

*marine drugs*

# Synthesis of Marine Natural Products and Molecules Inspired by Marine Substances II

---

Edited by  
Emiliano Manzo

Printed Edition of the Special Issue Published in *Marine Drugs*

# **Synthesis of Marine Natural Products and Molecules Inspired by Marine Substances II**



# Synthesis of Marine Natural Products and Molecules Inspired by Marine Substances II

Editor

**Emiliano Manzo**

MDPI • Basel • Beijing • Wuhan • Barcelona • Belgrade • Manchester • Tokyo • Cluj • Tianjin



*Editor*

Emiliano Manzo  
Institute of Biomolecular  
Chemistry (CNR-Italy)  
Pozzuoli  
Italy

*Editorial Office*

MDPI  
St. Alban-Anlage 66  
4052 Basel, Switzerland

This is a reprint of articles from the Special Issue published online in the open access journal *Marine Drugs* (ISSN 1660-3397) (available at: [www.mdpi.com/journal/marinedrugs/special\\_issues/Synthesis\\_Immunomodulatory](http://www.mdpi.com/journal/marinedrugs/special_issues/Synthesis_Immunomodulatory)).

For citation purposes, cite each article independently as indicated on the article page online and as indicated below:

LastName, A.A.; LastName, B.B.; LastName, C.C. Article Title. <i>Journal Name</i> <b>Year</b> , <i>Volume Number</i> , Page Range.
--

**ISBN 978-3-0365-1941-8 (Hbk)**

**ISBN 978-3-0365-1940-1 (PDF)**

© 2021 by the authors. Articles in this book are Open Access and distributed under the Creative Commons Attribution (CC BY) license, which allows users to download, copy and build upon published articles, as long as the author and publisher are properly credited, which ensures maximum dissemination and a wider impact of our publications.

The book as a whole is distributed by MDPI under the terms and conditions of the Creative Commons license CC BY-NC-ND.

# Contents

<b>About the Editor</b> . . . . .	<b>vii</b>
<b>Preface to "Synthesis of Marine Natural Products and Molecules Inspired by Marine Substances II"</b> . . . . .	<b>ix</b>
<b>Emiliano Manzo</b> Synthesis of Marine Natural Products and Molecules Inspired by Marine Substances II Reprinted from: <i>Marine Drugs</i> <b>2021</b> , <i>19</i> , 518, doi:10.3390/md19090518 . . . . .	<b>1</b>
<b>Uli Kazmaier and Lukas Junk</b> Recent Developments on the Synthesis and Bioactivity of Ilamycins/Rufomycins and Cyclomarins, Marine Cyclopeptides That Demonstrate Anti-Malaria and Anti-Tuberculosis Activity Reprinted from: <i>Marine Drugs</i> <b>2021</b> , <i>19</i> , 446, doi:10.3390/md19080446 . . . . .	<b>3</b>
<b>Paulo E. S. Munekata, Mirian Pateiro, Carlos A. Conte-Junior, Rubén Domínguez, Asad Nawaz, Noman Walayat, Elena Movilla Fierro and José M. Lorenzo</b> Marine Alkaloids: Compounds with <i>In Vivo</i> Activity and Chemical Synthesis Reprinted from: <i>Marine Drugs</i> <b>2021</b> , <i>19</i> , 374, doi:10.3390/md19070374 . . . . .	<b>31</b>
<b>Hong-Xiu Xiao, Qing-Xiang Yan, Zhi-Hui He, Zheng-Biao Zou, Qing-Qing Le, Ting-Ting Chen, Bing Cai, Xian-Wen Yang and Su-Lan Luo</b> Total Synthesis and Anti-Inflammatory Bioactivity of (-)-Majusculoic Acid and Its Derivatives Reprinted from: <i>Marine Drugs</i> <b>2021</b> , <i>19</i> , 288, doi:10.3390/md19060288 . . . . .	<b>55</b>
<b>Antonio Rosales Martínez, Ignacio Rodríguez-García and Josefa L. López-Martínez</b> Divergent Strategy in Marine Tetracyclic Meroterpenoids Synthesis Reprinted from: <i>Marine Drugs</i> <b>2021</b> , <i>19</i> , 273, doi:10.3390/md19050273 . . . . .	<b>69</b>
<b>Mohammed Othman Aljhdali, Mohammad Habibur Rahman Molla and Foysal Ahammad</b> Compounds Identified from Marine Mangrove Plant ( <i>Avicennia alba</i> ) as Potential Antiviral Drug Candidates against WDSV, an In-Silico Approach Reprinted from: <i>Marine Drugs</i> <b>2021</b> , <i>19</i> , 253, doi:10.3390/md19050253 . . . . .	<b>85</b>



## About the Editor

### **Emiliano Manzo**

Dr. Manzo Emiliano was born in Naples on 3 March 1973. He received his degree in chemistry at the University of Naples Federico II on 19 July 1996 with the votes 110/110 cum laude, discussing the experimental thesis "Structural determination of polysaccharides from phytopathogenic bacteria". In November 1996, he entered the profession of chemistry. On 6/03/2001, he obtained his Ph.D. in "Chemical Sciences" (Cycle XIII) at the University of Naples "Federico II". Since 2001, he has been a researcher and as of January of 2021 he has been a senior researcher at the Institute of Biomolecular Chemistry of the National Research Council (CNR), where he works on marine natural substances and in particular on chemical synthesis of marine metabolites with pharmacological activity developing synthetic strategies. His research activity is summarized in more than 80 papers in peer-reviewed international journals, 5 intern. patents and 50 communications to international conferences on chemistry of marine natural products.





# **Preface to "Synthesis of Marine Natural Products and Molecules Inspired by Marine Substances II"**

The sea covers more than 70% of Earth's surface and contains more than 300,000 organisms with huge biodiversity. These organisms represent an enormous tank of substances whose chemical structures are the result of the enormous ecological pressure for survival. Given their high chemical diversity, biological activity, biochemical specificity and other crucial molecular properties, marine natural products have always played a crucial role in the search and discovery of novel bioactive molecules that are potentially useful for pharmacological applications. In fact, the development of new 'lead' compounds from the sea has always been and is one of the main purposes of drug discovery.

The study and advanced progress of these products cannot be separated from the development of chemical synthesis and synthetic strategies aimed at the preparation and optimization of these substances and/or analogs, leading the way to new classes of biologically active compounds with pharmacological potential.

**Emiliano Manzo**

*Editor*



Editorial

# Synthesis of Marine Natural Products and Molecules Inspired by Marine Substances II

Emiliano Manzo 

Institute of Biomolecular Chemistry (ICB), Consiglio Nazionale delle Ricerche (CNR), Via Campi Flegrei 34, 80078 Pozzuoli, Italy; emanzo@icb.cnr.it

The sea occupies more than 70% of the Earth's surface and includes more than 300,000 organisms with huge biodiversity. These organisms represent an enormous source of substances with relevant potential in the pharmacological field. The diversity and potential bioactivity of structures isolated from marine organisms have always played a crucial role in the search for and discovery of novel bioactive molecules that are potentially useful in pharmacological applications. The development of new lead compounds from the sea has always been the crucial aim of drug discovery [1]. In this regard, the progress of chemical synthesis and synthetic strategies, leading to preparation and biological optimization of these substances, paves the way for new classes of biologically active compounds with pharmacological potential.

This Special Issue, as a continuation of the previous Special Issue, 'Synthesis of Marine Natural Products and Molecules Inspired by Marine Substances', includes three reviews and two articles that describe the synthetic strategies and biological activities of different classes of bioactive marine metabolites and analogs essential for future pharmacological applications.

A review by Munekata et al. [2] focuses on the development of synthetic chemical strategies for the preparation of marine alkaloid compounds and analogs to ameliorate the biological behavior of these substances. In particular, for the research and validation of the bioactivities, an increasing number of *in vivo* studies with animals, especially mice and zebrafish, have evidenced the potential health benefits against several important and debilitating pathologies *in vivo*.

In a review by Kazmaier and Junk [3], cycloheptapeptides molecules as ilamycins, rufomycins, and cyclomarins, including unusual amino acids with important biological activities, are treated. These substances are specifically active against a range of mycobacteria with no significant activity towards other Gram-positive and Gram-negative bacteria or fungi. A wide range of these derivatives can be obtained by fermentation, while bioengineering also allows the synthesis of derivatives, especially cyclomarins. Other derivatives are accessible by semisynthesis or total syntheses, reported for both natural product classes. This review examines all aspects of the research conducted in the synthesis of these interesting cyclopeptides.

A review by Martinez et al. [4] focuses on divergent total synthesis strategies applied to the preparation of families of natural products using a common late-stage pluripotent intermediate and offering the opportunities for preparation of structurally related compounds. Aureol is the main topic of this review.

In an article of Aljahdali et al. [5], a docking study useful for the finding of new antiviral agents was performed. In this regard Walleye dermal sarcoma virus (WDSV), responsible for the induction of a multifocal benign cutaneous tumor, is particularly prevalent in some localities. Efficient therapeutics against this virus have not been developed yet. This study utilizes computer-aided drug design approaches to develop molecules through homology modeling, molecular docking, and ADMET methods, and three potential antiviral candidates, Friedlein, Phytosterols, and 1-Triacontanol are identified.



**Citation:** Manzo, E. Synthesis of Marine Natural Products and Molecules Inspired by Marine Substances II. *Mar. Drugs* **2021**, *19*, 518. <https://doi.org/10.3390/md19090518>

Received: 3 September 2021

Accepted: 7 September 2021

Published: 13 September 2021

**Publisher's Note:** MDPI stays neutral with regard to jurisdictional claims in published maps and institutional affiliations.



**Copyright:** © 2021 by the author. Licensee MDPI, Basel, Switzerland. This article is an open access article distributed under the terms and conditions of the Creative Commons Attribution (CC BY) license (<https://creativecommons.org/licenses/by/4.0/>).

In an article by Xiao et al. [6], the first total synthesis of marine natural product, (-)-majusculoic acid and its seven analogs, is performed. This strategy features the application of conformational and stereochemical controlled reactions. The promising anti-inflammatory activity of the synthetic derivatives is evaluated with significant effect. Moreover, they do not show cytotoxicity against RAW264.7 cells, indicating that they might be potential anti-inflammatory agents.

As guest editor, I am grateful to all the authors who contributed their excellent results to this Special Issue, all the reviewers who carefully evaluated the submitted manuscripts, and *Marine Drugs* for their support and kind help.

**Funding:** This research received no external funding.

**Conflicts of Interest:** The authors declare no conflict of interest.

## References

1. Carroll, A.R.; Copp, B.R.; Davis, R.A.; Keyzers, R.A.; Prinsep, M.R. Marine natural products. *Nat. Prod. Rep.* **2020**, *37*, 175–223. [[CrossRef](#)] [[PubMed](#)]
2. Munekata, P.E.S.; Pateiro, M.; Conte-Junior, C.A.; Domínguez, R.; Nawaz, A.; Walayat, N.; Movilla Fierro, E.; Lorenzo, J.M. Marine Alkaloids: Compounds with In Vivo Activity and Chemical Synthesis. *Mar. Drugs* **2021**, *19*, 374. [[CrossRef](#)] [[PubMed](#)]
3. Kazmaier, U.; Junk, L. Recent Developments on the Synthesis and Bioactivity of Ilamycins/Rufomycins and Cyclomarins, Marine Cyclopeptides That Demonstrate Anti-Malaria and Anti-Tuberculosis Activity. *Mar. Drugs* **2021**, *19*, 446. [[CrossRef](#)] [[PubMed](#)]
4. Rosales Martínez, A.; Rodríguez-García, I.; López-Martínez, J.L. Divergent Strategy in Marine Tetracyclic Meroterpenoids Synthesis. *Mar. Drugs* **2021**, *19*, 273. [[CrossRef](#)] [[PubMed](#)]
5. Aljahdali, M.O.; Molla, M.H.R.; Ahammad, F. Compounds Identified from Marine Mangrove Plant (*Avicennia alba*) as Potential Antiviral Drug Candidates against WDSV, an In-Silico Approach. *Mar. Drugs* **2021**, *19*, 253. [[CrossRef](#)] [[PubMed](#)]
6. Xiao, H.-X.; Yan, Q.-X.; He, Z.-H.; Zou, Z.-B.; Le, Q.-Q.; Chen, T.-T.; Cai, B.; Yang, X.-W.; Luo, S.-L. Total Synthesis and Anti-Inflammatory Bioactivity of (-)-Majusculoic Acid and Its Derivatives. *Mar. Drugs* **2021**, *19*, 288. [[CrossRef](#)] [[PubMed](#)]

Review

# Recent Developments on the Synthesis and Bioactivity of Ilamycins/Rufomycins and Cyclomarins, Marine Cyclopeptides That Demonstrate Anti-Malaria and Anti-Tuberculosis Activity

Uli Kazmaier<sup>1,2,\*</sup>  and Lukas Junk<sup>1,2</sup>

<sup>1</sup> Organic Chemistry, Saarland University, Campus Building C4.2, 66123 Saarbrücken, Germany; l.junk@mx.uni-saarland.de

<sup>2</sup> Helmholtz Institute for Pharmaceutical Research Saarland (HIPS)—Helmholtz Centre for Infection Research (HZI), Campus Building E8 1, 66123 Saarbrücken, Germany

\* Correspondence: u.kazmaier@mx.uni-saarland.de; Tel.: +49-681-302-3409

**Abstract:** Ilamycins/rufomycins and cyclomarins are marine cycloheptapeptides containing unusual amino acids. Produced by *Streptomyces* sp., these compounds show potent activity against a range of mycobacteria, including multidrug-resistant strains of *Mycobacterium tuberculosis*. The cyclomarins are also very potent inhibitors of *Plasmodium falciparum*. Biosynthetically the cyclopeptides are obtained via a heptamodular nonribosomal peptide synthetase (NRPS) that directly incorporates some of the nonproteinogenic amino acids. A wide range of derivatives can be obtained by fermentation, while bioengineering also allows the mutasynthesis of derivatives, especially cyclomarins. Other derivatives are accessible by semisynthesis or total syntheses, reported for both natural product classes. The anti-tuberculosis (anti-TB) activity results from the binding of the peptides to the N-terminal domain (NTD) of the bacterial protease-associated unfoldase ClpC1, causing cell death by the uncontrolled proteolytic activity of this enzyme. Diadenosine triphosphate hydrolase (PfAp3Aase) was found to be the active target of the cyclomarins in *Plasmodia*. SAR studies with natural and synthetic derivatives on ilamycins/rufomycins and cyclomarins indicate which parts of the molecules can be simplified or otherwise modified without losing activity for either target. This review examines all aspects of the research conducted in the syntheses of these interesting cyclopeptides.

**Keywords:** ilamycins; rufomycins; cyclomarins; tuberculosis; malaria; cyclopeptides; biosynthesis; total synthesis; natural products



**Citation:** Kazmaier, U.; Junk, L. Recent Developments on the Synthesis and Bioactivity of Ilamycins/Rufomycins and Cyclomarins, Marine Cyclopeptides That Demonstrate Anti-Malaria and Anti-Tuberculosis Activity. *Mar. Drugs* **2021**, *19*, 446. <https://doi.org/10.3390/md19080446>

Academic Editor: Emiliano Manzo

Received: 20 July 2021

Accepted: 30 July 2021

Published: 3 August 2021

**Publisher's Note:** MDPI stays neutral with regard to jurisdictional claims in published maps and institutional affiliations.



**Copyright:** © 2021 by the authors. Licensee MDPI, Basel, Switzerland. This article is an open access article distributed under the terms and conditions of the Creative Commons Attribution (CC BY) license (<https://creativecommons.org/licenses/by/4.0/>).

## 1. Introduction

Marine organisms produce a wealth of natural products, creating a universe of fascinating new chemical structures [1,2]. These natural products are often the result of an evolutionary process providing competitive advantages to their producers in their natural environments. Therefore, many of these natural products have notable biological activities, making them good candidates for drug development [3–5], including against infectious diseases such as malaria and tuberculosis.

Malaria is one of the most common tropical diseases, with more than 200 million infections and 600,000 deaths annually worldwide [6], mainly in the poorest population. Tuberculosis (TB) is also common: in 2019, approximately 10 million people fell ill with the disease and 1.5 million died [7]. In addition, in 2018, 500,000 people demonstrated resistance to rifampicin, the most effective first-line drug, 80% of whom suffer from multidrug-resistant tuberculosis (MDR-TB). The development of antibiotic resistance is widespread, and these multi-resistant pathogens are a particularly serious problem. Therefore, new drugs are required [8]. Most first- and second-line drugs were discovered or developed between 1940 and 1980, often with a similar mode of action, facilitating the development of resistance [9,10]. Modern drugs should therefore work via new modes of action against not

only the MDR-TB strains but also the largely drug-resistant tuberculosis (XDR-TB) strains, which are now almost resistant to all drugs. In addition, any new drug should effectively destroy dormant bacteria, beneficial for short-term therapies, and be nontoxic (because of the generally long treatment times required). Natural products are excellent candidates for developing anti-TB drugs, and more than 60% of drugs under current development are natural products or derived from natural products [11–13].

## 2. Discovery of Anti-Tubercular Cycloheptapeptides

### 2.1. Discovery of the Ilamycins/Rufomycins

In 1962, two independent research groups investigated marine *Streptomyces* from soil samples found on Japanese islands. Takita et al. observed that the culture filtrate of a new strain, *Streptomyces insulates* (A-165-Z1), later renamed *Streptomyces islandicus*, inhibited the growth of *Mycobacterium* 607 and *Mycobacterium phlei*. They isolated two antibiotics and named them ilamycin A and B (IIaA and IIaB) [14,15].

In addition, at this time Shibata et al. isolated two new antibiotics, rufomycin I and II (Ruf I and Ruf II), from the newly discovered *Streptomyces atratus* (46408), found to be especially active against acid-fast bacteria [16,17]. The compounds were also active against *Mycobacterium tuberculosis* and *Mycobacterium smegmatis* but almost inactive against most other bacteria, fungi, and yeasts. Subsequent research indicated that these two antibiotics possess very similar chemical structures [18–23].

The structures of ilamycins/rufomycins (Figure 1) are unusual, as these cyclic heptapeptides contain a series of atypical amino acids. Most prominent is the *N*-prenylated tryptophan ①, which can also be found in the epoxidized form [24,25]. At the *N*-terminus of the tryptophan, a  $\gamma,\delta$ -unsaturated amino acid is incorporated ⑦ [26]. Common to all derivatives is a unique 3-nitrotyrosine ③, a building block not found in any other natural product. The greatest variability is observed in the leucine building block ⑤, which can be oxidized to different oxidation levels at a terminal methyl group. In its original description, ilamycin was proposed to contain an aldehyde functionality [23], but structural elucidation by NMR and X-ray crystallography showed that the aldehyde functionality undergoes cyclization with the nearby amide bond [27–29]. Very recently, a wide range of new ilamycins/rufomycins were described, differing mainly in the combination of different amino acid oxidation levels ⑤ and the *N*-prenyl substituent of ① (alkene, epoxide, diol) [27–29].

### 2.2. Discovery of the Cyclomarins

In 1999, the research groups of Fenical and Clardy reported the isolation of three new anti-inflammatory cyclic peptides from extracts of a *Streptomyces* sp. collected in Mission Bay, California [30]. These secondary metabolites from the strain CNB-982, called cyclomarins (Cym) A–C, are structurally related to the rufomycins. Very similar amino acid building blocks are incorporated, although in a different sequence. As in the rufomycins, an *N*-prenylated tryptophan ① (CymC) is a notable building block that can also be epoxidized (CymA). However, in contrast to the rufomycins, in the cyclomarin series, the tryptophan units are  $\beta$ -hydroxylated. At the *N*-terminus of the tryptophan, a  $\gamma,\delta$ -unsaturated amino acid is incorporated, not a linear one as found in the rufomycins, but one that is branched and dimethylated ⑦. One of the leucines is also oxidized at the  $\delta$  position ②, at least in CymA and C, but at another position, as in the rufomycins. Most obvious is the replacement of the unique nitrotyrosine by another aromatic amino acid, *syn*- $\beta$ -methoxyphenylalanine ④.

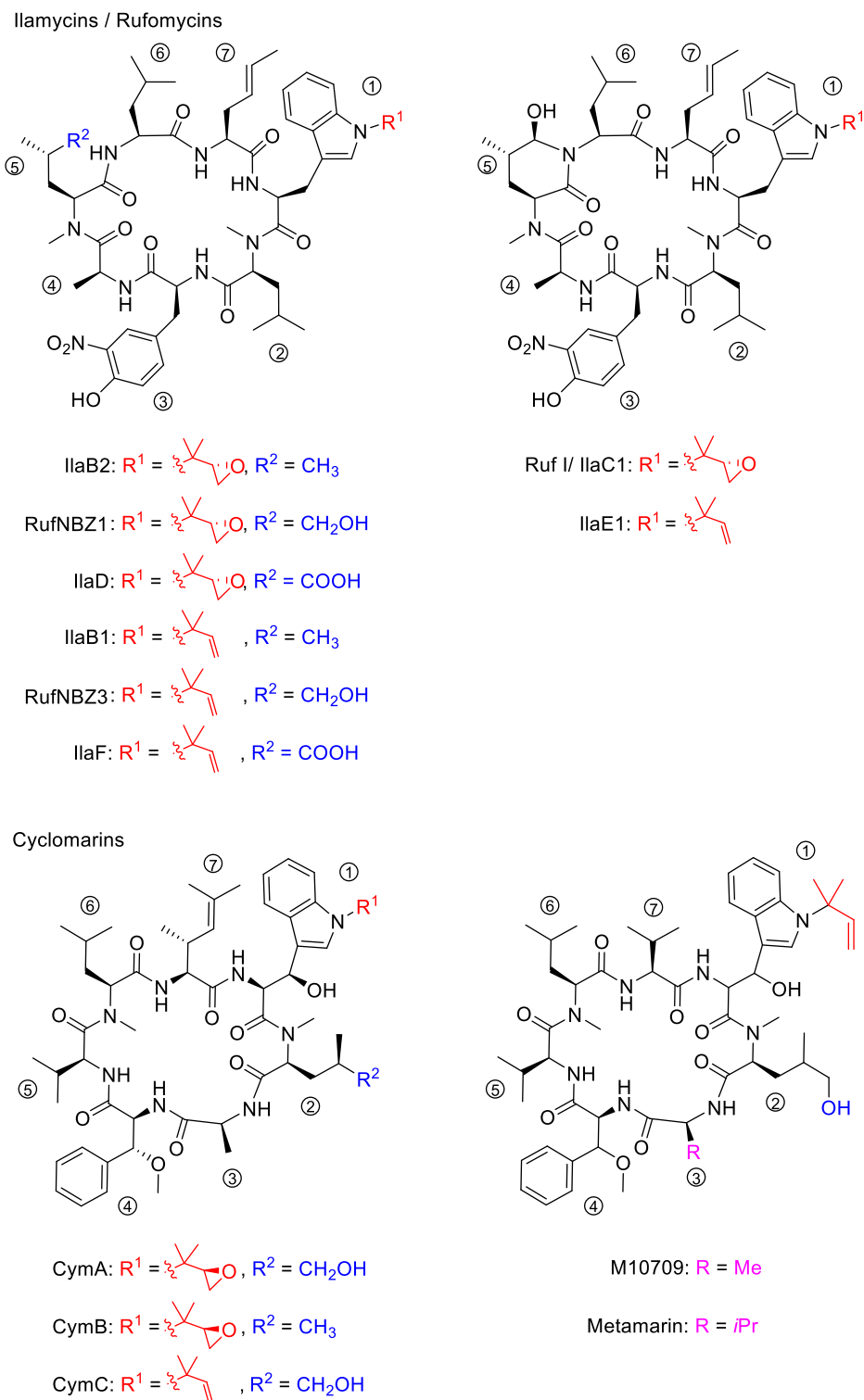


**Figure 1.** Selected ilamycins/rufomycins and cyclomarins.

In 2010, the group of Mikami described the extraction of a new cyclomarin derivative M10709 from clinically isolated *Streptomyces* sp. IFM 10,709 [31]. Although not all stereogenic centers were determined properly, results revealed the compound was different from cyclomarin C only by the replacement of the unsaturated amino acid ⑦ by valine. The same structural motif was also found in a recently isolated metamarine in which a valine



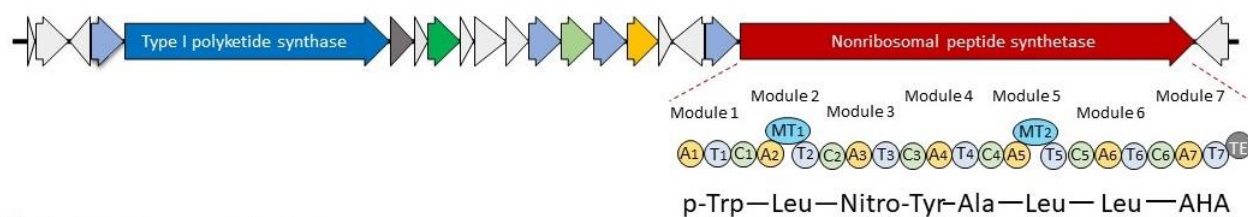
at position ③ replaced an alanine. The discovery of metamarine resulted from a larger soil metagenome project undertaken to discover rufomycin/cyclomarins-like antibiotics [32].

### 3. Biosynthesis of Anti-Tubercular Cycloheptapeptides

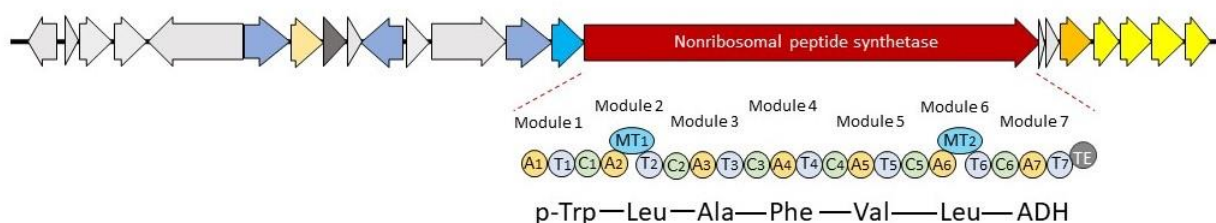
Although the ilamycins/rufomycins were originally described in the early 1960s, biosynthetic studies of these unusual cyclopeptides were reported only recently [27,33]. The first investigations of cyclomarins were conducted in 2008 by the Moore group [34,35], while Brady et al. reported their results on metamarine biosynthesis in 2021 [32].

Although there are significant differences in the structures of these cycloheptapeptides, they also have structural similarities and common biosynthetic features (Figure 2). A key feature of the biosynthetic gene cluster is a gene encoding a heptamodular nonribosomal peptide synthetase (NRPS). This NRPS is surrounded by a set of open reading frames (ORF) that encodes tailoring enzymes (P450, oxygenases) and provides the required building blocks for peptide synthesis. They contain the unusual amino acids *N*-prenyl-tryptophan (p-Trp), 3-nitrotyrosine (Nitro-Tyr, ilamycins), as well as the unsaturated amino acids (2*S*,4*E*)-2-amino-4-hexenoic acid (AHA, ilamycins) and (2*S*,3*R*)-2-amino-3,5-dimethylhexenoic acid (ADH, cyclomarins). These building blocks are directly incorporated into the NRPS, while oxidative tailoring enzymes encoded in the ORFs modify the protein-bound peptide during synthesis. All biosyntheses start with the p-Trp ① and end with a cyclization between ① and the C-terminal amino acids ⑦.

#### a) Rufomycin gene cluster



#### b) Cyclomarins gene cluster



#### c) Metamarin gene cluster

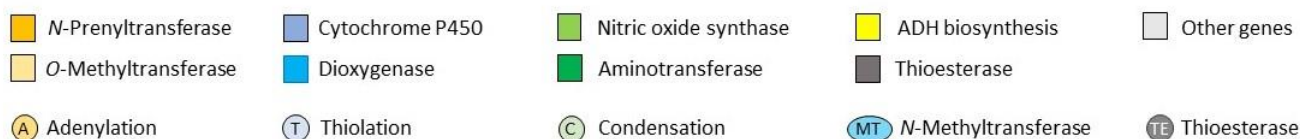
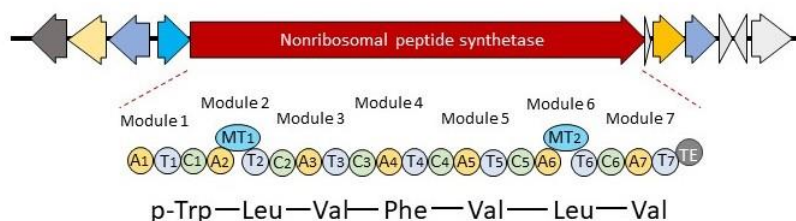


**Figure 2.** Biosynthesis of rufomycins and (modified) cyclomarins; (a) Rufomycin gene cluster, (b) Cyclomarins gene cluster, (c) Metamarin gene cluster.

### 3.1. Biosynthesis of the Ilamycins/Rufomycins

A total of 20 genes are involved in the biosynthesis of these cyclopeptides (Figure 2a) [27,36]. Besides the gene encoding the NRPS, a second large gene encodes a type I polyketide synthase (PKS), which is involved in AHA synthesis. (*E*)-4-Hexenic acid is obtained from AcCoA, and is further hydroxylated, oxidized (P450), and transaminated to AHA [33]. An *N*-prenyltransferase is responsible for the generation of the first amino acid of the sequence from tryptophan. The unusual 3-nitrotyrosine is obtained by P450-catalyzed nitrosation of tyrosine, and the NO required is provided by a nitric acid synthase from arginine [33]. Additional P450 cytochrome controls the final oxidation steps to create the different ilamycin family members [27].

### 3.2. Biosynthesis of Cyclomarins

Although the cyclomarins are structurally related to the ilamycins, they are significantly different, at least from a biosynthetic point of view (Figure 2b) [34,35]. In contrast to the ilamycins, the linear unsaturated amino acid AHA is replaced by the dimethylated derivative ADH, which has a completely different biosynthetic origin. While AHA is obtained by a classical polyketide synthase, ADH is formed from valine and pyruvate [35]. Of the 23 ORFs of the biosynthetic gene cluster, several genes are responsible for ADH synthesis. Another significant difference is the  $\beta$ -OH functionality of the prenylated tryptophan (p-Trp), which is found in all cyclomarins but not in the ilamycins and rufomycins. Its introduction is catalyzed by a tryptophan- $\beta$ -hydroxylase, a dioxygenase, and occurs on the protein-bound peptide in the early stages of the biosynthesis. In contrast, epoxidation of the *N*-prenyl side chain by a P450 epoxidase occurs post-NRPS assembly. Gene inactivation of the prenyltransferase eliminated the production of cyclomarin, indicating that p-Trp is the initiator of the peptide assembly line and that the unmodified p-Trp is not a good substrate for the first acceptor domain [34]. The  $\beta$ -hydroxylation must occur during the first two steps of the peptide synthesis, since inactivation of the corresponding gene does not result in the formation of a desoxycyclomarin but the formation of a dioxopiperazine called cyclomarazine (Figure 3), containing only the first two amino acids of the biosynthesis.

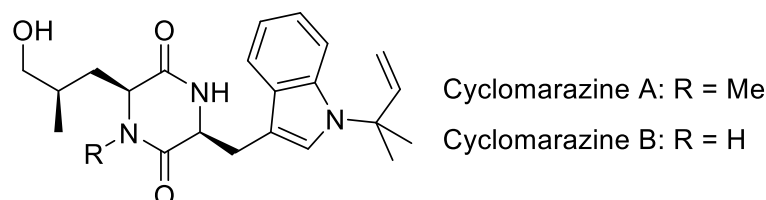


**Figure 3.** Cyclomarazines.

CymA and CymB were isolated from the *Streptomyces* sp. CNB-982, together with CymD that was missing the *N*-methyl group on the  $\delta$ -hydroxyleucine ②. It is clear that  $\delta$ -hydroxylation by P450 leucine hydroxylase occurs faster than *N*-methylation, and tryptophan hydroxylation is essential for prolonging the peptide chain. If this hydroxylation does not occur properly, the incompletely processed dipeptide is cleaved from the NRPS due to ineffective processing by the next module. This reaction is a unique example in which a megasynthetase can produce two different natural products of different sizes simply by triggering the level of  $\beta$ -oxidation on the priming Trp unit. Notably, cyclomarazines do not show significant biological activity.

The second major way in which cyclomarins differ from ilamycins is the incorporation of  $\beta$ -methoxyphenylalanine (MeOPhe) instead of nitrotyrosine. This amino acid is obtained from a peptide-bound Phe via a P450-catalyzed  $\beta$ -hydroxylation followed by *O*-methylation [35].

During their soil metagenome project, Brady et al. also investigated the biosynthesis of metamarin. In this cyclomarin derivative, the unsaturated amino acid is replaced by valine (Figure 2c) [32]. Another valine is incorporated instead of alanine ③. Therefore, it is

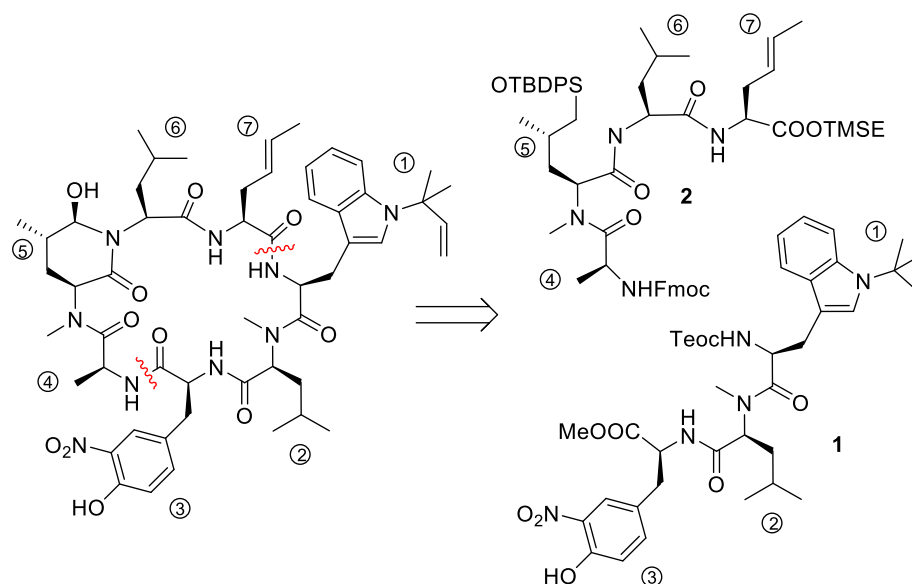
not surprising that the gene cluster is comparable to the cyclomarins cluster, and only the genes responsible for ADH biosynthesis are missing.

#### 4. Total Syntheses of Marine Cycloheptapeptides

The interesting biological properties and unusual building blocks of marine cycloheptapeptides sparked the interest of synthetic chemists, and the syntheses of several different amino acids and fragments have been reported in a recent review [37]. Therefore, they will not be discussed in detail here, and the focus will be on the total syntheses of the natural products.

##### 4.1. Total Synthesis of Ilamycins/Rufomycins

To date, only one synthetic route has been described for ilamycins E1 and F by Guo and Ye et al. [38]. In their highly convergent strategy, the ilamycins were synthesized from two parts (**1** and **2**) that were linked between **1** and **7** to the macrocyclic lactam (Scheme 1). The lower right tripeptide part **1** (**1**–**3**) was prepared in five steps from tryptophan, while the upper left tetrapeptide **2** (**4**–**7**) required 13 steps from glutamic acid. Final oxidation of the  $\delta$ -hydroxyleucine **5** resulted in the described ilamycins.

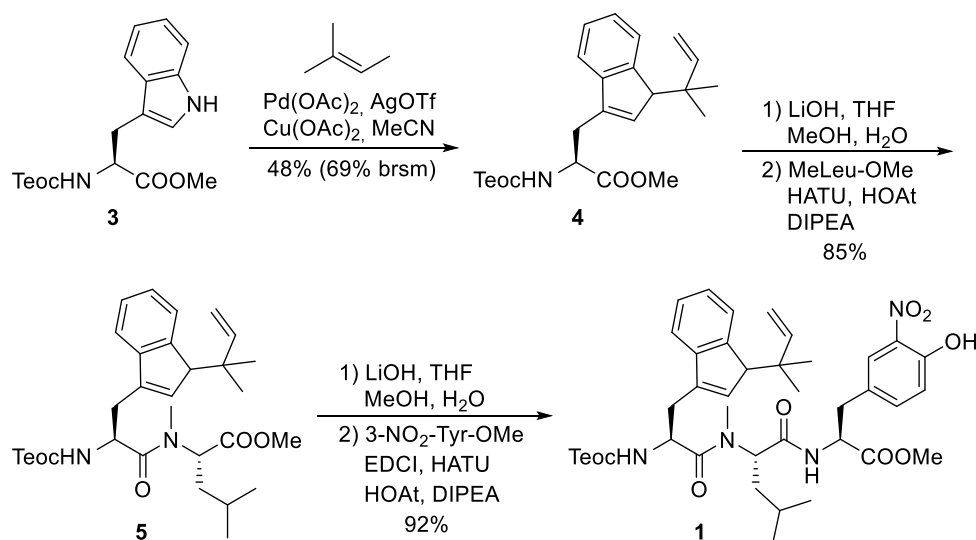


**Scheme 1.** Retrosynthesis of ilamycins (Guo and Ye).

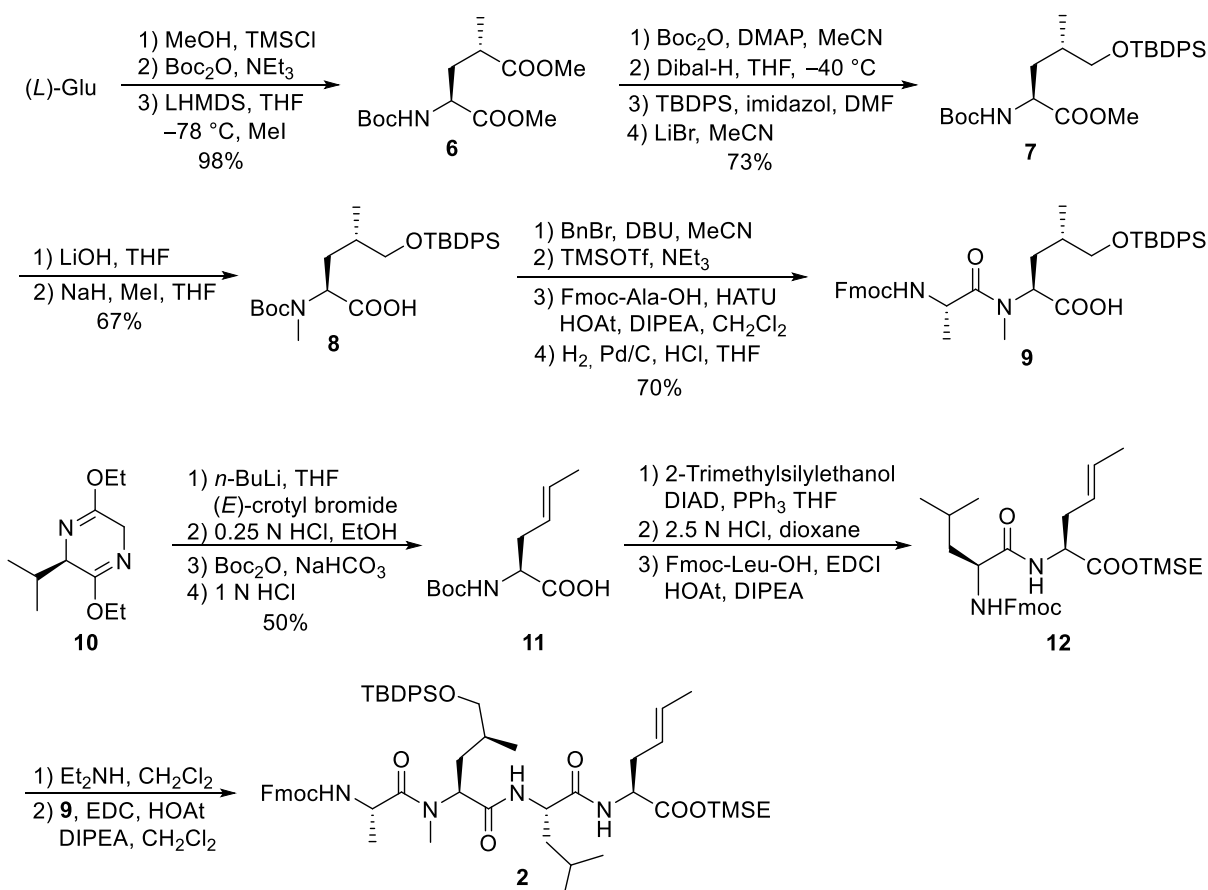
The synthesis of peptide fragment **1** was rather straightforward (Scheme 2). 2-(Trimethylsilyl)ethoxycarbonyl (Teoc)-protected tryptophan methyl ester **3** was subjected to a Pd-catalyzed *N-tert*-prenylation according to a protocol developed by Baran et al. [39]. Saponification of the ester moiety of **4** and peptide coupling with *N*-methylated Leu-OMe produced dipeptide **5**, which was further elongated to tripeptide **1**.

For the larger fragment **2**, glutamic acid was converted into protected **8** (Scheme 3) according to a synthetic route developed during the synthesis of dysithiazolamide [40]. The glutamic acid was converted into the dimethyl ester and *N*-Boc protected before it was stereoselectively  $\alpha$ -methylated at the sterically least-hindered ester moiety [41,42]. For the chemoselective reduction of the  $\gamma$ -ester **6**, a second *N*-Boc-protecting group was introduced, and the sterically least-hindered ester functionality was reduced with DIBAL-H. Silyl protection of the primary alcohol and subsequent mono-Boc deprotection yielded **7**. The methyl ester was saponified (to avoid  $\alpha$ -methylation), and the Boc-amide was selectively *N*-methylated to **8** with NaH/MeI. The free carboxylic acid **8** was converted into the corresponding benzyl ester. TMSOTf/NEt<sub>3</sub> was used for selective cleavage of the *N*-Boc-protecting group without affecting the OTBDPS group. The free amine could

be coupled with Fmoc-protected alanine, and the C-terminal benzyl ester was cleaved by catalytic hydrogenation to provide the free acid **9**.



Scheme 2. Synthesis of peptide fragment 1.

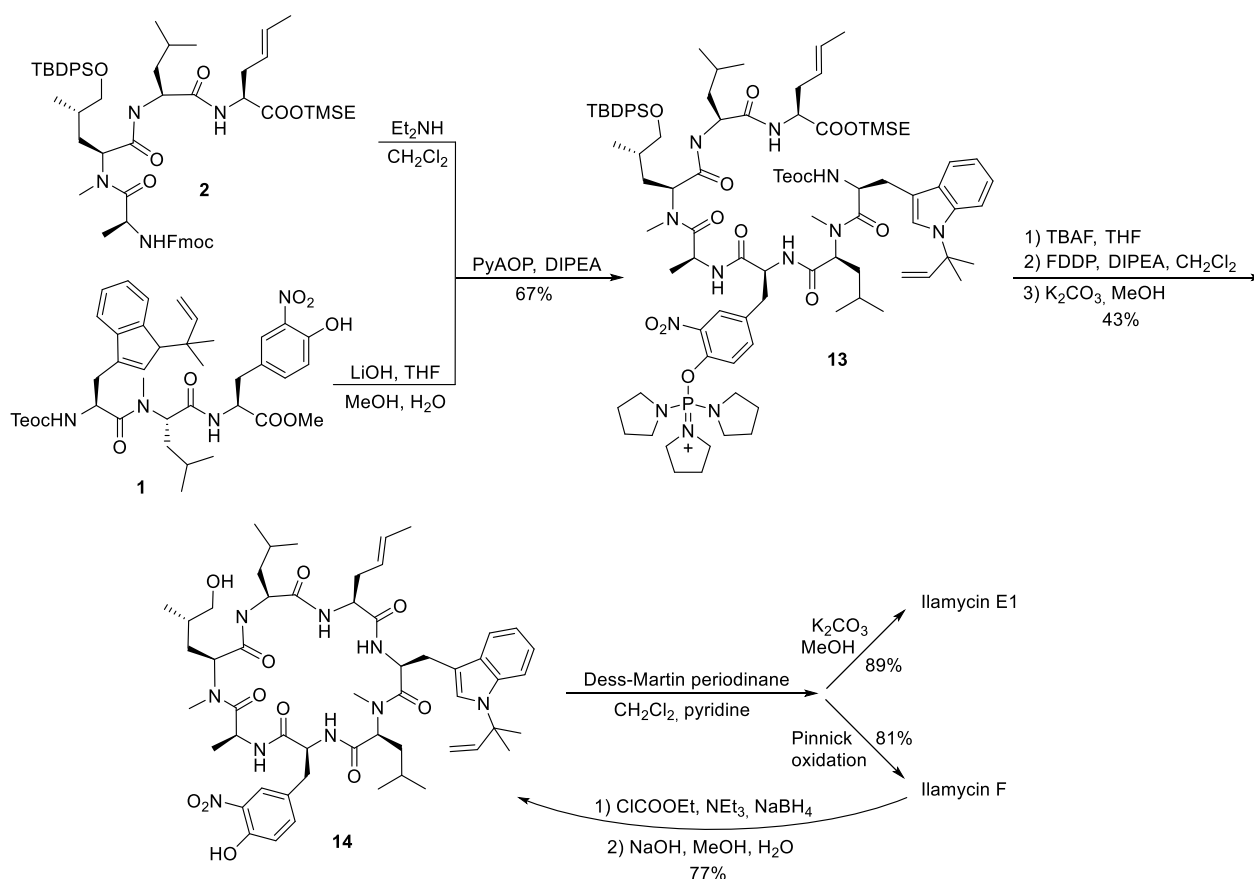


Scheme 3. Synthesis of peptide fragment 2.

Schöllkopf auxiliary **10** [43] was subjected to stereoselective crotylation to generate the C-terminal unsaturated amino acid of **2** (Scheme 3). Subsequent auxiliary cleavage provided *N*-Boc-protected amino acid **11**, which was converted into the corresponding

TMSE ester. Boc-deprotection and peptide coupling produced dipeptide **12**. Subsequent Fmoc deprotection and coupling with **9** generated the linear tetrapeptide **2**.

With the two major building blocks produced, ilamycin synthesis could proceed to the final step (Scheme 4). Mild saponification of the methylester **1** and coupling with Fmoc-deprotected **2** using (2-azabenzotriazol-1-yloxy)tripyrrolidinophosphonium hexafluorophosphate (PyAOP) [44] yielded **13** without significant epimerization. Global deprotection with TBAF resulted in the linear heptapeptide, which was subjected to macro-lactamization. While many peptide coupling reagents have been investigated, the best results were obtained using pentafluorophenyl diphenylphosphinate (FDPP) [45]. As a side product in addition to the expected cyclopeptide **14**, the diphenylphosphinylated ester was formed, which could directly be converted into **14** by treatment with  $K_2CO_3$  in methanol, providing an overall yield of 43% of the desired **14**. Finally, only the primary OH-functionality needed to be oxidized. Depending on the oxidation protocol, both ilamycin E1 and F could be obtained. Ilamycin E1 was obtained as a single stereoisomer. Notably, ilamycin F is also available on a gram scale via fermentation, but the derivative E1, which is approximately 100-fold more potent, is not. Therefore, the authors developed a protocol to convert ilamycin F into intermediate **14** by reducing the mixed anhydride, permitting an interconversion of ilamycin F into ilamycin E1 [38].

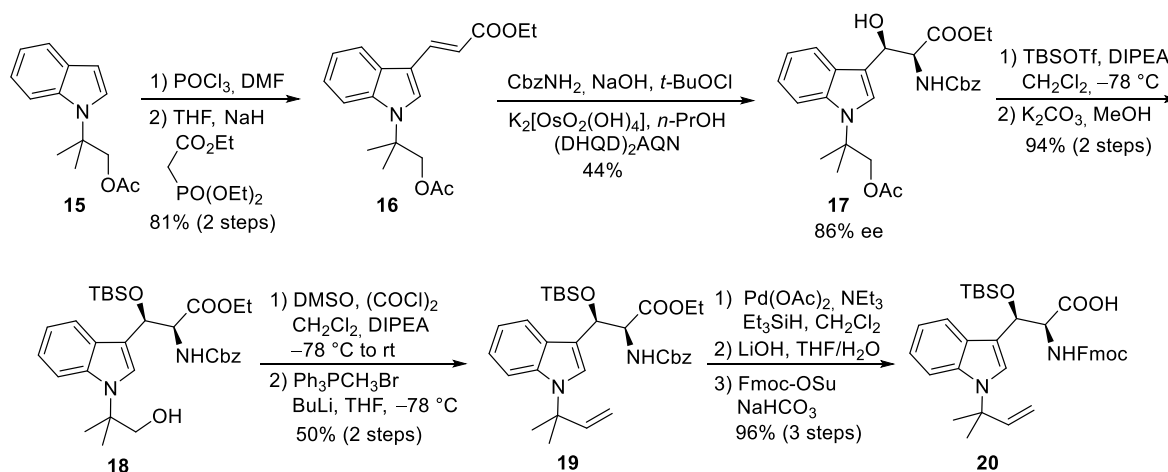


**Scheme 4.** Synthesis of ilamycinE1 and F.

#### 4.2. Total Synthesis of Cyclomarins

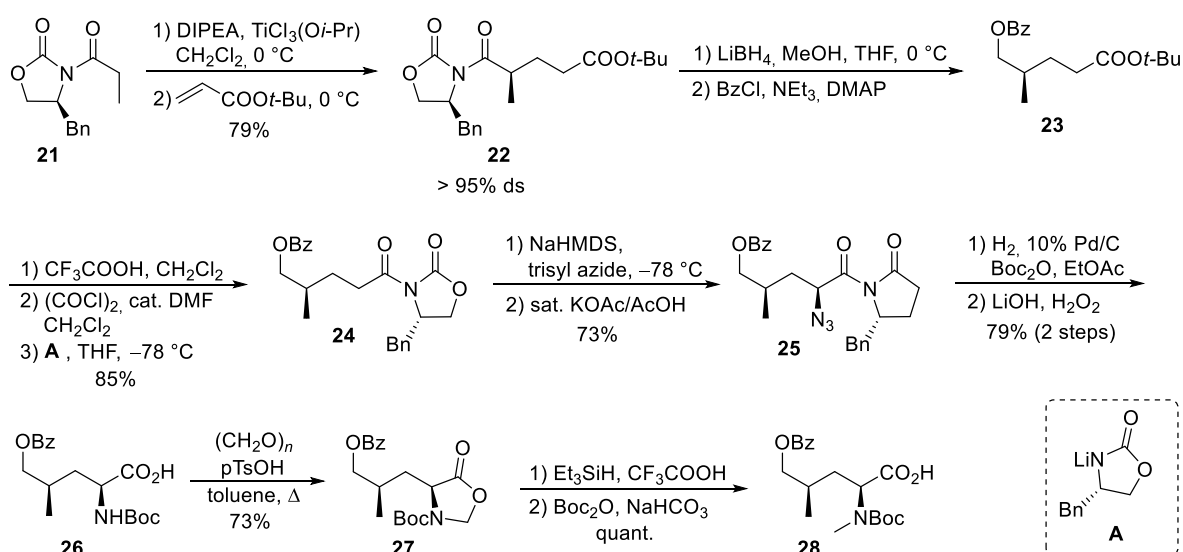
The amino acids present in the cyclomarins are slightly more complex than in the ilamycins, and various synthetic approaches have been undertaken to produce these building blocks and partial structures of cyclomarin [46]. These are covered in a recent review [37], and therefore only the routes applicable to the synthesis of cyclomarins and derivatives will be discussed here.

The first synthesis of cyclomarins C was reported in 2004 by Yao and coworkers [47]. The unusual *tert*-prenylated  $\beta$ -hydroxy-tryptophan ① was obtained from indole derivative **15** (Scheme 5). This compound is available from indole via *N*-alkylation with ethyl- $\alpha$ -bromo-propionate, subsequent  $\alpha$ -methylation of the ester, LAH-reduction, and acetylation [48]. Formylation and a subsequent Horner–Wadsworth–Emmons reaction yielded  $\alpha,\beta$ -unsaturated ester **16**, which could be subjected to a Sharpless aminohydroxylation [49]. Moderate yield and enantioselectivity of the desired  $\beta$ -hydroxytryptophan derivative **17** was obtained. Unfortunately, no comment was made concerning the regioselectivity of the reaction. Silylation of the  $\beta$ -hydroxy group and selective transesterification of the acetate gave rise to primary alcohol **18**, which could be oxidized to the aldehyde and methenylated via Wittig reaction. Finally, the Cbz-protecting group from **19** was removed selectively without affecting the generated double bond. Furthermore, the free amine was Fmoc-protected after saponification of the ester. The use of the Fmoc- or Alloc-protecting group is essential for the synthesis of cyclomarins because other protecting groups, such as Boc, cannot be removed later on without side reactions, such as the elimination of the  $\beta$ -hydroxy functionality [50].



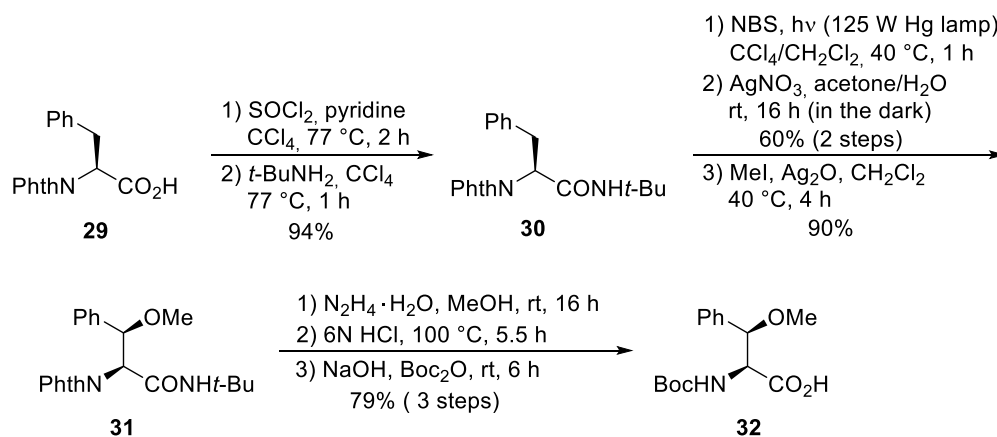
**Scheme 5.** Synthesis of protected tryptophan **20** (building block ①).

The synthesis of  $\delta$ -hydroxyleucine building block ②, with the opposite configuration of the  $\gamma$ -methyl group than in amino acid ⑤ in the ilamycins, was obtained by classical asymmetric synthesis using chiral auxiliary chemistry (Scheme 6). According to Evans et al. [51], chiral oxazolidinone **21** was subjected as its titanium enolate in a Michael addition to *tert*-butyl acrylate to provide a good yield of **22** with high stereoselectivity. The imide was selectively reduced in the presence of the *tert*-butyl ester using  $\text{LiBH}_4$ , and the resulting primary alcohol was *O*-benzoylated to **23**. Acidic cleavage of the *tert*-butyl ester, activation of the carboxylic acid, and reapplication of the Evans auxiliary **A** provided oxazolidinone **24**. Deprotonation of **24** and stereoselective azidation produced azide **25**. Catalytic hydrogenation in the presence of  $\text{Boc}_2\text{O}$  resulted in the formation of the *N*-Boc-protected amino derivative, which was saponified to the corresponding amino acid **26**. The desired *N*-methyl group was introduced by conversion of **26** into the corresponding oxazolidinone **27**, which was reduced using triethylsilane in presence of trifluoroacetic acid. Subsequent cleavage of the Boc-protecting group required its reintroduction to **28**.



**Scheme 6.** Synthesis of protected hydroxyleucine **28** (building block ②).

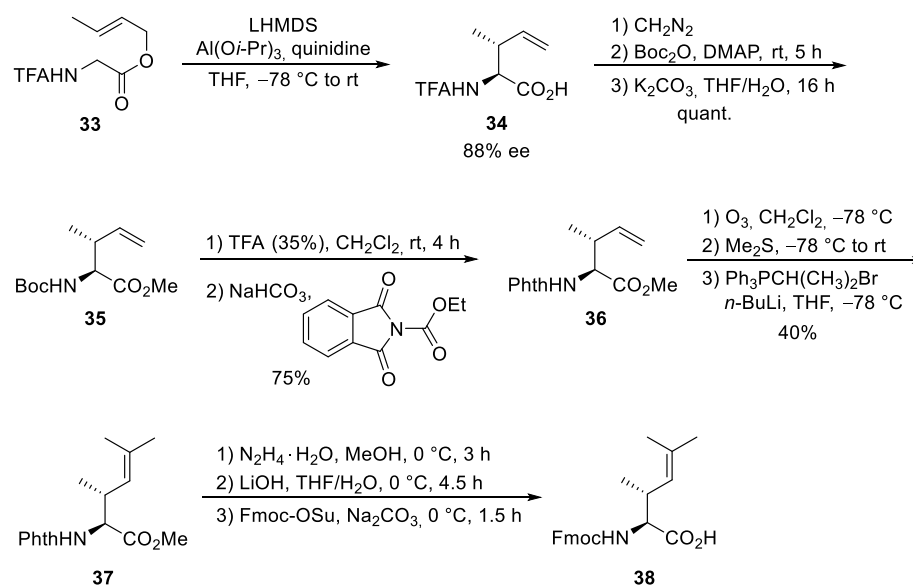
The unusual  $\beta$ -methoxyphenylalanine④ was obtained from *N*-phthaloyl-protected phenylalanine **29**, which was converted into the corresponding *tert*-butylamide **30** (Scheme 7). Oxygen functionality was introduced into the  $\beta$ -position by subjecting **30** to a Wohl–Ziegler bromination, providing a 1:1 diastereomeric mixture of the desired  $\beta$ -bromo derivative [52]. According to Easton et al., treatment of the diastereomeric mixture with  $\text{AgNO}_3$  in aqueous acetone produced the desired (2*S*,3*R*)- $\beta$ -hydroxyphenylalanine enantio- and diastereoselectively [53]. The stereochemical outcome can be explained by a preferred conformation of the benzylic carbenium ion in the substitution step. The best selectivities were obtained with the *tert*-butylamide. Subsequent *O*-methylation provided the methoxy derivative **31**, converted into the *N*-Boc-protected amino acid **32** under standard conditions.



**Scheme 7.** Synthesis of protected  $\beta$ -methoxy phenylalanine **32** (building block ④).

Finally, the unsaturated amino acid ⑦ was obtained via an asymmetric chelate enolate Claisen rearrangement, developed by Kazmaier et al. (Scheme 8) [54,55]. Trifluoroacetyl (TFA)-protected glycine crotyl ester **33** was deprotonated and converted into a chelated aluminum ester enolate, which in the presence of quinidine underwent a [3,3]-sigmatropic rearrangement to unsaturated amino acid **34** with good yield and enantioselectivity. Epimerization of the  $\alpha$ -stereogenic center was avoided by first converting **34** into the Boc-protected ester **35** and then, in a second step, into the corresponding phthaloyl-protected derivative **36**. A direct epimerization-free conversion (**34** to **36**) was not possible. Ozonolysis of the

double bond and subsequent Wittig reaction produced protected amino acid **37**, finally converted into the Fmoc-protected acid **38**.

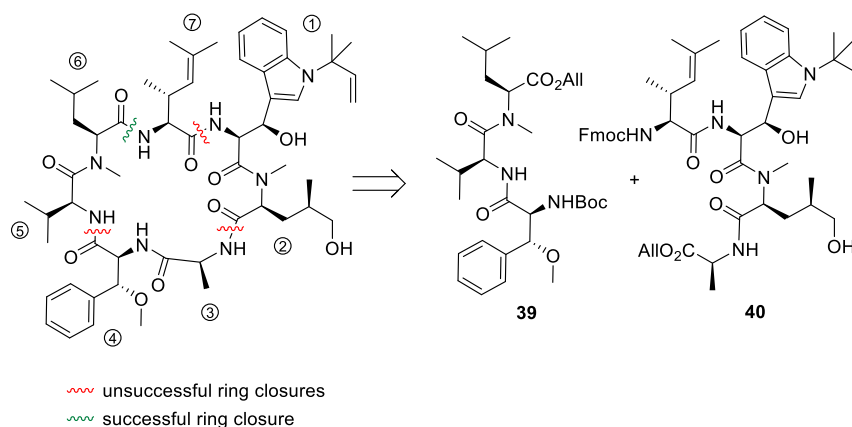


**Scheme 8.** Synthesis of protected dehydroamino acid **38** (building block **7**).

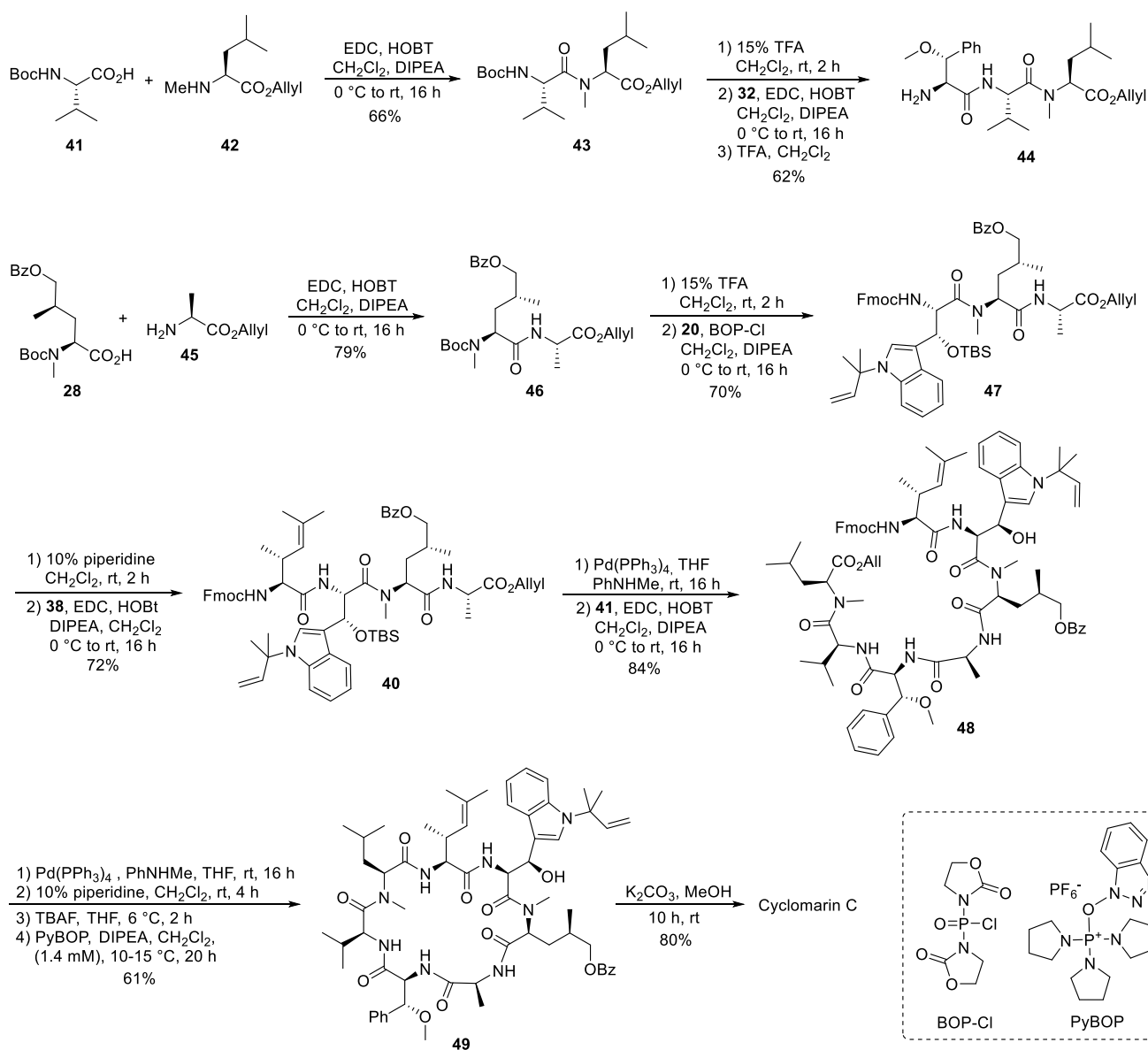
After the desired building blocks were created, the synthesis of cyclomarin C and especially the best position for macrocyclization was investigated (Scheme 9) [47,56]. An attempt to align the synthesis to the biosynthetic pathway and to cyclize the linear heptapeptide precursor between the unusual tryptophan **1** and the unsaturated amino acid **7** failed. Although obtaining the linear peptide in a [3+3+1] peptide fragment coupling strategy was straightforward, the final deprotection and ring closure yielded only trace amounts of the desired product. The same was true for attempts to cyclize the linear heptapeptide between the methoxyphenylalanine **4** and valine **5**. The trial to cyclize between the sterically less demanding hydroxyleucine **2** and alanine **3** failed early in the synthesis stage. All attempts to prolong the **1**,**2** dipeptide at the *N*-terminus failed. Under the basic conditions for Fmoc-deprotection, spontaneous cyclization to the corresponding diketopiperazine occurred, comparable to the previously discussed biosynthetic side reaction, which resulted in the formation of the cyclomarazines. The ultimately successful route was the cyclization between the unsaturated amino acid **7** and the *C*-terminal *N*-methylleucine **6**. The linear heptapeptide was obtained via a [4+3]-coupling strategy. An allyl ester was used as the *C*-terminal protecting group to avoid the basic reaction conditions required for the saponification of the *C*-terminal ester, which caused problems in previous cyclization attempts.

The desired tri- and tetrapeptide **39** and **40** were synthesized using classical peptide coupling reactions and a combination of Boc- and Fmoc-protecting groups (Scheme 10). Because of the acid lability of  $\beta$ -hydroxytryptophan, Fmoc had to be used after incorporating this building block into the growing peptide chain. The synthesis of the peptide fragments was straightforward. An adequate yield of the tripeptide **39** was obtained from *N*-Boc-valine **41** and *N*-methylleucine allyl ester **42**. Boc-cleavage and coupling with methoxyphenylalanine **32** produced **39**, which was also *N*-deprotected to tripeptide **44**.





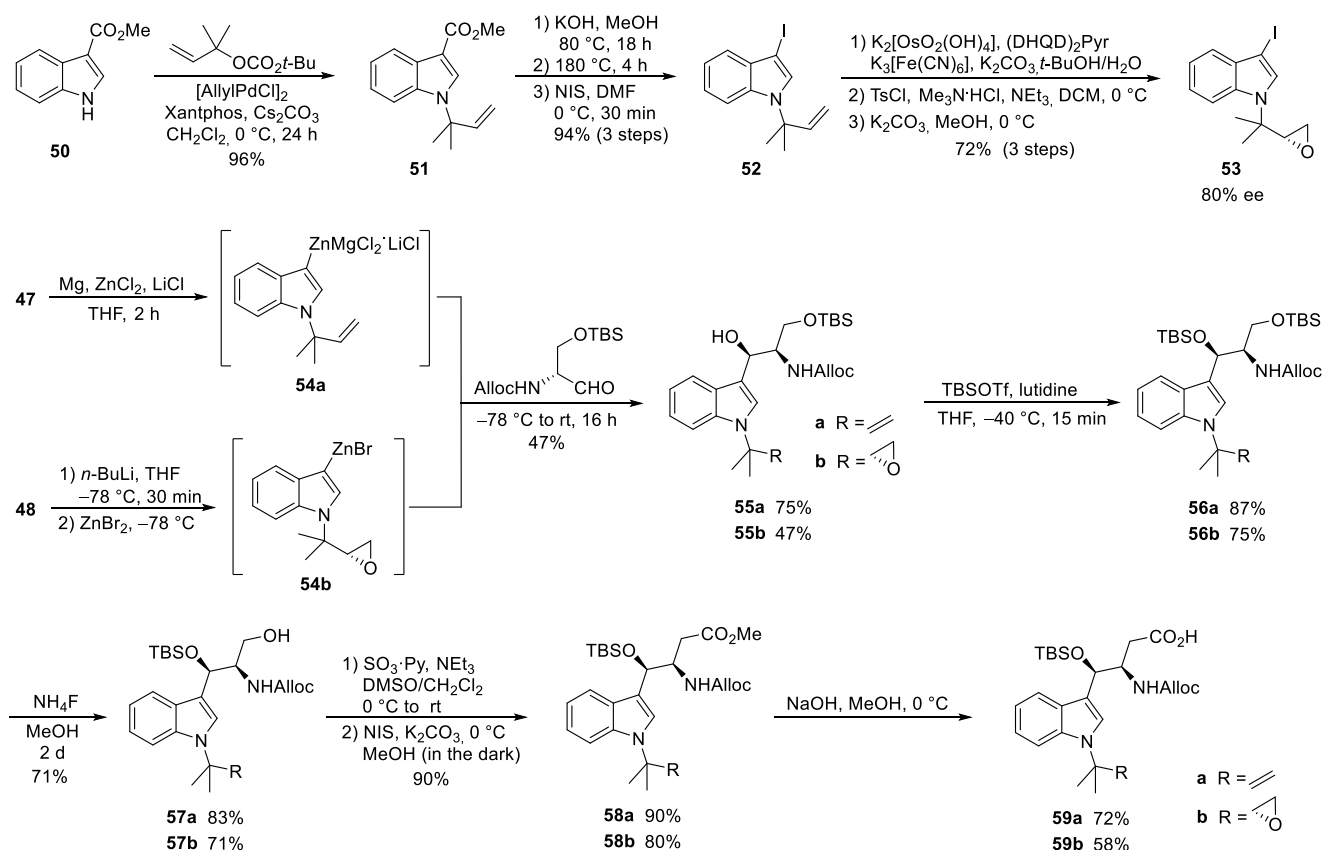
Scheme 9. Cyclization attempts for cyclomarín C [56].



Scheme 10. Synthesis of cyclomarín C.

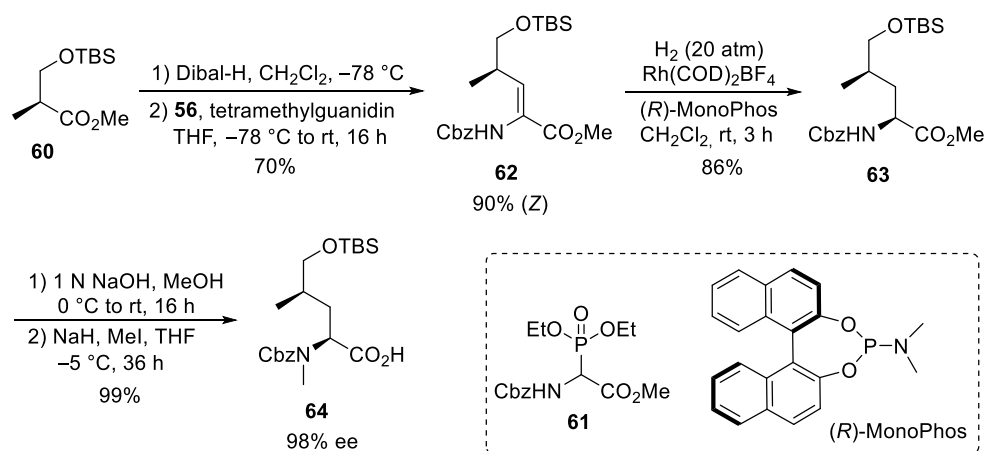
The synthesis of the tetrapeptide started with the coupling of protected  $\delta$ -hydroxy-leucine **28** with alanine allyl ester **45**. After *N*-deprotection, the Fmoc-protected tryptophan **20** was coupled using Bop-Cl/DIPEA [57]. Careful removal of the Fmoc-protecting group from **47** and EDC/HOBT-coupling with the unsaturated building block **38** provided tetrapeptide **40**. Finally, the C-terminal allyl ester was cleaved under mild Pd-catalyzed conditions, and the two peptide fragments were ready for the fragment coupling. An excellent yield of **48** was obtained using EDC/HOAt, which proved more suitable than HOBT. Subsequent deprotection of the C- and the N-terminus and removal of the OTBS-protecting group from the hydroxytryptophan provided the linear peptide precursor, which could be cyclized to **49** using PyBOP [58] under high dilution conditions and providing good yields. Finally, the benzoyl group had to be removed from the hydroxy-leucine and cyclomarin C was purified via preparative HPLC.

The second synthesis of cyclomarin C and the first for cyclomarin A were reported in 2016 by Barbie and Kazmaier [59]. Both natural products differ only in the oxidation state of the prenylated  $\beta$ -hydroxytryptophan unit ①, which is epoxidized in cyclomarin A. Therefore, a synthetic protocol was developed which gave access to both tryptophan derivatives (Scheme 11). The synthesis started with a relatively new method for regioselective *tert*-prenylation of electron-demanding indoles [60]. Using indole ester **50**, a palladium-catalyzed protocol delivered the required product **51** in almost quantitative yield. At 0 °C, no competitive *n*-prenylation was observed. In the next step, the activating ester functionality needed to be replaced by iodine. Saponification of the ester and heating the neat acid to 180 °C resulted in a clean decarboxylation to the *N*-prenylated indole, which could be iodinated in almost quantitative yield. Iodide **52** was used as a key building block for the synthesis of cyclomarin C, and after epoxidation, cyclomarin A. According to Yokohama et al. [61], **52** was subjected to a Sharpless dihydroxylation, which unfortunately demonstrated only moderate stereoselectivity. The best results were obtained with (DHQD)<sub>2</sub>Pyr as chiral ligand, but the ee did not exceed 80 % [62]. Subsequent tosylation of the primary OH-group and treatment with a base provided a good yield of the desired epoxide **53**. The iodides **52** and **53** were next converted into organometallic reagents and reacted with a protected serinal. While the corresponding Grignard reagents provided only moderate yields and selectivities, zinc reagents were found to be superior. According to Knochel et al. [63,64], **52** was presumably converted into the indole-zinc-magnesium complex **54a**, which was reacted with freshly prepared protected serinal to give the desired *syn*-configured **55a** as a single diastereomer. In the case of the epoxyindole **53**, a slightly different protocol was used. To avoid side reactions during the metalation step, **53** was lithiated at -78 °C with *n*-BuLi and transmetalated with ZnBr<sub>2</sub> [63,64]. The zinc reagent **54b** was directly reacted with the aldehyde to create **55b**. According to NMR and HPLC, only two diastereomers (ratio 9:1) could be detected following the Sharpless dihydroxylation step. Obviously, the carbonyl addition also here was highly stereoselective. Next, the secondary OH-functionality was TBS-protected under the assumption that a primary OTBS-group could be removed selectively [65]. Notably, only a combination of TBSOTf and lutidine gave the desired product **56a** in high yield, while all other methods failed and resulted in the decomposition of **55a**. Interestingly, no complete conversion was obtained for **55b**, but the silyl ether **56b** was obtained as a single stereoisomer. Obviously, the undesirable diastereomer did not undergo silylation. Next, the primary silyl protecting group was removed using NH<sub>4</sub>F in MeOH [66]. The free alcohols **57** had to be oxidized to the desired carboxylic acids **59**, which were found to be highly sensitive and not very stable. By far, the best results were obtained using a two-step protocol beginning with a Parikh-Doering oxidation [67]. The also very labile aldehydes were directly oxidized to the corresponding methyl esters **58** with *N*-iodosuccinimide in MeOH [68]. These are stable, can be stored under standard refrigeration, and should be saponified to the free acids **59** on demand.



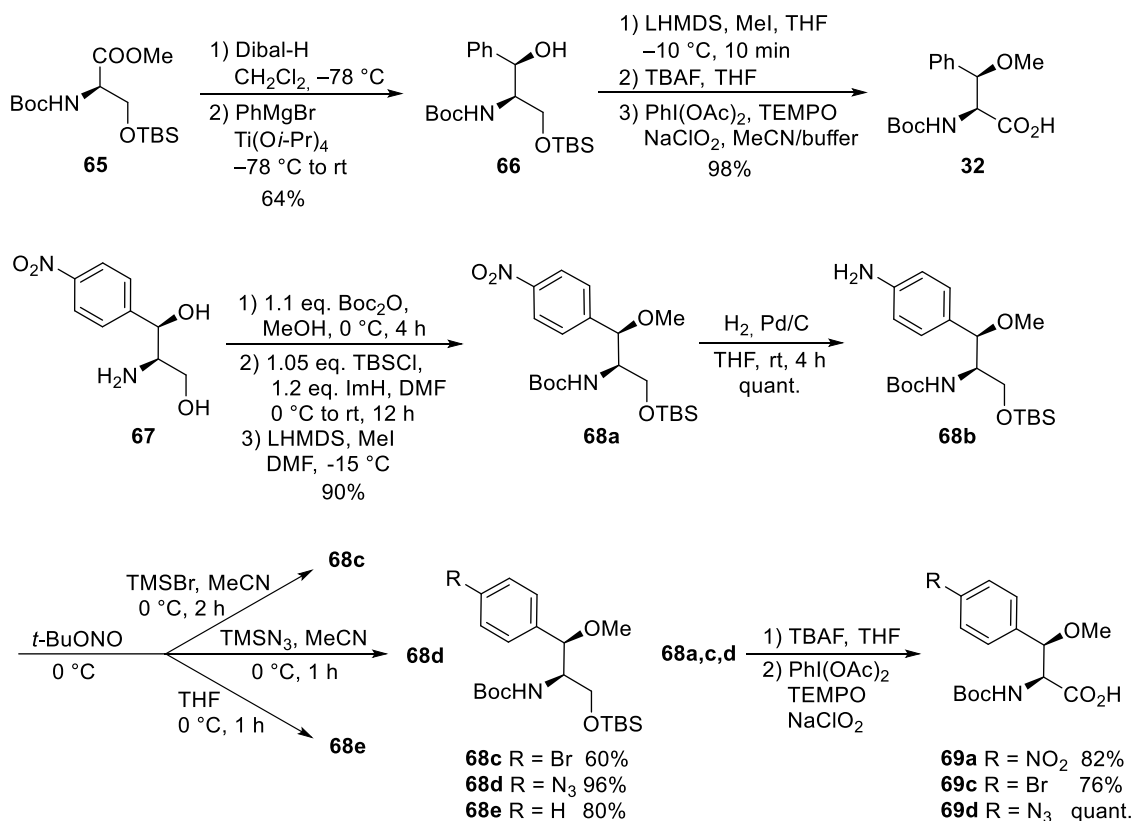
Scheme 11. Synthesis of tryptophan derivative 59 (building block ①).

A straightforward protocol was developed for the protected  $\delta$ -hydroxy-leucine<sup>②</sup>, starting with the commercially available (*S*)-Roche ester, which was *O*-silylated to **60** (Scheme 12). Subsequent Dibal-H reduction provided the corresponding aldehyde, which was subjected to a Horner–Wadsworth–Emmons reaction using Schmidt’s phosphonoglycinate **61** [69]. The unsaturated amino acid **62** obtained was subjected to asymmetric hydrogenation [70] using (*R*)-MonoPhos as a chiral ligand [71,72]. Subsequent saponification of **63** and *N*-methylation yielded the desired building block **64**.

Scheme 12. Synthesis of  $\delta$ -hydroxy-leucine derivative 59 (building block ②).

The third unusual amino acid,  $\beta$ -methoxyphenylalanine<sup>④</sup>, could be obtained similarly to the tryptophan building block ① (Scheme 13). Protected (*R*)-serine **65** was reduced

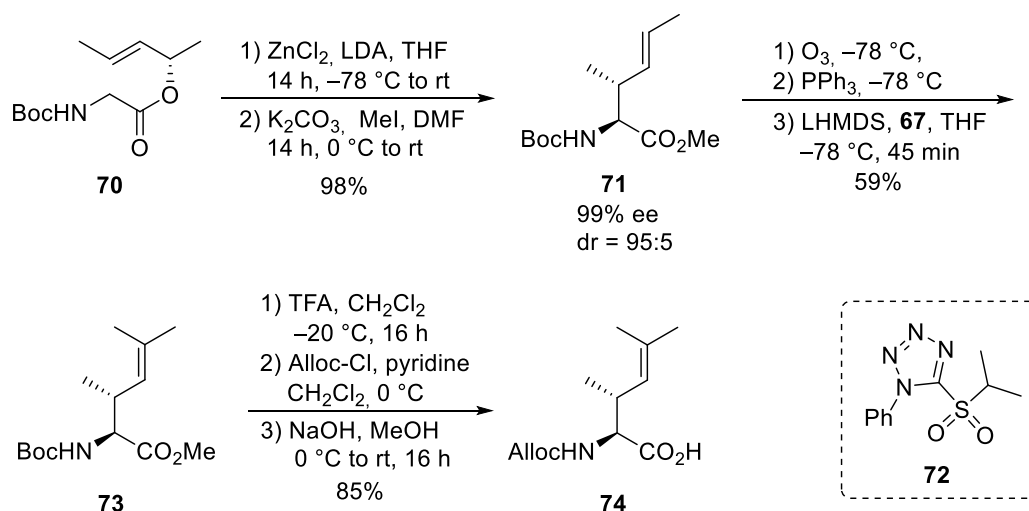
to the corresponding aldehyde, which was subjected to a chelate-controlled aryl-metal addition. The addition of phenylmagnesium bromide provided an acceptable yield but only moderate diastereoselectivity (7:3). In contrast, in the presence of titanium salts, the desired coupling product **66** could be obtained as a single diastereomer in enantiomerically pure form. Further standard transformations yielded building block **32**.



**Scheme 13.** Synthesis of  $\beta$ -methoxyphenylalanine derivatives (building block **4**).

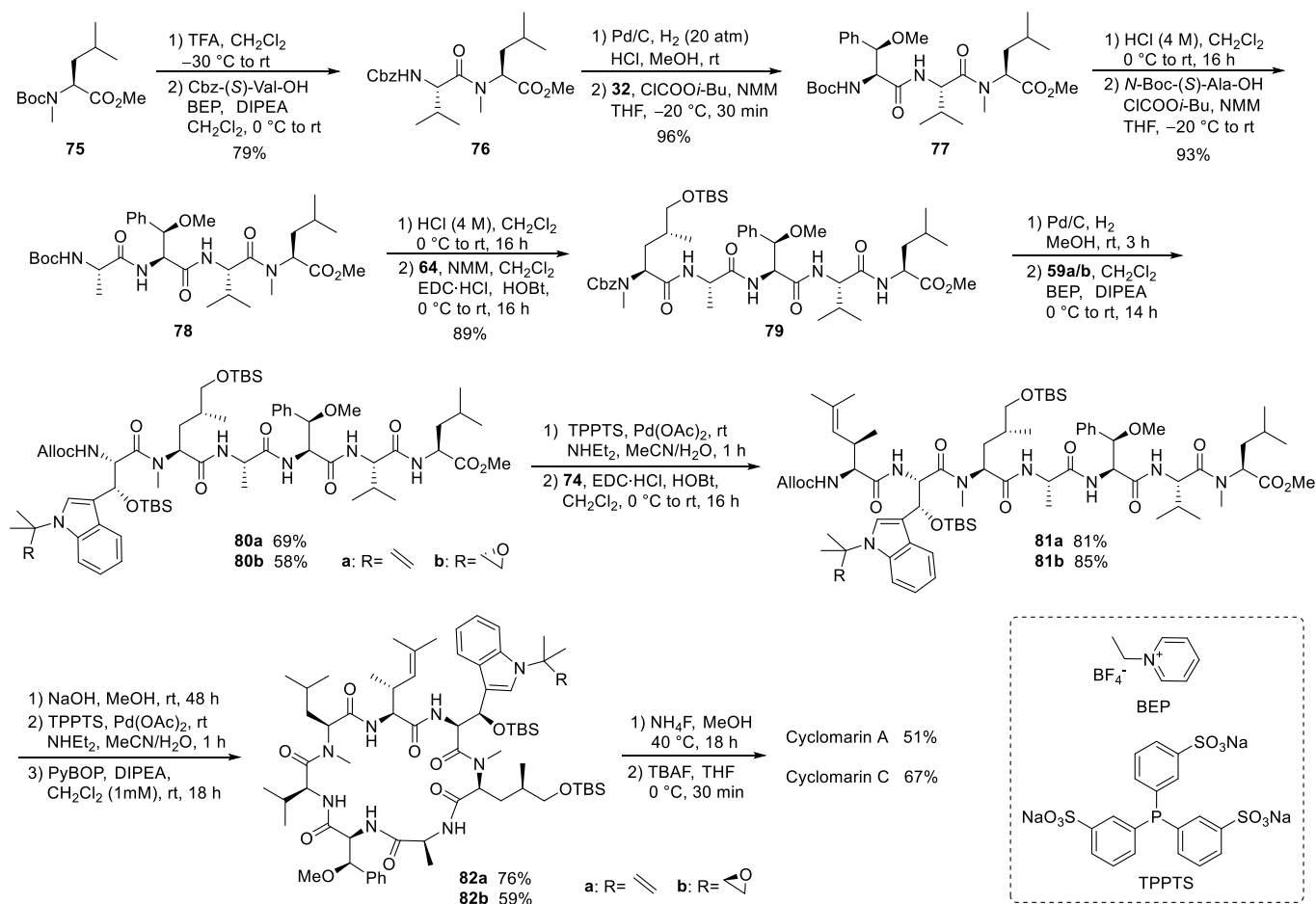
An alternative protocol, which also permitted the synthesis of substituted building blocks, was developed starting from commercially available chloramphenicol base **67** (Scheme 13) [73]. Thus, the amino diol was first converted stepwise into the protected derivative **68a**. The nitro functionality could easily be reduced to the corresponding aniline derivative **68b**, an ideal candidate for further structural variations via diazonium chemistry. Depending on the reaction conditions and additives used, several new derivatives **68c-e** could be obtained, which could be oxidized to the corresponding amino acids **69a-d**, while deamination of **68b** provided the unsubstituted building block **32**.

For the synthesis of the fourth, the unsaturated amino acid **7**, also a chelate enolate Claisen rearrangement, was used starting with chiral ester **70** (Scheme 14) [74–76]. Rearrangement of the corresponding zinc enolate proceeded with complete chirality transfer and high stereoselectivity, and ester **71** was obtained after *O*-methylation. Ozonolysis provided the desired aldehyde, which was subjected to a Wittig reaction. However, only tiny amounts of the desired product could be obtained, even with a large excess of the Wittig reagents, which also caused the chiral aldehyde's epimerization. Better results were obtained with a modified Julia–Kocienski reagent **72**, normally used for (*E*)-selective olefination [77]. Under these conditions, the desired unsaturated building block **73** could be obtained almost epimerization-free. Saponification and change in the *N*-protecting group provided amino acid **74**.



Scheme 14. Synthesis of unsaturated amino acid 69 (building block 7).

With all required building blocks synthesized, the linear synthesis of cyclomarins A and C started with protected *N*-methylleucine **75** (6) to cyclize the linear heptapeptide at the same position as achieved by Yao et al. (Scheme 15) [47,56]. The linear strategy was chosen to avoid epimerizations during fragment couplings, and three of the unusual building blocks were incorporated at the end of the synthesis, also allowing for modification of these building blocks and to obtain derivatives for structure-activity relationship (SAR) studies.



Scheme 15. Syntheses of cyclomarins A and C.

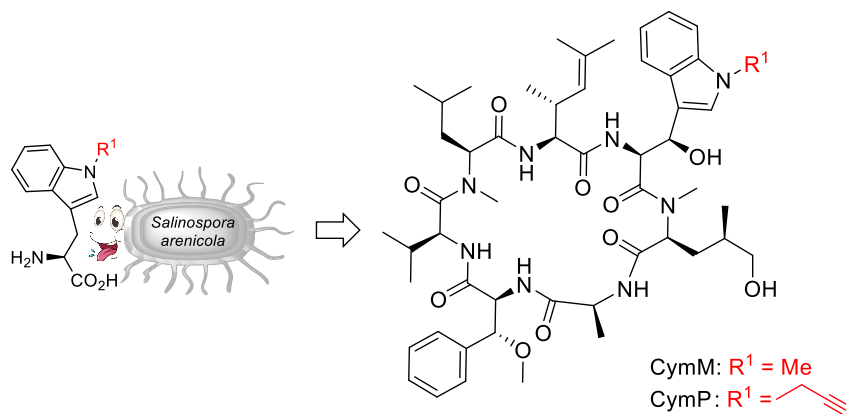
The hydrogenolysis of the Cbz-protecting group in dipeptide **76** was not a trivial task. The reaction required an H<sub>2</sub> pressure of 20 bar to proceed, and two equivalents of HCl had to be added to avoid diketopiperazine formation. The hydrochloride salt was directly coupled with the activated amino acid **32** in the presence of excess base. The next steps were standard peptide couplings. BEP [78,79] was used to incorporate the sensitive tryptophan building blocks **59**. The Alloc protecting group was removed, Pd-catalyzed, and the linear heptapeptide was cyclized using Yao's protocol [47,56]. Finally, a two-step protocol was needed to remove the two OTBS protecting groups separately, providing good yields of cyclomarins A and C. Notably, cyclomarin D (desmethylcyclomarin C), missing only the *N*-methyl group of the  $\delta$ -hydroxyleucin, was also obtained by this protocol [80].

## 5. Syntheses of Cyclomarin Derivatives

Given the outstanding biological properties of the cyclomarins, it is not surprising that multiple investigations have been undertaken to obtain modified cyclomarins for SAR studies.

### 5.1. Mutasyntheses of Cyclomarin Derivatives

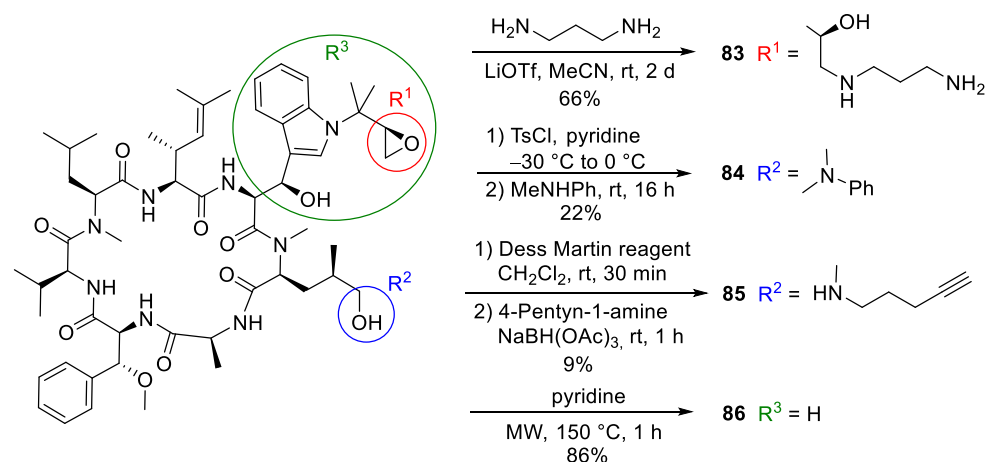
In studies of cyclomarin biosynthesis, Moore et al. identified an *N*-prenyltransferase to prenylate tryptophan prior to loading the modified amino acid onto the NRPS [35]. A knockout mutant of *Salinospora arenicola* CNS-205 with a disrupted prenyltransferase gene failed to produce cyclomarins but did produce desprenylcyclomarin C, although at a 100-fold lower production rate. Obviously, tryptophan is not a good substrate for the cyclomarin NRPS, but other *N*-alkylated tryptophans are well accepted [34]. These can be obtained by simple alkylation of suitably protected tryptophan derivatives [81]. Feeding the bacteria with methylated and propargylated tryptophan resulted in the production of new cyclomarin derivatives CymM and CymP (Scheme 16).



**Scheme 16.** Synthesis of cyclomarin derivatives via mutasyntheses.

### 5.2. Semisyntheses of Cyclomarin Derivatives

Researchers at Novartis observed that cyclomarin A might be a good candidate for drug development since it kills not only *Mycobacterium tuberculosis* (Mtb) but also the malaria parasite *Plasmodium falciparum* [82]. Thus, cyclomarin A is a rare example of a natural product with two distinct and specific modes of action. The researchers modified cyclomarin A, obtained by fermentation (Scheme 17) [83]. Ring-opening of the prenylepoxide with 1,3-propanediamine provided amine **83**, which was linked to sepharose beads and processed by affinity chromatography to identify the target. Interestingly, **83** inhibits the growth of Mtb similarly to cyclomarin A [83,84]. Obviously, the epoxide of the *N*-prenyl side chain is not responsible for the biological activity, at least against Mtb. In contrast, replacing the terminal OH-group of the  $\delta$ -hydroxyleucin **2** by an *N*-methylanilin (**84**) caused a significant drop (>200 fold) in activity [83].



**Scheme 17.** Synthesis of cyclomarins derivatives via semisyntheses.

Notably, the amine **77**, which was very active against Mtb, demonstrated little activity against *Plasmodium falciparum*. Therefore, the Novartis researchers also synthesized acetylenic amine **85** for target fishing [82]. This compound was almost as active as cyclomarin A in biochemical assays toward the biological target PfAp3Aase. As an inactive control, a “minimized” cyclomarins **86** with a missing tryptophan side chain was used. This compound was obtained by retro aldol reaction.

### 5.3. Total Synthesis of Cyclomarin Derivatives

Retro aldol reaction of the  $\beta$ -hydroxytryptophan seems to be a serious stability issue, also during synthesis. This building block undergoes the discussed side reaction proceeding under slightly basic conditions. Under acidic conditions, water is rapidly eliminated, resulting in the formation of the  $\alpha,\beta$ -unsaturated dehydrotryptophan derivative. To avoid these problems, Kazmaier et al. synthesized a series of cyclomarins derivatives containing non-hydroxylated tryptophans (desoxycyclomarins), e.g., the building blocks found in ilamycins/rufomycin [85,86]. *N*-Isopropyltryptophan was obtained via Negishi coupling of 3-iodo-*N*-isopropylindole with protected zincated iodoalanine [86]. Other derivatives can be obtained by an improved protocol for tryptophan alkylations [81]. Several modifications have also been made on the  $\beta$ -methoxyphenylalanine unit **4** [73]. Other derivatives were synthesized utilizing further modifications on building blocks **2** and **7** (Figure 4).

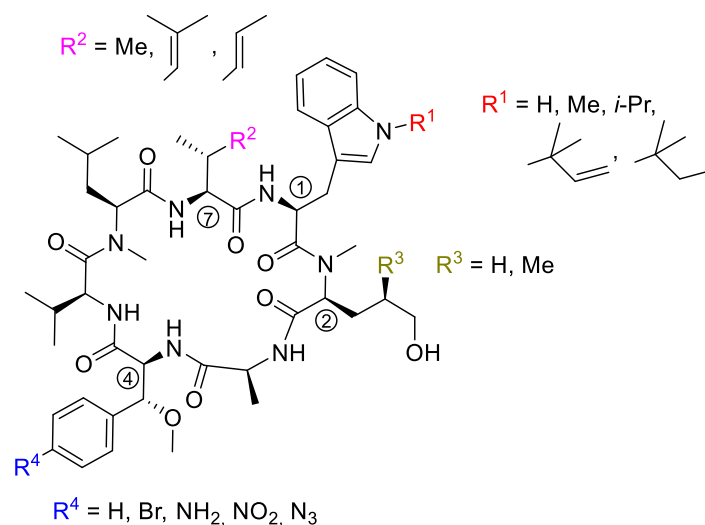


**Figure 4.** Desoxycyclomarins obtained by total syntheses.

## 6. Biological Activities and Mode of Action

### 6.1. Biological Activities of Ilamycins/Rufomycins

Both the ilamycins [14,15] and rufomycins [16,17] were isolated independently from *Streptomyces* in 1962 as new antibiotics, active against acid-fast bacteria, especially *Mycobacterium*. Ilamycin A was reported to inhibit *Mycobacterium* 607 at 0.5 µg/mL, while ilamycin B was less active (3 µg/mL). The rufomycins were reported to be highly active against *Mycobacterium smegmatis* (RufA: 0.2 µg/mL, RufB: 0.5 µg/mL) and *Mycobacterium tuberculosis* (RufA: 0.1–0.4 µg/mL, RufB: 1–5 µg/mL), also strains resistant to other antibiotics such as streptomycin (SM), neomycin (NM), kanamycin (KM), and isonicotinic acid hydrazide (INHA). The compounds are almost inactive against other Gram-positive and Gram-negative bacteria, fungi, and yeasts. In addition, no significant toxicity was observed on four-week-old mice by intraperitoneal injection (Ruf A, LD<sub>0</sub> 200 mg/kg and LD<sub>100</sub> 360 mg/kg) [16].

Ma and Ju et al. recently isolated 12 new ilamycin analogs (IIaG–R) from a 200 L scale culture of mutant *Streptomyces atratus* ZH16 ΔIlaR. The analogs demonstrated a slightly different oxidation pattern compared to the previously isolated ilamycins [27,28]. Most derivatives showed the same antibacterial activity as the other ilamycins and rufomycins with MIC's in the range of 1–2 µM against *Mycobacterium tuberculosis*, while the most active examples thus far have been ilamycin E and J (Figure 5), both more active than rifampicin used as a positive control.

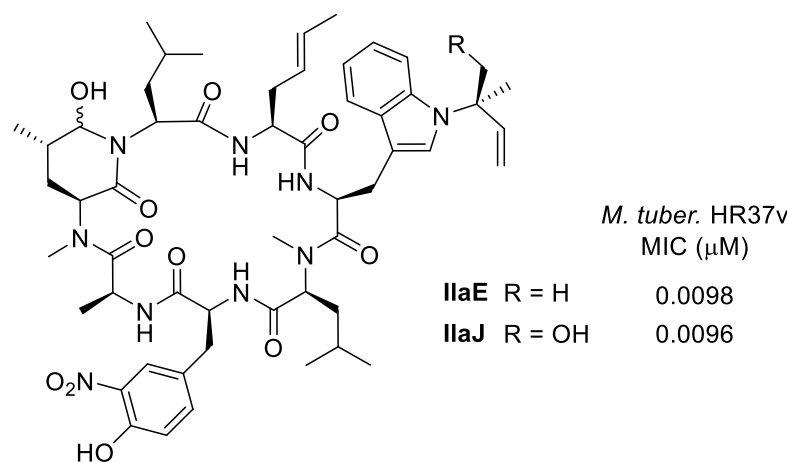


**Figure 5.** Most active ilamycins.

Based on the bioassay data, some structure-activity relationships became evident. Cyclized compounds such as IIaE and IIaJ demonstrated greater activity than open-chain leucine derivatives such as IIaB, IIaD, or IIaF (Figure 1). Oxidation of the prenyl side chain did not affect activity. The nitro group on the tyrosine seems to play an important role [27,28].

In 2020, Pauli et al. isolated eight new rufomycins (rufNBZ1–NBZ8) together with five already known derivatives from the *Streptomyces atratus* strain MJM3502 [29]. Analogous to the ilamycins, the most active derivatives contain a cyclic oxidized leucine such as RufNBZ8 or the previously isolated Ruf I (Figure 6) with an MIC (*M. tuber.* HR37v) similar to rifampicin (0.03 µM). Ruf I maintained activity against mono-resistant, MDR, and XDR strains, indicating that the Rufs most likely have a different molecular target than current drugs used in TB therapy. Additionally, Ruf I retained its activity against strains from the five global *M. tuberculosis* clades representative of clinical TB disease worldwide [87]. Especially interesting is its activity against *M. abscessus*, one of the more difficult-to-treat mycobacteria [88].



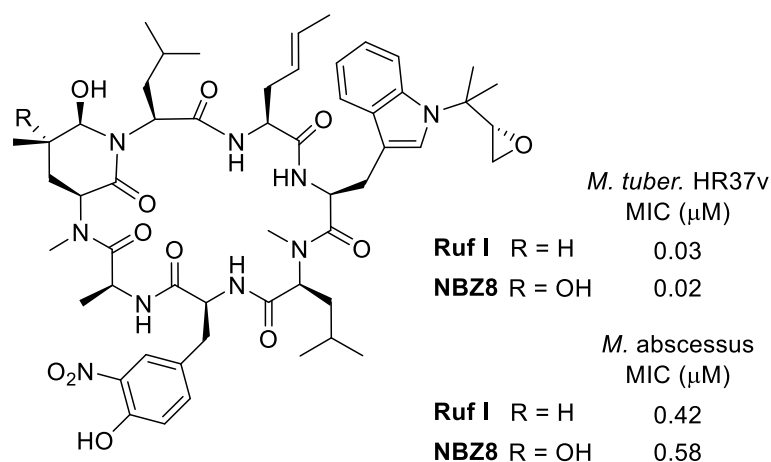


**Figure 6.** Most active rufomycins.

Detailed studies indicated that the ilamycins/rufomycins inhibit ClpC1, an enzyme currently not targeted for TB treatment. ClpC1 is the ATP-dependent homolog of the ClpC class of chaperone proteins present in *M. tuberculosis* [89] and is highly conserved among mycobacteria. Unlike in many other bacteria, ClpC proteins are essential for the viability of mycobacteria, especially *M. tuberculosis*. In this species, the strictly regulated ClpC1 associates with the proteolytic domains, ClpP1 and ClpP2, and together they are responsible for waste protein degradation within the cell [90]. Without functional ClpC1, cellular protein degradation is reduced or stopped completely. Ruf I significantly decreases the proteolytic capabilities of the ClpC1/P1/P2 complex while having no significant effect on the ATPase activity of ClpC1 [87]. In this respect, it differs from ecumicin (Ecu), another anti-tubercular cyclic peptide, which inhibits ClpC1 but stimulates ATPase activity. Details of the binding topology and chemical mode of (inter)action of these cyclopeptides were reported by Cho et al. [91]. The X-ray structure of a complex of the N-terminal helical domain (NTD) of ClpC1 and Ruf I reveals distinct differences from the corresponding ClpC1-NTD-cyclomarin A structure. Surprisingly, the complex structure shows that the epoxide moiety of Ruf I is opened and covalently bound to ClpC1-NTD via the sulfur atom of a methionine in the binding pocket [92,93].

Although the anti-tubercular activity is the most prominent effect of ilamycins/rufomycins, certain derivatives show some anti-cancer activities, while others do not. IlaC (Ruf I) was found to be preferentially cytotoxic towards triple-negative breast cancer (TNBC) cell lines, the most aggressive subtype of breast cancer with poor prognoses. IlaC can induce Bax/Bcl-2-related caspase-dependent apoptosis and inhibit migration and invasion in TNBC by suppressing IL-6-induced STAT3 phosphorylation [94]. IlaE, but not IlaF, decreases cell viability, inhibits G1/S cell cycle progression, and promotes apoptosis in the TNBC cell lines HCC1937 (IC<sub>50</sub> 14.2 μM) and MDA-MB-468 (IC<sub>50</sub> 24.5 μM). It promotes apoptosis via activation of endoplasmic reticulum (ER) stress, increasing CHOP expression and down-regulating the expression of anti-apoptotic protein Bcl-2 [94].

### 6.2. Biological Activities of Cyclomarins

Fenical and Clardy et al., who isolated the cyclomarins A–C in 1999, reported that the major metabolite cyclomarin A (CymA) showed anti-inflammatory activity in vivo and in vitro [30]. Lateron, Pittayakhajonwut et al. reported that CymC shows anti-malarial activity against multidrug-resistant *Plasmodium falciparum* strains (IC<sub>50</sub> 0.25 μM) as well as anti-TB activity (MIC: 0.1 μM) [95]. No significant activity was observed against cancer cells or *Candida albicans* (IC<sub>50</sub> > 50 μM). Schmitt et al. at Novartis investigated the mode of action in detail [83]. CymA was found to bind specifically and with a high affinity to ClpC1 and did not interfere with ATP binding by the two ATPase domains of ClpC1. The antimycobacterial activity of cyclomarin derivatives correlates well with binding to ClpC1.

For example, amino alcohol **83** (Scheme 17) demonstrated high affinity (MIC: 0.1  $\mu\text{M}$ ), while no binding was observed for the inactive amine **84**. The hydroxy functionality on leucine ② is clearly important for binding, but not the epoxide.

The exact binding of CymA toward the NTD of ClpC1 was determined by high-resolution co-crystal structure analysis [84]. The overall sequence identity of ClpC1 from various *Mycobacterium* species is close to 95%, but the NTD of mycobacterial ClpC1 is 100% conserved. This phenomenon explains why all tested mycobacteria were found to be sensitive to CymA. Based on the structure of the complex, several mutations were engineered into ClpC1, which showed reduced CymA binding in vitro. The ClpC1 mutants were overexpressed in mycobacteria and two showed resistance to CymA, providing clear evidence that ClpC1 is the target of CymA.

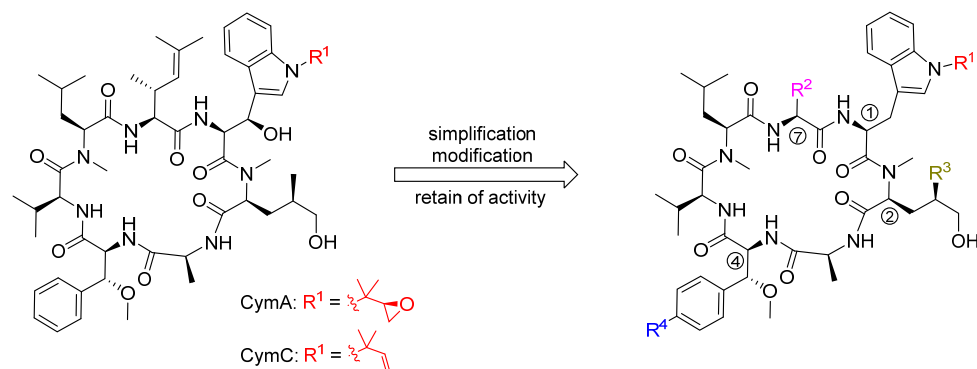
Using NMR and small-angle X-ray scattering, Schanda and Fraga et al. demonstrated that arginine-phosphate binding to the ClpC1 NTD induces millisecond dynamics [96]. Cyclomarin binding to this domain specifically blocks these dynamics. Based on these results, a proposed mechanism of action involves the cyclomarin-induced restriction of ClpC1 dynamics, which modulates the chaperone enzymatic activity leading eventually to cell death [96]. Very recently, Mogk et al. showed that CymA activates an ATP-driven bacterial AAA+ protease (e.g., ClpP) and that cell death is induced by uncontrolled proteolytic activity of these enzymes [97].

However, anti-TB activity is not the only interesting feature of the cyclomarins. Schmitt et al. showed that CymA is a potent growth inhibitor of *Plasmodium falciparum*, and its molecular target, diadenosine triphosphate hydrolase (PfAp3Aase), was identified by chemical proteomics [82]. CymA is a specific inhibitor of the plasmodial enzyme (IC<sub>50</sub>: 0.004  $\mu\text{M}$ ) but not of the closest human homolog hFHIT (IC<sub>50</sub> > 10  $\mu\text{M}$ ). Co-crystallization experiments demonstrated a unique inhibitor binding mode. One molecule of CymA binds a dimeric PfAp3Aase and prevents the formation of the enzyme-substrate complex. These results validate PfAp3Aase as a new drug target for the treatment of malaria. Thus, CymA is a rare example of a natural product with two distinct and specific modes of action.

Unfortunately, CymA as a natural product lacks satisfactory pharmacokinetic properties, making it challenging for optimization into an (orally) bioavailable drug. Therefore, Kazmaier et al. tried to simplify the complex structure of the cyclomarins without losing significant biological activity. Because the  $\beta$ -hydroxytryptophan unit ① is the most critical building block, they removed the hydroxy functionality completely, and the desoxycyclomarins obtained were further modified on the prenyl side chain of ①, the hydroxylated leucine ②, the  $\beta$ -methoxyphenylalanine ④ and the unsaturated amino acid ⑦ [37,73,85,86]. Selected biological data are summarized in Table 1.

Certain modifications at R<sup>1</sup> were well-tolerated (series **87**). Reduction to an isopropyl group (**87c**) provides an especially promising simplification retaining antimycobacterial activity. In general, manipulations at this position do not result in dramatic effects on potency measured against *Mtb* and *Pfalcp*. Interestingly, the methyl group in **87d** is an appropriate balance between reducing synthetic complexity and loss of activity.

Results obtained for the modifications at R<sup>2</sup> were consistent with the data obtained by X-ray structure analysis [82]. In the case of *Pfalcp*, where this residue is completely buried between the target and the ligand scaffold, large changes are not accepted. However, it is important that removing the terminal methyl group in the *cis* position of the  $\gamma,\delta$ -unsaturated side chain led to an equivalent or even slightly improved activity. Further simplifications, however, are not advisable, as they lead to dramatic activity losses, which are seen in the comparison of **87a** and **88a**. In contrast, the anti-TB activity was not influenced.

**Table 1.** Biological data of cyclomarins and selected desoxycyclomarins.

Compound	R <sup>1</sup>	R <sup>2</sup>	R <sup>3</sup>	R <sup>4</sup>	Mtb		Pfalcp	
					wt Erdman MIC[μM]	3D7 IC <sub>50</sub> [nM]	Dd2 IC <sub>50</sub> [nM]	
Isoniazid					0.9			
CQ						3.4	233.9	
Cyclomarin A			Me	H	0.125	36.8	27.7	
Cyclomarin C			Me	H	0.25	42.8		
Desoxycyclomarin C			Me	H	0.9	39.8		
87a			Me	H	0.5	9.0	12.9	
87b			Me	H	1.7	4.4	6.5	
87c	<i>i</i> Pr		Me	H	0.4	47.8	76.0	
87d	Me		Me	H	0.9	13.4	17.8	
87e	H		Me	H	1.5	28.1	27.5	
88a	<i>i</i> Pr		Me	H	0.4	355.7	300.3	
88b	Me		Me	H	1.6	230.3	256.7	
88c	H		Me	H	0.5	314.2	421.5	
89a			H	H	2.3	47.9	36.7	
89b	<i>i</i> Pr		H	H	1.8	177.5	287.8	
89c	Me		H	H	3.4	362.4	318.4	
90a			Me	NH <sub>2</sub>	0.25			
90b			Me	N <sub>3</sub>	0.26			
90c			Me	NO <sub>2</sub>	0.13			
90d			Me	Br	4.1			

Removal of the methyl group at R<sup>3</sup> led to a decrease in potency against both pathogens (89). This result was indeed expected for the Mtb target ClpC1-NTD [96]. This group interacts well with the target, which is also closely packed with the indole motif of the tryptophan core. However, it is not yet clear why deletion of this methyl residue impairs activity towards *Pfalcp*.

Modifications of R<sup>4</sup> on  $\beta$ -methoxyphenylalanine (4) were also well tolerated (90). The amino- and azido-derivatives 90a and 90b were equipotent to cyclomarin C, and the nitro compound 90c was even twice as active. Only in the case of bromo derivative 90d was a significant drop in activity observed.

## 7. Conclusions

The ilamycins/rufomycins and the cyclomarins are highly interesting marine cycloheptapeptides characterized by their incorporation of unusual amino acids. The natural products are produced by *Streptomyces* sp. and show potent activity against a range of mycobacteria, including multidrug-resistant strains of *Mycobacterium tuberculosis*. No significant activity has been observed towards other Gram-positive and Gram-negative bacteria or fungi.

The cyclomarins are also very potent inhibitors of *Plasmodium falciparum*, the organism that causes malaria. Biosynthetically, the cyclopeptides are obtained via a heptamodular NRPS that directly incorporates some of the nonproteinogenic amino acids, while oxidations at certain positions allow the compounds to proceed to protein-bound biosynthetic intermediates. Cyclized ilamycins/rufomycins are obtained by oxidative post-NRPS cyclization of leucine (7), the last introduced amino acid in the biosynthesis. A wide range of derivatives can be obtained by fermentation, while bioengineering also allows the mutasynthesis of derivatives, especially cyclomarins. Other derivatives are accessible by semisynthesis or total syntheses, reported for both natural product classes. Some of these derivatives were used to identify the biological targets of these peptides. The anti-TB activity results from the binding of the peptides to the N-terminal domain (NTD) of the protease ClpC1, causing cell death by the uncontrolled proteolytic activity of associated enzymes.

Diadenosine triphosphate hydrolase (PfAp3Aase) was found to be the active target of the cyclomarins in Plasmodia, and this enzyme might be a good candidate for the treatment of malaria. SAR studies of natural and synthetic derivatives on the ilamycins/rufomycins and cyclomarins indicate which parts of the molecules can be simplified/modified without losing activity towards either target.

**Author Contributions:** U.K. and L.J., writing review and editing. All authors have read and agreed to the published version of the manuscript.

**Funding:** This research was funded by Saarland University and received no external funding.

**Data Availability Statement:** Not applicable.

**Conflicts of Interest:** The authors declare no conflict of interest.

## References

1. Carroll, A.R.; Copp, B.R.; Davis, R.A.; Keyzers, R.A.; Prinsep, M.R. Marine natural products. *Nat. Prod. Rep.* **2020**, *37*, 175–223. [[CrossRef](#)]
2. Carroll, A.R.; Copp, B.R.; Davis, R.A.; Keyzers, R.A.; Prinsep, M.R. Marine natural products. *Nat. Prod. Rep.* **2021**, *38*, 362–413. [[CrossRef](#)] [[PubMed](#)]
3. Barreca, M.; Spane, V.; Montalbano, A.; Cueto, M.; Marrero, A.R.D.; Deniz, I.; Erdogan, A.; Bilela, L.L.; Moulin, C.; Taffin-de-Givenchy, E.; et al. Marine Anticancer Agents: An Overview with a Particular Focus on Their Chemical Classes. *Mar. Drugs* **2020**, *18*, 619. [[CrossRef](#)] [[PubMed](#)]
4. McCauley, E.P.; Pina, I.C.; Thompson, A.D.; Bashir, K.; Weinberg, M.; Kurz, S.L.; Crews, P. Highlights of marine natural products having parallel scaffolds found from marine-derived bacteria, sponges, and tunicates. *J. Antibiot.* **2020**, *73*, 504–525. [[CrossRef](#)] [[PubMed](#)]
5. Qamar, H.; Hussain, K.; Soni, A.; Khan, A.; Hussain, T.; Chenais, B. Cyanobacteria as natural therapeutics and pharmaceutical potential: Role in antitumor activity and as nanovectors. *Molecules* **2021**, *26*, 247. [[CrossRef](#)] [[PubMed](#)]

6. Njoroge, M.; Njuguna, N.M.; Mutai, P.; Ongarora, D.S.B.; Smith, P.W.; Chibale, K. Recent approaches to chemical discovery and development against malaria and the neglected tropical diseases human african trypanosomiasis and schistosomiasis. *Chem. Rev.* **2014**, *114*, 11138–11163. [[CrossRef](#)] [[PubMed](#)]
7. WHO. Available online: [https://www.who.int/health-topics/tuberculosis#tab=tab\\_1](https://www.who.int/health-topics/tuberculosis#tab=tab_1) (accessed on 30 July 2021).
8. De Opitz, C.L.M.; Sass, P. Tackling antimicrobial resistance by exploring new mechanisms of antibiotic action. *Future Microbiol.* **2020**, *15*, 703–708. [[CrossRef](#)] [[PubMed](#)]
9. Dooley, K.E.; Park, J.G.; Swindells, S.; Allen, R.; Haas, D.W.; Cramer, Y.; Aweeka, F.; Wiggins, I.; Gupta, A.; Lizak, P.; et al. Safety, tolerability, and pharmacokinetic interactions of the antituberculous agent TMC207 (bedaquiline) with efavirenz in healthy volunteers: AIDS clinical trials group study A5267. *J. Acq. Imm. Def.* **2012**, *59*, 455–462. [[CrossRef](#)] [[PubMed](#)]
10. Zumla, A.; Nahid, P.; Cole, S.T. Advances in the development of new tuberculosis drugs and treatment regimens. *Nat. Rev. Drug Discov.* **2013**, *12*, 388–404. [[CrossRef](#)]
11. Igarashi, M.; Ishizaki, Y.; Takahashi, Y. New antituberculous drugs derived from natural products: Current perspectives and issues in antituberculous drug development. *J. Antibiot.* **2018**, *71*, 15–25. [[CrossRef](#)]
12. Lee, H.; Suh, J.W. Anti-tuberculosis lead molecules from natural products targeting *Mycobacterium tuberculosis* ClpC1. *J. Ind. Microbiol. Biotechnol.* **2016**, *43*, 205–212. [[CrossRef](#)]
13. Newman, D.J.; Cragg, G.M. Natural products as sources of new drugs over the 30 years from 1981 to 2010. *J. Nat. Prod.* **2012**, *75*, 311–335. [[CrossRef](#)] [[PubMed](#)]
14. Nakayama, Y.; Takita, T.; Ozawa, H.; Umezawa, H.; Tahara, K. Studies on ilamycin. *J. Antibiot.* **1962**, *15*, 49–50.
15. Takita, T.; Ohi, K.; Maeda, K.; Okami, Y.; Umezawa, H. New antibiotics, ilamycins. *J. Antibiot.* **1962**, *15*, 46–48.
16. Higashidani, E.; Ueyanagi, J.; Shibata, M.; Nakazawa, K.; Miyake, A.; Iwasaki, H.; Yamamoto, H. Studies on *Streptomyces*. 2. Rufomycin A and A, new antituberculous antibiotics. *Agric. Biol. Chem.* **1962**, *26*, 234–237.
17. Shibata, M.; Yamamoto, H.; Higashidani, E.; Nakazawa, K. Studies on *Streptomyces*. 1. *Streptomyces atratus* nov. sp. producing new antituberculous antibiotics rufomycin A and B. *Agric. Biol. Chem.* **1962**, *26*, 228–233.
18. Cary, L.W.; Takita, T.; Ohnishi, M. Study of secondary structure of ilamycin-B1 by 300 MHz proton magnetic resonance. *FEBS Lett.* **1971**, *17*, 145–148. [[CrossRef](#)]
19. Iitaka, Y.; Nakamura, H.; Takada, K.; Takita, T. X-RAY study of ilamycin B1, a cyclic heptapeptide antibiotic. *Acta Cryst. B* **1974**, *30*, 2817–2825. [[CrossRef](#)]
20. Iwasaki, H.; Witkop, B. New methods for nonenzymatic peptide cleavage. Electrolytic differential + solvolytic cleavage of antibiotic cyclopeptide rufymacin. *J. Am. Chem. Soc.* **1964**, *86*, 4698–4708. [[CrossRef](#)]
21. Takita, T. Amino acid sequence of ilamycin and ilamycin B. *J. Antibiot.* **1963**, *16*, 211–212.
22. Takita, T.; Maeda, K.; Naganawa, H.; Umezawa, H. Structures of ilamycin and ilamycin B2. *J. Antibiot.* **1964**, *17*, 129–131.
23. Takita, T.; Naganawa, H.; Maeda, K.; Umezawa, H. The structural difference among ilamycin, ilamycin C1 and ilamycin C2. *J. Antibiot.* **1965**, *18*, 135–136.
24. Fujino, M.; Kamiya, T.; Miyake, A.; Iwasaki, H.; Ueyanagi, J. Tryptophan moiety of rufomycin homologs. *Chem. Pharm. Bull.* **1964**, *12*, 390–392. [[CrossRef](#)] [[PubMed](#)]
25. Takita, T.; Naganawa, H.; Maeda, K.; Umezawa, H. Further studies on tryptophan parts of ilamycins. *J. Antibiot.* **1964**, *17*, 264–265.
26. Takita, T.; Naganawa, H. L-2-Amino-4-hexenoic acid in ilamycins. *J. Antibiot.* **1963**, *16*, 246.
27. Ma, J.Y.; Huang, H.B.; Xie, Y.C.; Liu, Z.Y.; Zhao, J.; Zhang, C.Y.; Jia, Y.X.; Zhang, Y.; Zhang, H.; Zhang, T.Y.; et al. Biosynthesis of ilamycins featuring unusual building blocks and engineered production of enhanced anti-tuberculosis agents. *Nat. Commun.* **2017**, *8*, 391. [[CrossRef](#)]
28. Sun, C.L.; Liu, Z.Y.; Zhu, X.C.; Fan, Z.Y.; Huang, X.M.; Wu, Q.L.; Zheng, X.H.; Qin, X.J.; Zhang, T.Y.; Zhang, H.; et al. Antitubercular ilamycins from marine-derived *Streptomyces atratus* SCSIO ZH16  $\Delta$  ilaR. *J. Nat. Prod.* **2020**, *83*, 1646–1657. [[CrossRef](#)]
29. Zhou, B.; Shetye, G.; Yu, Y.; Santarsiero, B.D.; Klein, L.L.; Abad-Zapatero, C.; Wolf, N.M.; Cheng, J.; Jin, Y.; Lee, H.; et al. Antimycobacterial rufomycin analogues from *Streptomyces atratus* strain MJM3502. *J. Nat. Prod.* **2020**, *83*, 657–667. [[CrossRef](#)]
30. Renner, M.K.; Shen, Y.C.; Cheng, X.C.; Jensen, P.R.; Frankmoelle, W.; Kauffman, C.A.; Fenical, W.; Lobkovsky, E.; Clardy, J. Cyclomarins A–C, new antiinflammatory cyclic peptides produced by a marine bacterium (*Streptomyces* sp.). *J. Am. Chem. Soc.* **1999**, *121*, 11273–11276. [[CrossRef](#)]
31. Kumamoto, T.; Koshino, H.; Watanabe, D.; Matsumoto, Y.; Aoyama, K.; Harada, K.; Ishikawa, T.; Mikami, Y. M10709, a new peptide antibiotic from clinically isolated *Streptomyces* sp. *Heterocycles* **2010**, *80*, 281–288.
32. Li, L.; MacIntyre, L.W.; Ali, T.; Russo, R.; Koirala, B.; Hernandez, Y.; Brady, S.F. Biosynthetic interrogation of soil metagenomes reveals metamarin, an uncommon cyclomarin congener with activity against *Mycobacterium tuberculosis*. *J. Nat. Prod.* **2021**, *84*, 1056–1066. [[CrossRef](#)]
33. Tomita, H.; Katsuyama, Y.; Minami, H.; Ohnishi, Y. Identification and characterization of a bacterial cytochrome P450 monooxygenase catalyzing the 3-nitration of tyrosine in rufomycin biosynthesis. *J. Biol. Chem.* **2017**, *292*, 15859–15869. [[CrossRef](#)] [[PubMed](#)]
34. Schultz, A.W.; Lewis, C.A.; Luzung, M.R.; Baran, P.S.; Moore, B.S. Functional characterization of the cyclomarin/cyclomarine prenyltransferase CymD directs the biosynthesis of unnatural cyclic peptides. *J. Nat. Prod.* **2010**, *73*, 373–377. [[CrossRef](#)] [[PubMed](#)]

35. Schultz, A.W.; Oh, D.C.; Carney, J.R.; Williamson, R.T.; Udworthy, D.W.; Jensen, P.R.; Gould, S.J.; Fenical, W.; Moore, B.S. Biosynthesis and structures of cyclomarins and cyclomarazines, prenylated cyclic peptides of marine actinobacterial origin. *J. Am. Chem. Soc.* **2008**, *130*, 4507–4516. [[CrossRef](#)] [[PubMed](#)]
36. He, J.Q.; Wei, X.; Yang, Z.J.; Li, Y.; Ju, J.H.; Ma, J.Y. Characterization of regulatory and transporter genes in the biosynthesis of anti-tuberculosis ilamycins and production in a heterologous host. *Mar. Drugs* **2020**, *18*, 216. [[CrossRef](#)]
37. Kiefer, A.; Kazmaier, U. Syntheses of cyclomarins—Interesting marine natural products with distinct mode of action towards malaria and tuberculosis. *Synthesis* **2019**, *51*, 107–121. [[CrossRef](#)]
38. Cheng, Y.Y.; Tang, S.B.; Guo, Y.; Ye, T. Total synthesis of anti-tuberculosis natural products ilamycins E-1 and F. *Org. Lett.* **2018**, *20*, 6166–6169. [[CrossRef](#)]
39. Luzung, M.R.; Lewis, C.A.; Baran, P.S. Direct, chemoselective *N*-*tert*-prenylation of indoles by C-H functionalization. *Angew. Chem. Int. Ed.* **2009**, *48*, 7025–7029. [[CrossRef](#)]
40. Arda, A.; Soengas, R.G.; Nieto, M.I.; Jimenez, C.; Rodriguez, J. Total synthesis of (-)-dysithiazolamide. *Org. Lett.* **2008**, *10*, 2175–2178. [[CrossRef](#)]
41. Hanessian, S.; Margarita, R. 1,3-asymmetric induction in dianionic allylation reactions of amino acid derivatives—synthesis of functionally useful enantiopure glutamates, pipecolates and pyroglutamates. *Tetrahedron Lett.* **1998**, *39*, 5887–5890. [[CrossRef](#)]
42. Padron, J.M.; Kokotos, G.; Martin, T.; Markidis, T.; Gibbons, W.A.; Martin, V.S. Enantiospecific synthesis of alpha-amino acid semialdehydes: A key step for the synthesis of unnatural unsaturated and saturated alpha-amino acids. *Tetrahedron Asymmetry* **1998**, *9*, 3381–3394. [[CrossRef](#)]
43. Schöllkopf, U.; Groth, U.; Deng, C. Asymmetric synthesis via heterocyclic intermediates. 6. Enantioselective synthesis of (*R*)-amino acids using valine as a chiral agent. *Angew. Chem. Int. Ed. Engl.* **1981**, *20*, 798–799. [[CrossRef](#)]
44. Albericio, F.; Cases, M.; Alsina, J.; Triolo, S.A.; Carpino, L.A.; Kates, S.A. On the use of PyAOP, a phosphonium salt derived from HOAt, in solid-phase peptide synthesis. *Tetrahedron Lett.* **1997**, *38*, 4853–4856. [[CrossRef](#)]
45. Chen, S.Q.; Xu, J.C. Pentafluorophenyl diphenylphosphinate—A new efficient coupling reagent in peptide chemistry. *Tetrahedron Lett.* **1991**, *32*, 6711–6714. [[CrossRef](#)]
46. Sathish, K.; Reddy, G.P.K.; Mainkar, P.S.; Chandrasekhar, S. Synthesis of the ‘southern’ tripeptide of Cyclomarins A and C having novel anti-tuberculocidal mode of action. *Tetrahedron Asymmetry* **2011**, *22*, 1568–1573. [[CrossRef](#)]
47. Wen, S.J.; Yao, Z.J. Total synthesis of cyclomarin C. *Org. Lett.* **2004**, *6*, 2721–2724. [[CrossRef](#)]
48. Wen, S.J.; Zhang, H.W.; Yao, Z.J. Synthesis of a fully protected (2*S*,3*R*)-*N*-(1',1'-dimethyl-2'-propenyl)-3-hydroxytryptophan from tryptophan. *Tetrahedron Lett.* **2002**, *43*, 5291–5294. [[CrossRef](#)]
49. Tao, B.; Schlingloff, G.; Sharpless, K.B. Reversal of regioselection in the asymmetric aminohydroxylation of cinnamates. *Tetrahedron Lett.* **1998**, *39*, 2507–2510. [[CrossRef](#)]
50. Barbie, P.; Kazmaier, U. Synthesis of fully protected, reverse *N*-prenylated (2*S*,3*R*)-3-hydroxytryptophan, a unique building block of the cyclomarins. *Org. Biomol. Chem.* **2015**, *13*, 9267–9275. [[CrossRef](#)] [[PubMed](#)]
51. Evans, D.A.; Ripin, D.H.B.; Halstead, D.P.; Campos, K.R. Synthesis and absolute stereochemical assignment of (+)-miyakolide. *J. Am. Chem. Soc.* **1999**, *121*, 6816–6826. [[CrossRef](#)]
52. Easton, C.J.; Hutton, C.A.; Roselt, P.D.; Tiekink, E.R.T. Synthesis and molecular structure of stable derivatives of (*E*)-dehydrophenylalanine and (*Z*)-dehydrophenylalanine. *Aust. J. Chem.* **1991**, *44*, 687–694. [[CrossRef](#)]
53. Easton, C.J.; Hutton, C.A.; Roselt, P.D.; Tiekink, E.R.T. Stereocontrolled synthesis of  $\beta$ -hydroxyphenylalanine and  $\beta$ -hydroxytyrosine derivatives. *Tetrahedron* **1994**, *50*, 7327–7340. [[CrossRef](#)]
54. Kazmaier, U.; Krebs, A. Synthesis of chiral  $\gamma,\delta$ -unsaturated amino acids by asymmetric ester enolate Claisen rearrangement. *Angew. Chem. Int. Ed. Engl.* **1995**, *34*, 2012–2014. [[CrossRef](#)]
55. Kazmaier, U.; Mues, H.; Krebs, A. Asymmetric chelated Claisen rearrangements in the presence of chiral ligands—Scope and limitations. *Chem. Eur. J.* **2002**, *8*, 1850–1855. [[CrossRef](#)]
56. Wen, S.J.; Hu, T.S.; Yao, Z.J. Macrocyclization studies and total synthesis of cyclomarin C, an anti-inflammatory marine cyclopeptide. *Tetrahedron* **2005**, *61*, 4931–4938. [[CrossRef](#)]
57. Cabre, J.; Palomo, A.L. New experimental strategies in amide synthesis using *N,N*-Bis-2-oxo-3-oxazolidinyl phosphordiamidic chloride. *Synthesis* **1984**, 413–417. [[CrossRef](#)]
58. Coste, J.; Lenguyen, D.; Castro, B. PYBOP—A new peptide coupling reagent devoid of toxic byproducts. *Tetrahedron Lett.* **1990**, *31*, 205–208. [[CrossRef](#)]
59. Barbie, P.; Kazmaier, U. Total Synthesis of Cyclomarin A, a Marine Cycloheptapeptide with Anti-Tuberculosis and Anti-Malaria Activity. *Org. Lett.* **2016**, *18*, 204–207. [[CrossRef](#)] [[PubMed](#)]
60. Johnson, K.F.; Van Zeeland, R.; Stanley, L.M. Palladium-catalyzed synthesis of *N*-*tert*-prenylindoles. *Org. Lett.* **2013**, *15*, 2798–2801. [[CrossRef](#)]
61. Sugiyama, H.; Shioiri, T.; Yokokawa, F. Syntheses of four unusual amino acids, constituents of cyclomarin A. *Tetrahedron Lett.* **2002**, *43*, 3489–3492. [[CrossRef](#)]
62. Della Sala, G.; Izzo, I.; Spinella, A. A Pd-mediated approach to the synthesis of an unusual  $\beta$ -hydroxytryptophan amino acid constituent of cyclomarin A. *Synlett* **2006**, 1319–1322.
63. Metzger, A.; Bernhardt, S.; Manolikakes, G.; Knochel, P. MgCl<sub>2</sub>-accelerated addition of functionalized organozinc reagents to aldehydes, ketones, and carbon dioxide. *Angew. Chem. Int. Ed.* **2010**, *49*, 4665–4668. [[CrossRef](#)] [[PubMed](#)]

64. Piller, F.M.; Metzger, A.; Schade, M.A.; Haag, B.A.; Gavryushin, A.; Knochel, P. Preparation of polyfunctional arylmagnesium, arylzinc, and benzylic zinc reagents by using magnesium in the presence of LiCl. *Chem. Eur. J.* **2009**, *15*, 7192–7202. [[CrossRef](#)]
65. Corey, E.J.; Venkateswarlu, A. Protection of hydroxyl groups as *tert*-Butyldimethylsilyl derivatives. *J. Am. Chem. Soc.* **1972**, *94*, 6190–6191. [[CrossRef](#)]
66. Futagawa, S.; Inui, T.; Shiba, T. Nuclear magnetic-resonance study of stereoisomeric 2-oxazolidone and 2-phenyl-2-oxazoline derivatives of  $\alpha$ -amino- $\beta$ -hydroxy acids. *Bull. Chem. Soc. Jpn.* **1973**, *46*, 3308–3310. [[CrossRef](#)]
67. Parikh, J.R.; Doering, W.V.E. Sulfur trioxide in oxidation of alcohols by dimethyl sulfoxide. *J. Am. Chem. Soc.* **1967**, *89*, 5505–5507. [[CrossRef](#)]
68. McDonald, C.; Holcomb, H.; Kennedy, K.; Kirkpatrick, E.; Leathers, T.; Vanemon, P. *N*-iodosuccinimide-mediated conversion of aldehydes to methyl esters. *J. Org. Chem.* **1989**, *54*, 1213–1215. [[CrossRef](#)]
69. Schmidt, U.; Griesser, H.; Leitenberger, V.; Lieberknecht, A.; Mangold, R.; Meyer, R.; Riedl, B. Amino-acids and peptides. 81. Diastereoselective formation of (*Z*)-didehydroamino acid-esters. *Synthesis* **1992**, 487–490. [[CrossRef](#)]
70. Schmidt, U.; Lieberknecht, A.; Kazmaier, U.; Griesser, H.; Jung, G.; Metzger, J. Amino-acids and peptides. 75. Synthesis of dihydroxyamino and trihydroxyamino acids—Construction of lipophilic tripalmitoyldihydroxy- $\alpha$ -amino acids. *Synthesis* **1991**, 49–55. [[CrossRef](#)]
71. Panella, L.; Aleixandre, A.M.; Kruidhof, G.J.; Robertus, J.; Feringa, B.L.; de Vries, J.G.; Minnaard, A.J. Enantioselective Rh-catalyzed hydrogenation of *N*-formyl dehydroamino esters with monodentate phosphoramidite ligands. *J. Org. Chem.* **2006**, *71*, 2026–2036. [[CrossRef](#)]
72. Van den Berg, M.; Minnaard, A.J.; Schudde, E.P.; van Esch, J.; de Vries, A.H.M.; de Vries, J.G.; Feringa, B.L. Highly enantioselective rhodium-catalyzed hydrogenation with monodentate ligands. *J. Am. Chem. Soc.* **2000**, *122*, 11539–11540. [[CrossRef](#)]
73. Kiefer, A.; Kazmaier, U. Synthesis of modified  $\beta$ -methoxyphenylalanines via diazonium chemistry and their incorporation in desoxycyclomarin analogues. *Org. Biomol. Chem.* **2019**, *17*, 88–102. [[CrossRef](#)] [[PubMed](#)]
74. Kazmaier, U.; Schneider, C. Stereoselective synthesis of unsaturated polyhydroxylated amino acids via ester enolate Claisen rearrangement. *Synlett* **1996**, *10*, 975–977. [[CrossRef](#)]
75. Kazmaier, U.; Schneider, C. Application of the asymmetric chelate enolate Claisen rearrangement to the synthesis of unsaturated polyhydroxylated amino acids. *Synthesis* **1998**, 1321–1326. [[CrossRef](#)]
76. Kazmaier, U.; Schneider, C. Application of the asymmetric chelate-enolate Claisen rearrangement to the synthesis of 5-epi-isofagomine. *Tetrahedron Lett.* **1998**, *39*, 817–818. [[CrossRef](#)]
77. Marti, C.; Carreira, E.M. Total synthesis of (-)-spirotryprostatin B: Synthesis and related studies. *J. Am. Chem. Soc.* **2005**, *127*, 11505–11515. [[CrossRef](#)]
78. Li, P.; Xu, J.C. 1-Ethyl 2-halopyridinium salts, highly efficient coupling reagents for hindered peptide synthesis both in solution and the solid-phase. *Tetrahedron* **2000**, *56*, 8119–8131. [[CrossRef](#)]
79. Li, P.; Xu, J.C. 2-Bromo-1-ethyl pyridinium tetrafluoroborate (BEP): A powerful coupling reagent for *N*-methylated peptide synthesis. *Chem. Lett.* **2000**, *29*, 204–205. [[CrossRef](#)]
80. Barbie, P.; Kazmaier, U. Total synthesis of cyclomarins A, C and D, marine cyclic peptides with interesting anti-tuberculosis and anti-malaria activities. *Org. Biomol. Chem.* **2016**, *14*, 6036–6054. [[CrossRef](#)]
81. Junk, L.; Papadopoulos, E.; Kazmaier, U. Tryptophan *N*-1-alkylation: Quick and simple access to diversely substituted tryptophans. *Synthesis* **2021**, *53*, 2503–2511. [[CrossRef](#)]
82. Bürstner, N.; Roggo, S.; Ostermann, N.; Blank, J.; Delmas, C.; Freuler, F.; Gerhartz, B.; Hinniger, A.; Hoepfner, D.; Liechty, B.; et al. Gift from Nature: Cyclomarin A Kills Mycobacteria and Malaria Parasites by Distinct Modes of Action. *ChemBioChem* **2015**, *16*, 2433–2436. [[CrossRef](#)]
83. Schmitt, E.K.; Riwanto, M.; Sambandamurthy, V.; Roggo, S.; Miault, C.; Zwingelstein, C.; Krastel, P.; Noble, C.; Beer, D.; Rao, S.P.S.; et al. The natural product cyclomarin kills *Mycobacterium tuberculosis* by targeting the ClpC1 subunit of the caseinolytic protease. *Angew. Chem. Int. Ed.* **2011**, *50*, 5889–5891. [[CrossRef](#)]
84. Vasudevan, D.; Rao, S.P.S.; Noble, C.G. Structural basis of mycobacterial inhibition by cyclomarin A. *J. Biol. Chem.* **2013**, *288*, 30883–30891. [[CrossRef](#)]
85. Barbie, P.; Kazmaier, U. Total synthesis of desoxycyclomarin C and the cyclomarazines A and B. *Org. Biomol. Chem.* **2016**, *14*, 6055–6064. [[CrossRef](#)] [[PubMed](#)]
86. Kiefer, A.; Bader, C.D.; Held, J.; Esser, A.; Rybniker, J.; Empting, M.; Müller, R.; Kazmaier, U. Synthesis of new cyclomarin derivatives and their biological evaluation towards *Mycobacterium tuberculosis* and *plasmodium falciparum*. *Chem. Eur. J.* **2019**, *25*, 8894–8902. [[CrossRef](#)] [[PubMed](#)]
87. Choules, M.P.; Wolf, N.M.; Lee, H.; Anderson, J.R.; Grzelak, E.M.; Wang, Y.H.; Ma, R.; Gao, W.; McAlpine, J.B.; Jin, Y.Y.; et al. Rufomycin targets ClpC1 proteolysis in *Mycobacterium tuberculosis* and *M. abscessus*. *Antimicrob. Agents Chemother.* **2019**, *63*, e02204-18. [[CrossRef](#)] [[PubMed](#)]
88. Nessar, R.; Cambau, E.; Reytrat, J.M.; Murray, A.; Gicquel, B. *Mycobacterium abscessus*: A new antibiotic nightmare. *J. Antimicrob. Chemother.* **2012**, *67*, 810–818. [[CrossRef](#)] [[PubMed](#)]
89. Kar, N.P.; Sikriwal, D.; Rath, P.; Choudhary, R.K.; Batra, J.K. *Mycobacterium tuberculosis* ClpC1. *FEBS J.* **2008**, *275*, 6149–6158. [[CrossRef](#)]





90. Schmitz, K.R.; Sauer, R.T. Substrate delivery by the AAA+ ClpX and ClpC1 unfoldases activates the mycobacterial ClpP1P2 peptidase. *Mol. Microbiol.* **2014**, *93*, 617–628. [[CrossRef](#)]
91. Wolf, N.M.; Lee, H.; Choules, M.P.; Pauli, G.F.; Phansalkar, R.; Anderson, J.R.; Gao, W.; Ren, J.H.; Santarsiero, B.D.; Lee, H.; et al. High-resolution structure of ClpC1-rufomycin and ligand binding studies provide a framework to design and optimize anti-tuberculosis leads. *ACS Infect. Dis.* **2019**, *5*, 829–840. [[CrossRef](#)]
92. Wolf, N.; Lee, H.; Choules, M.; Klein, L.; Petukhova, V.; Tufano, M.; Phansalkar, R.; Gao, W.; Santarsiero, B.; Lee, H.; et al. High-resolution structure of ClpC1-Ntd-Rufomycin complex provides three-dimensional framework for optimization of cyclopeptide anti-Tb drug leads. *Protein Sci.* **2018**, *27*, 119–120.
93. Wolf, N.M.; Lee, H.; Nam, J.; Hong, J.; Duc, N.M.; Ho, N.A.; Lee, H.; Suh, J.W.; Pauli, G.F.; Franzblau, S.G.; et al. Structures of ClpC1-NTD with potent anti-TB cyclic peptides Rufomycin and Ecumicin: Implications for the mechanism of action and design of therapeutic agents. *Acta Cryst. A* **2019**, *75*, A59. [[CrossRef](#)]
94. Xie, Q.; Yang, Z.J.; Huang, X.M.; Zhang, Z.K.; Li, J.B.; Ju, J.H.; Zhang, H.; Ma, J.Y. Ilamycin C induces apoptosis and inhibits migration and invasion in triple-negative breast cancer by suppressing IL-6/STAT3 pathway. *J. Hematol. Oncol.* **2019**, *12*, 60. [[CrossRef](#)] [[PubMed](#)]
95. Intaraudom, C.; Rachtawee, P.; Suvannakad, R.; Pittayakhajonwut, P. Antimalarial and antituberculosis substances from *Streptomyces* sp. BCC26924. *Tetrahedron* **2011**, *67*, 7593–7597. [[CrossRef](#)]
96. Weinhäupl, K.; Brennich, M.; Kazmaier, U.; Lelievre, J.; Ballell, L.; Goldberg, A.; Schanda, P.; Fraga, H. The antibiotic cyclomarin blocks arginine-phosphate-induced millisecond dynamics in the N-terminal domain of ClpC1 from *Mycobacterium tuberculosis*. *J. Biol. Chem.* **2018**, *293*, 8379–8393. [[CrossRef](#)]
97. Maurer, M.; Linder, D.; Franke, K.B.; Jager, J.; Taylor, G.; Gloge, F.; Gremer, S.; Le Breton, L.; Mayer, M.P.; Weber-Ban, E.; et al. Toxic activation of an AAA plus protease by the antibacterial drug cyclomarin A. *Cell Chem. Biol.* **2019**, *26*, 1169–1179. [[CrossRef](#)] [[PubMed](#)]





Review

# Marine Alkaloids: Compounds with *In Vivo* Activity and Chemical Synthesis

Paulo E. S. Munekata <sup>1</sup>, Mirian Pateiro <sup>1</sup>, Carlos A. Conte-Junior <sup>2</sup>, Rubén Domínguez <sup>1</sup>, Asad Nawaz <sup>3</sup>,  
Noman Walayat <sup>4</sup>, Elena Movilla Fierro <sup>5</sup> and José M. Lorenzo <sup>1,6,\*</sup>

- <sup>1</sup> Centro Tecnológico de la Carne de Galicia, Parque Tecnológico de Galicia, rúa Galicia No. 4, San Cibrao das Viñas, 32900 Ourense, Spain; paulosichetti@ceteca.net (P.E.S.M.); mirianpateiro@ceteca.net (M.P.); rubendominguez@ceteca.net (R.D.)
- <sup>2</sup> Centro de Tecnologia, Programa de Pós-Graduação em Ciência de Alimentos, Instituto de Química, Universidade Federal do Rio de Janeiro, Avenida Athos da Silveira Ramos 149, Cidade Universitária, Rio de Janeiro 21941-909, RJ, Brazil; carlosconte@id.uff.br
- <sup>3</sup> Jiangsu Key Laboratory of Crop Genetics and Physiology, College of Agriculture, Yangzhou University, Yangzhou 225009, China; 007298@yzu.edu.cn
- <sup>4</sup> Department of Food Science and Engineering, College of Ocean, Zhejiang University of Technology, Hangzhou 310014, China; Noman.raii66@gmail.com
- <sup>5</sup> Complejo Hospitalario Universitario de Ourense, 32005 Ourense, Spain; elena.movilla.fierro@sergas.es
- <sup>6</sup> Área de Tecnología de los Alimentos, Facultad de Ciencias de Ourense, Universidad de Vigo, 32004 Ourense, Spain
- \* Correspondence: jmlorenzo@ceteca.net



**Citation:** Munekata, P.E.S.; Pateiro, M.; Conte-Junior, C.A.; Domínguez, R.; Nawaz, A.; Walayat, N.; Movilla Fierro, E.; Lorenzo, J.M. Marine Alkaloids: Compounds with *In Vivo* Activity and Chemical Synthesis. *Mar. Drugs* **2021**, *19*, 374. <https://doi.org/10.3390/md19070374>

Academic Editor: Emiliano Manzo

Received: 28 May 2021

Accepted: 24 June 2021

Published: 28 June 2021

**Publisher's Note:** MDPI stays neutral with regard to jurisdictional claims in published maps and institutional affiliations.



**Copyright:** © 2021 by the authors. Licensee MDPI, Basel, Switzerland. This article is an open access article distributed under the terms and conditions of the Creative Commons Attribution (CC BY) license (<https://creativecommons.org/licenses/by/4.0/>).

**Abstract:** Marine alkaloids comprise a class of compounds with several nitrogenated structures that can be explored as potential natural bioactive compounds. The scientific interest in these compounds has been increasing in the last decades, and many studies have been published elucidating their chemical structure and biological effects *in vitro*. Following this trend, the number of *in vivo* studies reporting the health-related properties of marine alkaloids has been increasing and providing more information about the effects in complex organisms. Experiments with animals, especially mice and zebrafish, are revealing the potential health benefits against cancer development, cardiovascular diseases, seizures, Alzheimer's disease, mental health disorders, inflammatory diseases, osteoporosis, cystic fibrosis, oxidative stress, human parasites, and microbial infections *in vivo*. Although major efforts are still necessary to increase the knowledge, especially about the translation value of the information obtained from *in vivo* experiments to clinical trials, marine alkaloids are promising candidates for further experiments in drug development.

**Keywords:** animal studies; marine alkaloids; biological activity; cancer; cardiovascular diseases; inflammation; chemical synthesis

## 1. Introduction

The use of natural products in the treatment and management of human diseases dates back to ancient times. In modern times, the consumption of natural bioactive compounds remains in the habits of modern society as a complementary or alternative strategy to ameliorate the effects of many diseases [1,2]. The role of natural products in human health has been generating increasing interest among researchers, physicians, pharmacists, and professionals of the health sector. This scenario is based on the vast diversity of chemical structures found in natural sources that can be studied as potential drugs or inspire the synthesis of derivatives to improve the management and treatment of diseases at a global scale [3].

Although terrestrial plants are in the focus of numerous studies about bioactive compounds from natural sources, marine organisms have been gaining more space and

interest [4]. A growing number of studies have been revealing the rich diversity of compounds found in marine organisms that can be explored as new drugs for human diseases. Among them, alkaloids stand out as one of the most diverse and largely studied groups of compounds [5,6]. This relatively young field of research is growing fast, and many studies have focused on the accurate identification of chemical structures and evaluation of biological potential *in vitro*. For instance, a recent review compiled around 800 indole alkaloids isolated from algae, microorganisms, sponges, and invertebrate sources [5]. Moreover, several studies have been carried out to screen and characterize the biological activity of marine alkaloids *in vitro* against cancer [6], inflammatory diseases [7], and parasites [8], for instance.

Although several studies characterized the biological effect of marine alkaloids *in vitro*, the evaluation at the animal level is a more recent progression to understand the applications and limitations of marine alkaloids. This progression is a step towards the evaluation at the human level that allows a more comprehensive evaluation of the effects that cannot be obtained from chemical methods and cellular models [9]. Thus, this review aims to provide an overview of the current knowledge about the *in vivo* effect of marine alkaloids, the synthetic production of their derivative compounds, and considerations about animal studies with marine alkaloids.

## 2. Marine Alkaloids with Biological Activity *In Vivo*

### 2.1. Antitumor Effect

The antitumor activity of marine alkaloids has been investigated by many research groups (Table 1). For instance, the recent study carried out by Choi et al. [10] reported the effect of (–)-agelamide D (1) (Figure 1) in assisting the treatment of cancer with radiation in mice with xenograft tumors (hepatocellular carcinoma). According to the authors, the treatment with this alkaloid improved the efficiency of radiation therapy wherein the proposed mechanism involved an increase in the stress in the endoplasmic reticulum (increased levels of activating transcription factor 4) and eventual apoptosis during the radiotherapy treatment. In another experiment with mice, Wang et al. [11] explored the effect of ascomylactam A (2) against human lung cancer (A549, NCI-H460, and NCI-H1975). The main effects of the treatment with this alkaloid were the significant reduction in the volume and weight of NCI-H460 tumor and the reduction in the volume of A549 tumors in mice treated with 6 mg/kg/day. Conversely, no effect was observed in animals with NCI-H1975 tumors.

**Table 1.** Antitumor and cardiovascular protective activities of marine alkaloids and derivative compounds evaluated *in vivo*.

Compound and Source	Experimental Conditions	Effect	Ref.
Anticancer activity			
(–)-Agelamide D (1) from marine sponge <i>Agelas</i> sp.	6–7-week-old male Balb/c nude mice; intraperitoneal injection; 1.25 mg/kg/day; 3 times a week; mice euthanized after 21 days	Increased the efficacy of radiation therapy in xenograft Hep3B cells with reduced systemic toxicity	[10]
Ascomylactam A (2) from mangrove endophytic fungus <i>Ascomycota</i> sp.	Male BALB/c-nu mice; intraperitoneal injection; 3 and 6 (A549 and NCI-H460), 5 or 10 (NCI-H1975) mg/kg/day; every 3 days for 21 days	Suppression of A549 (6 mg/kg/day; volume) and NCI-H460 (6 mg/kg/day; volume and weight) and lung tumor growth; no effect in NCI-H1975 tumor	[11]
Synthetic 4-chloro faspaplysin (3) (found in marine sponge)	4–6-week-old C57B/6J female mice; oral administration; 1, 3, and 5 mg/kg/day for 5 days (tumor angiogenesis assay); 4 and 7 mg/kg/day for 8 days (Ehrlich solid tumor model)	Reduced the formation of VEGF-mediated microvessels and blood vessel formation of xenograft breast cancer cells (1, 3, and 5 mg/kg/day) and Ehrlich solid tumor formation (4 and 7 mg/kg/day)	[12]

Table 1. Cont.

Compound and Source	Experimental Conditions	Effect	Ref.
Synthetic derivative (C2-substituted) of 7-deazahypoxanthine (4) from rigidin D	4–6-week-old female athymic nude mice; intraperitoneal injection; 3 mg/kg; 5 times per week for 17 days	Reduced tumor growth; no effect on weight	[13]
Synthetic FBA-TPQ (5); makaluvamine analog from marine sponge <i>Zyzyya</i> sp.	4–6-week-old female athymic nude mice; intraperitoneal injection; 5 mg/kg/day, 3 days/week for 3 weeks; 10 mg/kg, 3 days/week for 2 weeks; and 20 mg/kg, 3 days/week for 1 week	Reduced tumor growth; weight loss with doses of 10 and 20 mg/kg	[14]
Synthetic FBA-TPQ (5); makaluvamine analog from marine sponge <i>Zyzyya</i> sp.	5-week-old female athymic nude mice; intraperitoneal injection; 1 and 10 mg/kg/day; 5 days/week for two and half weeks	Reduced tumor growth and no significant effect on body weight	[15]
Synthetic FBA-TPQ (5); makaluvamine analog from marine sponge <i>Zyzyya</i> sp.	4–6-week-old female athymic nude mice; intraperitoneal injection; 5 and 10 mg/kg/day; 5 days per week for 3 weeks	Reduced tumor growth and induced remission	[16]
Neoamphimedine (6) from marine sponge <i>Xestospongia</i> sp.	Nude mice; intraperitoneal injection; 50 mg/kg; 4 q.d.	Reduced tumor growth	[17]
Synthetic lamellarin 14 (7); lamellarin analog from mollusk <i>Lamellaria</i> sp	BALB/c nu/nu mice; 5 and 10 mg/kg; once a day for 17 days	Reduced tumor growth with no effect on body weight	[18]
Isofistularin-3 (8) from marine sponge <i>Aplysina aerophoba</i>	Zebrafish embryos; 15, 20, and 25 $\mu$ M; incubation for 24 h	Reduced neuroblastoma (15–25 $\mu$ M) and prostate (20 and 25 $\mu$ M) cancer development	[19]
Crambescidine-816 (9) from marine sponge <i>Crambe crambe</i>	Zebrafish embryos; 0.5, 1, and 2 $\mu$ M; 48 h after fertilization	Reduced tumor development; no effect on survival rate	[20]
Cardioprotective activity			
Manzamine A (10) from marine sponge <i>Acanthostrongylophora ingens</i>	6-week-old apoE-deficient mice; oral administration; 30 mg/kg for 80 days	Reduced total, free, and LDL cholesterol and triglyceride levels; atherosclerotic lesions were diminished	[21]
Fungi fibrinolytic compound 1 (11) from marine fungus <i>Stachbotrys longispora</i> FG216	Wistar rats; 5, 10, and 25 mg/kg (morphological effect in lungs; euglobulin lysis time); injection in caudal vein	Reduced morphological changes from induced thrombosis and reduced euglobulin lysis time; no effect on fibrinogen degradation concentrations (5–25 mg/kg)	[22]
4 alkaloids (12–15) from marine fungus <i>Penicillium expansum</i>	Zebrafish embryos; 1, 10, and 100 $\mu$ g/mL; incubation for 24 h	Reduced bradycardia; induced angiogenesis	[23]
4 alkaloids (16–19) from marine fungus <i>Aspergillus austroafricanus</i>	Zebrafish embryos; 30, 70, 120 $\mu$ g/mL; incubation for 24 h	Induced angiogenesis	[24]
Agelanemoechine (20) from marine sponge <i>Agelas nemoechinata</i>	Zebrafish embryos; 1.25, 2.5, 5, 10, and 20 $\mu$ M	Induced angiogenesis	[25]

n.i.: not indicated; FBA-TPQ (5): 7-(4-fluorobenzylamino)-1,3,4,8-tetrahydropyrrolo[4,3,2-de]quinolin-8(1H)-one.

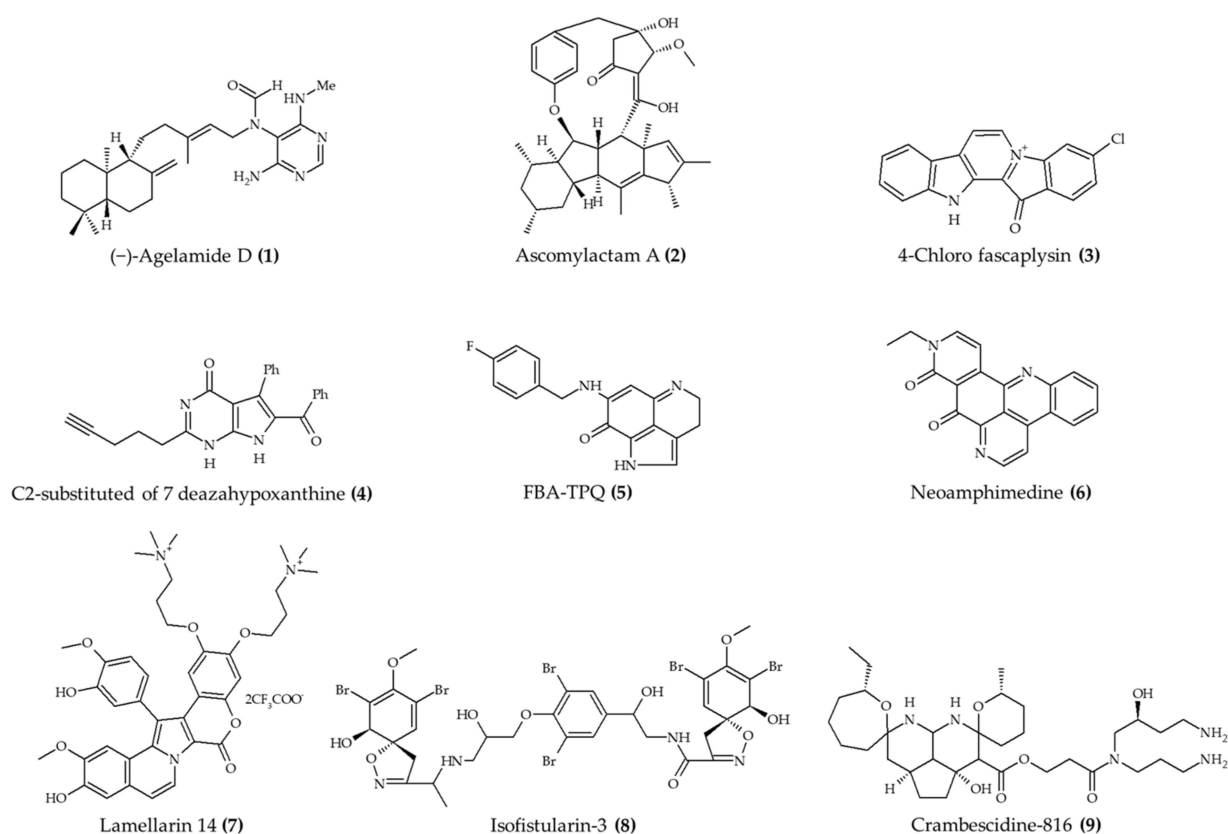


**Figure 1.** Marine alkaloids with antitumor activity *in vivo*.

A relevant marine alkaloid with antitumor activity is 4-chloro fascaplysin (3) [12]. This compound displayed antiangiogenic capacity in mice with human breast cancer MDAMB-231 by reducing the levels of vascular endothelial growth factor (VEGF). Another outcome from this study was the inhibition of Ehrlich ascites carcinoma growth. The authors also observed that 4-chloro fascaplysin (3) limited the growth of this carcinoma by activating the phosphoinositide 3-kinases, protein kinase B, and mechanistic target of rapamycin (PI3K/Akt/mTOR) pathway.

A similar inhibitory effect *in vivo* against tumor development was reported by Medellin et al. [13] for C2-substituted 7-deazahypoxanthine (4). The animals xenografted with colon cancer SW620 and treated with this alkaloid displayed a significant reduction in total tumor volume. Moreover, no weight loss was observed in the alkaloid-treated group. In the same line of thought, a series of studies against different types of cancer were performed to evaluate the anticancer activity of 7-(4-fluorobenzylamino)-1,3,4,8-tetrahydropyrrolo[4,3,2-de]quinolin-8(1H)-one (FBA-TPQ, compound 5), which is a synthetic derivative from makaluvamine (naturally found in marine sponge *Zyzzya* sp.) [14]. In the case of breast cancer, this compound reduced tumor growth in athymic nude mice at the three tested levels (5, 10, and 20 mg/kg). However, the authors indicated that animals treated with 10 and 20 mg/kg lost weight during the treatment period. In a subsequent experiment, Chen et al. [15] observed that FBA-TPQ (5) slowed the growth of ovarian tumor *in vivo* in a dose-dependent manner (by 20.5% and 69.4% at 1 and 10 mg/kg, respectively). Additionally, no significant changes were observed in the weight of treated animals. According to the authors, this effect was attributed to the formation of radical oxygen species and mitochondrial collapse, which led to apoptosis and interruption of cell cycle progression and proliferation.

Zhang et al. [16] explored the inhibitory effect of FBA-TPQ (5) against pancreatic cancer. These authors observed that tumors in animals treated with this alkaloid were reduced gradually during the treatment time and achieved remission at the end of the trial.

Moreover, no changes in the weight of animals were observed. The authors also indicated that this effect was attributed to the induction of cell cycle arrest and apoptosis (observed in the *in vitro* experiments).

The experiment carried out by Marshall et al. [17] is another example of the anticancer effect of marine alkaloids. In this study, these authors observed a significant reduction in the tumor growth (epidermoid-nasopharyngeal and colon cell lines) in mice treated with neoamphimedine (obtained from marine sponge *Xestospongia* sp.; compound 6). Another relevant synthetic derivative from marine alkaloids with anticancer potential is lamellarin 14 (inspired by naturally occurring lamellarins from mollusk *Lamellaria* sp.; compound 7) [18]. This compound reduced the growth of adenocarcinoma *in vivo* after 17 days of treatment without significant loss of weight.

Similar to observations in experiments with mouse models, some studies using zebrafish as a model organism indicate the anticancer effect of marine alkaloids. For instance, Florean et al. [19] studied the effect of isofistularin-3 (isolated from marine sponge *Aplysina aerophoba*; compound 8) against neuroblastoma and prostate cancer. The authors reported that this alkaloid (at 20 and 25  $\mu\text{M}$ ) displayed the capacity to inhibit tumor growth by binding to DNA methyltransferase 1 and causing cell cycle arrest (inducing the expression of p21 and p27 cyclin-dependent kinase inhibitors) and apoptosis (favoring the production of tumor necrosis factor). A similar experiment with a zebrafish model indicated that crambescidine-816 (isolated from marine sponge *Crambe crambe*; compound 9) induced colorectal carcinoma regression [20]. This experiment also revealed that crambescidine-816 (9) affected the tumor adhesion capacity, cytoskeletal integrity, and mitochondrial membrane potential leading to apoptosis.

## 2.2. Cardioprotective Activity

Marine alkaloids have also been investigated as potential drugs to assist in the management of cardiovascular diseases (Figure 2). In this context, Eguchi et al. [21] explored the effect of manzamine A (naturally found in the marine sponge *Acanthostrongylophora ingens*) in the blood of apoE-deficient mice (naturally prone to developing atherosclerosis). The animals treated with this alkaloid displayed lower blood levels of total, free, and LDL cholesterol and triglyceride than animals in the untreated group. Moreover, manzamine A also reduced the lesions in the arteries of animals in the treated group.

Yan et al. [22] evaluated the thrombolytic effect of fungi fibrinolytic compound 1 (FGC1; 2,5-bis-[8-(4,8-dimethyl-nona-3,7-dienyl)-5,7-dihydroxy-8-methyl-3-keto-1,2,7,8-tetrahydro-6H-pyran[a]isoindol-2-yl]-pentanoic acid; compound 11). The authors observed a significant improvement in the thrombolysis of pulmonary capillaries and a reduction in the formation of blood clots in mice. Another relevant outcome from this study was the lack of effect in the fibrinogen levels, which indicated that FGC1 (11) did not affect the blood coagulation of treated mice. Moreover, the treatment with FGC1 (11) also ameliorated the morphological alterations in the walls of the alveolus caused by the induced pulmonary thrombosis.

Interesting outcomes were also obtained in a zebrafish model. Fan et al. [23] explored the effect of several alkaloids obtained from the marine fungus *Penicillium expansum* in controlling blood pressure and inducing angiogenesis. Among all alkaloids, eight compounds displayed the capacity to induce both beneficial effects in the treated group, especially fumiquinazoline Q (12), prelapatin B (13), and protuboxepin B (14) and E (15). Likewise, Li et al. [24] observed a significant increase in the formation of new blood vessels in zebrafish embryos treated with alkaloids extracted from marine fungus *Aspergillus austroafricanus*. The alkaloids with the highest angiogenic activity were dinotoamide J (16), 2-hydroxy-6-N-isopentenyl-adenine (17), cyclophenol (18), and decumbenones A (19). Similarly, Li et al. [25] observed a similar angiogenic effect in zebrafish treated with age-lanemoechine (20), especially at 5  $\mu\text{M}$ , from marine sponge *Agelas nemoechinata*.

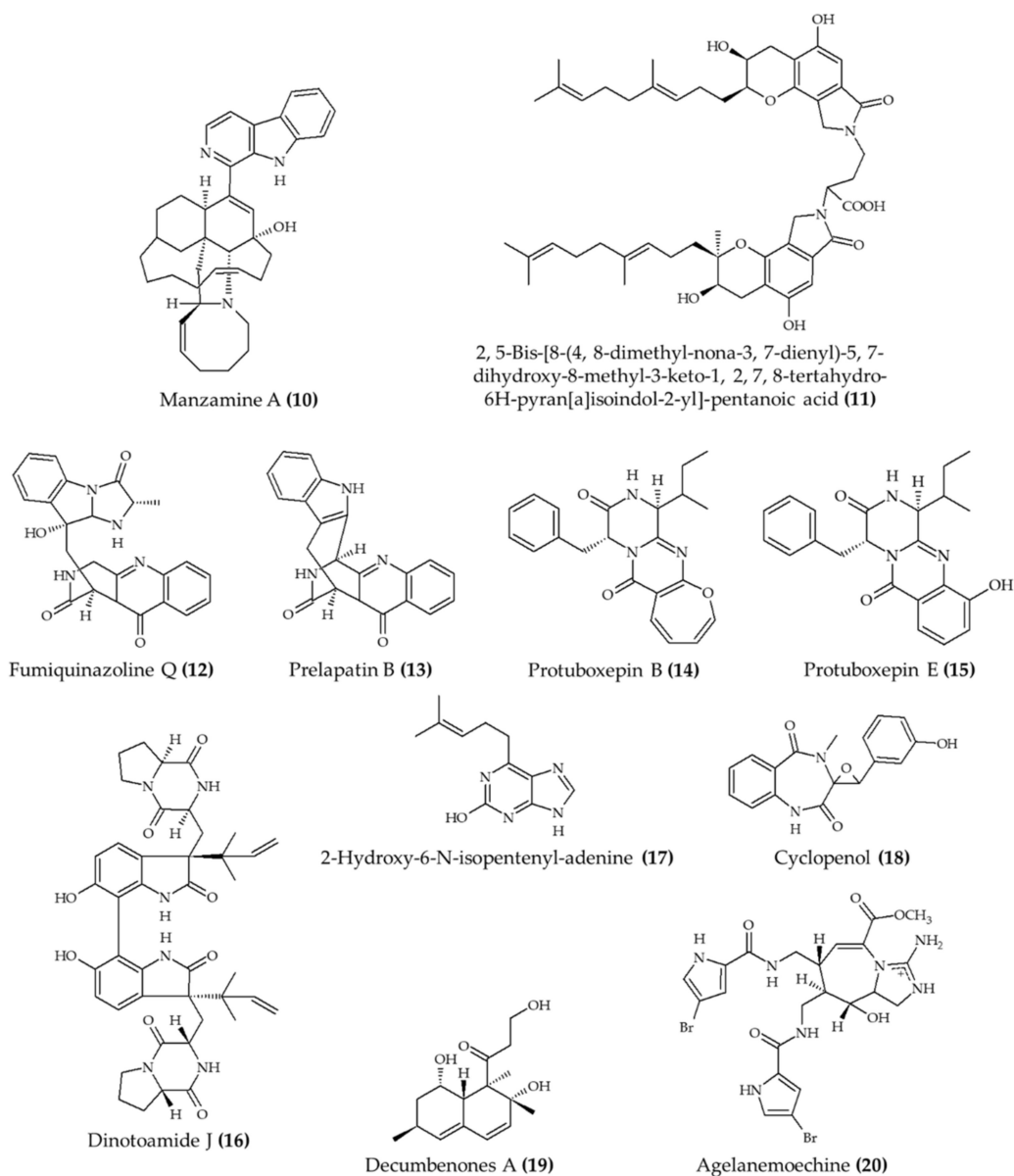


**Figure 2.** Marine alkaloids with cardioprotective activity *in vivo*.

### 2.3. Antiseizure Activity, Alzheimer's Disease, and Mental Health

The potential of marine alkaloids to assist in the management of seizures has been explored *in vivo* (Table 2). A recent experiment evaluated the antiseizure effect of TMC-120A and -120B (Figure 3; compounds 21 and 22, respectively) in both mouse and zebrafish models [26]. In the mouse model, a significant reduction in seizure duration was observed using 10 mg/kg of any of the two alkaloids. Likewise, the duration of seizure behavior and the percentage of animals displaying epileptiform activity in zebrafish model were also reduced by both compounds (20 µg/mL).

**Table 2.** Effects of marine alkaloids and derivative compounds on seizures, Alzheimer’s disease, mental health, and inflammation evaluated *in vivo*.

Compound and Source	Experimental Conditions	Effect	Ref.
Antiseizure activity, Alzheimer’s disease, and mental health			
TMC-120A (21) and TMC-120B (22) isoquinoline alkaloids from marine fungus <i>Aspergillus insuetus</i>	Male NMRI mice; intraperitoneal injection; TMC-120A (1.25, 2.5, 5, and 10 mg/kg) and TMC-120B (2.5, 5, 10, and 20 mg/kg); 30 min before electrical stimulation	Reduced seizure duration (at 10 mg/kg for both alkaloids)	[26]
TMC-120A (21) and TMC-120B (22) isoquinoline alkaloids from marine fungus <i>Aspergillus insuetus</i>	Zebrafish larvae; 5, 10, and 20 µg/mL; 2 h incubation	Reduced the proportion of animals and seizure duration (20 µg/mL)	[26]
1 alkaloid (23); grassystatin A analog from marine cyanobacterium <i>Symploca</i> sp.	8-week-old CF-1 mice; intraperitoneal injection; 30 mg/kg; single day	Reduced the Aβ40 level in the brain	[27]
9-Methylfascaplysin (24); Fascaplysin analog from marine sponge <i>Fascaplysinopsis</i> sp.	4-month-old male ICR mice; intrahippocampal injection; scopolamine with 7.3 ng and 21.9 ng; once a day for 10 days	Ameliorated cognitive dysfunction; inhibited Aβ-induced tau hyperphosphorylation; no effect in locomotor function	[28]
Circumdatin D (25) from marine fungus <i>Aspergillus ochraceus</i>	<i>Caenorhabditis elegans</i> ; 50, 100, and 200 mM incubation for 36 h	Reduced paralysis rate	[29]
Veranamine (26) from marine sponge <i>Verongula rigida</i>	Male Swiss Webster mice; intraperitoneal injection; 20 mg/kg; single day	Reduced immobility time; no effect on locomotor activity	[30]
3 alkaloids (27–29) from marine sponge <i>Aplysina fulva</i>	Zebrafish adult; 0.1, 0.5, and 1.0 mg/mL; 1 h incubation	Induced anxiolytic effect and involved the GABAergic system	[31]
Anti-inflammatory			
6-Bromoisatin (30) isolated from Muricidae mollusk <i>Dicathais orbita</i>	Male and female C57 black/6 mice; oral administration; 0.5 and 0.1 mg/g HBG extract and 0.05 and 0.1 mg/g 6-bromoisatin (30); 48, 24, and 1 h prior to the administration of LPS; mice euthanized after 3 h	Reduce acute lung inflammation, TNFα, IL-1β, and total protein levels in BALF, attenuated physiological changes	[32]
Viridicatol (31) isolated from marine fungus <i>Penicillium griseofulvum</i>	6–7-week-old female BALB/c mice; oral administration; 5, 10, and 20 mg/kg for 13 days	Reduced OVA-specific IgE, serum histamine, mMCP-1, and TNF-α; increased IL10 level	[33]
Caulerpin (32) from seaweed <i>Caulerpa racemosa</i>	6–8-week-old male C57BL/6 mice; oral administration; 0.4, 4, and 40 mg/kg for 7 days	Reduced colon damage and shortening and DAI (4 mg/kg)	[34]
Dysidinoid B (33) from marine sponge <i>Dysidea septosa</i>	Zebrafish embryos; 20, 40, and 80 µM; incubation for 2 h	Reduced inflammation (40 and 80 µM)	[35]
3 alkaloids (18, 19, and 31) from marine fungus <i>Aspergillus austroafricanus</i>	Zebrafish embryos; 30, 70, and 120 µg/mL; incubation for 2 h	Induced anti-inflammatory response	[24]

Aβ: amyloid-β peptide; BALF: bronchoalveolar lavage fluid; DAI: disease activity index; HBG: hypobranchial gland; IL10: interleukin 10; IL-1β: interleukin-1 beta; LPS: lipopolysaccharide; mMCP-1: mast cell protease-1; OVA: ovalbumin; TNF-α: tumor necrosis factor-α.



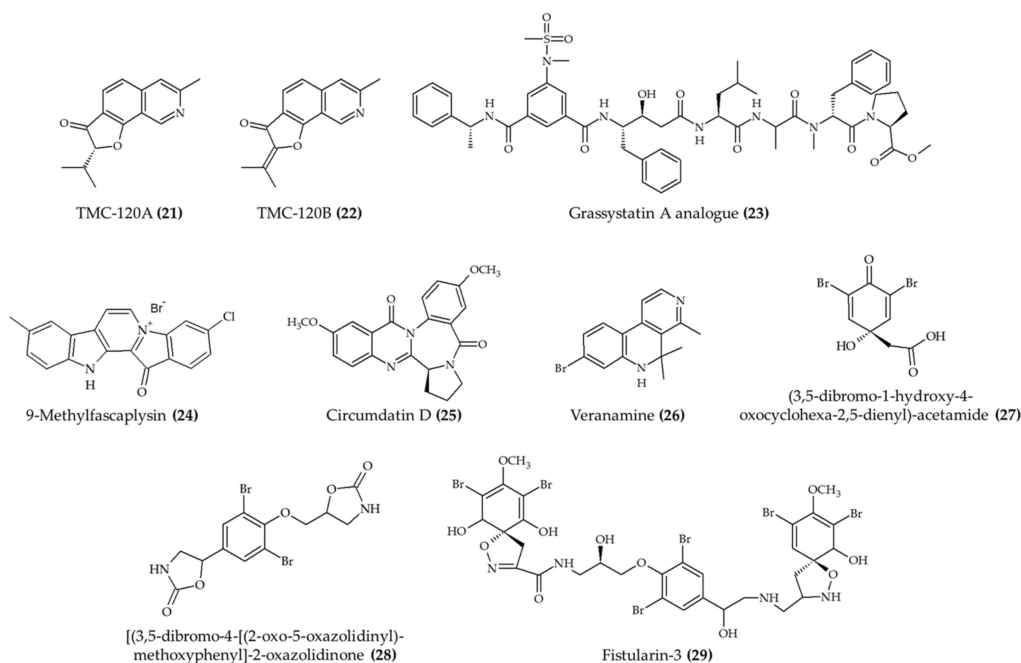


**Figure 3.** Marine alkaloids with antiseizure activity and health benefits related to Alzheimer’s disease and mental health *in vivo*.

Marine alkaloids have also been exerting beneficial effects in the management of Alzheimer’s disease. For instance, the experiment carried out by Liu et al. [27] indicated that a grassystatin A analog (23) reduced the levels of amyloid- $\beta$  peptide ( $A\beta_{40}$ ) in the brain of treated animals. Likewise, 9-methylfascaplysin (analog of fascaplysin, an alkaloid found in marine sponge *Fascaplysinopsis* sp.; compound 24) ameliorated the cognitive dysfunction and inhibited the phosphorylation of amyloid- $\beta$  peptide by tau protein in mice exposed to scopolamine [28]. Additionally, the locomotor function of 9-methylfascaplysin (24)-treated animals was not affected. A related experiment with *Caenorhabditis elegans* indicated the role of circumdatin D (25) in assisting in the management of Alzheimer’s disease [29]. In this case, temperature-induced paralysis was significantly lower in the group of animals treated with circumdatin D (25) in comparison to untreated animals.

Another relevant biological effect related to marine alkaloids is the capacity to exert antidepressant-like activity. This outcome was obtained from the use of veranamine (naturally found in marine sponge *Verongula rigida*; compound 26) [30]. The main effect was observed in the reduction immobility time of treated animals in relation to untreated ones. However, no significant differences were reported in terms of locomotor activity.

The anxiolytic activity is another interesting effect of marine alkaloids observed *in vivo*. Cesário et al. [31] observed an anxiolytic effect upon exposure to (3,5-dibromo-1-hydroxy-4-oxocyclohexa-2,5-dienyl)-acetamide, [(3,5-dibromo-4-[(2-oxo-5-oxazolidinyl)methoxy]phenyl)-2-oxazolidinone or fistularin-3 (extracted marine sponge *Aplysina fulva*; compounds 27, 28, and 29, respectively) in a zebrafish model. The other six identified alkaloids from the same extract displayed low anxiolytic activity.

#### 2.4. Anti-Inflammatory Activity

The management of the inflammatory process is another relevant health benefit that has been observed for marine alkaloids (Figure 4) *in vivo*. For instance, 6-bromoisatin (obtained from Muricidae mollusk *Dicathais orbita*; compound 30) exerted a protective effect in the lung tissue of mice with induced inflammation [32]. These results were attributed to the reduction in tumor necrosis factor- $\alpha$  (TNF- $\alpha$ ), interleukin-1 beta (IL-1 $\beta$ ), and total protein levels in the bronchoalveolar lavage fluid.

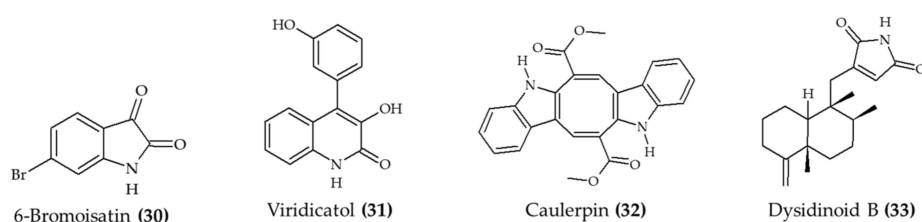


**Figure 4.** Alkaloids from marine sources associated with anti-inflammatory activity *in vivo*.

The anti-inflammatory effect of marine alkaloids was also observed in the reduction in the allergic reaction induced by ovalbumin [33]. In this case, viridicatol (20 mg/kg; compound **31**) reduced the circulating levels of histamine, mast cell protease-1, and TNF- $\alpha$ , as well as the levels of ovalbumin-specific immunoglobulin E. At the physiological level, the treatment with viridicatol (**31**) also attenuated the lymphocytic infiltration in the jejunum villi and the degranulation of intestinal mast cells. A similar protective effect was reported by Lucena et al. [34], who reported the anticolitis effect of caulerpin (**32**) in mice. These authors observed that a dose of 4 mg/kg ameliorated the damage of the inflammatory response in the colon.

The use of a zebrafish model has also revealed relevant effects of marine alkaloids against inflammation. For instance, dysidinoid B (**33**) reduced the number of inflammatory cells induced by CuSO<sub>4</sub> at 40 and 80  $\mu$ M [35]. Similarly, Li et al. [24] reported a significant reduction in the count of macrophages induced by CuSO<sub>4</sub> in a mouse model due to the treatment with cyclophenol (**18**), decumbenones A (**19**), or viridicatol (**31**) (extracted from marine fungus *Aspergillus austroafricanus*).

### 2.5. Antiparasitic and Antimicrobial Activity

Ameliorating the infection of parasites (Table 3) is another important health benefit associated with marine alkaloids (Figure 5). Davis et al. [36] observed that mice treated with makaluvamine G (obtained from marine sponge *Zyzzya* sp.; compound **34**) had lower blood levels of *Plasmodium berghei* in comparison to animals in the untreated group. Additionally, the authors indicated that the dose administered to the animals did not induce toxic effects. A similar experiment was carried with 10-(4,5-dihydrothiazol-2-yl)thio)decan-1-ol (**35**), a derivative of 3-alkylpyridine (naturally found in marine sponge *Theonella* sp.), against the *P. berghei* infection in mice [37]. According to the authors, the treatment with 50 mg/kg suppressed the parasitemia by 20% in comparison to the untreated group. It is noteworthy that this experiment was carried out with an encapsulated material, which is a relevant approach to protect the active compounds during gastric digestion and facilitate the intestinal absorption of compounds administered orally. Likewise, Mani et al. [38] indicated that haliclonyclamine A (isolated from marine sponge *Haliclona* sp.; compound **36**) reduced *Plasmodium falciparum* level by 45% in mice after 4 days of treatment. Only the treatment with 10 mg/kg increased the survival rate after 18 days of treatment.

Antimicrobial activity is another biologically relevant effect of marine alkaloids. For instance, Pech-Puch et al. [39] evaluated the antimicrobial activity of bromoageliferin (**37**) against *Pseudomonas aeruginosa* in mice. The authors observed a significant increase in the survival rate in the group of animals treated with the marine alkaloid. Similarly, the synthetic 3-(3-((12-azidododecyl)oxy)propyl)-1-benzylpyridin-1-ium chloride (**38**) displayed a protective effect against *Candida albicans* in the kidney and spleen of mice [40]. The marine alkaloids (especially at 1.0 mg/kg) also did not affect the weight of animals during the treatment period. However, no protective effect against *Candida albicans* was observed in the liver.

**Table 3.** Antiparasitic and antimicrobial activity and health benefits related to osteoporosis, cystic fibrosis, and antioxidant activity of marine alkaloids *in vivo*.

Compound and Source	Experimental Conditions	Effect	Ref.
Antiparasitic activity			
Makaluvamine G (34) from marine sponge <i>Zyzzya</i> sp.	7–9-week-old male and female Swiss albino mice; subcutaneous injection; 8 mg/kg/day for 4 days	Reduced the growth of <i>Plasmodium berghei</i> in infected mice	[36]
10-(4,5-Dihydrothiazol-2-yl)thio)decan-1-ol) (thiazoline) (35), a synthetic analog of 3-alkylpyridine	6–8-week-old female C57BL/6 mice; oral administration; 25 and 50 mg/kg (nanoemulsion) and 25 mg/kg (free compound); 4 h after infection for 4 days; samples collected after 5, 8, and 10 days	Reduced parasitemia for 8 days (especially with 50 mg/kg)	[37]
Haliclonacyclamine A (36) from marine sponge <i>Haliclona</i> sp.	Swiss female mice; 0.1, 1, and 10 mg/kg; once a day for 4 days	Reduced parasitemia by 45% after 4 days of treatment (10 mg/kg)	[38]
Antimicrobial activity			
Bromoageliferin (37) from marine sponge <i>Agelas dilatata</i>	<i>Galleria mellonella</i> larvae; 2 mg/kg	Increased survival rate after infection with <i>Pseudomonas aeruginosa</i>	[39]
3-(3-((12-Azidododecyl)oxy)propyl)-1-benzylpyridin-1-ium chloride (38), a synthetic 3-alkylpyridine analog	6–8-week-old Swiss male mice; 0.5 and 1.0 mg/kg; 2, 24, and 48 h postinfection	Reduced microbial infection in kidney and spleen (1.0 mg/kg); no effect in liver	[40]
2 alkaloids (39 and 40), hyrtinadine A analogs from Red Sea sponge <i>Hyrtios</i> sp.	BALB/c female mice; topical administration and intraperitoneal injection; 5 mg/kg; single application	Improved wound skin wound healing; increased survival rate	[41]
Osteoporosis			
Hymenialdisine (41) from marine sponge	11-week-old female C57BL/6j mice; intraperitoneal injection; 1 mg/kg; every 2 days for 6 weeks	Reduced the loss of bone volume and trabecular thickness	[42]
Cystic fibrosis			
Latonduine A (42) from marine sponge <i>Stylissa carteri</i>	10–12-week-old F508del-CFTR homozygous mice; gavage; 50 mg/kg once daily for 2 days	Reduced salivary secretion	[43]
Antioxidant activity			
Fronodoplysin A (43) from marine sponge <i>Dysidea frondosa</i>	Zebrafish embryos; 20 µM	Induced antioxidant response	[44]

The antimicrobial activity of marine alkaloids was also reported in the study carried out by Rehberg et al. [41] with methicillin-resistant *Staphylococcus aureus*. These authors observed significant reductions in the size and microbial counts in contaminated skin wounds of animals treated with either 3,3'-(pyrimidine-2,5-diyl)bis(5-chloro-1H-indole) (39) or 2,6-bis(5-chloro-1H-indol-3-yl)pyridine (40) after 12 days. Additionally, these alkaloids also increased the survival rate of animals intraperitoneally injected with methicillin-resistant *Staphylococcus aureus* by 12 h in relation to control mice (without antibiotic).

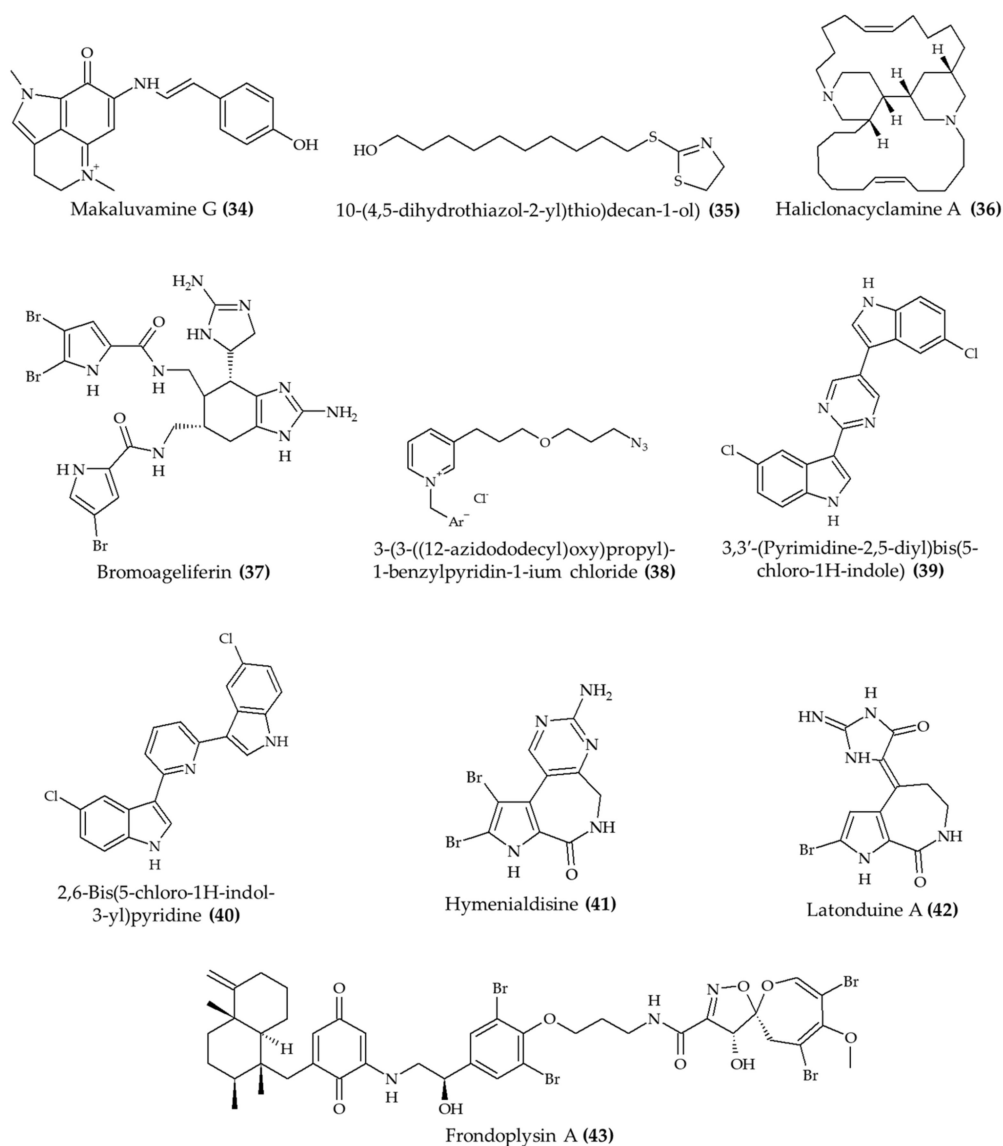


**Figure 5.** Alkaloids from marine sources with antiparasitic and antimicrobial activity and health benefits related to osteoporosis, cystic fibrosis, and antioxidant activity *in vivo*.

### 2.6. Other Health-Related Effects

The biological activity of marine alkaloids *in vivo* is also related to effects other than those aforementioned. Osteoporosis is a disease with a major impact, especially in the elderly population [45]. In this sense, Wang et al. [42] studied the effect of hymenialdisine (Figure 5; compound 41) in the bone health of mice. The authors observed that treated animals displayed lower levels of bone volume and trabecular thickness levels than non-treated animals. Moreover, this outcome was related to the activation of nuclear factor kappa B (NF- $\kappa$ B); mitogen-activated protein kinase (MAPK); and nuclear factor of activated T-cells, cytoplasmic 1 (NFATc1) signaling pathways.

Marine alkaloids can also assist in the management of cystic fibrosis. This outcome was reported by Carlile et al. [43] for latonduine A (42) in a mouse model. These authors observed a significant reduction in the salivary secretion of treated animals. According to the authors, this effect was related to the binding of latonduine A (42) to poly(ADP-ribose) polymerases that leads to a correction in the cystic fibrosis transmembrane conductance regulator trafficking to the cell surface. Finally, marine alkaloids can also induce an antioxi-

dant response *in vivo*. Jiao et al. [44] observed a significant increase in the fluorescence of mutant zebrafish treated with frondoplysin A (43).

### 3. Chemical Modification and Synthesis of Marine Alkaloids

Several studies described in the last section disclose the potential health benefits of marine alkaloids. Although this scenario is an important advance towards the use of marine alkaloids in disease management, the majority of marine alkaloids do not reach the *in vivo* level. A relevant example that shows the small fraction of compounds with potential biological effects from the huge number of candidates is the screening carried out by Copmans et al. [26]. In this study, more than 2000 marine extracts were screened for *in vivo* characterization of antiseizure activity. Only 43 candidates displayed the target activity and did not induce toxicological effects in both embryonic and larval zebrafish. Eventually, only alkaloids were further evaluated *in vivo*. This study also indicated another important result: 1764 compounds were considered inactive.

This outcome is observed in other natural sources, and major advances are necessary to explore these compounds. Moreover, these compounds with low biological activity may also present low solubility, metabolic instability, and unknown mechanisms of action, and they may be too large for oral administration and gut absorption [46,47]. Consequently, no wide interest from researchers has been generated regarding their pharmacological activity.

One of the possible approaches to overcome this barrier is the modification of the chemical structure of the natural compounds with different substituents and further evaluation of the relationship between each derived compound and the target biological effect [46]. This strategy has been explored in the context of marine alkaloids, and several studies provide valuable information about the structure–activity relationship *in vitro* [48–51].

In terms of derivatives and synthetic compounds inspired from marine alkaloids sources with biological activity *in vivo*, some studies explored interesting modifications. For instance, Sharma et al. [12] evaluated the antitumor effect of the synthetic compound 4-chloro faspaplysin (Figure 6A; compound 3). The authors synthesized this derivative by reacting tryptamine (44) with 2,4-dichlorophenyl glyoxal (45) with Pd/C in acetic acid to produce the intermediary compound  $\beta$ -carboline (46). Further heating (20 min at 220 °C) led to the generation of 4-chloro faspaplysin (3) by intramolecular ring closure. According to the authors, 75% reaction yield was obtained using this route.

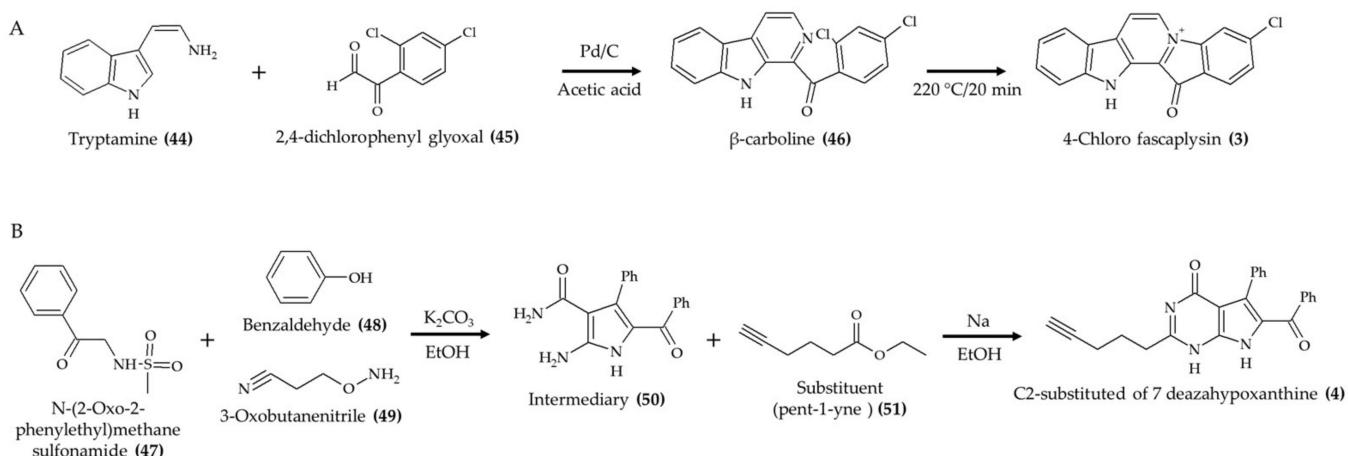


**Figure 6.** Schematic representation of 4-chlorofaspaplysin (3) (A) and C2-substituted 7-deazahypoxanthine (4) (B) syntheses (according to Sharma et al. [12] and Medellín et al. [13], respectively).

Medellin et al. [13] explored the effect of structural modifications in the anticancer activity of rigin D derivatives. The factors evaluated in this study were carbon chain length, elemental composition (Br, N, O, and S), and functional groups (carboxylic acid, phenol, furan, and nitrile) of the substituent group. A schematic representation of the route used by these authors is displayed in Figure 6B. The authors reacted N-(2-Oxo-2-phenylethyl)methanesulfonamide (47) with benzaldehyde (48) and 3-oxobutanenitrile (49) in the presence of potassium carbonate and ethanol under reflux to produce the intermediary compound (50). Then, different substituents were coupled to this intermediary compound (50) in the presence of sodium in ethanol to produce the rigin D derivatives. According to the authors, increasing chain length reduced the antitumor activity of the rigin D derivatives against HeLa (CCL-2) and MCF-7 cell lines. Conversely, the alkaline substituents with carbon chains containing 5 or 6 C had the most intense inhibitory effects in these cell lines, especially the compound with pent-1-yne substituent (51). Additionally, the presence of Br, N, O, S, carboxylic acid, phenol, furan, or nitrile in the carbon chain led to intermediary activity in relation to the large and the 5 or 6 carbon chain groups. Further evaluation *in vivo* confirmed the antitumor potential of the rigin D derivative with pent-1-yne substituent (4). Moreover, the authors also indicated that a 72% yield was obtained for this compound.

FBA-TPQ (5) is another bioactive alkaloid obtained by chemical synthesis [16]. In order to produce this compound (Figure 7A), the authors reacted a pyrroloiminoquinone derivative (52) [52] with 1-(4-fluorophenyl)methanamine (53) in methanol to generate the intermediary compound (54). Then, this intermediary compound (54) was further reacted with sodium methoxide and methanol in trifluoroacetic acid (TFA) to generate FBA-TPQ (5). A previous experiment from this research group indicated a purity of 99% using this route [53]. A related study carried out by Guimarães et al. [54] reported the chemical synthesis 10-((4,5-dihydrothiazol-2-yl)thio)decan-1-ol (Figure 7B; compound 35). These authors produced this synthetic compound using a two-step reaction. First, 1,10-decanediol (55) reacted with HBr in toluene to generate 10-bromo-decan-1-ol (56) as an intermediary compound. Then, 10-bromo-decan-1-ol (56) was reacted with 2-thiazoline-2-thiol (57) and potassium hydroxide in hydroethanolic solution to produce 10-(4,5-dihydrothiazol-2-yl)thio)decan-1-ol (35) with a yield of 97%.

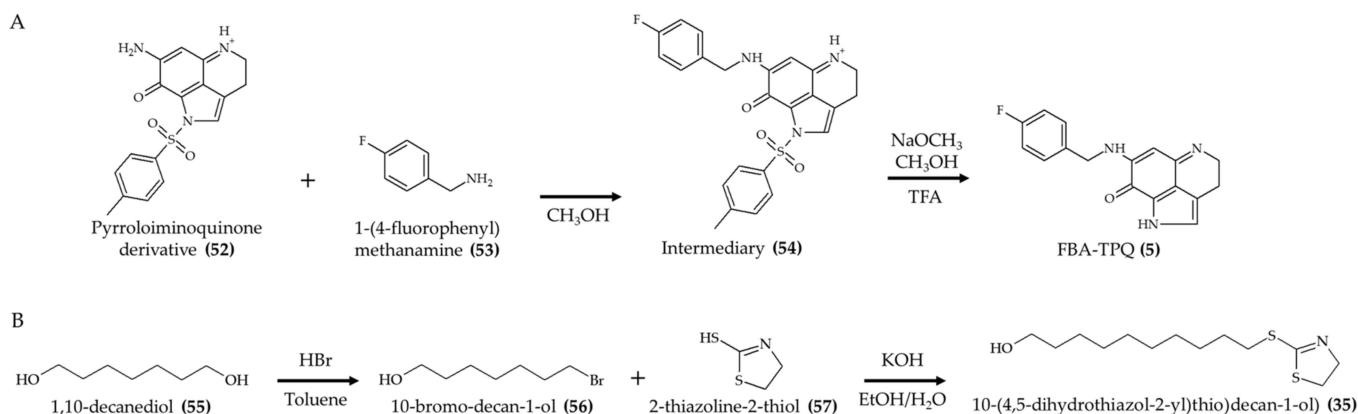


**Figure 7.** Schematic representation of FBA-TPQ (5) (A) and 10-((4,5-dihydrothiazol-2-yl)thio)decan-1-ol (35) (B) syntheses (according to Wang et al. [53] and Guimarães et al. [54], respectively).

The synthesis of neoamphimedine (6) was successfully completed by Li et al. [55]. These authors proposed starting the synthesis with 2,5-dimethoxy-3-nitrobenzoate (58) with Pd/C to produce the intermediate 8 $\alpha$  (Figure 8; compound 59). Subsequently, the intermediate 8 $\alpha$  (59) was treated with Meldrum's acid and trimethyl orthoformate to generate the intermediate 8 $\beta$  (60). Then, the intermediate 8 $\gamma$  (61) was produced via thermal ring closure from compound 8 $\beta$  (60). In the next step, dry dichloromethane and trifluoro-

romethanesulfonic anhydride with dimethyl amino pyridine (as catalyst) were reacted with compound 8 $\gamma$  (61) to generate the intermediate 8 $\delta$  (62). Once this intermediate was obtained, the Stille coupling reaction with trimethyl-(2-nitrophenyl)stannane was carried out using Pd as catalyst to produce the intermediate 8 $\epsilon$  (63). Then, the intermediate 8 $\zeta$  (64) was produced from a two-step reaction: hydrolyses with lithium hydroxide followed by a coupling reaction with methylamino acetaldehyde dimethylacetal. After this step, an acid-catalyzed ring closure was carried out, which produce the mixture of intermediates 8 $\eta$  and 8 $\theta$  (quinone (65) and dimetoxy (66) intermediates, respectively). Finally, the neoamphimedine (6) was produced in a two-step reaction: a reduction reaction catalyzed by Pd followed by oxidative demetallation in the presence of ceramic ammonium nitrate. According to the authors, the final step to produce neoamphimedine (6) had a yield of 46%. It is noteworthy that this described route comprised fewer steps than another study on the production of neoamphimedine (6) published by this research group [56].

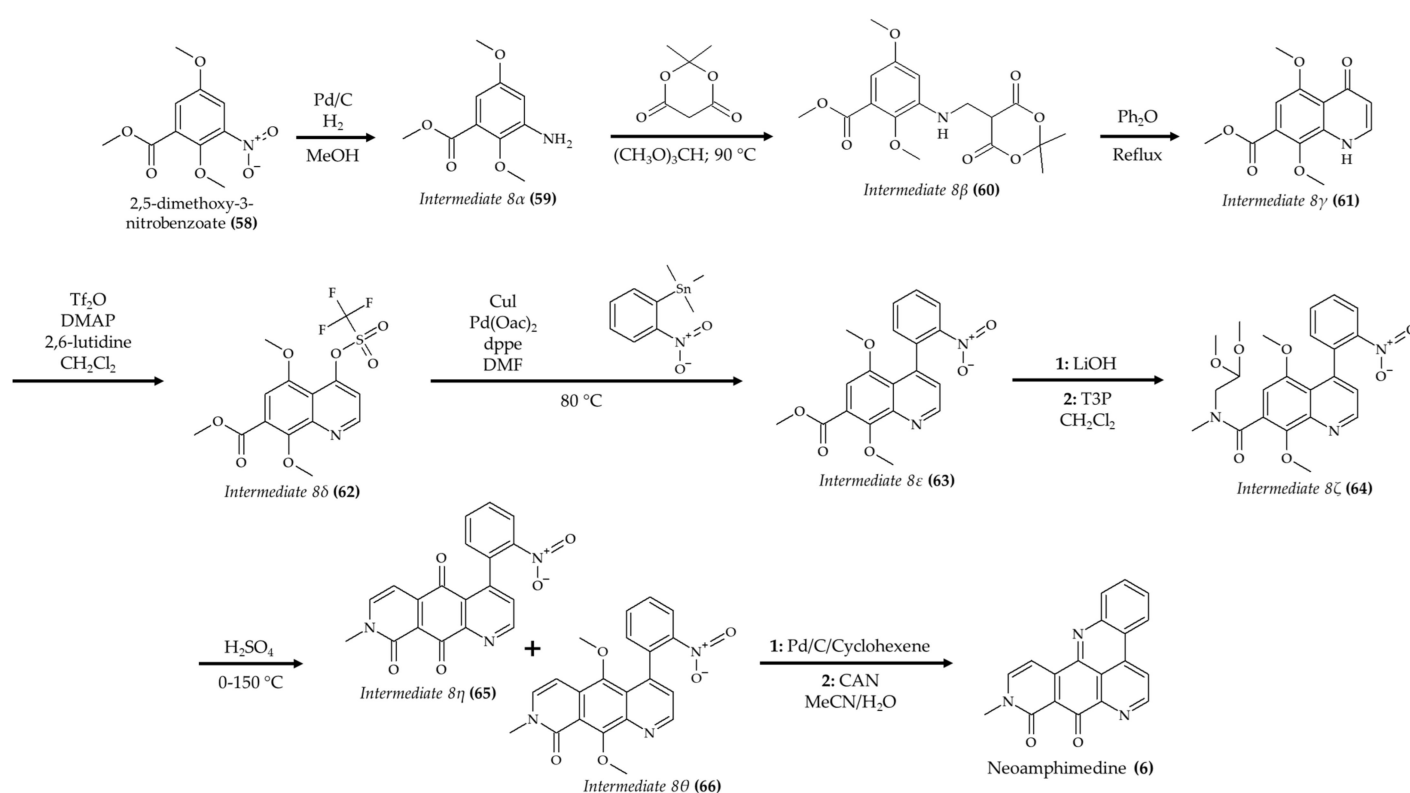


**Figure 8.** Schematic representation of neoamphimedine (6) synthesis (according to Li et al. [55]).

The synthesis of lamellarin 14 (Figure 9; compound 7) was developed by Fukuda et al. [57]. These authors initiated the synthesis by carrying out a six-step reaction using *N*-*boc*-2,5-dibromopyrrole (67) to produce the tetra-substituted pyrrole intermediate 9 $\alpha$  (68) from a previous study [58]. Once this intermediate was obtained, alkylation with bromoacetaldehyde dimethyl acetal at the pyrrole nitrogen was carried out to yield the intermediate 9 $\beta$  (69). Then, the tricyclic compound 9 $\gamma$  (70) was produced via trifluoromethanesulfonic acid (TfOH)-catalyzed cyclization. This was followed by Suzuki–Miyaura coupling with a 2-(methoxymethoxy)aryl boronic acid (71) to produce the intermediate 9 $\delta$  (72). A subsequent direct lactonization of *O*-protected lamellarins was carried out to generate the intermediate 9 $\epsilon$  (73). Once this intermediate was obtained, hydrogenolysis was performed to remove the *O*-benzyl groups and generate the compound 9 $\zeta$  (74). Then, 3-(dimethylamino)propyl chloride was used to produce the compound 9 $\eta$  (75). Finally, the *O*-isopropyl groups were removed to produce lamellarin 14 (7). The authors indicated that the last step of lamellarin 14 (7) synthesis had a quantitative yield.

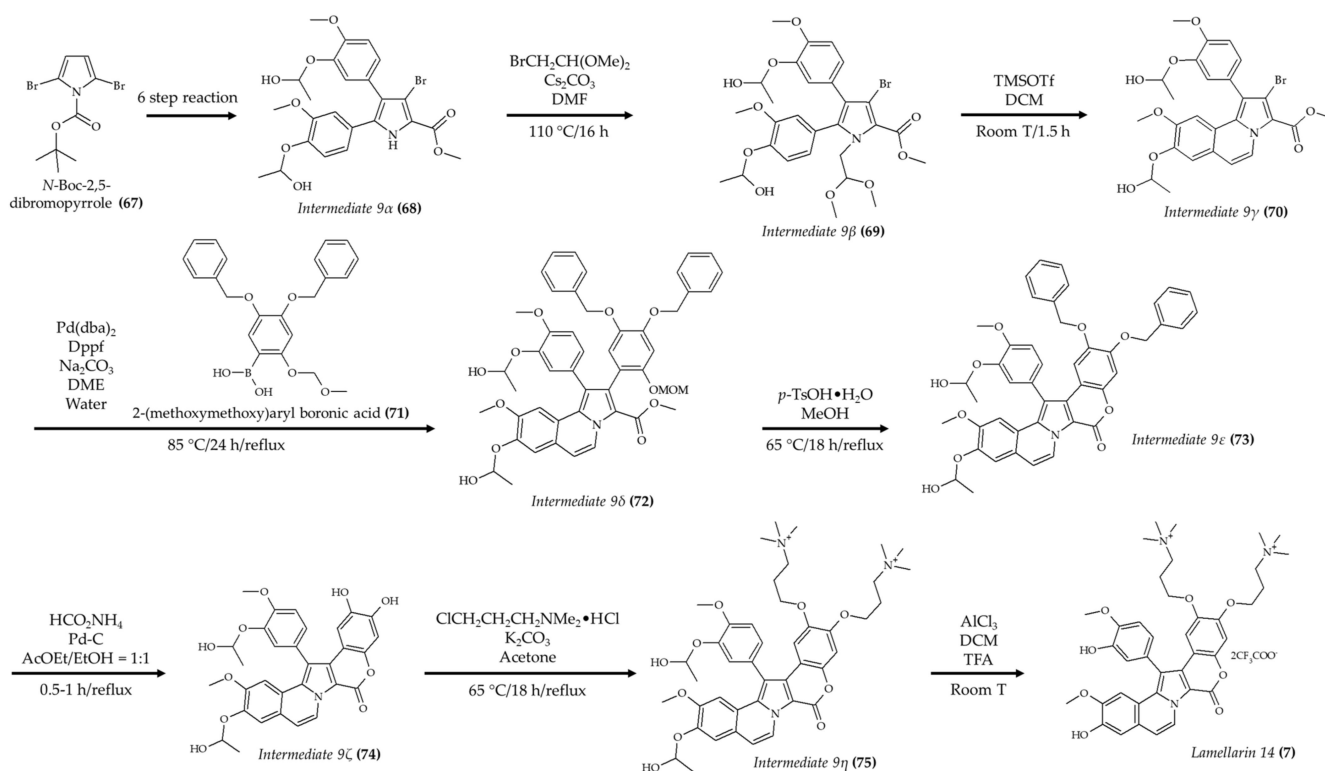


**Figure 9.** Schematic representation of lamellarin 14 (7) synthesis (according to Fukuda et al. [57]).

Manzamine A (10) is another marine alkaloid for which chemical synthesis has been achieved. Jakubec et al. [59] synthesized this marine alkaloid by starting with 2-(bromomethyl)-2-vinyl-1,3-dioxolane (76) to generate the key intermediate 10ε (Figure 10; compound 81). Once the compound 10ε (81) was obtained, a reaction with a selected bicyclic reagent (82) took place to produce intermediate 10ζ (83) in the presence of 18-crown-6 and KHMDS. In the following reaction, formaldehyde and hex-5-en-1-amine were used to produce intermediate 10η (84). Then, the nitro group was removed from this intermediate to produce the compound 10θ (85). Subsequently, the intermediate 10ι (86) was produced by adding HI in the double bond via anti-Markovnikov addition. In the next step, silver nitrite was used to produce intermediate 10κ (87). Then, a selective reduction with DIBAL and toluene was applied to produce the intermediate 10λ (88). After the generation of this intermediate, a new ring was formed by using  $\text{Ti}(\text{OiPr})_4$ ,  $\text{Ph}_2\text{SiH}_2$ , and hexane to produce the compound 10μ (89). Subsequently, the intermediate 10ν (90) was generated by replacing the  $\text{NO}_2$  group with a ketone. Then, a two-step reaction was carried out to add a 3-butenylcerium-derived organometallic substituent and remove the 1,3-dioxolan-2-yl radical from intermediate 10ν (90) and produce compound 10ξ (91). In the subsequent step, the intermediate 10ξ (91) was reacted with TMSOTf in the presence of  $\text{Et}_3\text{N}$  and  $\text{Et}_2\text{O}$  to generate the compound 10o (92). After generating this compound, Commin's reagent, KHMDS, and THF were added to the reaction to produce the intermediate 10π (93), which produced a new ring. Finally, manzamine A (10) was formed (52% yield) with Grubb's first-generation catalyst in the presence of  $\text{CH}_2\text{Cl}_2$  from compound 10π (93). The authors also indicated that a yield of 73% was obtained using this route. Moreover, other authors have provided insights for core structures [60] and additional routes for manzamine A (10) synthesis [61–63].



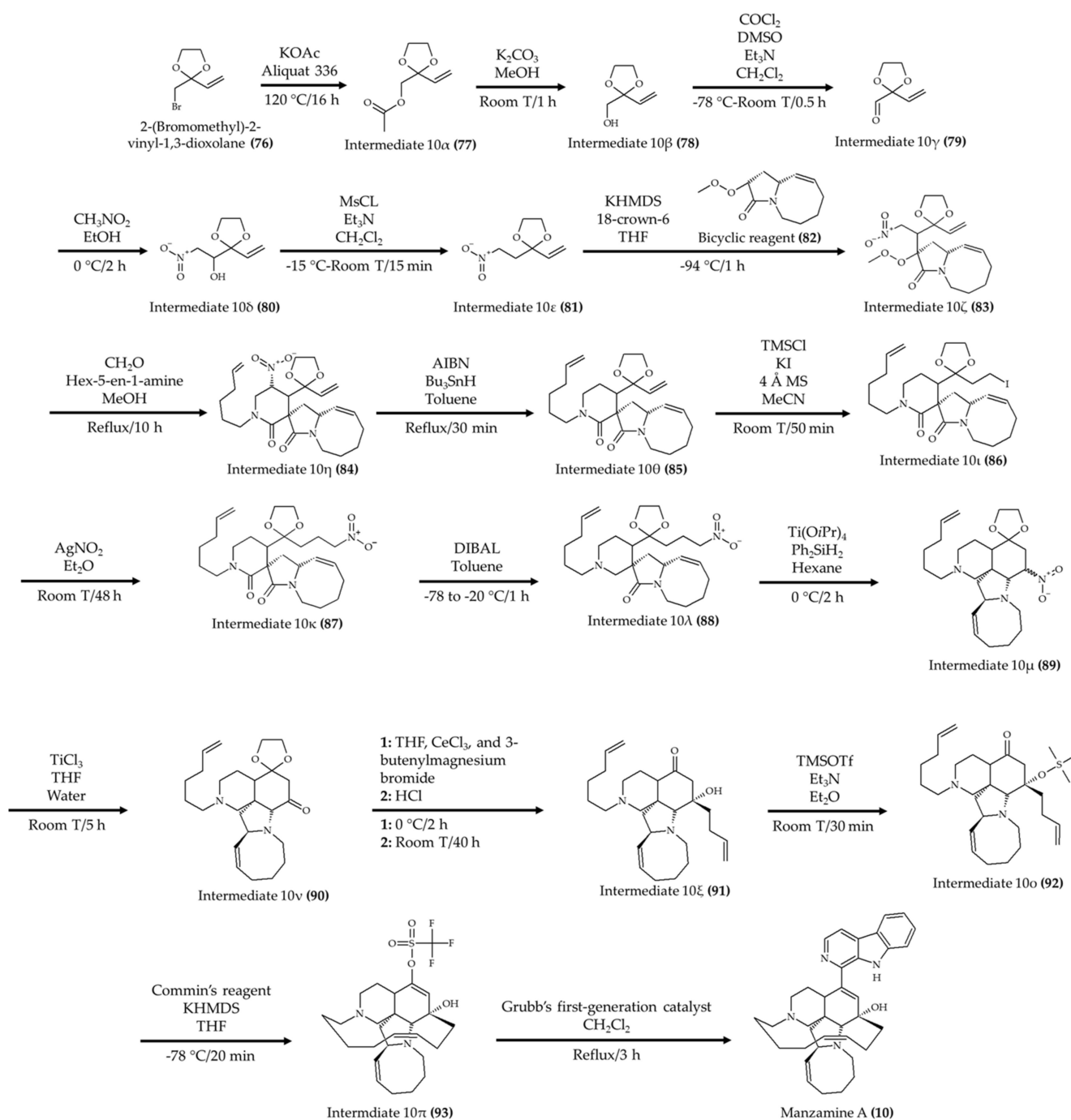


**Figure 10.** Schematic representation of manzamine A (**10**) synthesis (according to Jakubec et al. [59]).

The synthesis of 9-methylfascaplysin (Figure 11A; compound **24**) was carried out using 5-methyltryptamine (**94**) with *o*-bromoacetophenone in the presence of  $\text{I}_2$  and DMSO [28]. Once the intermediary adduct product (**95**) was formed, the reaction mixture was heated to obtain 9-methylfascaplysin (**24**) by closing an inner ring. A synthetic route to produce 3-(3-((12-azidododecyl)oxy)propyl)-1-benzylpyridin-1-ium chloride (Figure 11B; compound **38**) was also proposed by Andrade et al. [40]. In this study, the synthesis was initiated with the reaction between 1,11-undecanediol (**96**) and HBr in toluene to yield 11-bromo-1-undecanol (**97**). Then, this compound was reacted with  $\text{NaN}_3$  in DMSO to produce 11-azide-1-undecanol (**98**). Next, the addition of a methanesulfonyl group in this compound was carried out to generate 11-methanesulfonyl-1-undecanol (**99**). Subsequently, 3-(3-((12-azidododecyl)oxy)propyl)pyridine (**101**) was produced by the reaction

between 11-methanesulfonyl-1-undecanol (**99**) and 3-pyridinepropanol (**100**). Finally, the 3-(3-((12-azidododecyl)oxy)propyl)pyridine (**101**) was reacted with BnCl to generate 3-(3-((12-azidododecyl)oxy)propyl)-1-benzylpyridin-1-ium chloride (**38**).

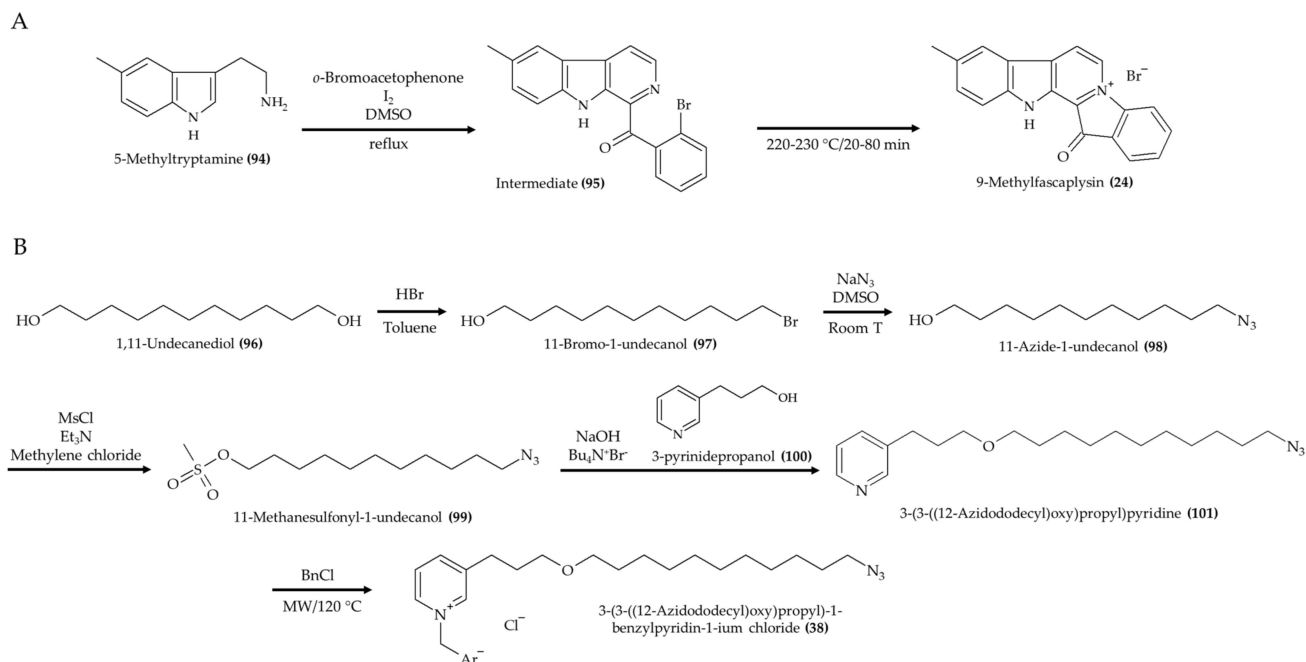


**Figure 11.** Schematic representation of 9-methylfascaplysin (**24**) (**A**) and 3-(3-((12-azidododecyl)oxy)propyl)-1-benzylpyridin-1-ium chloride (**38**) (**B**) syntheses (according to Pan et al. [28] and Andrade et al. [40], respectively).

Other relevant synthetic alkaloids are 3,3'-(pyrimidine-2,5-diyl)bis(5-chloro-1H-indole) (**39**) and 2,6-bis(5-chloro-1H-indol-3-yl)pyridine (**40**) [41]. The synthesis of 3,3'-(pyrimidine-2,5-diyl)bis(5-chloro-1H-indole) (Figure 12A; compound **39**) was possible with a one-pot reaction composed of three steps initiated with 5-chloro-3-iodoindole (**102**). A similar strategy was applied in the generation of 2,6-bis(5-chloro-1H-indol-3-yl)pyridine (Figure 12B; compound **40**) from 5-chloro-3-iodo-1-tosyl-1H-indole (**103**).

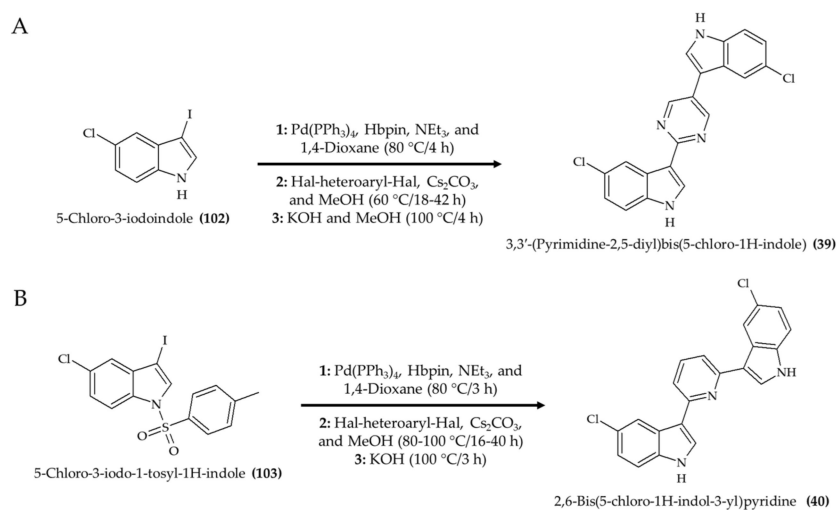


**Figure 12.** Schematic representation of 3,3'-(pyrimidine-2,5-diyl)bis(5-chloro-1H-indole) (**39**) (**A**) and 2,6-bis(5-chloro-1H-indol-3-yl)pyridine (**40**) (**B**) syntheses (according to Rehberg et al. [41]).

Another interesting synthetic marine alkaloid is the grassystatin A analog (**23**) produced by Liu et al. [27]. These authors proposed a building block strategy to produce this compound by generating the key intermediates **13 $\delta$**  (Figure 13A; compound **108**) and **13 $\eta$**  (Figure 13B; compound **112**). In order to obtain the compound **13 $\delta$**  (**108**), the authors initiated the synthesis with dimethyl 5-[methyl(methylsulfonyl)amino]isophthalate (**104**) and carried out a coupling reaction with (R)-1-phenylethylamine to produce the intermediate **13 $\alpha$**  (**105**). Subsequently, a coupling reaction was performed between intermediate **13 $\alpha$**  (**105**) and **13 $\beta$**  (**106**) with preparatory steps (with NaOH in THF/MeOH/H<sub>2</sub>O and with Pd-C, H<sub>2</sub>, and MeOH for compounds **13 $\alpha$**  (**105**) and **13 $\beta$**  (**106**), respectively). Once these preparatory reactions were accomplished, the coupling reaction was carried out with EDC, HOAt, DIEA, and DCM to generate the compound **13 $\gamma$**  (**107**). Then, the key intermediate **13 $\delta$**  (**108**) was produced from compound **13 $\gamma$**  (**107**) in TFA and DCM.

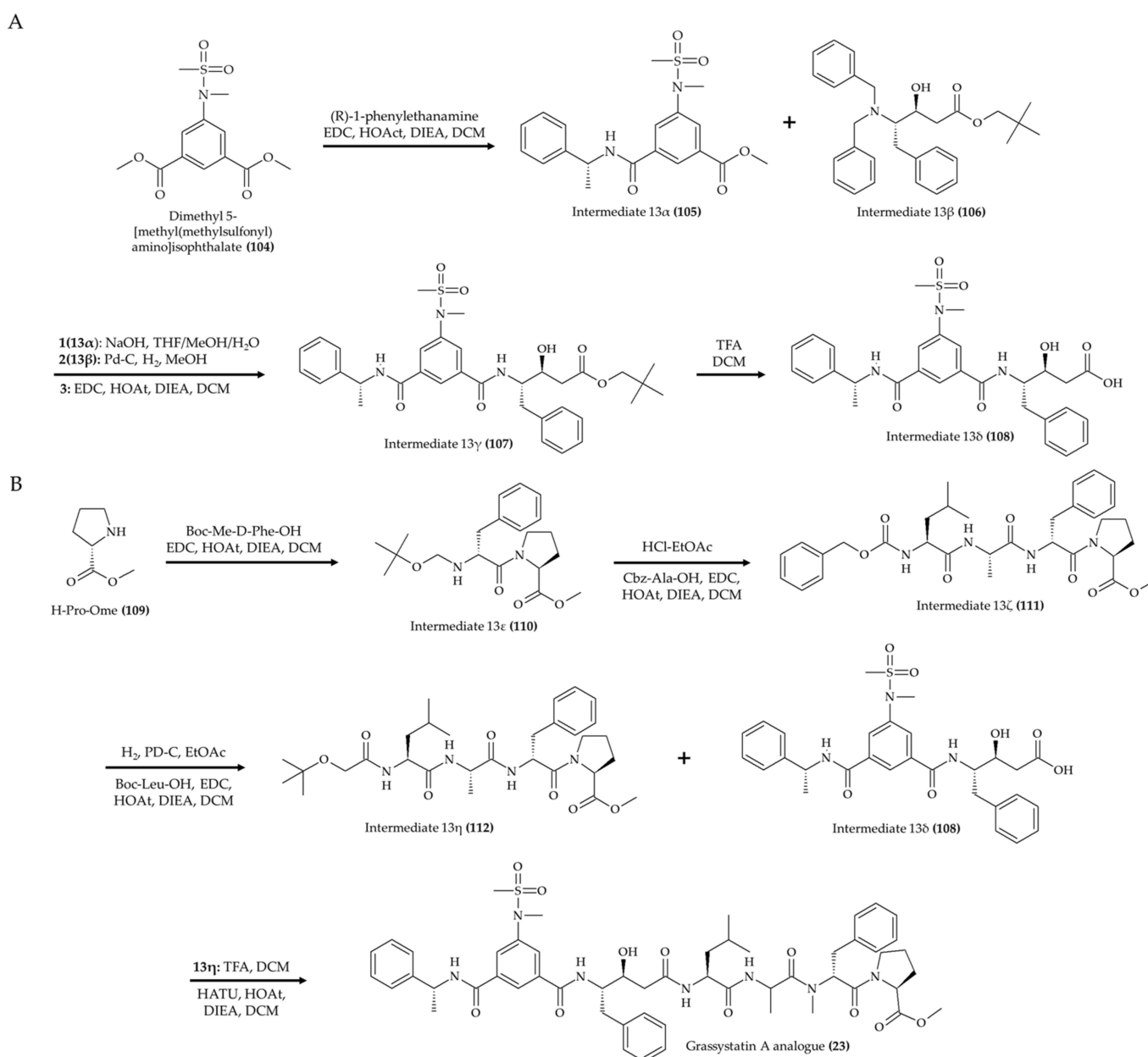


**Figure 13.** Schematic representation of Grassystatin A analog (**23**) (**A,B**) synthesis (according to Liu et al. [27]).

The production of key intermediate 13 $\eta$  (**112**) was initiated with the reaction between H-Pro-OMe (**109**) with Boc-Me-D-Phe-OH in the presence of EDC, HOAt, DIEA, and DCM to produce the intermediate 13 $\epsilon$  (**110**) [27]. In the next step, this intermediate was treated with HCl-EtOAc and then coupled to Cbz-Ala-OH (in EDC, HOAt, DIEA, and DCM) to generate the compound 13 $\zeta$  (**111**). Subsequently, the key intermediate 13 $\eta$  (**112**) was generated from the reaction between intermediate 13 $\zeta$  (**111**) (treated with H<sub>2</sub>, PD-C, and EtOAc) and Boc-Leu-OH (in EDC, HOAt, DIEA, and DCM). Finally, intermediate 13 $\eta$  (**112**) (treated with TFA and DCM) was coupled to intermediate 13 $\delta$  (**108**) in HATU, HOAt, DIEA, and DCM to produce the grassystatin A analog (reaction yield of 60%; compound **23**).

#### 4. Animal Model Context and Further Considerations for Bioactive Marine Alkaloids

The previous sections provide an overview of the current research about the biological effects related to marine alkaloids at the animal level and alternatives to modify their chemical structure. However, it is also important to consider the role of animal models and their application in drug development. Traditionally, animals have been used in the study of diseases and drug development in order to obtain information that cannot be comprehensively determined using *in vitro* methods (cellular and subcellular/molecular tests), such as the efficacy, potential toxicological effects, and pharmacokinetics [9].

Although different animal models can be considered in the study of diseases, such as mice [64], rabbits [65], pigs [66], and fish [67], selecting an appropriate model to study is a complex and multifactorial challenge. Ideally, an animal model should provide a replication of the same elicitors, symptoms, physiological changes, therapeutic responses, resolution mechanisms, and side effects observed in humans. Since it is not possible to carry out an experiment and comply with all these conditions, understanding the similarities and limitations of each animal model is a necessary step to strengthen the progression of *in vitro* data to more complex organisms and the conclusions from these studies [9].

In this line of thought, Denayer et al. [68] discuss these aspects and advise considering multiple aspects for validating an animal model for drug development: species similarity (human > nonhuman primate > nonhuman mammal > nonmammal), complexity of the model (*in vivo* > tissue > cellular > subcellular/molecular), disease simulation (true > complex > pharmacological > no), face validity (more than one core symptom > one core symptom > no), and predictivity (graded for all pharmacology principles > graded for certain pharmacology principles > all or none for certain pharmacology principles > no or not shown).

Another important aspect in animal trials is the humanization of animal models in order to increase the similarities of specific conditions to human physiological characteristics, pathologies, and metabolic processes. The development of mutant strains of animals with specific genetic modifications to match with these necessities in animal studies is the most common approach [69]. Additionally, some specific cases, such as the tumor xenograft in cancer studies, can be cited [70].

To the best of our knowledge, only two animal models have been applied to test marine alkaloids: mice and zebrafish (Tables 1–3). In the case of mice, this animal model has been widely applied for several diseases. Mice are the most widely used animals for disease studies and drug development. Some of the advantages associated with choice are the ease of breeding, availability of many strains, genetic modification, relatively low cost of maintenance, and small quantity of tested compounds [68,71]. Moreover, mice have been used as an animal model for many diseases, such as cancer [72], cardiovascular diseases [73], and seizures [74].

In a similar way, the zebrafish (*Danio rerio*, a teleost species or bony fish) has emerged as a potential animal model in the studies of diseases and drug development. This animal model has relevant molecular and physiological processes that are similar to those observed in humans and can be explored to discover and characterize the biological properties of new drugs such as marine alkaloids. In general, the embryonic, larval, and adult phases of zebrafish have been used in drug discovery. Interesting aspects related to the zebrafish

model are its high fecundity, fast growth, relatively low maintenance cost, small size (either as embryos or adults), fluorescent receptor production, and optical clarity (allowing the visualization of internal organs and structures) [75–77]. Zebrafish have been applied in the context of studying specific diseases such as cancer [78–80], cardiovascular diseases [81], inflammatory diseases [75,76], and neurological disorders and mental health [82].

However, animal models may not provide the whole spectrum of physiological changes associated with a disease [9]. Moreover, each model has limitations that limit or preclude its use. In the case of mice, the limitations are known to be disease- and process-specific due to the long history and widespread utilization of these animals in disease and drug development studies [83,84]. For the zebrafish model, the limitations are mainly related to the respiratory, reproductive, and locomotion systems; small organ size; and the aquatic habitat [85].

An interesting approach to overcome the individual limitations of each animal model is the evaluation using more than one animal model in order to obtain a more comprehensive, detailed, and better replication of a given human disease [68]. For instance, Copmans et al. [26] explored the use of both mice and zebrafish models to test the anti-seizure effect of TMC-120A (21) and TMC-120B (22). The results from both animal models indicate a congruent interpretation of the potential biological effect to manage seizures. Therefore, it is necessary to increase efforts to explore different animal models, whenever possible, by means of combining strengths and reducing the limitations of each animal model in the area of marine alkaloid drug development.

Finally, it is worth commenting that the translation of results and conclusions from animal studies and successful clinical application is another factor that imposes a persistent necessity to improve animal studies. The rate of translation of animal study results to clinical experiments is low, and such studies may not effectively predict the biological effect in humans. Different authors have indicated that less than 10% of all experiments are translated into actual drugs [9,86,87]. In addition, failure to provide the target therapeutic effect in patients at clinical levels is also accompanied by the concern of generation of acute symptoms and side effects not observed at the animal level [9]. The marine alkaloids included in this review can be considered as potential candidates to manage and treat some of the main diseases imposing a heavy burden on our society. Proper and solid information must be generated in order to reduce misinterpretation and the raising of premature expectations in further clinical evaluation.

## 5. Conclusions

The progression of scientific knowledge about the biological effects of marine alkaloids and their derivatives (especially those obtained from chemical synthesis) *in vitro* has been also observed *in vivo*. An increasing number of studies indicate that these compounds can exert beneficial effects in complex organisms such as mice and zebrafish. Although each animal model has its own limitations, both are valuable models to obtain information and improve the knowledge about the protective effects of the mechanisms activated by marine alkaloids and should be seen as complementary models rather than competitive. However, major efforts are still necessary to improve the validation and define the actual role of the zebrafish model in animal drug discovery.

Further experiments *in vivo* should target other relevant diseases such as stroke, respiratory diseases, diabetes, and Alzheimer's disease. The studies in chemical synthesis are also relevant for marine alkaloids in order to obtain active compounds from relatively inactive ones. Additionally, the synthetic production of those compounds with promising effects for clinical trials is also advised in order to circumvent the exploration of natural sources and preserve the marine environment.

**Author Contributions:** Conceptualization, P.E.S.M. and J.M.L.; writing—original draft preparation, P.E.S.M.; writing—review and editing, P.E.S.M., M.P., R.D., C.A.C.-J., A.N., N.W., E.M.F., and J.M.L. All authors have read and agreed to the published version of the manuscript.

**Funding:** This research received no external funding.

**Data Availability Statement:** Data sharing is not applicable to this article.

**Acknowledgments:** Thanks are extended to GAIN (Axencia Galega de Innovación) for supporting this review (grant number IN607A2019/01).

**Conflicts of Interest:** The authors declare no conflict of interest.

## References

- Kemppainen, L.M.; Kemppainen, T.T.; Reippainen, J.A.; Salmenniemi, S.T.; Vuolanto, P.H. Use of complementary and alternative medicine in Europe: Health-related and sociodemographic determinants. *Scand. J. Public Health* **2018**, *46*, 448–455. [[CrossRef](#)]
- Lucas, S.; Leach, M.; Kumar, S. Complementary and alternative medicine utilisation for the management of acute respiratory tract infection in children: A systematic review. *Complement. Ther. Med.* **2018**, *37*, 158–166. [[CrossRef](#)]
- Thomford, N.E.; Senthane, D.A.; Rowe, A.; Munro, D.; Seele, P.; Maroyi, A.; Dzobo, K. Natural products for drug discovery in the 21st century: Innovations for novel drug discovery. *Int. J. Mol. Sci.* **2018**, *19*, 1578. [[CrossRef](#)]
- Altmann, K.H. Drugs from the oceans: Marine natural products as leads for drug discovery. *Chimia* **2017**, *71*, 646–651. [[CrossRef](#)] [[PubMed](#)]
- Netz, N.; Opatz, T. Marine indole alkaloids. *Mar. Drugs* **2015**, *13*, 4814–4914. [[CrossRef](#)]
- Elissawy, A.M.; Dehkordi, E.S.; Mehdinezhad, N.; Ashour, M.L.; Pour, P.M. Cytotoxic alkaloids derived from marine sponges: A comprehensive review. *Biomolecules* **2021**, *11*, 258. [[CrossRef](#)] [[PubMed](#)]
- Souza, C.R.M.; Bezerra, W.P.; Souto, J.T. Marine alkaloids with anti-inflammatory activity: Current knowledge and future perspectives. *Mar. Drugs* **2020**, *18*, 147. [[CrossRef](#)]
- Tempone, A.G.; Pieper, P.; Borborema, S.E.T.; Thevenard, F.; Lago, J.H.G.; Croft, S.L.; Anderson, E.A. Marine alkaloids as bioactive agents against protozoal neglected tropical diseases and malaria. *Nat. Prod. Rep.* **2021**. [[CrossRef](#)]
- Mak, I.W.Y.; Evaniew, N.; Ghert, M. Lost in translation: Animal models and clinical trials in cancer treatment. *Am. J. Transl. Res.* **2014**, *6*, 114–118.
- Choi, C.; Cho, Y.; Son, A.; Shin, S.W.; Lee, Y.J.; Park, H.C. Therapeutic potential of (-)-Agelamide D, a diterpene alkaloid from the marine sponge *Agelas* sp., as a natural radiosensitizer in hepatocellular carcinoma models. *Mar. Drugs* **2020**, *18*, 500. [[CrossRef](#)] [[PubMed](#)]
- Wang, L.; Huang, Y.; Huang, C.H.; Yu, J.C.; Zheng, Y.C.; Chen, Y.; She, Z.G.; Yuan, J. A Marine Alkaloid, Ascomylactam A, suppresses lung tumorigenesis via inducing cell cycle G1/S arrest through ROS/Akt/Rb pathway. *Mar. Drugs* **2020**, *18*, 494. [[CrossRef](#)]
- Sharma, S.; Guru, S.K.; Manda, S.; Kumar, A.; Mintoo, M.J.; Prasad, V.D.; Sharma, P.R.; Mondhe, D.M.; Bharate, S.B.; Bhushan, S. A marine sponge alkaloid derivative 4-chloro faspalylin inhibits tumor growth and VEGF mediated angiogenesis by disrupting PI3K/Akt/mTOR signaling cascade. *Chem. Biol. Interact.* **2017**, *275*, 47–60. [[CrossRef](#)] [[PubMed](#)]
- Medellin, D.C.; Zhou, Q.; Scott, R.; Hill, R.M.; Frail, S.K.; Dasari, R.; Ontiveros, S.J.; Pelly, S.C.; Van Otterlo, W.A.L.; Betancourt, T.; et al. Novel microtubule-targeting 7-Deazahypoxanthines derived from marine alkaloid rigidins with potent in vitro and in vivo anticancer activities. *J. Med. Chem.* **2016**, *59*, 480–485. [[CrossRef](#)] [[PubMed](#)]
- Wang, W.; Rayburn, E.R.; Velu, S.E.; Nadkarni, D.H.; Murugesan, S.; Zhang, R. In vitro and in vivo anticancer activity of novel synthetic makaluvamine analogues. *Clin. Cancer Res.* **2009**, *15*, 3511–3518. [[CrossRef](#)] [[PubMed](#)]
- Chen, T.; Xu, Y.; Guo, H.; Liu, Y.; Hu, P.; Yang, X.; Li, X.; Ge, S.; Velu, S.E.; Nadkarni, D.H.; et al. Experimental therapy of ovarian cancer with synthetic makaluvamine analog: In Vitro and In vivo anticancer activity and molecular mechanisms of action. *PLoS ONE* **2011**, *6*, e20729. [[CrossRef](#)]
- Zhang, X.; Xu, H.; Zhang, X.; Voruganti, S.; Murugesan, S.; Nadkarni, D.H.; Velu, S.E.; Wang, M.H.; Wang, W.; Zhang, R. Preclinical evaluation of anticancer efficacy and pharmacological properties of FBA-TPQ, a novel synthetic Makaluvamine analog. *Mar. Drugs* **2012**, *10*, 1138–1155. [[CrossRef](#)]
- Marshall, K.M.; Matsumoto, S.S.; Holden, J.A.; Concepción, G.P.; Tasdemir, D.; Ireland, C.M.; Barrows, L.R. The anti-neoplastic and novel topoisomerase II-mediated cytotoxicity of neoamphimedine, a marine pyridoacridine. *Biochem. Pharmacol.* **2003**, *66*, 447–458. [[CrossRef](#)]
- Nishiya, N.; Oku, Y.; Ishikawa, C.; Fukuda, T.; Dan, S.; Mashima, T.; Ushijima, M.; Furukawa, Y.; Sasaki, Y.; Otsu, K.; et al. Lamellarin 14, a derivative of marine alkaloids, inhibits the T790M/C797S mutant epidermal growth factor receptor. *Cancer Sci.* **2021**, *112*, 1963–1974. [[CrossRef](#)]
- Florea, C.; Schneckeburger, M.; Lee, J.Y.; Kim, K.R.; Mazumder, A.; Song, S.; Kim, J.M.; Grandjette, C.; Kim, J.G.; Yoon, A.Y.; et al. Discovery and characterization of Isofistularin-3, a marine brominated alkaloid, as a new DNA demethylating agent inducing cell cycle arrest and sensitization to TRAIL in cancer cells. *Oncotarget* **2016**, *7*, 24027–24049. [[CrossRef](#)] [[PubMed](#)]
- Roel, M.; Rubiolo, J.A.; Guerra-Varela, J.; Silva, S.B.L.; Thomas, O.P.; Cabezas-Sainz, P.; Sánchez, L.; López, R.; Botana, L.M. Marine guanidine alkaloids crambescidins inhibit tumor growth and activate intrinsic apoptotic signaling inducing tumor regression in a colorectal carcinoma zebrafish xenograft model. *Oncotarget* **2016**, *7*, 83071–83087. [[CrossRef](#)] [[PubMed](#)]

21. Eguchi, K.; Fujiwara, Y.; Hayashida, A.; Horlad, H.; Kato, H.; Rotinsulu, H.; Losung, F.; Mangindaan, R.E.P.; De Voogd, N.J.; Takeya, M.; et al. Manzamine A, a marine-derived alkaloid, inhibits accumulation of cholesterol ester in macrophages and suppresses hyperlipidemia and atherosclerosis *in vivo*. *Bioorganic Med. Chem.* **2013**, *21*, 3831–3838. [[CrossRef](#)]
22. Yan, T.; Wu, W.; Su, T.; Chen, J.; Zhu, Q.; Zhang, C.; Wang, X.; Bao, B. Effects of a novel marine natural product: Pyrano indolone alkaloid fibrinolytic compound on thrombolysis and hemorrhagic activities *in vitro* and *in vivo*. *Arch. Pharm. Res.* **2015**, *38*, 1530–1540. [[CrossRef](#)] [[PubMed](#)]
23. Fan, Y.Q.; Li, P.H.; Chao, Y.X.; Chen, H.; Du, N.; He, Q.X.; Liu, K.C. Alkaloids with cardiovascular effects from the marine-derived fungus *Penicillium expansum* Y32. *Mar. Drugs* **2015**, *13*, 6489–6504. [[CrossRef](#)]
24. Li, P.; Zhang, M.; Li, H.; Wang, R.; Hou, H.; Li, X.; Liu, K.; Chen, H. New prenylated indole homodimeric and pteridine alkaloids from the marine-derived fungus *Aspergillus austroafricanus* Y32-2. *Mar. Drugs* **2021**, *19*, 98. [[CrossRef](#)] [[PubMed](#)]
25. Li, T.; Tang, X.; Luo, X.; Wang, Q.; Liu, K.; Zhang, Y.; De Voogd, N.J.; Yang, J.; Li, P.; Li, G. Agelanemoechine, a dimeric bromopyrrole alkaloid with a pro-angiogenic effect from the south China sea sponge *Agelas nemoechinata*. *Org. Lett.* **2019**, *21*, 9483–9486. [[CrossRef](#)] [[PubMed](#)]
26. Copmans, D.; Kildgaard, S.; Rasmussen, S.A.; Ślezak, M.; Dirx, N.; Partoens, M.; Esguerra, C.V.; Crawford, A.D.; Larsen, T.O.; De Witte, P.A.M. Zebrafish-based discovery of antiseizure compounds from the north sea: Isoquinoline alkaloids TMC-120A and TMC-120B. *Mar. Drugs* **2019**, *17*, 607. [[CrossRef](#)]
27. Liu, Y.; Zhang, W.; Li, L.; Salvador, L.A.; Chen, T.; Chen, W.; Felsenstein, K.M.; Ladd, T.B.; Price, A.R.; Golde, T.E.; et al. Cyanobacterial peptides as a prototype for the design of potent  $\beta$ -secretase inhibitors and the development of selective chemical probes for other aspartic proteases. *J. Med. Chem.* **2012**, *55*, 10749–10765. [[CrossRef](#)]
28. Pan, H.; Qiu, H.; Zhang, K.; Zhang, P.; Liang, W.; Yang, M.; Mou, C.; Lin, M.; He, M.; Xiao, X.; et al. Fascaplysin derivatives are potent multitarget agents against Alzheimer's disease: *In vitro* and *in vivo* evidence. *ACS Chem. Neurosci.* **2019**. [[CrossRef](#)]
29. Zhang, C.; Hu, L.; Liu, D.; Huang, J.; Lin, W. Circumdatin D exerts neuroprotective effects by attenuating LPS-induced pro-inflammatory responses and downregulating acetylcholinesterase activity *in vitro* and *in vivo*. *Front. Pharmacol.* **2020**, *11*, 760. [[CrossRef](#)]
30. Kochanowska-Karamyan, A.J.; Araujo, H.C.; Zhang, X.; El-Alfy, A.; Carvalho, P.; Avery, M.A.; Holmbo, S.D.; Magolan, J.; Hamann, M.T. Isolation and synthesis of veranamine, an antidepressant lead from the marine sponge *Verongula rigida*. *J. Nat. Prod.* **2020**, *83*, 1092–1098. [[CrossRef](#)]
31. Cesário, H.P.S.F.; Silva, F.C.O.; Ferreira, M.K.A.; de Menezes, J.E.S.A.; dos Santos, H.S.; Nogueira, C.E.S.; de L. Silva, K.S.B.; Hajdu, E.; Silveira, E.R.; Pessoa, O.D.L. Anxiolytic-like effect of brominated compounds from the marine sponge *Aplysina fulva* on adult zebrafish (*Danio rerio*): Involvement of the GABAergic system. *Neurochem. Int.* **2021**, *146*, 105021. [[CrossRef](#)]
32. Ahmad, T.B.; Rudd, D.; Benkendorff, K.; Mahdi, L.K.; Pratt, K.A.; Dooley, L.; Wei, C.; Kotiw, M. Brominated indoles from a marine mollusc inhibit inflammation in a murine model of acute lung injury. *PLoS ONE* **2017**, *12*, e0186904. [[CrossRef](#)] [[PubMed](#)]
33. Shu, Z.; Liu, Q.; Xing, C.; Zhang, Y.; Zhou, Y.; Zhang, J.; Liu, H.; Cao, M.; Yang, X.; Liu, G. Viridicatol isolated from deep-sea *Penicillium Griseofulvum* alleviates anaphylaxis and repairs the intestinal barrier in mice by suppressing mast cell activation. *Mar. Drugs* **2020**, *18*, 517. [[CrossRef](#)] [[PubMed](#)]
34. Lucena, A.M.M.; Souza, C.R.M.; Jales, J.T.; Guedes, P.M.M.; De Miranda, G.E.C.; de Moura, A.M.A.; Araújo-Júnior, J.X.; Nascimento, G.J.; Scortecchi, K.C.; Santos, B.V.O.; et al. The bisindole alkaloid caulerpipin, from seaweeds of the genus *Caulerpa*, attenuated colon damage in murine colitis model. *Mar. Drugs* **2018**, *16*, 318. [[CrossRef](#)]
35. Gui, Y.H.; Liu, L.; Wu, W.; Zhang, Y.; Jia, Z.L.; Shi, Y.P.; Kong, H.T.; Liu, K.C.; Jiao, W.H.; Lin, H.W. Discovery of nitrogenous sesquiterpene quinone derivatives from sponge *Dysidea septosa* with anti-inflammatory activity *in vivo* zebrafish model. *Bioorg. Chem.* **2020**, *94*, 103435. [[CrossRef](#)] [[PubMed](#)]
36. Davis, R.A.; Buchanan, M.S.; Duffy, S.; Avery, V.M.; Charman, S.A.; Charman, W.N.; White, K.L.; Shackelford, D.M.; Edstein, M.D.; Andrews, K.T.; et al. Antimalarial activity of pyrroloiminoquinones from the Australian marine sponge *Zyzzya* sp. *J. Med. Chem.* **2012**, *55*, 5851–5858. [[CrossRef](#)]
37. Da Silva, M.G.; Cardoso, J.F.; Perasoli, F.B.; Branquinho, R.T.; Mourão, R.S.; Tavares, H.D.S.; Xocaira, M.L.C.T.; Guimarães, D.S.M.; Viana, G.H.R.; Varotti, F.D.P.; et al. Nanoemulsion composed of 10-(4,5-dihydrothiazol-2-yl)thio)decan-1-ol, a synthetic analog of 3-alkylpyridine marine alkaloid: Development, characterization, and antimalarial activity. *Eur. J. Pharm. Sci.* **2020**, *151*, 105382. [[CrossRef](#)] [[PubMed](#)]
38. Mani, L.; Petek, S.; Valentin, A.; Chevalley, S.; Folcher, E.; Aalbersberg, W.; Debitus, C. The *in vivo* anti-plasmodial activity of haliclonaclamine A, an alkaloid from the marine sponge, *Haliclona* sp. *Nat. Prod. Res.* **2011**, *25*, 1923–1930. [[CrossRef](#)] [[PubMed](#)]
39. Pech-Puch, D.; Pérez-Povedano, M.; Martínez-Guitián, M.; Lasarte-Monterrubio, C.; Vázquez-Ucha, J.C.; Bou, G.; Rodríguez, J.; Beceiro, A.; Jimenez, C. *In vitro* and *in vivo* assessment of the efficacy of bromoageliferin, an alkaloid isolated from the sponge *Agelas dilatata*, against *Pseudomonas aeruginosa*. *Mar. Drugs* **2020**, *18*, 326. [[CrossRef](#)] [[PubMed](#)]
40. Andrade, J.T.; Lima, W.G.; Sousa, J.F.; Saldanha, A.A.; De Sá, N.P.; Morais, F.B.; Prates Silva, M.K.; Ribeiro Viana, G.H.; Johann, S.; Soares, A.C.; et al. Design, synthesis, and biodistribution studies of new analogues of marine alkaloids: Potent *in vitro* and *in vivo* fungicidal agents against *Candida* spp. *Eur. J. Med. Chem.* **2021**, *210*, 113048. [[CrossRef](#)]
41. Rehberg, N.; Sommer, G.A.; Drießen, D.; Kruppa, M.; Adeniyi, E.T.; Chen, S.; Wang, L.; Wolf, K.; Tasch, B.O.A.; Ioerger, T.R.; et al. Nature-inspired (di)azine-bridged bisindole alkaloids with potent antibacterial *in vitro* and *in vivo* efficacy against methicillin-resistant *Staphylococcus aureus*. *J. Med. Chem.* **2020**, *63*, 12623–12641. [[CrossRef](#)]



42. Wang, Q.; Chen, D.; Jin, H.; Ye, Z.; Wang, C.; Chen, K.; Kuek, V.; Xu, K.; Qiu, H.; Chen, P.; et al. Hymenialdisine: A marine natural product that acts on both osteoblasts and osteoclasts and prevents estrogen-dependent bone loss in mice. *J. Bone Miner. Res.* **2020**, *35*, 1582–1596. [[CrossRef](#)]
43. Carlile, G.W.; Keyzers, R.A.; Teske, K.A.; Robert, R.; Williams, D.E.; Lington, R.G.; Gray, C.A.; Centko, R.M.; Yan, L.; Anjos, S.M.; et al. Correction of F508del-CFTR trafficking by the sponge alkaloid latonduine is modulated by interaction with PARP. *Chem. Biol.* **2012**, *19*, 1288–1299. [[CrossRef](#)] [[PubMed](#)]
44. Jiao, W.H.; Li, J.; Zhang, M.M.; Cui, J.; Gui, Y.H.; Zhang, Y.; Li, J.Y.; Liu, K.C.; Lin, H.W. Frondoplysins A and B, unprecedented terpene-alkaloid bioconjugates from *Dysidea frondosa*. *Org. Lett.* **2019**, *21*, 6190–6193. [[CrossRef](#)] [[PubMed](#)]
45. Ballane, G.; Cauley, J.A.; Luckey, M.M.; El-Hajj Fuleihan, G. Worldwide prevalence and incidence of osteoporotic vertebral fractures. *Osteoporos. Int.* **2017**, *28*, 1531–1542. [[CrossRef](#)] [[PubMed](#)]
46. Yao, H.; Liu, J.; Xu, S.; Zhu, Z.; Xu, J. The structural modification of natural products for novel drug discovery. *Expert Opin. Drug Discov.* **2017**, *12*, 121–140. [[CrossRef](#)]
47. Lam, K.S. New aspects of natural products in drug discovery. *Trends Microbiol.* **2007**, *15*, 279–289. [[CrossRef](#)]
48. Chen, M.; Shao, C.L.; Fu, X.M.; Xu, R.F.; Zheng, J.J.; Zhao, D.L.; She, Z.G.; Wang, C.Y. Bioactive indole alkaloids and phenyl ether derivatives from a marine-derived *Aspergillus* sp. fungus. *J. Nat. Prod.* **2013**, *76*, 547–553. [[CrossRef](#)]
49. Lyakhova, I.A.; Bryukhovetsky, I.S.; Kudryavtsev, I.V.; Khotimchenko, Y.S.; Zhidkov, M.E.; Kantemirov, A.V. Antitumor activity of faspachysin derivatives on glioblastoma model in vitro. *Bull. Exp. Biol. Med.* **2018**, *164*, 666–672. [[CrossRef](#)]
50. Parra, L.L.L.; Bertonha, A.F.; Severo, I.R.M.; Aguiar, A.C.C.; De Souza, G.E.; Oliva, G.; Guido, R.V.C.; Grazzia, N.; Costa, T.R.; Miguel, D.C.; et al. Isolation, derivative synthesis, and structure-activity relationships of antiparasitic bromopyrrole alkaloids from the marine sponge *Tedania brasiliensis*. *J. Nat. Prod.* **2018**, *81*, 188–202. [[CrossRef](#)]
51. Zheng, L.; Gao, T.; Ge, Z.; Ma, Z.; Xu, J.; Ding, W.; Shen, L. Design, synthesis and structure-activity relationship studies of glycosylated derivatives of marine natural product Lamellarin D. *Eur. J. Med. Chem.* **2021**, *214*, 113226. [[CrossRef](#)]
52. Shinkre, B.A.; Raisch, K.P.; Fan, L.; Velu, S.E. Analogs of the marine alkaloid makaluvamines: Synthesis, topoisomerase II inhibition, and anticancer activity. *Bioorganic Med. Chem. Lett.* **2007**, *17*, 2890–2893. [[CrossRef](#)]
53. Wang, F.; Ezell, S.J.; Zhang, Y.; Wang, W.; Rayburn, E.R.; Nadkarni, D.H.; Murugesan, S.; Velu, S.E.; Zhang, R. FBA-TPQ, a novel marine-derived compound as experimental therapy for prostate cancer. *Invest. New Drugs* **2010**, *28*, 234–241. [[CrossRef](#)] [[PubMed](#)]
54. Guimarães, D.S.M.; de Sousa Luz, L.S.; do Nascimento, S.B.; Silva, L.R.; de Miranda Martins, N.R.; de Almeida, H.G.; de Souza Reis, V.; Maluf, S.E.C.; Budu, A.; Marinho, J.A.; et al. Improvement of antimalarial activity of a 3-alkylpyridine alkaloid analog by replacing the pyridine ring to a thiazole-containing heterocycle: Mode of action, mutagenicity profile, and Caco-2 cell-based permeability. *Eur. J. Pharm. Sci.* **2019**, *138*, 105015. [[CrossRef](#)]
55. Li, L.; Abraham, A.D.; Zhou, Q.; Ali, H.; O'Brien, J.V.; Hamill, B.D.; Arcaroli, J.J.; Messersmith, W.A.; LaBarbera, D.V. An improved high yield total synthesis and cytotoxicity study of the marine alkaloid neoamphimedine: An ATP-competitive inhibitor of topoisomerase II $\alpha$  and potent anticancer agent. *Mar. Drugs* **2014**, *12*, 4833–4850. [[CrossRef](#)]
56. LaBarbera, D.V.; Bugni, T.S.; Ireland, C.M. The total synthesis of neoamphimedine. *J. Org. Chem.* **2007**, *72*, 8501–8505. [[CrossRef](#)] [[PubMed](#)]
57. Fukuda, T.; Umeki, T.; Tokushima, K.; Xiang, G.; Yoshida, Y.; Ishibashi, F.; Oku, Y.; Nishiya, N.; Uehara, Y.; Iwao, M. Design, synthesis, and evaluation of A-ring-modified lamellarin N analogues as noncovalent inhibitors of the EGFR T790M/L858R mutant. *Bioorganic Med. Chem.* **2017**, *25*, 6563–6580. [[CrossRef](#)]
58. Komatsubara, M.; Umeki, T.; Fukuda, T.; Iwao, M. Modular synthesis of lamellarins via regioselective assembly of 3,4,5-differentially arylated pyrrole-2-carboxylates. *J. Org. Chem.* **2014**, *79*, 529–537. [[CrossRef](#)] [[PubMed](#)]
59. Jakubec, P.; Hawkins, A.; Felzmann, W.; Dixon, D.J. Total synthesis of manzamine A and related alkaloids. *J. Am. Chem. Soc.* **2012**, *134*, 17482–17485. [[CrossRef](#)]
60. Martin, S.F.; Humphrey, J.M.; Ali, A.; Hillier, M.C. Enantioselective total syntheses of ircinal A and related manzamine alkaloids. *J. Am. Chem. Soc.* **1999**, *121*, 866–867. [[CrossRef](#)]
61. Winkler, J.D.; Axten, J.M. The first total syntheses of ircinol A, ircinal A, and manzamines A and D. *J. Am. Chem. Soc.* **1998**, *120*, 6425–6426. [[CrossRef](#)] [[PubMed](#)]
62. Humphrey, J.M.; Liao, Y.; Ali, A.; Rein, T.; Wong, Y.L.; Chen, H.J.; Courtney, A.K.; Martin, S.F. Enantioselective total syntheses of manzamine A and related alkaloids. *J. Am. Chem. Soc.* **2002**, *124*, 8584–8592. [[CrossRef](#)]
63. Toma, T.; Kita, Y.; Fukuyama, T. Total synthesis of (+)-Manzamine A. *J. Am. Chem. Soc.* **2010**, *132*, 10233–10235. [[CrossRef](#)] [[PubMed](#)]
64. Kapourchali, F.R.; Surendiran, G.; Chen, L.; Uitz, E.; Bahadori, B.; Moghadasian, M.H. Animal models of atherosclerosis. *World J. Clin. Cases WJCC* **2014**, *2*, 126–132. [[CrossRef](#)] [[PubMed](#)]
65. Fan, J.; Kitajima, S.; Watanabe, T.; Xu, J.; Zhang, J.; Liu, E.; Chen, Y.E. Rabbit models for the study of human atherosclerosis: From pathophysiological mechanisms to translational medicine. *Pharmacol. Ther.* **2015**, *146*, 104–119. [[CrossRef](#)] [[PubMed](#)]
66. Fan, N.; Lai, L. Genetically modified pig models for human diseases. *J. Genet. Genomics* **2013**, *40*, 67–73. [[CrossRef](#)] [[PubMed](#)]
67. Kirla, K.T.; Erhart, C.; Groh, K.J.; Stadnicka-Michalak, J.; Eggen, R.I.L.; Schirmer, K.; Kraemer, T. Zebrafish early life stages as alternative model to study ‘designer drugs’: Concordance with mammals in response to opioids. *Toxicol. Appl. Pharmacol.* **2021**, *419*, 115483. [[CrossRef](#)] [[PubMed](#)]



68. Denayer, T.; Stöhrn, T.; Van Roy, M. Animal models in translational medicine: Validation and prediction. *New Horizons Transl. Med.* **2014**, *2*, 5–11. [[CrossRef](#)]
69. McGonigle, P.; Ruggeri, B. Animal models of human disease: Challenges in enabling translation. *Biochem. Pharmacol.* **2014**, *87*, 162–171. [[CrossRef](#)]
70. Jung, J. Human tumor xenograft models for preclinical assessment of anticancer drug development. *Toxicol. Res.* **2014**, *30*, 1–5. [[CrossRef](#)]
71. Getz, G.S.; Reardon, C.A. Animal models of Atherosclerosis. *Arterioscler. Thromb. Vasc. Biol.* **2012**, *32*, 1104–1115. [[CrossRef](#)]
72. Teng, M.W.L.; Galon, J.; Fridman, W.H.; Smyth, M.J. From mice to humans: Developments in cancer immunoediting. *J. Clin. Invest.* **2015**, *125*, 3338–3346. [[CrossRef](#)]
73. Camacho, P.; Fan, H.; Liu, Z.; He, J.Q. Small mammalian animal models of heart disease. *Am. J. Cardiovasc. Dis.* **2016**, *6*, 70–80. [[PubMed](#)]
74. Löscher, W.; Ferland, R.J.; Ferraro, T.N. The relevance of inter- and intrastrain differences in mice and rats and their implications for models of seizures and epilepsy. *Epilepsy Behav.* **2017**, *73*, 214–235. [[CrossRef](#)]
75. Xie, Y.; Meijer, A.H.; Schaaf, M.J.M. Modeling inflammation in zebrafish for the development of anti-inflammatory drugs. *Front. Cell Dev. Biol.* **2021**, *8*, 620984. [[CrossRef](#)]
76. Zandrea, R.; Bonan, C.D.; Campos, M.M. Zebrafish as a model for inflammation and drug discovery. *Drug Discov. Today* **2020**, *25*, 2201–2211. [[CrossRef](#)]
77. Brown, H.K.; Schiavone, K.; Tazzyman, S.; Heymann, D.; Chico, T.J.A. Zebrafish xenograft models of cancer and metastasis for drug discovery. *Expert Opin. Drug Discov.* **2017**, *12*, 379–389. [[CrossRef](#)] [[PubMed](#)]
78. Nathan, J.; Kannan, R.R. Antiangiogenic molecules from marine actinomycetes and the importance of using zebrafish model in cancer research. *Heliyon* **2020**, *6*, e05662. [[CrossRef](#)] [[PubMed](#)]
79. Hason, M.; Bartůněk, P. Zebrafish models of cancer—new insights on modeling human cancer in a non-mammalian vertebrate. *Genes* **2019**, *10*, 935. [[CrossRef](#)] [[PubMed](#)]
80. Letrado, P.; De Miguel, I.; Lamberto, I.; Díez-Martínez, R.; Oyarzabal, J. Zebrafish: Speeding up the cancer drug discovery process. *Cancer Res.* **2018**, *78*, 6048–6058. [[CrossRef](#)]
81. Giardoglou, P.; Beis, D. On zebrafish disease models and matters of the heart. *Biomedicines* **2019**, *7*, 15. [[CrossRef](#)]
82. Fontana, B.D.; Mezzomo, N.J.; Kalueff, A.V.; Rosemberg, D.B. The developing utility of zebrafish models of neurological and neuropsychiatric disorders: A critical review. *Exp. Neurol.* **2018**, *299*, 157–171. [[CrossRef](#)] [[PubMed](#)]
83. Cekanova, M.; Rathore, K. Animal models and therapeutic molecular targets of cancer: Utility and limitations. *Drug Des. Devel. Ther.* **2014**, *8*, 1911–1922. [[CrossRef](#)]
84. Turner, A.S. Animal models of osteoporosis - Necessity and limitations. *Eur. Cells Mater.* **2001**, *1*, 66–81. [[CrossRef](#)] [[PubMed](#)]
85. Gut, P.; Reischauer, S.; Stainier, D.Y.R.; Arnaout, R. Little fish, big data: Zebrafish as a model for cardiovascular and metabolic disease. *Physiol. Rev.* **2017**, *97*, 889–938. [[CrossRef](#)] [[PubMed](#)]
86. Hay, M.; Thomas, D.W.; Craighead, J.L.; Economides, C.; Rosenthal, J. Clinical development success rates for investigational drugs. *Nat. Biotechnol.* **2014**, *32*, 40–51. [[CrossRef](#)]
87. He, H.; Liu, L.; Morin, E.E.; Liu, M.; Schwendeman, A. Survey of clinical translation of cancer nanomedicines - Lessons learned from successes and failures. *Acc. Chem. Res.* **2019**, *52*, 2673–2683. [[CrossRef](#)]

## Article

# Total Synthesis and Anti-Inflammatory Bioactivity of (–)-Majusculoic Acid and Its Derivatives

Hong-Xiu Xiao <sup>1,2</sup>, Qing-Xiang Yan <sup>2</sup>, Zhi-Hui He <sup>2</sup>, Zheng-Biao Zou <sup>2</sup>, Qing-Qing Le <sup>2</sup>, Ting-Ting Chen <sup>2</sup>, Bing Cai <sup>2</sup>, Xian-Wen Yang <sup>2,\*</sup>  and Su-Lan Luo <sup>1,\*</sup> 

<sup>1</sup> Key Laboratory of Tropical Biological Resources of Ministry of Education, Hainan University, Haikou 570228, China; xiaohongxiu97@hainanu.edu.cn

<sup>2</sup> Key Laboratory of Marine Biogenetic Resources, Third Institute of Oceanography, Ministry of Natural Resources, 184 Daxue Road, Xiamen 361005, China; youngqx@126.com (Q.-X.Y.); hezhihui@tio.org.cn (Z.-H.H.); zhengbiaozou@njjust.edu.cn (Z.-B.Z.); leqingqing@tio.org.cn (Q.-Q.L.); chentingting@tio.org.cn (T.-T.C.); caibing@tio.org.cn (B.C.)

\* Correspondence: yangxianwen@tio.org.cn (X.-W.Y.); luosulan2003@163.com (S.-L.L.)

**Abstract:** The first total synthesis of marine natural product, (–)-majusculoic acid (**1**) and its seven analogs (**9–15**), was accomplished in three to ten steps with a yield of 3% to 28%. The strategy featured the application of the conformational controlled establishment of the *trans*-cyclopropane and stereochemical controlled bromo-olefination or olefination by Horner–Wadsworth–Emmons (HWE) reaction. The potential anti-inflammatory activity of the eight compounds (**1** and **9–15**) was evaluated by determining the nitric oxide (NO) production in the lipopolysaccharide (LPS)-induced mouse macrophages RAW264.7. (–)-Majusculoic acid (**1**), methyl majusculoate (**9**), and (1*R*,2*R*)-2-((3*E*,5*Z*)-6-bromonona-3,5-dien-1-yl)cyclopropane-1-carboxylic acid (**12**) showed significant effect with inhibition rates of 33.68%, 35.75%, and 43.01%, respectively. Moreover, they did not show cytotoxicity against RAW264.7 cells, indicating that they might be potential anti-inflammatory agents.

**Keywords:** marine natural products; (–)-majusculoic acid; anti-inflammation; LPS; CCK-8



**Citation:** Xiao, H.-X.; Yan, Q.-X.; He, Z.-H.; Zou, Z.-B.; Le, Q.-Q.; Chen, T.-T.; Cai, B.; Yang, X.-W.; Luo, S.-L. Total Synthesis and Anti-Inflammatory Bioactivity of (–)-Majusculoic Acid and Its Derivatives. *Mar. Drugs* **2021**, *19*, 288. <https://doi.org/10.3390/md19060288>

Academic Editor: Emiliano Manzo

Received: 2 May 2021

Accepted: 18 May 2021

Published: 21 May 2021

**Publisher's Note:** MDPI stays neutral with regard to jurisdictional claims in published maps and institutional affiliations.



**Copyright:** © 2021 by the authors. Licensee MDPI, Basel, Switzerland. This article is an open access article distributed under the terms and conditions of the Creative Commons Attribution (CC BY) license (<https://creativecommons.org/licenses/by/4.0/>).

## 1. Introduction

Inflammation can be triggered by tissue injury, infection, and malfunction. Chronic inflammatory conditions are related to a wide range of diseases, such as atherosclerosis and type II diabetes [1]. Lipopolysaccharide (LPS) is one of the main components of the Gram-negative bacteria membrane, which could be recognized by toll-like receptors and then result in inflammatory reaction [2]. LPS-mediated activation of toll-like receptors can activate the downstream nuclear transcription factor  $\kappa$ B (NF- $\kappa$ B), activator protein 1 (AP-1), and mitogen-activated protein kinase signaling pathway (MAPK) [3]. Inducible nitric oxide synthase (iNOS) plays an important role in up-regulating NO levels [4]. Overexpression of iNOS can facilitate the production of NO. When immune cells are stimulated by microbial endotoxins and inflammatory mediators, etc., they will generate a large amount of iNOS to generate NO for immune response. Therefore, inhibition of NO production is a direct indicator of the anti-inflammatory activity.

Fatty acids (FAs) were reported to be effective in the suppression of inflammatory mediator production, including halogenated FAs and polyunsaturated FAs [5,6]. Those FAs could inhibit pathophysiological mediator production such as TNF- $\alpha$ , NO, and IL-6 in LPS-activated RAW 264.7 macrophages [7]. Therefore, FAs are regarded as lead compounds in the drug research and development, especially for anti-inflammatory medicines [8].

Cyclopropane fatty acids (CFAs, Figure 1) are commonly found in terrestrial plants and marine organisms including sponges and bacteria [9–12]. Since a cyclopropane motif can provide specific steric, stereo-electronic, and electronic properties [9], many CFAs showed intriguing bioactivities, such as anticancer [13], antimicrobial [11,12], antitrypanosomal [14],  $\beta$ -arrestin-biased agonist [12], and topoisomerase I inhibitory activity [15].

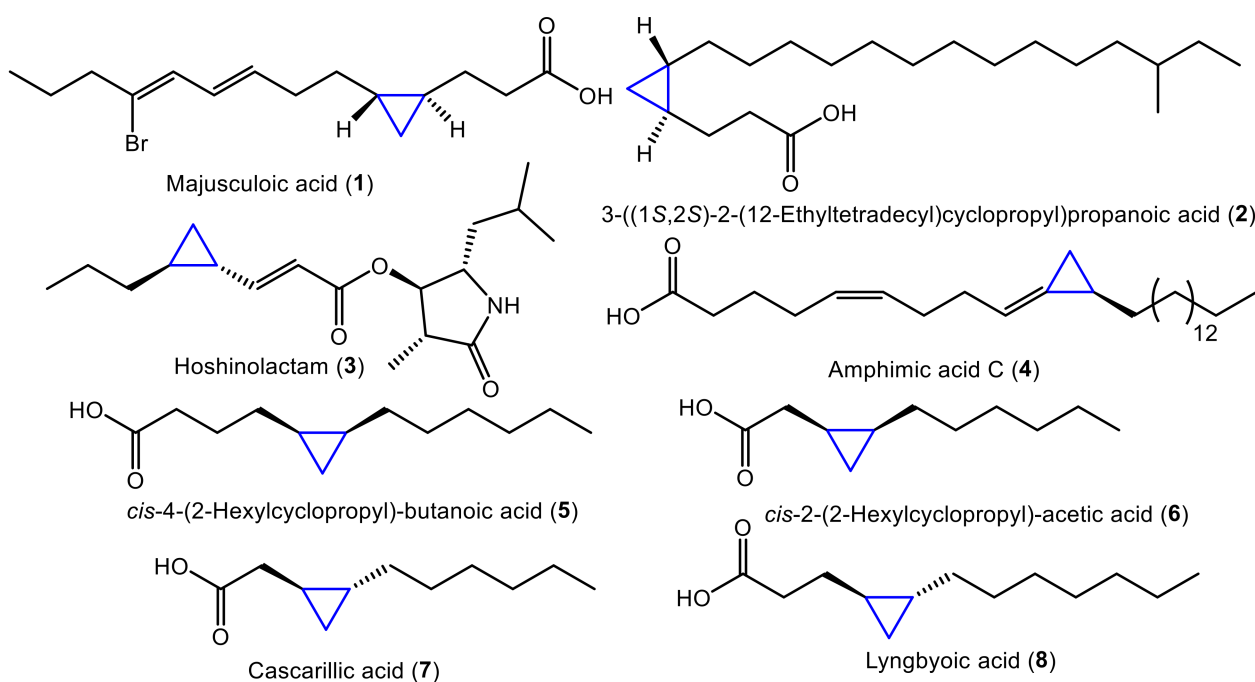


**Figure 1.** Marine-derived cyclopropane fatty acids (CFAs).

Majusculoic acid (**1**), a marine-derived CFA with a halogen atom substituted conjugated diene, was first isolated from the community of cyanobacterial mat microbial in 2005 [11]. Its enantiomer, (+)-majusculoic acid, was total synthesized in 2018 using the dimerization–cyclopropanation–dedimerization strategy in 13 steps [16]. In this study, a more concise strategy was designed to construct a series of FAs with a *trans*-cyclopropane motif. Herein, we report total synthesis and anti-inflammatory activity of (–)-majusculoic acid and its analogs (Figure 2).

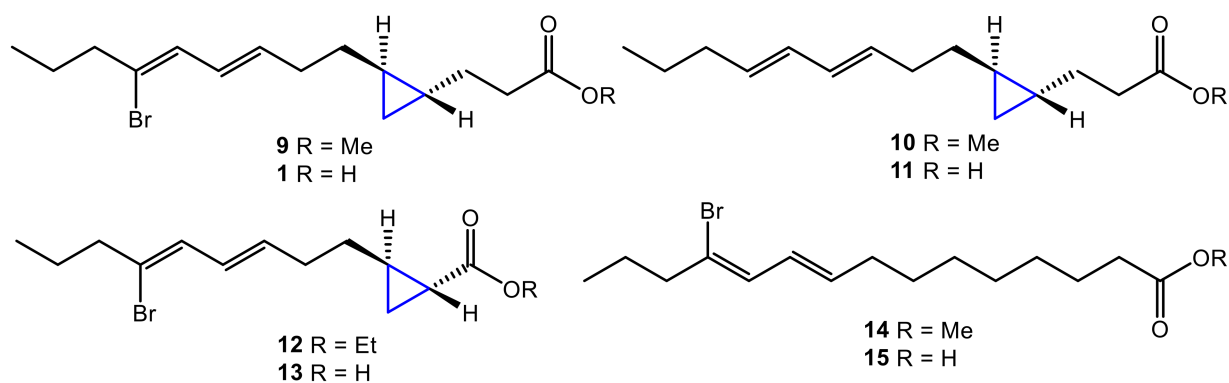


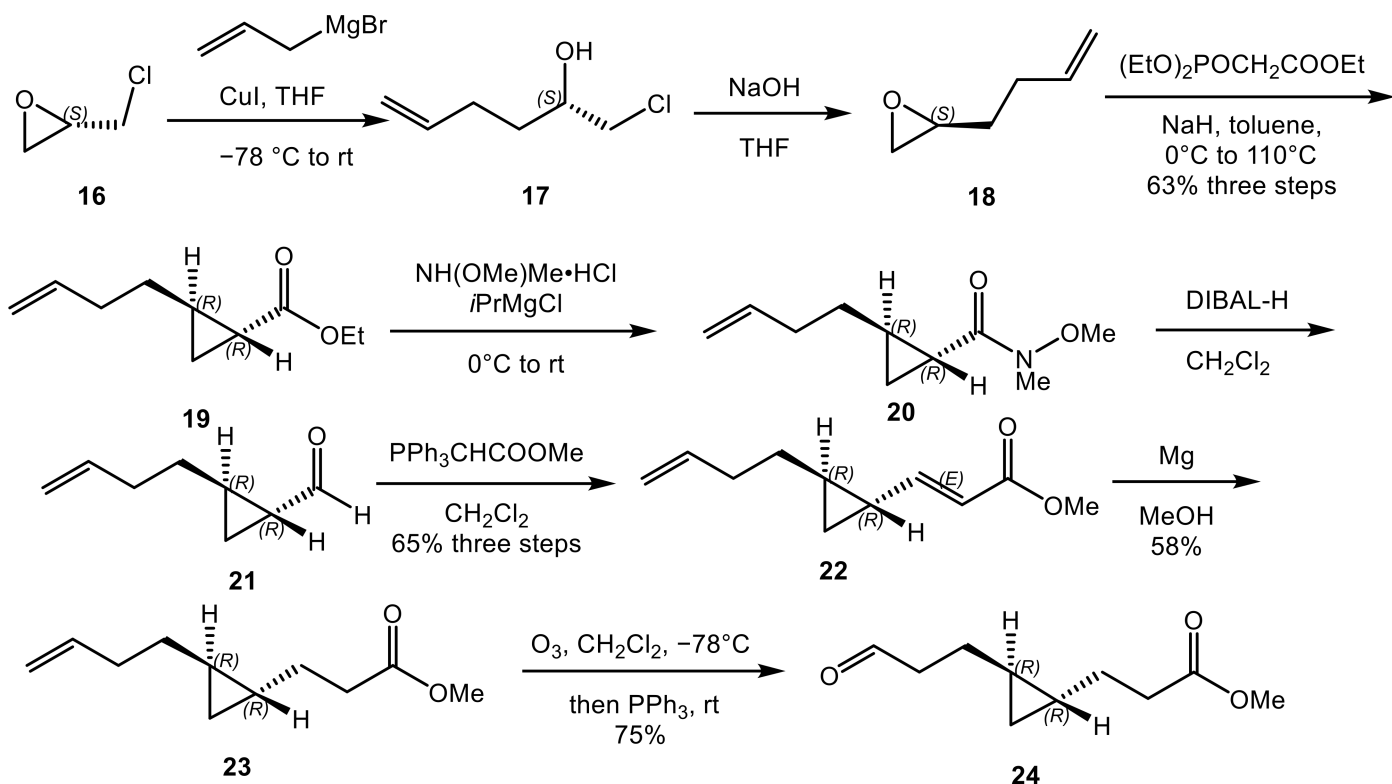
**Figure 2.** Design of majusculoic acid and its derivatives.

## 2. Results

### 2.1. Total Synthesis of Majusculoic Acid

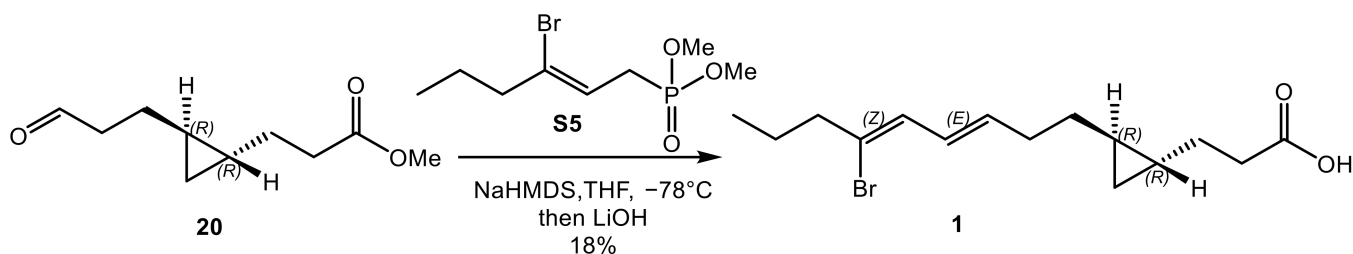
As shown in Scheme 1, the aldehyde **24** was obtained through eight steps. The chiral epoxide **16**, after the nucleophilic addition reaction with the allyl magnesium bromide, provided the chlorinated secondary alcohol **17**, which was transformed into the new epoxide **18** by the treatment with NaOH [17]. By conformationally controlled establishment of the *trans*-4,6-dialkylcyclopropane through Horner reagent in the presence of NaH [18], the ester **19** was treated with isopropylmagnesium chloride and *N,O*-dimethylhydroxylamine hydrochloride to afford the Weinreb amide **20**. After reduction by diisobutylaluminium

hydride (DIBAL-H), the amide **20** was transformed to aldehyde. Wittig reagent was used to extend the length of the chain from aldehyde **21** to alkene ester **22**. Before the ozonolytic cleavage of the double bond, the alkene ester **22** was selectively reduced by magnesium in MeOH. After the aldehyde **24** was synthesized, HWE reaction was applied to establish the conjugated diene motif. It is concise to construct the *trans*-cyclopropane unit and extend the chain.



Scheme 1. Synthesis of aldehyde **24**.

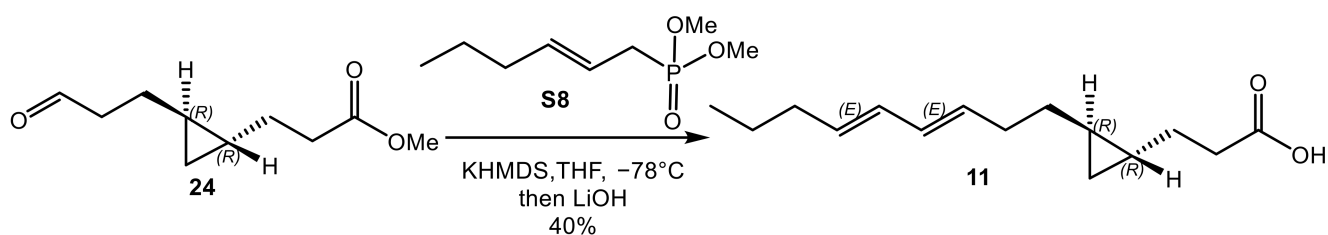
According to the reported strategy [16], the HWE reaction was applied to construct the conjugated (*E,Z*)-bromodiene moiety. And (*E,Z*)-bromodiene **9** was obtained by the treatment of Horner reagent and NaHMDS at  $-78\text{ }^{\circ}\text{C}$ . Compound **9** was hydrolyzed by LiOH to give (–)-majusculoic acid (**1**) in two steps with a yield of 18% (Scheme 2). The synthesized (–)-majusculoic acid (**1**) has the same spectroscopic properties as that of the natural counterpart [11].



Scheme 2. Synthesis of majusculoic acid.

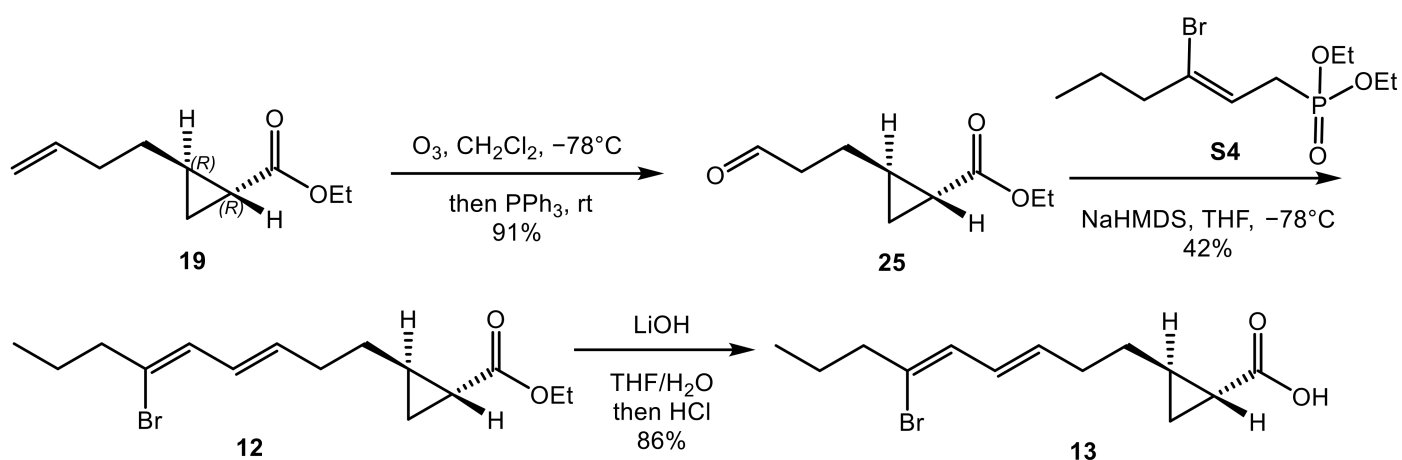
## 2.2. Total Synthesis of Majusculoic Acid Derivatives

By the same strategy for the total synthesis of majusculoic acid, the construction of the conjugated (*E,E*)-diene element in **10** and **11** can also be realized (Scheme 3).



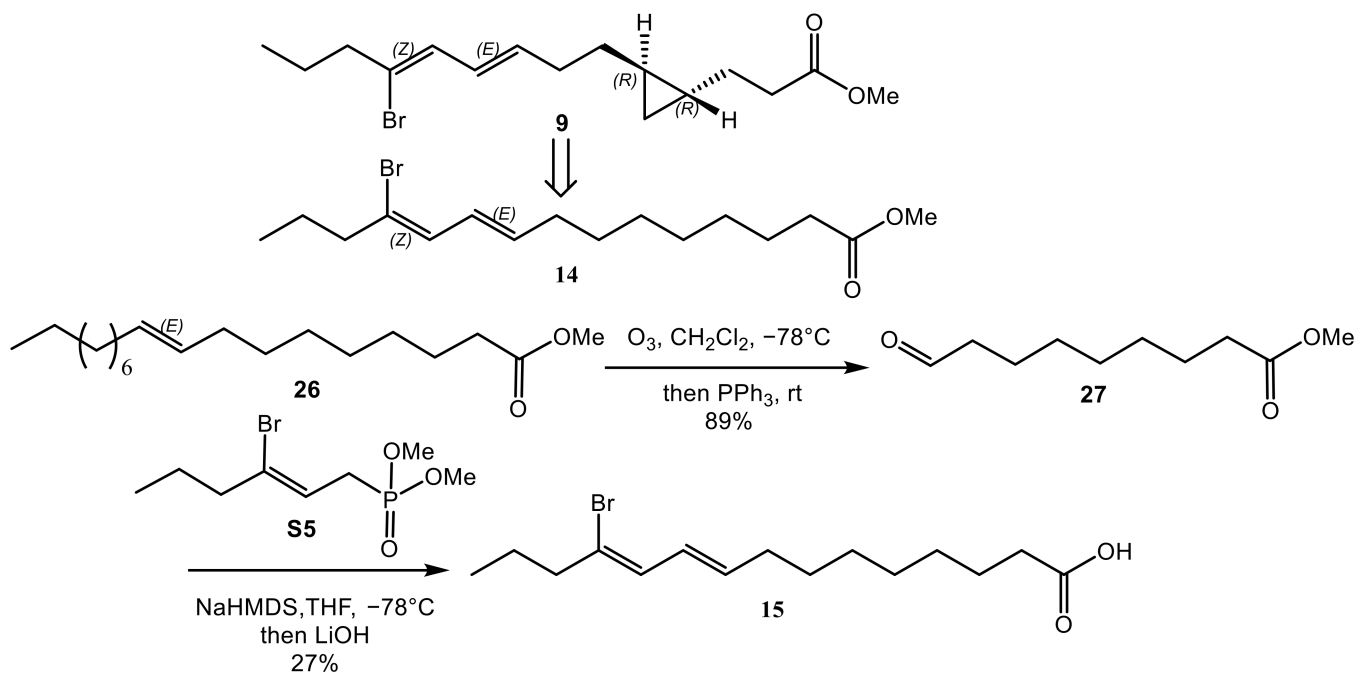
**Scheme 3.** Synthesis of derivatives **10** and **11**.

To investigate the effect between the length of carbon chain and the anti-inflammatory activity, compound **19** was transformed into aldehyde **25** by ozonolytic cleavage of the double bond. The homolog of majusculoic acid was realized after the HWE reaction (Scheme 4).



**Scheme 4.** Synthesis of derivatives **12** and **13**.

For the transformation of **9** to **14**, the direct opening of cyclopropane by the treatment of  $\text{PtO}_2$  or  $\text{Pd/C}$  under  $\text{H}_2$  was failed. Alternatively, **14** was constructed by the reaction between aldehyde **27** and Horner reagent. Aldehyde **27** was synthesized with methyl oleate **26**, by the ozonolytic cleavage of the double bond (Scheme 5).

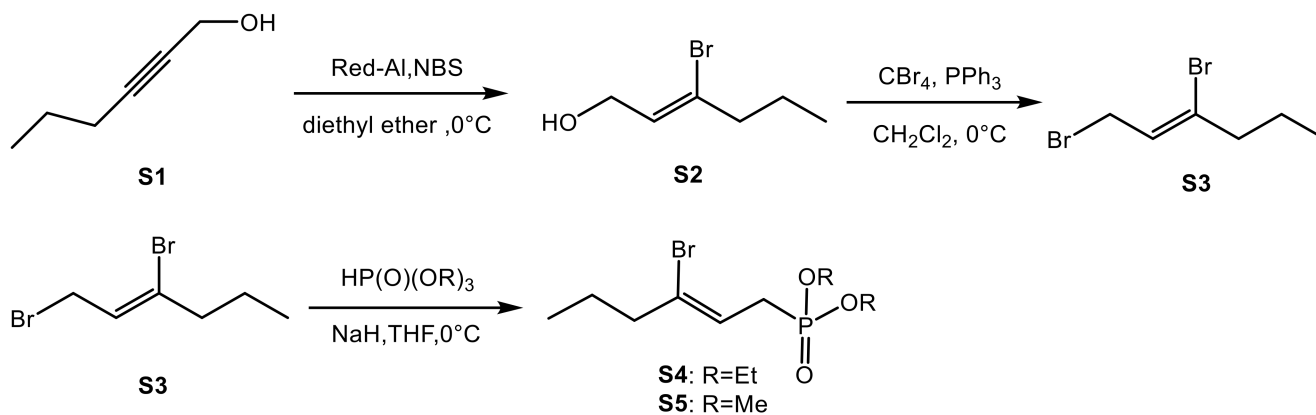


**Scheme 5.** Synthesis of derivatives 14 and 15.

### 2.3. Synthesis of Horner Reagent

#### 2.3.1. Synthesis of Horner Reagent for Bromo-Olefination (S4 and S5)

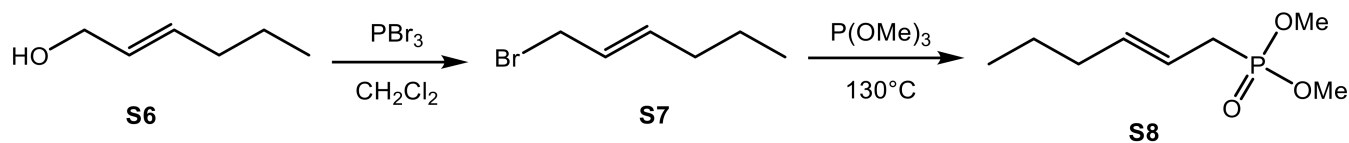
The construction of Horner reagent for bromo-olefination was conducted based on the reported strategy (Scheme 6) [16].



**Scheme 6.** Synthesis of Horner reagent for bromo-olefination.

#### 2.3.2. Synthesis of Horner Reagent (S8)

The construction of Horner reagent was commenced with (*E*)-hex-2-en-1-ol (S6), by the treatment of PBr<sub>3</sub> and trimethyl phosphate (Scheme 7).



**Scheme 7.** Synthesis of Horner reagent for olefination.

#### 2.4. Anti-Inflammatory Effect of Majusculoic Acid and Its Analogs

The anti-inflammatory activity of majusculoic acid and its analogs was determined in the LPS-induced RAW264.7 macrophages. (–)-Majusculoic acid (**1**), methyl majusculoate (**9**) and ethyl-(1*R*,2*R*)-2-((3*E*,5*Z*)-6-bromonona-3,5-dien-1-yl)cyclopropane-1-carboxylate (**12**) showed weak inhibitory activity. Noteworthy, all three compounds showed dose-dependent effects (Table 1).

**Table 1.** Inhibitory rate of NO production for **1** and **9–15**.

Compound	Concentration (μM)	NO Inhibition Rate (%)
<b>1</b>	30	35.75 ± 4.4
	10	12.95 ± 4.4
<b>9</b>	30	33.68 ± 7.33
	10	9.84 ± 2.93
<b>10</b>	30	11.92 ± 8.79
	10	8.81 ± 7.33
<b>11</b>	30	18.13 ± 8.79
	10	6.74 ± 7.33
<b>12</b>	30	43.01 ± 2.93
	10	7.77 ± 5.86
<b>13</b>	30	26.42 ± 14.66
	10	28.5 ± 2.93
<b>14</b>	30	15.03 ± 7.33
	10	9.84 ± 5.86
<b>15</b>	30	19.17 ± 7.33
	10	9.84 ± 8.79

#### 2.5. Cytotoxicity of Majusculoic Acid and Its Analogs

To investigate their cytotoxic effects, all eight compounds were tested for the cell proliferation by Cell Counting Kit 8 (CCK-8) assay. As shown in Table 2, they did not show cytotoxicity even under the concentration of 30 μM.

**Table 2.** Anti-proliferative effect of majusculoic acid (**1**) and its derivatives (**9–15**).

Compound	Concentration (μM)	Inhibition Rate of Cell Proliferation (%)
<b>1</b>	30	−24.38 ± 3.15
	10	−16.02 ± 5.37
<b>9</b>	30	−21.59 ± 0.07
	10	−15.32 ± 10.95
<b>10</b>	30	−22.05 ± 6.3
	10	−10.66 ± 6.52
<b>11</b>	30	−16.88 ± 1.15
	10	−0.13 ± 19.26
<b>12</b>	30	−6.25 ± 9.59
	10	1.54 ± 0.57
<b>13</b>	30	11.01 ± 1.22
	10	7.16 ± 0.07
<b>14</b>	30	−25.74 ± 11.53
	10	−8.33 ± 3.51
<b>15</b>	30	−15.16 ± 17.04
	10	−14.15 ± 5.87

### 3. Discussion

Inflammation occurs when organisms receive stimuli, and manifests as pain, redness, heat, swelling, and dysfunction [19,20]. Monocytes can differentiate into macrophages after the stimulation at the site of infection, followed by the release of inflammatory mediators including prostaglandin E-2 (PGE-2), NO, and other cytokines. Inhibiting the production of those cytokines can control the inflammatory response. Therefore, finding

out efficient molecules that could down-regulate the levels of those factors is a way to find potential drugs.

FAs are reported to be effective in inflammatory inhibition activity [5–7]. Yet the anti-inflammatory activity of the marine-derived CFAs that have a cyclopropane motif, such as majusculoic acid, remains unknown. Therefore, an efficient way to realize the total synthesis of majusculoic acid and its derivatives, as well as a primary structure–activity relationship (SAR) study on anti-inflammatory effect were figured out. A conformational controlled strategy was applied in the building of *trans*-4,6-dialkylcyclopropane and an efficient homologation strategy was involved. To construct the conjugated (*E,E*)-diene element and (*E,Z*)-bromodiene moiety stereospecificly, we developed three Horner reagents for different substrates. These derivatives were designed to identify the impact of halogen atom, length of chain, esterification as well as the unique *trans*-4,6-dialkylcyclopropane on the influence of anti-inflammatory activity.

As a result, an efficient synthetic strategy was developed to totally synthesize majusculoic acid and its derivatives with yields over 3%. Majusculoic acid (**1**), methyl majusculoate (**9**) and ethyl-(1*R*,2*R*)-2-((3*E*,5*Z*)-6-bromonona-3,5-dien-1-yl)-cyclopropane-1-carboxylate (**12**) showed weak effects on the NO production. As shown in Figure 3, the primary SAR result indicated that the existence of the *trans*-4,6-dialkylcyclopropane and (*E,Z*)-bromodiene are crucial for the activity and the length of the chain is key to the effect. However, the methyl esterification will not influence its bioactivity.

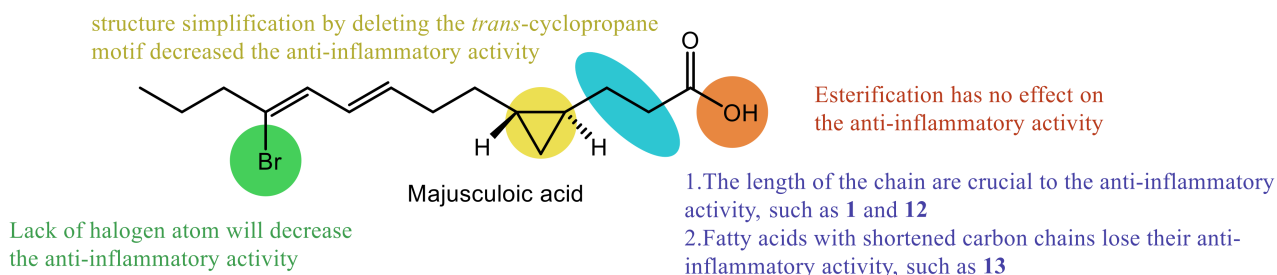


**Figure 3.** Structure and activity relationship of majusculoic acid (**1**) and its derivatives (**9**–**15**).

## 4. Materials and Methods

### 4.1. Reagents and Materials

Unless otherwise stated, all reactions were conducted under an argon atmosphere and anhydrous conditions in the dry organic solvent. Super-dry MeOH was purchased from Innochem Science & Technology Co., Ltd. (Beijing, China). The synthesized products were monitored by thin layer chromatography (TLC), and visualized by  $\text{KMnO}_4$  or ultra-violet (UV) lights. The high-resolution electron spray ionization mass spectra (HRESIMS) were obtained by Micromass Quadrupole/Time-of-Flight (Q-TOF) mass spectrometer (Waters Corporation, Milford, MA, USA). The nuclear magnetic resonance (NMR) spectra were measured on  $\text{CDCl}_3$  ( $\delta_{\text{H}} = 7.26$  and  $\delta_{\text{C}} = 77.0$ ) by Bruker AV-400 spectrometer (Bruker, Fällanden, Switzerland).

The RAW264.7 cells were bought from Shanghai Kanglang Biological Technology Co., Ltd. (Beijing, China). The Griess reagent kit and the CCK-8 kit were bought from the Thermo Fisher Scientific (Shanghai, China) and MedChemExpress (Shanghai, China), respectively.

### 4.2. Total Synthesis of Majusculoic Acid and Its Derivates

#### 4.2.1. Synthesis of (S)-2-(but-3-en-1-yl)oxirane (**18**)

To a solution of **16** (10.0 g, 108.0 mmol) in THF was added CuI (2.06 g, 10.8 mmol) and the solution was stirred for 20 min. Then Grignard reagent allyl magnesium bromide was added (118.9 mmol, 2 mol/L in THF) dropwise. The reaction mixture was warmed to 23 °C slowly and quenched by saturated  $\text{NH}_4\text{Cl}$  solution (60 mL). The mixture was



extracted with EtOAc. The combined organic layer was washed with brine, dried over  $\text{MgSO}_4$  and concentrated in vacuo to give a crude (*S*)-1-chlorohex-5-en-2-ol (**17**) (16.1 g), to which NaOH (8.64 g, 216 mmol) was added at 0 °C. After stirring for 10 h, NaOH was removed by filtration and the mixture was washed by diethyl ether. The combined organic layer was washed with brine, dried over  $\text{MgSO}_4$  and concentrated in vacuo to afford crude epoxide (**18**) (6.2 g) as yellow oil.

#### 4.2.2. Synthesis of Ethyl (1*R*,2*R*)-2-(but-3-en-1-yl) cyclopropane-1-carboxylate (**19**)

To a solution of NaH in toluene (100 mL) at 0 °C was added  $(\text{EtO})_2\text{POCH}_2\text{COOEt}$  (35.5 g, 158.2 mmol) dropwise. The mixture was stirred for 30 min before adding the crude epoxide **18** (6.2 g, 63.3 mmol) in toluene (15 mL). The mixture was heated at 110 °C and stirred for 6 h. Then it was quenched with saturated  $\text{NH}_4\text{Cl}$  solution (60 mL), followed by extraction with diethyl ether. The combined organic layer was washed with brine, dried over  $\text{MgSO}_4$  and concentrated in vacuo. Purification of the residue by flash chromatography (PE/EtOAc = 40:1) afforded **19** (11.36 g, 63% yield of three steps) as colorless oil.

#### 4.2.3. Synthesis of (1*R*,2*R*)-2-(but-3-en-1-yl)-*N*-methoxy-*N*-methylcyclopropane-1-carboxamide (**20**)

To a solution of ester **19** (2.8 g, 16.7 mmol) and  $\text{NH}(\text{OMe})\text{Me}\cdot\text{HCl}$  (1.7 g, 18.0 mmol) in THF (100 mL) at 0 °C was added *i*PrMgCl (33 mL, 66 mmol, 2.0 mol/L in THF) dropwise. The reaction mixture was slowly warmed to 23 °C and then stirred for 4 h before adding saturated  $\text{NH}_4\text{Cl}$  solution (60 mL) dropwise. The mixture was extracted with EtOAc. The combined organic layer was washed with brine, dried over  $\text{MgSO}_4$  and concentrated in vacuo. The crude amide **20** (3.1 g, 16.7 mmol) was used for next step without further purification.

#### 4.2.4. Synthesis of (1*R*,2*R*)-2-(but-3-en-1-yl) cyclopropane-1-carbaldehyde (**21**)

To a solution of crude amide **20** (3.1 g, 16.7 mmol) in  $\text{CH}_2\text{Cl}_2$  (5 mL) at  $-78$  °C was added DIBAL-H (27.8 mL, 41.6 mmol, 1.5 mol/L in  $\text{Et}_2\text{O}$ ) dropwise. The mixture was stirred for 2 h before the addition of HCl (45 mL, 1 mol/L) dropwise until the solution turned to be clear. The mixture was extracted with EtOAc. The combined organic layer was washed with brine, dried over  $\text{MgSO}_4$  and concentrated in vacuo to afford crude aldehyde **21** (2.1 g).

#### 4.2.5. Synthesis of Methyl (*E*)-3-((1*R*,2*R*)-2-(but-3-en-1-yl) cyclopropyl) Acrylate (**22**)

To a solution of crude aldehyde **21** (2.1 g, 16.7 mmol) in  $\text{CH}_2\text{Cl}_2$  (50 mL) was added Wittig reagent (13.9 g, 41.5 mmol). The mixture was stirred overnight. Then silica gel was added, and the mixture was concentrated in vacuo. Purification of the residue by flash chromatography (PE/EtOAc = 80:1) afforded **22** (1.9 g, 65% yield in three steps).

#### 4.2.6. Synthesis of Methyl 3-((1*R*,2*R*)-2-(but-3-en-1-yl) cyclopropyl) Propanoate (**23**)

To a solution of **22** (1.0 g, 5.56 mmol) in MeOH (50 mL) at 0 °C was added Mg (667.0 mg, 27.8 mmol). The mixture was stirred for 1 h before adding 1 mol/L HCl (60 mL). The mixture was extracted with EtOAc. The EtOAc was combined and washed with brine, dried over  $\text{MgSO}_4$  and concentrated in vacuo. Purification of the residue by flash chromatography (PE/EtOAc = 100:1) afforded **23** (592 mg, 58% yield).

#### 4.2.7. Synthesis of Methyl 3-((1*R*,2*R*)-2-(3-oxopropyl) cyclopropyl) Propanoate (**24**)

Ozone was bubbled into a solution of **23** in  $\text{CH}_2\text{Cl}_2$  at  $-78$  °C until the solution turned to blue and the  $\text{O}_2$  was bubbled into the blue solution at  $-78$  °C until the disappearance of the blue color.  $\text{PPh}_3$  (476 mg, 1.8 mmol) was added, and the resulting solution was slowly warmed to room temperature. Then it was stirred overnight. The crude mixture was combined with silica gel and concentrated in vacuo. Purification of the residue by flash chromatography (PE/EtOAc = 20:1) afforded **24** (62.2 mg, 75% yield) as a colorless oil.

#### 4.2.8. Synthesis of Methyl Majusculoate (**9**)

To a solution of **S5** [16] (415.5 mg, 1.53 mmol) in THF (20 mL) at  $-78\text{ }^{\circ}\text{C}$  was added NaHMDS (0.76 mL, 2 mmol/L in THF). The mixture was stirred at  $-78\text{ }^{\circ}\text{C}$  for 30 min before **24** (113.0 mg, 0.61 mmol) in THF (5 mL) was added. The mixture was stirred at  $-78\text{ }^{\circ}\text{C}$  for 2 h before the addition of saturated  $\text{NH}_4\text{Cl}$  solution (10 mL). Extraction with EtOAc and the combination of organic layer was washed with brine, dried over  $\text{MgSO}_4$  and concentrated in vacuo. Purification of the residue by flash chromatography (PE/EtOAc = 100:1) afforded **9** (40.4 mg, 20% yield).

#### 4.2.9. Synthesis of Majusculoic Acid (**1**)

To a solution of **9** (40.4 mg, 0.12 mmol) in THF (10 mL) and  $\text{H}_2\text{O}$  (3 mL) was added LiOH (5.9 mg, 0.24 mmol). The mixture was stirred for 5 h. After the pH of the mixture was adjusted to about 5 with HCl (2 mol/L), it was extracted with EtOAc. The combination of organic layer was washed with brine, dried over  $\text{MgSO}_4$  and concentrated in vacuo. Purification of the residue by flash chromatography (PE/EtOAc = 6:1) afforded **1** (35.2 mg, 93% yield).

### 4.3. General Method for the Synthesis of Majusculoic Acid Analogs

#### 4.3.1. Synthesis of Methyl 3-((1*R*,2*R*)-2-((3*E*,5*E*)-nona-3,5-dien-1-yl) cyclopropyl) Propanoate (**10**)

To a solution of **S8** [21] (101.9 mg, 0.53 mmol) in THF (20 mL) at  $-78\text{ }^{\circ}\text{C}$  was added KHMDS (0.76 mL, 2 mmol/L in THF). The mixture was stirred at  $-78\text{ }^{\circ}\text{C}$  for 30 min before **24** (39.4 mg, 0.21 mmol) in THF (10 mL) was added. The mixture was stirred at  $-78\text{ }^{\circ}\text{C}$  for 1.5 h before adding the saturated  $\text{NH}_4\text{Cl}$  solution (10 mL). It was extracted with EtOAc and the combination of organic layer was washed with brine, dried over  $\text{MgSO}_4$  and concentrated in vacuo. Purification of the residue by flash chromatography (PE/EtOAc = 100:1) afforded **6** (26.3 mg, 50% yield).

#### 4.3.2. Synthesis of Methyl 3-((1*R*,2*R*)-2-((3*E*,5*E*)-nona-3,5-dien-1-yl) cyclopropyl) Propanoic Acid (**11**)

To a solution of **6** (26.3 mg, 0.11 mmol) in THF (10 mL) and  $\text{H}_2\text{O}$  (3 mL) was added LiOH (5.7 mg, 0.24 mmol). The mixture was stirred for 5 h. The pH of the mixture was adjusted to about 5 with HCl (2 mol/L) and then extraction with EtOAc was conducted. The combination of organic layer was washed with brine, dried over  $\text{MgSO}_4$  and concentrated in vacuo. Purification of the residue by flash chromatography (PE/EtOAc = 6:1) afforded **11** (21.2 mg, 82% yield) as a colorless oil.

#### 4.3.3. Synthesis of Ethyl (1*R*,2*R*)-2-(3-oxopropyl) cyclopropane-1-carboxylate (**25**)

Ozone was bubbled into a solution of **19** in  $\text{CH}_2\text{Cl}_2$  at  $-78\text{ }^{\circ}\text{C}$  until the solution turned to blue and the  $\text{O}_2$  was bubbled into the blue solution at  $-78\text{ }^{\circ}\text{C}$  until the disappearance of the blue color.  $\text{PPh}_3$  (1.2 g, 4.6 mmol) was added, and the resulting solution was slowly warmed to room temperature. Then it was stirred overnight. The crude mixture was combined with silica gel and concentrated in vacuo. Purification of the residue by flash chromatography (PE/EtOAc = 20:1) afforded **25** (179.2 mg, 91% yield) as a colorless oil.

#### 4.3.4. Synthesis of Ethyl (1*R*,2*R*)-2-((3*E*,5*Z*)-6-bromonona-3,5-dien-1-yl) cyclopropane-1-carboxylate (**12**)

To a solution of **S4** (143.7 mg, 0.53 mmol) in THF (20 mL) at  $-78\text{ }^{\circ}\text{C}$  was added NaHMDS (0.27 mL, 2 mmol/L in THF). The mixture was stirred at  $-78\text{ }^{\circ}\text{C}$  for 30 min before **25** (36.5 mg, 0.21 mmol) in THF (10 mL) was added. The mixture was stirred at  $-78\text{ }^{\circ}\text{C}$  for 1.5 h before adding the saturated  $\text{NH}_4\text{Cl}$  solution (10 mL). Extraction with EtOAc was performed and the combination of organic layer was washed with brine, dried over  $\text{MgSO}_4$  and concentrated in vacuo. Purification of the residue by flash chromatography (PE/EtOAc = 100:1) afforded **12** (27.8 mg, 42% yield).

#### 4.3.5. Synthesis of (1*R*,2*R*)-2-((3*E*,5*Z*)-6-bromonona-3,5-dien-1-yl)cyclopropane-1-carboxylic Acid (**13**)

To a solution of **12** (27.8 mg, 0.09 mmol) in THF (10 mL) and H<sub>2</sub>O (3 mL) was added LiOH (4.32 mg, 0.18 mmol). The mixture was stirred for 5 h. The pH of the mixture was adjusted to about 5 with HCl (2 mol/L) and then extraction with EtOAc was carried out. The combination of organic layer was washed with brine, dried over MgSO<sub>4</sub> and concentrated in vacuo. Purification of the residue by flash chromatography (PE/EtOAc = 6:1) afforded **13** (22.0 mg, 86% yield) as a colorless oil.

#### 4.3.6. Synthesis of Methyl 9-oxononanoate (**27**)

Ozone was bubbled into a solution of **26** (276.4 mg, 0.93 mmol) in CH<sub>2</sub>Cl<sub>2</sub> at −78 °C until the solution turned to blue and the O<sub>2</sub> was bubbled into the blue solution at −78 °C until the disappearance of the blue color. PPh<sub>3</sub> (978.0 mg, 3.7 mmol) was added, and the resulting solution was slowly warmed to 25 °C to keep stirring overnight. The crude mixture was combined with silica gel and concentrated in vacuo. Purification of the residue by flash chromatography (PE/EtOAc = 20:1) afforded **27** (154.3 mg, 89% yield) as a colorless oil.

#### 4.3.7. Synthesis of Methyl (9*E*,11*Z*)-12-bromopentadeca-9,11-dienoate (**14**)

To a solution of **S5** (277.9 mg, 1.03 mmol) in THF (20 mL) at −78 °C was added NaHMDS (0.51 mL, 2 mmol/L in THF). The mixture was stirred at −78 °C for 30 min before **27** (75.6 mg, 0.41 mmol) in THF (5 mL) was added. The mixture was stirred at −78 °C for 2 h before the addition of saturated NH<sub>4</sub>Cl solution (10 mL). Extraction with EtOAc was performed and the combination of organic layer was washed with brine, dried over MgSO<sub>4</sub> and concentrated in vacuo. Purification of the residue by flash chromatography (PE/EtOAc = 100:1) afforded **14** (43.0 mg, 32% yield).

#### 4.3.8. Synthesis of (9*E*,11*Z*)-12-bromopentadeca-9,11-dienoic Acid (**15**)

To a solution of **14** (43.0 mg, 0.13 mmol) in THF (10 mL) and H<sub>2</sub>O (3 mL) was added LiOH (6.2 mg, 0.26 mmol). The mixture was stirred for 5 h. The pH of the mixture was adjusted to about 5 with HCl (2 mol/L). Then the mixture was extracted with EtOAc and the combination of organic layer was washed with brine, dried over MgSO<sub>4</sub> and concentrated in vacuo. Purification of the residue by flash chromatography (PE/EtOAc = 6:1) afforded **15** (36.1 mg, 88% yield).

### 4.4. General Method for the Synthesis of Horner Reagent

#### 4.4.1. Synthesis of Horner Reagent for Bromo-Olefination

The bromo-olefination of aldehyde was realized based on the reported strategy [16]. Similarly, the synthesis of (*Z*)-1,3-dibromohex-2-ene and (**S3**), diethyl (*Z*)-(3-bromohex-2-en-1-yl)phosphonate (**S4**) and dimethyl (*Z*)-(3-bromohex-2-en-1-yl)phosphonate (**S5**) were conducted according to the referenced approach [16].

#### 4.4.2. Synthesis of Horner Reagent for Olefination

The synthesis of dimethyl (*E*)-hex-2-en-1-ylphosphonate (**S8**) was commenced with (*E*)-hex-2-en-1-ol (**S6**). (*E*)-hex-2-en-1-ol (**S6**) (1.0 g, 7.5 mmol) was added into CH<sub>2</sub>Cl<sub>2</sub> and then PBr<sub>3</sub> (3.1 g, 11.3 mmol) was added slowly at 0 °C. The mixture was stirred for 30 min before adding the saturated NaHCO<sub>3</sub> solution (10 mL). It was extracted with EtOAc and the combination of organic layer was washed with brine, dried over MgSO<sub>4</sub> and concentrated in vacuo to obtain the crude (*E*)-1-bromohex-2-ene (**S7**, 875.9 mg). The mixture of **S7** (875.9 mg, 5.4 mmol) and P(OCH<sub>3</sub>)<sub>3</sub> was heated to 130 °C for 4 h, followed by evaporation for the low boiling point impurities. The mixture was purified by flash chromatography (PE/EtOAc = 4:1) afforded **S8** (761.7 mg, 74% yield).

## 4.5. Spectroscopic Data of Majusculoic Acid and Its Analogs

The NMR, optical rotations (OR), HRESIMS, and infrared (IR) data of majusculoic acid derivatives (**1**, **9–15**) were given below. Although the spectral characteristics of other intermediates (**19–27**) could be found in the Supplementary Materials.

**(1)**  $[\alpha]_D^{25} -4.3$  (c 1.0, MeOH);  $^1\text{H NMR}$  (400 MHz,  $\text{CDCl}_3$ )  $\delta$  6.33 (dd,  $J = 15.0, 9.9$  Hz, 1H), 6.23 (d,  $J = 9.9$  Hz, 1H), 5.89–5.79 (dt,  $J = 14.4, 7.2$  Hz, 1H), 2.45 (t,  $J = 7.4$  Hz, 4H), 2.21 (dd,  $J = 14.4$  Hz, 6.8 Hz, 2H), 1.70–1.49 (m, 4H), 1.44–1.36 (m, 1H), 1.29 (m, 1H), 0.92 (t,  $J = 7.4$  Hz, 3H), 0.56–0.46 (m, 2H), 0.32–0.23 (m, 2H).  $^{13}\text{C NMR}$  (100 MHz,  $\text{CDCl}_3$ )  $\delta$  179.5, 136.7, 128.1, 127.8, 127.0, 43.6, 34.1, 33.7, 33.0, 29.3, 21.5, 18.5, 18.2, 13.0, 11.9. IR (KBr,  $\text{cm}^{-1}$ )  $\nu$  2960, 2925, 2855, 1743, 1434, 1171, 986.83; HRMS (ESI,  $m/z$ ) calcd for  $\text{C}_{15}\text{H}_{23}\text{BrO}_2$   $[\text{M} + \text{Na}]^+$ , 337.0774 and 339.0753, found 337.0781 and 339.0762.

**(9)**  $^1\text{H NMR}$  (400 MHz,  $\text{CDCl}_3$ )  $\delta$  6.30 (ddt,  $J = 15.0, 9.9, 1.3$  Hz, 1H), 6.20 (d,  $J = 9.9$  Hz, 1H), 5.88–5.75 (m, 1H), 3.67 (s, 3H), a2.43 (t,  $J = 7.3$  Hz, 2H), 2.38 (t,  $J = 7.5$  Hz, 2H), 2.18 (dd,  $J = 14.3, 7.0$  Hz, 2H), 1.65–1.55 (m, 4H), 1.55–1.48 (m, 1H), 1.40–1.29 (m, 1H), 0.90 (t,  $J = 7.4$  Hz, 3H), 0.52–0.41 (m, 2H), 0.28–0.20 (m, 2H).  $^{13}\text{C NMR}$  (100 MHz,  $\text{CDCl}_3$ )  $\delta$  174.2, 136.7, 128.1, 127.8, 127.0, 51.4, 43.6, 34.2, 33.7, 33.0, 29.7, 29.6, 21.5, 18.5, 18.3, 13.0, 11.9. IR (KBr,  $\text{cm}^{-1}$ )  $\nu$  2961, 2927, 2871, 1557, 1742, 1459, 1377, 1261, 1188, 1081, 967, 801; HRMS (ESI,  $m/z$ ) calcd for  $\text{C}_{16}\text{H}_{25}\text{BrO}_2$   $[\text{M} + \text{Na}]^+$ , 351.0930 and 353.0910, found 351.0942 and 353.0925.

**(10)**  $[\alpha]_D^{25} -1.6$  (c 1.0, MeOH);  $^1\text{H NMR}$  (400 MHz,  $\text{CDCl}_3$ )  $\delta$  6.02 (dd,  $J = 9.9, 4.0$  Hz, 1H), 5.97 (dd,  $J = 10.0, 4.2$  Hz, 1H), 5.62–5.48 (m, 2H), 3.66 (s, 3H), 2.38 (t,  $J = 6.5$  Hz, 2H), 2.12 (dt,  $J = 14.5, 7.3$  Hz, 2H), 2.03 (dt,  $J = 14.4, 7.0$  Hz, 2H), 1.61–1.45 (m, 2H), 1.44–1.37 (m, 2H), 1.33–1.26 (m, 2H), 0.89 (t,  $J = 7.3$  Hz, 3H), 0.52–0.39 (m, 2H), 0.27–0.17 (m, 2H).  $^{13}\text{C NMR}$  (100 MHz,  $\text{CDCl}_3$ )  $\delta$  174.2, 132.3, 132.0, 130.5, 130.4, 51.4, 34.7, 34.2, 34.0, 32.6, 29.6, 22.6, 18.5, 18.3, 13.7, 11.8. IR (KBr,  $\text{cm}^{-1}$ )  $\nu$  2962, 2925, 1710, 1608, 1423, 868; HRMS (ESI,  $m/z$ ) calcd for  $\text{C}_{16}\text{H}_{26}\text{O}_2$   $[\text{M} + \text{Na}]^+$ , 273.1830, found 273.1828.

**(11)**  $[\alpha]_D^{25} -4.9$  (c 1.0, MeOH);  $^1\text{H NMR}$  (400 MHz,  $\text{CDCl}_3$ )  $\delta$  6.02 (dd,  $J = 10.1, 4.4$  Hz, 1H), 5.98 (dd,  $J = 10.8, 4.8$  Hz, 1H), 5.70–5.50 (m, 1H), 2.42 (t,  $J = 7.5$  Hz, 2H), 2.12 (dd,  $J = 14.2, 7.1$  Hz, 2H), 2.03 (q,  $J = 7.1$  Hz, 2H), 1.62–1.44 (m, 2H), 1.47–1.33 (m, 2H), 1.37–1.27 (m, 2H), 0.89 (t,  $J = 7.3$  Hz, 3H), 0.47 (m, 2H), 0.24 (m, 2H).  $^{13}\text{C NMR}$  (100 MHz,  $\text{CDCl}_3$ )  $\delta$  179.7, 132.4, 132.0, 130.5, 130.4(5), 34.7, 34.2, 34.0, 32.6, 29.3, 22.6, 18.6, 18.2, 13.7, 11.8. IR (KBr,  $\text{cm}^{-1}$ )  $\nu$  2959, 2926, 2858, 2371, 2323, 1710, 1453, 1287, 986; HRMS (ESI,  $m/z$ ) calcd for  $\text{C}_{15}\text{H}_{24}\text{O}_2$   $[\text{M} + \text{Na}]^+$ , 259.1674, found 259.1670.

**(12)**  $[\alpha]_D^{25} -39.8$  (c 1.0, MeOH);  $^1\text{H NMR}$  (400 MHz,  $\text{CDCl}_3$ )  $\delta$  6.31 (dd,  $J = 15.1, 9.8$  Hz, 1H), 6.20 (d,  $J = 9.9$  Hz, 1H), 5.87–5.75 (m, 1H), 4.11 (q,  $J = 7.1$  Hz, 2H), 2.43 (t,  $J = 7.2$  Hz, 2H), 2.22 (dd,  $J = 14.0, 7.0$  Hz, 2H), 1.65–1.56 (m, 2H), 1.43–1.35 (m, 4H), 1.25 (t,  $J = 7.1$  Hz, 3H), 1.16 (dt,  $J = 6.7, 4.5$  Hz, 1H), 0.90 (t,  $J = 7.4$  Hz, 3H), 0.73–0.67 (m, 1H).  $^{13}\text{C NMR}$  (100 MHz,  $\text{CDCl}_3$ )  $\delta$  174.4, 135.7, 128.5, 127.6, 127.3, 60.4, 43.6, 32.7, 32.5, 22.4, 21.4, 20.3, 15.4, 14.3, 12.9. IR (KBr,  $\text{cm}^{-1}$ )  $\nu$  3457, 2961, 2931, 2873, 1728, 1682, 1453, 1410, 1178, 1081, 970, 859.

**(13)**  $[\alpha]_D^{25} -17.5$  (c 1.0, MeOH);  $^1\text{H NMR}$  (400 MHz,  $\text{CDCl}_3$ )  $\delta$  6.34 (dd,  $J = 15.1, 9.8$  Hz, 1H), 6.23 (d,  $J = 9.9$  Hz, 1H), 5.90–5.75 (m, 1H), 2.46 (t,  $J = 7.2$  Hz, 2H), 2.26 (dd,  $J = 13.7, 6.9$  Hz, 2H), 1.62 (dd,  $J = 14.6, 7.3$  Hz, 2H), 1.50–1.44 (m, 2H), 1.46–1.38 (m, 1H), 1.28–1.23 (m, 2H), 0.92 (t,  $J = 7.4$  Hz, 3H), 0.86–0.78 (m, 1H).  $^{13}\text{C NMR}$  (100 MHz,  $\text{CDCl}_3$ )  $\delta$  180.0, 135.4, 128.7, 127.6, 127.4, 43.6, 32.7, 32.4, 23.4, 21.4, 20.0, 16.2, 12.9. IR (KBr,  $\text{cm}^{-1}$ )  $\nu$  2961, 2927, 2854, 1703, 1694, 1454, 1429, 1229, 1080, 968, 878, 802; HRMS (ESI,  $m/z$ ) calcd for  $\text{C}_{13}\text{H}_{19}\text{BrO}_2$   $[\text{M} + \text{Na}]^+$ , 309.0461 and 311.0440, found 309.0468 and 311.0449.

**(14)**  $^1\text{H NMR}$  (400 MHz,  $\text{CDCl}_3$ )  $\delta$  6.31 (dd,  $J = 14.9, 9.8$  Hz, 1H), 6.22 (d,  $J = 9.9$  Hz, 1H), 5.87–5.74 (m, 1H), 3.69 (s, 3H), 2.45 (t,  $J = 7.2$  Hz, 2H), 2.32 (t,  $J = 7.5$  Hz, 2H), 2.12 (q,  $J = 7.0$  Hz, 2H), 1.67–1.57 (m, 4H), 1.42 (m, 2H), 1.33 (m, 6H), 0.92 (t,  $J = 7.4$  Hz, 3H).  $^{13}\text{C NMR}$  (100 MHz,  $\text{CDCl}_3$ )  $\delta$  174.3, 137.1, 128.0, 127.8, 126.8, 51.5, 43.6, 34.1, 32.9, 29.1, 29.1, 29.0, 24.9, 21.5, 13.0. IR (KBr,  $\text{cm}^{-1}$ )  $\nu$  3648, 2927, 2854, 1742, 1621, 1260, 1016, 866; HRMS (ESI,  $m/z$ ) calcd for  $\text{C}_{16}\text{H}_{27}\text{BrO}_2$   $[\text{M} + \text{Na}]^+$ , 353.1087 and 355.1066, found 353.1099 and 355.1080.

**(15)**  $^1\text{H NMR}$  (400 MHz,  $\text{CDCl}_3$ )  $\delta$  6.29 (ddt,  $J = 14.8, 9.8, 1.3$  Hz, 1H), 6.20 (d,  $J = 9.9$  Hz, 1H), 5.85–5.74 (m, 1H), 2.43 (t,  $J = 7.2$  Hz, 2H), 2.35 (t,  $J = 7.5$  Hz, 2H), 2.10 (q,  $J = 6.9$  Hz, 2H),

1.67–1.55 (m, 4H), 1.45–1.33 (m, 4H), 1.35–1.27 (m, 6H), 0.90 (t,  $J = 7.4$  Hz, 3H).  $^{13}\text{C}$  NMR (100 MHz,  $\text{CDCl}_3$ )  $\delta$  179.6, 137.0, 128.0, 127.8, 126.8, 43.6, 34.0, 32.9, 29.1, 29.0(6), 29.0, 24.7, 21.5, 13.0. IR (KBr,  $\text{cm}^{-1}$ )  $\nu$  2960, 2929, 2855, 1710, 1462, 1464, 1428, 1259, 967; HRMS (ESI,  $m/z$ ) calcd for  $\text{C}_{15}\text{H}_{25}\text{BrO}_2$   $[\text{M} + \text{Na}]^+$ , 339.0930 and 341.0910, found 339.0945 and 341.0924.

#### 4.6. Anti-Inflammatory Activity Testing

Nitric oxide (NO) production in mouse macrophages (RAW264.7) was used to detect the inhibitory effect of compounds in inflammatory reaction. When immune cells are stimulated by microbial endotoxin and inflammatory mediators, many induced NO synthase (iNOS) will be generated to produce NO for immune response. Therefore, inhibition of NO production is a direct indicator of anti-inflammatory activity of compounds. The inhibitory activity of majusculoic acid and its analogs on NO production in LPS-induced inflammatory models were evaluated in our research.

Griss kit was used to detect NO content in the culture medium (Molecular probes, G-7921). Macrophages (RAW264.7) were cultured in Dulbecco modified eagle's medium (DMEM) medium which contained 10% fetal bovine serum (FBS). The cell concentration of macrophages was adjusted and then inoculated in a 24-well cell culture plate for 24 h. The test compounds of different concentrations were pretreated for 2 h before the incubating of LPS (100 ng/mL) for 24 h. The blank medium was used as control. After adding lipopolysaccharide (LPS, 1  $\mu\text{g}/\text{mL}$ ) for 24 h, the supernatant culture medium was combined with Griss reagent, and the absorbance value was measured at 548 nm by spectrometry.

$$\text{NO production inhibition rate} = (\text{OD}_{\text{control}} - \text{OD}_{\text{sample}}) / (\text{OD}_{\text{control}} - \text{OD}_{\text{blank}}) \times 100\%, \quad (1)$$

#### 4.7. Cytotoxicity Determination

It is expected that compounds inhibited the LPS-induced inflammatory response should not have cytotoxicity towards cells. Therefore, all eight compounds were also tested for cell proliferation by CCK-8 assay. Briefly, RAW264.7 cells were inoculated in 96-well plates and cultured for 24 h. The tested compounds were added, and incubation was continued for another 72 h. Then 10  $\mu\text{L}$  CCK-8 solution was added to each well. After 1.5 h, the OD values at 450 nm were determined.

$$\text{Cell proliferation inhibition rate (\%)} = (\text{OD}_{\text{control}} - \text{OD}_{\text{sample}}) / (\text{OD}_{\text{control}} - \text{OD}_{\text{blank}}) \times 100\%, \quad (2)$$

## 5. Conclusions

Our work provides a novel and efficient strategy to realize the total synthesis of natural majusculoic acid and other seven derivatives in ten steps with yield of 3% to 28%. Three compounds, majusculoic acid (**1**), methyl majusculoate (**9**), and ethyl (1*R*,2*R*)-2-((3*E*,5*Z*)-6-bromonona-3,5-dien-1-yl) cyclopropane-1-carboxylate (**12**), exhibited weak anti-inflammatory effects with inhibition rates of 33.68%, 35.75%, and 43.01% *in vitro*. This work could give assistance to more in-depth structure–activity relationship (SAR) research of CFAs.

**Supplementary Materials:** The following are available online at <https://www.mdpi.com/article/10.3390/md19060288/s1>, 1D and 2D NMR spectra of all synthetic compounds.

**Author Contributions:** X.-W.Y. and S.-L.L. designed the project; H.-X.X. synthesized all products, Q.-X.Y. and Z.-H.H. analyzed partial data. Z.-B.Z. purified some products. B.C., Q.-Q.L., and T.-T.C. performed the bioactive experiments. H.-X.X., S.-L.L., and X.-W.Y. wrote the paper, while critical revision of the publication was performed by all authors. All authors have read and agreed to the published version of the manuscript.

**Funding:** The work was supported by grants from the National Natural Science Foundation of China (21877022).

**Institutional Review Board Statement:** Not applicable.

**Informed Consent Statement:** Not applicable.

**Acknowledgments:** We thank Yandong Zhang, Renzhi Chen, and Yang Shen of Xiamen University for constructive suggestions on the synthetic strategy.

**Conflicts of Interest:** The authors declare no conflict of interest.



## References

1. Medzhitov, R. Origin and physiological roles of inflammation. *Nature* **2008**, *454*, 428–435. [[CrossRef](#)]
2. Beutler, B.; Rietschel, E.T. Innate immune sensing and its roots: The story of endotoxin. *Nat. Rev. Immunol.* **2003**, *3*, 169–176. [[CrossRef](#)] [[PubMed](#)]
3. Buchanan, M.M.; Hutchinson, M.; Watkins, L.R.; Yin, H. Toll-like receptor 4 in CNS pathologies. *J. Neurochem.* **2010**, *114*, 13–27. [[CrossRef](#)]
4. Kim, S.; Huri, D.; Snyder, S. Inducible Nitric Oxide Synthase Binds, S-Nitrosylates, and Activates Cyclooxygenase-2. *Science* **2006**, *310*, 1966–1970. [[CrossRef](#)] [[PubMed](#)]
5. Tungen, J.E.; Aursnes, M.; Vik, A.; Ramon, S.; Colas, R.A.; Dalli, J.; Serhan, C.N.; Hansen, T.V. Synthesis and Anti-inflammatory and Pro-resolving Activities of 22-OH-PD1, a Monohydroxylated Metabolite of Protectin D1. *J. Nat. Prod.* **2014**, *77*, 2241–2247. [[CrossRef](#)]
6. Aursnes, M.; Tungen, J.E.; Vik, A.; Colas, R.; Cheng, C.-Y.C.; Dalli, J.; Serhan, C.N.; Hansen, T.V. Total Synthesis of the Lipid Mediator PD1n-3 DPA: Configurational Assignments and Anti-inflammatory and Pro-resolving Actions. *J. Nat. Prod.* **2014**, *77*, 910–916. [[CrossRef](#)]
7. Dang, H.T.; Lee, H.J.; Yoo, E.S.; Shinde, P.B.; Lee, Y.M.; Hong, J.; Kim, D.K.; Jung, J.H. Anti-inflammatory Constituents of the Red Alga *Gracilaria verrucosa* and Their Synthetic Analogues. *J. Nat. Prod.* **2008**, *71*, 232–240. [[CrossRef](#)]
8. Tungen, J.E.; Primdahl, K.G.; Hansen, T.V. The First Total Synthesis of the Lipid Mediator PD2n-3 DPA. *J. Nat. Prod.* **2020**, *83*, 2255–2260. [[CrossRef](#)]
9. Wessjohann, L.; Brandt, W.; Thiemann, T. Biosynthesis and Metabolism of Cyclopropane Rings in Natural Compounds. *Chem. Rev.* **2003**, *103*, 1625–1647. [[CrossRef](#)] [[PubMed](#)]
10. Carballeira, N.; Montano, N.; Jan, V.; Rodriguez, D.A. Novel Cyclopropane Fatty Acids from the Phospholipids of the Caribbean Sponge *Pseudospongosorites suberitoides*. *Lipids* **2007**, *42*, 519–524. [[CrossRef](#)]
11. Macmillan, J.; Molinski, T. Majusculoic Acid, a Brominated Cyclopropyl Fatty Acid from a Marine Cyanobacterial Mat Assemblage. *J. Nat. Prod.* **2005**, *68*, 604–606. [[CrossRef](#)] [[PubMed](#)]
12. Amiri Moghaddam, J.; Dávila-Céspedes, A.; Kehraus, S.; Crüsemann, M.; Köse, M.; Müller, C.E.; König, G.M. Cyclopropane-Containing Fatty Acids from the Marine Bacterium *Labrenzia* sp. 011 with Antimicrobial and GPR84 Activity. *Mar. Drugs* **2018**, *16*, 369. [[CrossRef](#)]
13. Sitachitta, N.; Gerwick, W. Grenadadiene and Grenadamide, Cyclopropyl-Containing Fatty Acid Metabolites from the Marine Cyanobacterium *Lyngbya majuscula*. *J. Nat. Prod.* **1998**, *61*, 681–684. [[CrossRef](#)] [[PubMed](#)]
14. Ogawa, H.; Iwasaki, A.; Sumimoto, S.; Iwatsuki, M.; Ishiyama, A.; Hokari, R.; Otaguro, K.; Omura, S.; Suenaga, K. Isolation and Total Synthesis of Hoshinolactam, an Antitrypanosomal Lactam from a Marine Cyanobacterium. *Org. Lett.* **2017**, *19*, 890–893. [[CrossRef](#)] [[PubMed](#)]
15. Nemoto, T.; Yoshino, G.; Ojika, M.; Sakagami, Y. Amphimic Acids and Related Long-chain Fatty Acids as DNA Topoisomerase I Inhibitors from an Australian Sponge, *Amphimedon* sp.: Isolation, Structure, Synthesis, and Biological Evaluation. *Tetrahedron* **1997**, *53*, 16699–16710. [[CrossRef](#)]
16. Chen, R.; Li, L.; Lin, N.; Zhou, R.; Yuhui, H.; Deng, H.; Zhang, Y. Asymmetric Total Synthesis of (+)-Majusculoic Acid via a Dimerization–Dedimerization Strategy and Absolute Configuration Assignment. *Org. Lett.* **2018**, *20*, 1477–1480. [[CrossRef](#)]
17. Line, N.; Witherspoon, B.; Hancock, E.; Brown, M. Synthesis of ent-[3]-Ladderanol: Development and Application of Intramolecular Chirality Transfer [2+2] Cycloadditions of Allenic Ketones and Alkenes. *J. Am. Chem. Soc.* **2017**, *139*, 14392–14395. [[CrossRef](#)]
18. Shaw, M.H.; Croft, R.A.; Whittingham, W.G.; Bower, J.F. Modular Access to Substituted Azocanes via a Rhodium-Catalyzed Cycloaddition–Fragmentation Strategy. *J. Am. Chem. Soc.* **2015**, *137*, 8054–8057. [[CrossRef](#)]
19. Manzi, S.; Wasko, M.C. Inflammation-mediated rheumatic diseases and atherosclerosis. *Ann. Rheum. Dis.* **2000**, *59*, 321–325. [[CrossRef](#)]
20. Murdoch, J.; Lloyd, C. Chronic inflammation and asthma. *Mutat. Res.* **2009**, *690*, 24–39. [[CrossRef](#)]
21. Blau, N.; Wang, T.; Buess, C. Potential inhibitors of cholesterol biosynthesis phosphonates derived from geraniol and congeners. *J. Chem. Eng. Data* **2002**, *15*, 206–208. [[CrossRef](#)]



Review

# Divergent Strategy in Marine Tetracyclic Meroterpenoids Synthesis

Antonio Rosales Martínez <sup>1,\*</sup> , Ignacio Rodríguez-García <sup>2</sup>  and Josefa L. López-Martínez <sup>2</sup>

<sup>1</sup> Department of Chemical Engineering, Escuela Politécnica Superior, University of Sevilla, 41011 Sevilla, Spain

<sup>2</sup> Organic Chemistry, ceiA3, University of Almería, 04120 Almería, Spain; irodrigu@ual.es (I.R.-G.); pepaloma91@hotmail.com (J.L.L.-M.)

\* Correspondence: arosales@us.es

**Abstract:** The divergent total synthesis strategy can be successfully applied to the preparation of families of natural products using a common late-stage pluripotent intermediate. This approach is a powerful tool in organic synthesis as it offers opportunities for the efficient preparation of structurally related compounds. This article reviews the synthesis of the marine natural product aureol, as well as its use as a common intermediate in the divergent synthesis of other marine natural and non-natural tetracyclic meroterpenoids.

**Keywords:** divergent total synthesis; marine natural products; tetracyclic meroterpenoids; aureol



**Citation:** Rosales Martínez, A.; Rodríguez-García, I.; López-Martínez, J.L. Divergent Strategy in Marine Tetracyclic Meroterpenoids Synthesis. *Mar. Drugs* **2021**, *19*, 273. <https://doi.org/10.3390/md19050273>

Academic Editor: Emiliano Manzo

Received: 29 April 2021

Accepted: 12 May 2021

Published: 13 May 2021

**Publisher's Note:** MDPI stays neutral with regard to jurisdictional claims in published maps and institutional affiliations.



**Copyright:** © 2021 by the authors. Licensee MDPI, Basel, Switzerland. This article is an open access article distributed under the terms and conditions of the Creative Commons Attribution (CC BY) license (<https://creativecommons.org/licenses/by/4.0/>).

## 1. Introduction

The original definition of divergent total synthesis (Figure 1) was reported by Boger et al. [1] and was defined as the synthesis in which “at least two members of the class of compounds” can be separately prepared from a common, advanced synthetic intermediate. Therefore, the most important challenge in a divergent synthesis is the choice of a common intermediate which could be transformed into a target array of natural products and non-natural derivatives. This strategy is a powerful tool that has attracted the attention of numerous research groups as it improves the efficiency of chemical processes [2,3], and attains special relevance when structure-activity studies are the ultimate goals. Later, other terms such as “diverted total synthesis” [4] and “collective total synthesis” [5] were introduced, thus extending the amplitude of divergent synthesis. In this way, “diverted total synthesis” can be applied to the preparation of a natural product-like compound library by appropriate transformations of a common intermediate, avoiding the limitations inherent to partial syntheses from the natural product caused by the presence of multiple similar functional groups. In addition, the term “collective total synthesis” is used when the common intermediate is endowed with functional characteristics suitable for the preparation of structurally diverse natural products belonging to different families.

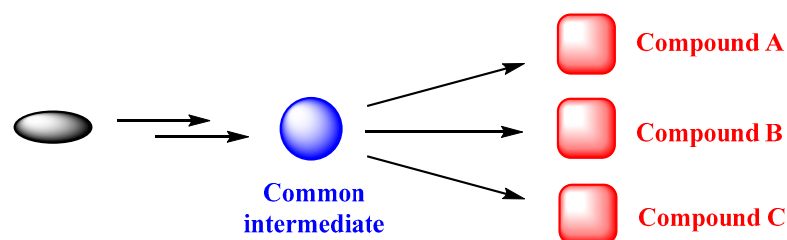
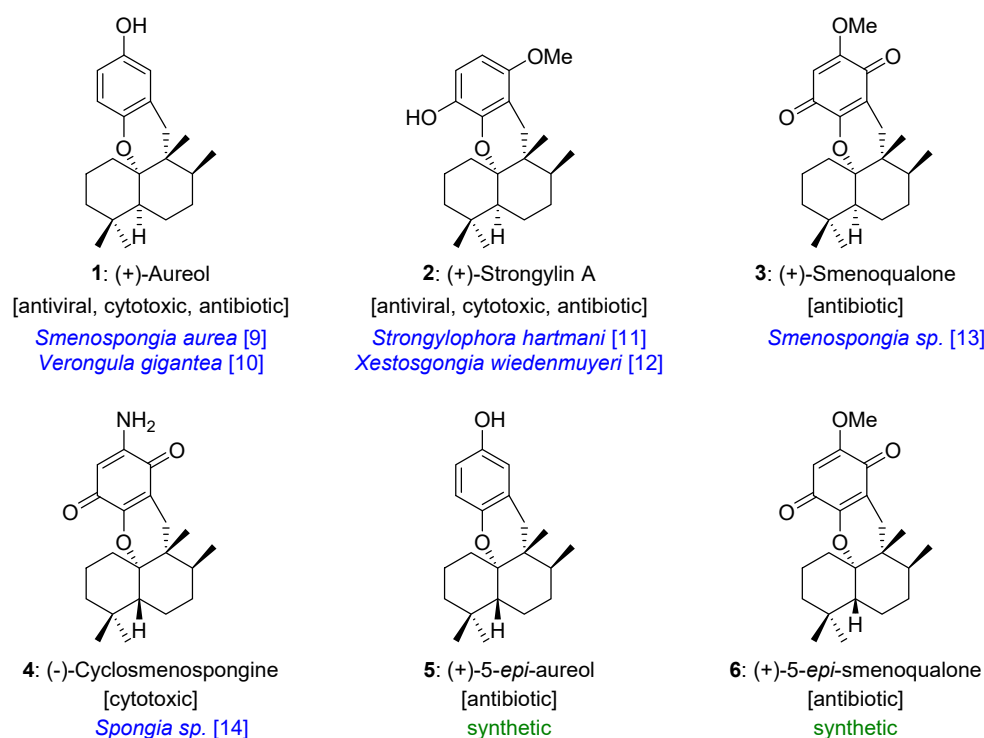


**Figure 1.** Divergent total synthesis.

On the other hand, tetracyclic meroterpenoids [6,7] are a unique class of marine natural compounds with significant biological activities. Representative examples of marine

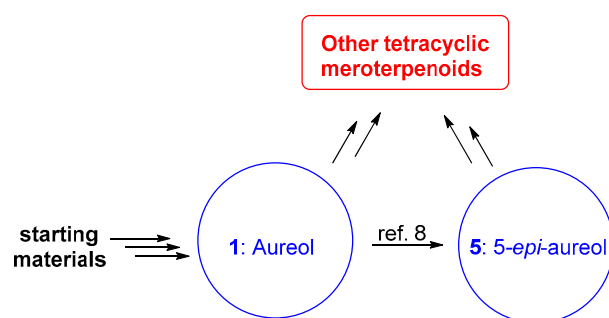


natural and non-natural tetracyclic meroterpenoids, including (+)-aureol (**1**) [8–10], (+)-strongylin A (**2**) [8,11,12], (+)-smenoqualone (**3**) [8,13], (–)-cyclosmenospongine (**4**) [8,14], (+)-5-*epi*-aureol (**5**) [8,15–17], and (+)-5-*epi*-smenoqualone (**6**) [8] have been considered of interest by the chemical community due to their interesting biological properties and unique molecular structures (Scheme 1). In fact, structure–activity relationship (SAR) studies show that variations on the nature and substituents on the aromatic ring have a strong impact on the observed activity [8,18]. These natural products (Scheme 1) contain a compact tetracyclic system with a substituted benzopyran moiety, four consecutive asymmetric carbon atoms, and a well-defined *trans*- or *cis*-relationship between the two cyclohexane rings of the decalin system. Although several synthetic methods have been described, a divergent approach to this class of compounds has not been previously reported as such.



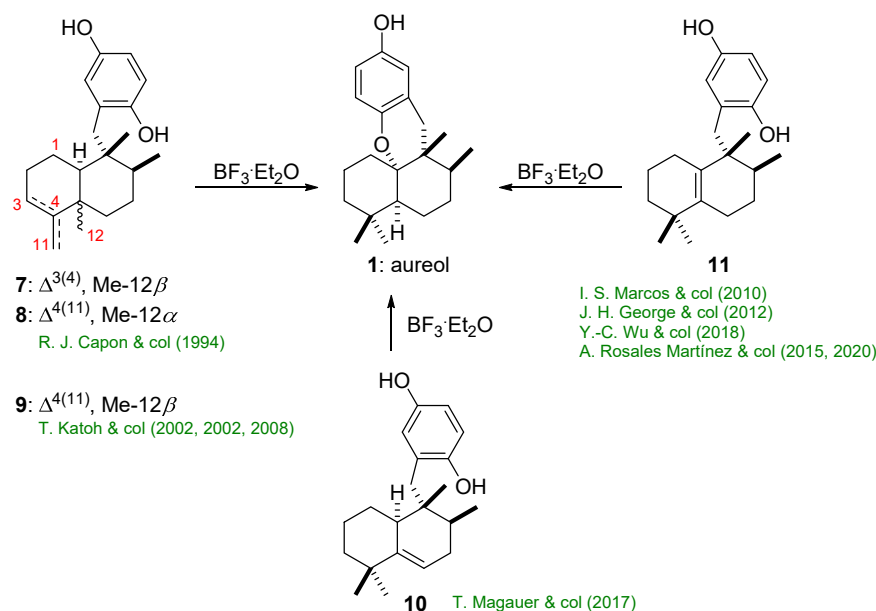
**Scheme 1.** Representative examples of marine natural and non-natural tetracyclic meroterpenoids and their reported biological activity.

This article focuses on the synthetic efforts towards aureol (**1**), a marine natural meroterpenoid present in the Caribbean sponges *Smenospongia aurea* [9] and *Verongula gigantea* [10] which has shown an important biological profile [8,19,20]. Aureol (**1**) can be an excellent advanced and common synthetic intermediate for the divergent synthesis of other natural and non-natural tetracyclic terpenoids. In this article, we present a unified and versatile approach for the diversification of this class of compounds with the aim to contribute to the development of new desirable drugs for the pharmaceutical industry and the medicinal chemistry. The divergent synthesis of either natural or fully synthetic derivatives could be achieved through aureol (**1**) as a common intermediate, by adequate sequential functionalization of the aromatic ring, or by epimerization of the decalin core of aureol (**1**) to 5-*epi*-aureol (**5**) followed by functionalization of the aromatic ring (Scheme 2).



**Scheme 2.** Conceptual model of the divergent synthesis of tetracyclic meroterpenoids using aureol (1) as a pluripotential late-stage intermediate.

Scheme 3 summarizes the last step of previous syntheses towards aureol (1). All of them have as key step a cationic cyclization of an olefinic intermediate (7–11).



**Scheme 3.** Key olefinic intermediates of previous syntheses of aureol (1).

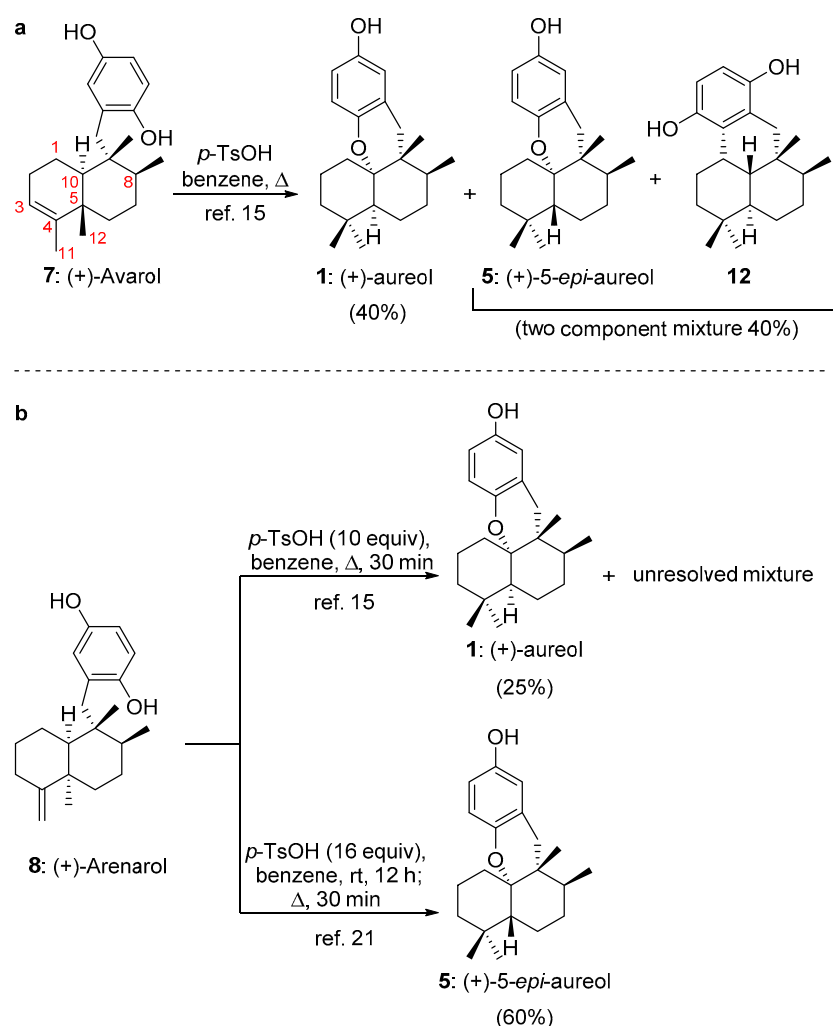
The different synthetic sequences for aureol (1) are listed below, classified according to the olefinic key intermediate shown in Scheme 3.

## 2. Synthesis of Aureol

### 2.1. Synthesis of Aureol from Key Intermediates 7–9

#### 2.1.1. Capon's Synthesis of (+)-Aureol

The first work on the synthesis of the marine product (+)-aureol (1) was published by the group of R. J. Capon [15] using natural sesquiterpene hydroquinones ((+)-avarol (7) and (+)-arenarol (8)) as starting materials (Scheme 4). In these processes (+)-aureol (1) could be formed via a concerted 1,2-migration of Me-12 and H-10. However, formation of (+)-*epi*-aureol (5) is better understood considering that, after methyl migration, there is a loss of the C-10 proton to give a  $\Delta^{5,10}$  olefin intermediate, which would later suffer *trans* addition of the OH group. This lack of stereocontrol of the process was later confirmed by Lakshmi et al. [21], as they could determine the structure of 5 by X-ray analysis (Scheme 4b).



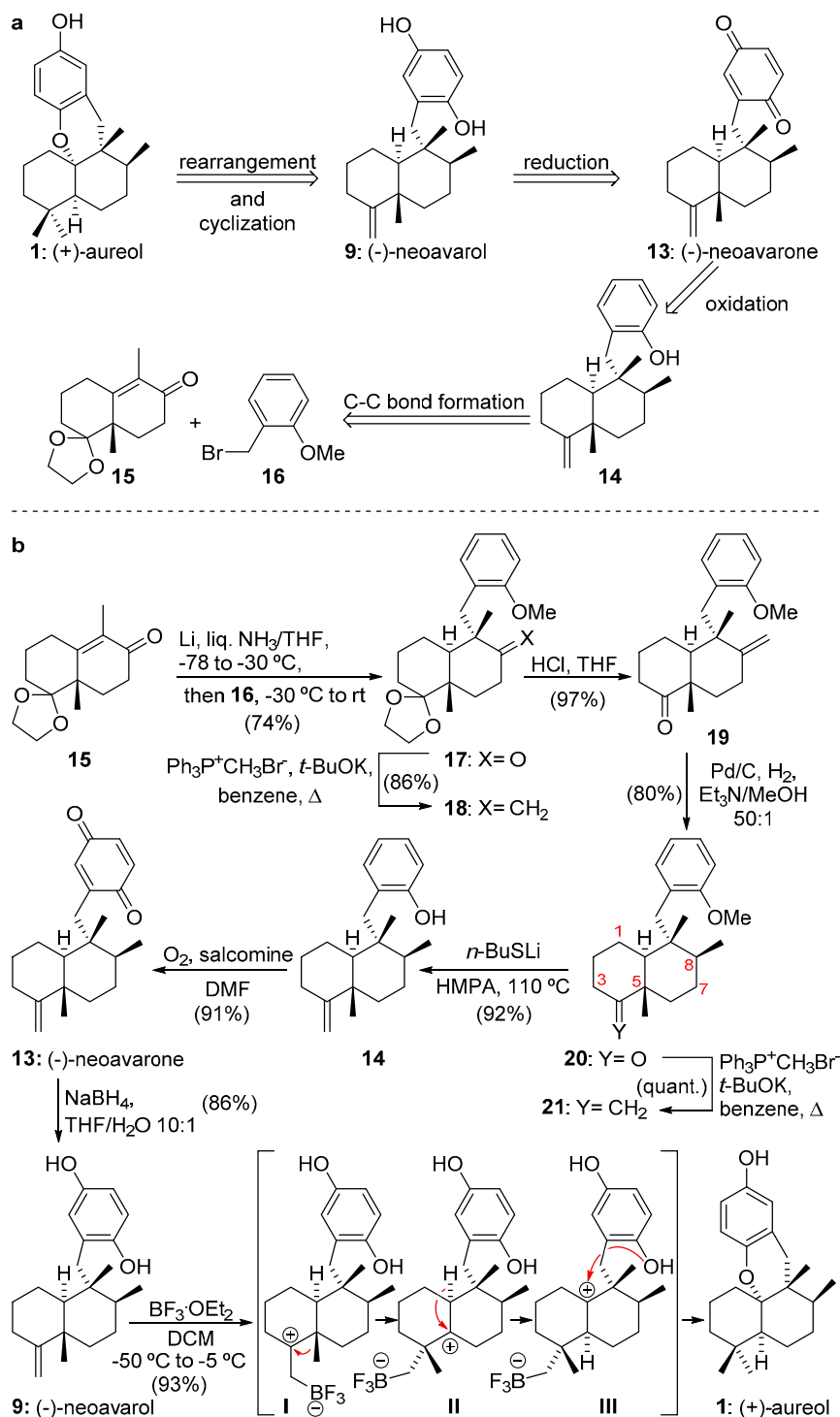
**Scheme 4.** (a): Acid-induced rearrangement of (+)-avarol (**7**). (b): Acid-induced rearrangement of (+)-arenarol (**8**).

### 2.1.2. Katoh's Synthesis of (+)-Aureol

Katoh and colleagues [22–24] reported the first enantioselective total synthesis of (+)-aureol (**1**) in 2002 [22], a process they later improved in 2003 [23]. The retrosynthetic plan of the improved synthesis is shown in Scheme 5a. This approach obtains aureol (**1**) in one step by acid-induced rearrangement/cyclization of (–)-neoavarol (**9**). In turn, **9** can be prepared by reduction of the quinone moiety present in (–)-neovarone (**13**), a compound which can be readily obtained by strategic salcomine oxidation of **14**. This can be assembled by stereocontrolled reductive alkylation of (+)-5-methyl-Wieland-Miescher ketone (**15**) with 2-methoxybenzyl bromide (**16**) (Scheme 5a).

As shown in Scheme 5b, Katoh's synthesis of (+)-aureol (**1**) used enantiopure (+)-5-methyl-Wieland-Miescher ketone (**15**) as the starting material. A C-C bond-forming reaction between **15** and a lithiated arene unit, prepared from 2-methoxybenzyl bromide (**16**), gave the coupling product **17** as a single diastereomer in 74%. The Wittig methylenation of **17** produced the *exo*-double bond present in decaline **18** in 86% yield. Removal of the acetal protective group by acid treatment (97% yield), followed by hydrogenation of the exocyclic double bond present in the resulting ketone **19**, led to the product **20** (80% yield) together with its C8 epimer (13% yield). Subsequent Wittig methylenation of **20** quantitatively gave **21**, which was submitted to a deprotection of the *O*-methyl group in order to form the phenol **14** (92% yield).  $O_2$ /salcomine oxidation of **14** gave the quinone **13** (91% yield). Finally,  $NaBH_4$  reduction of quinone **13** gave (–)-neoavarol (**9**) (86% yield). Once **9** was synthesized, the crucial step was the  $BF_3 \cdot Et_2O$ -induced rearrangement of **9**, which led to

the desired (+)-aureol (**1**) (93% yield). This rearrangement occurred via stereospecific 1,2-hydride and methyl shifts, as shown in Scheme 5b. In this reaction the three intermediate carbocations **I**, **II**, and **III** are involved. This synthesis was completed in nine steps (33% overall yield) from the starting material **15**.

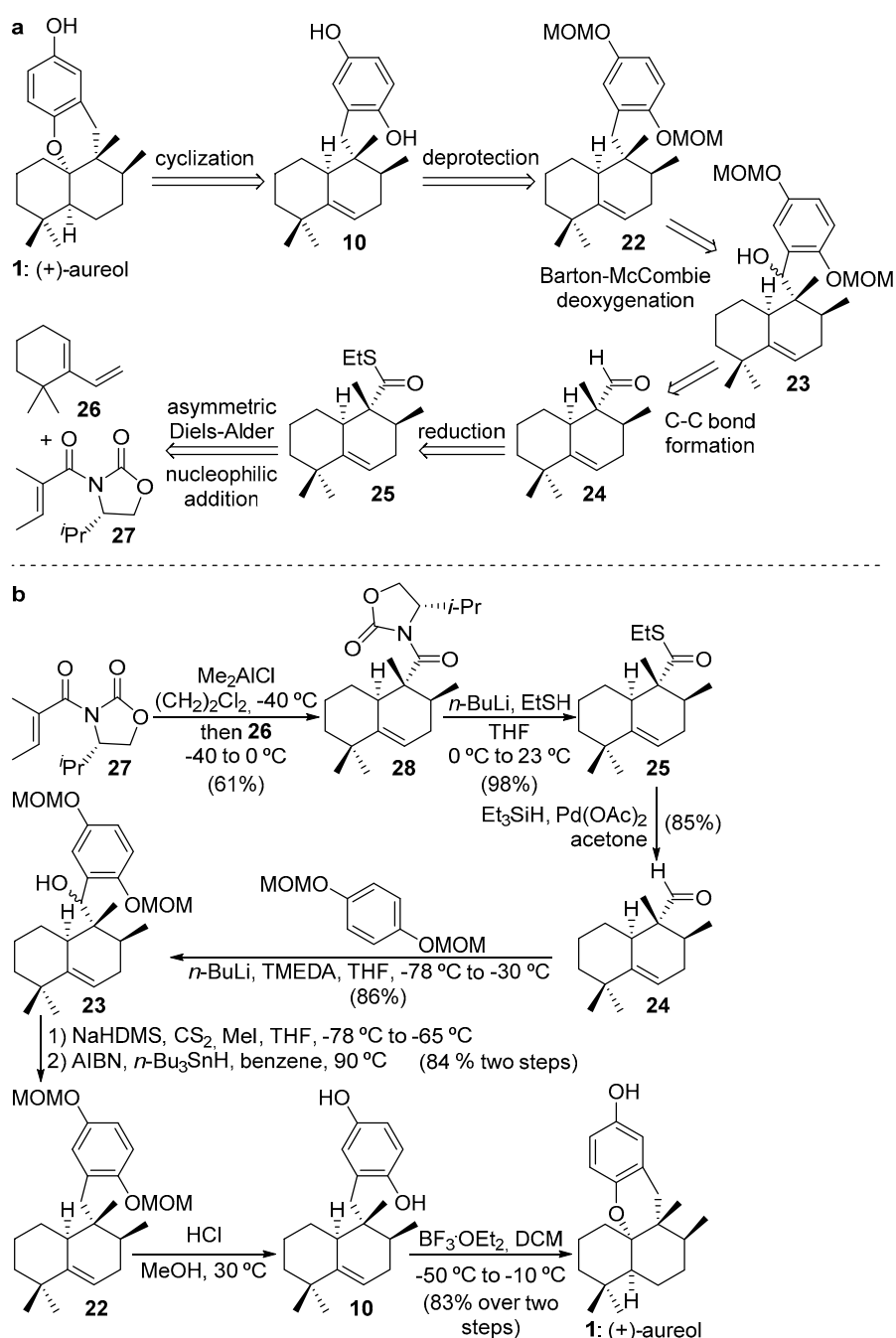


**Scheme 5.** Strategy for the synthesis of (+)-aureol (**1**) according to Katoh and colleagues [22–24]. (a): Retrosynthetic plan. (b): Synthesis of (+)-aureol (**1**). HMPA = hexamethylphosphoramide; salcomine = *N,N'*-bis(salicylidene)ethylenediamino cobalt(II); DMF = *N,N'*-dimethylformamide.

## 2.2. Synthesis of Aureol from Key Intermediate 10

## Magauer's Synthesis of (+)-Aureol

The synthesis of (+)-aureol (**1**) reported by Magauer and colleagues [8] used a highly robust and modular synthetic platform, developed for the preparation of natural and fully synthetic analogues of tetracyclic meroterpenoids. The retrosynthetic plan for (+)-aureol (**1**) (Scheme 6a) is based on the stereospecific acid-promoted cyclization of the  $\Delta^{5(6)}$  olefin intermediate **10**. Its methoxymethyl ether derivative **22** could be prepared from **23** following the Barton–McCombie deoxygenation protocol. This diastereoisomeric mixture of benzyl alcohols results from the addition of 2-lithiohydroquinone dimethyl ether to aldehyde **24**, which can be obtained by Fukuyama's reduction [25] of thioester **25**.



**Scheme 6.** Strategy for the synthesis of (+)-aureol (**1**) according to Magauer et al. [8]. (a): Retrosynthetic plan. (b): Synthesis of (+)-aureol (**1**). TMEDA = *N,N,N',N'*-tetramethylethane-1,2-diamine; NaHDMS = sodium bis(trimethylsilyl)amide; AIBN = 2,2'-azobis(2-methylpropanionitrile).

The keystone in the asymmetric process is the formation of the three chiral centers present in **25** through the asymmetric Diels–Alder reaction [26,27] between **26** and enantiopure **27** followed by lithium ethanethiolate removal of the chiral auxiliary (Scheme 6a).

Scheme 6b details the synthesis of (+)-aureol (**1**) from diene **26**. The first key step was the asymmetric construction of the 5,6-dehydrodecaline component **28** employing an *exo*-selective Diels–Alder cycloaddition between diene **26** and tiglic acid-derived dienophile **27** to afford **28** (61% yield). The oxazolidinone chiral auxiliary was replaced by nucleophilic 1,2-addition of lithium ethanethiolate to the carbonyl group of the Diels–Alder product **28**, a process which afforded thioester **25** in 98% yield. A smooth Fukuyama reduction [25] of **25** gave aldehyde **24** (85% yield), which was coupled with the lithiated arene unit to afford a mixture of diastereomeric benzylic alcohols **23** (86% yield). The free hydroxy group of **23** was removed using the two-step Barton–McCombie deoxygenation protocol, which afforded **22** in 84% yield (two steps). The subsequent deprotection of **22** with HCl/MeOH gave hydroquinone sesquiterpene **10**, which was directly subjected to cyclization conditions to give (+)-aureol (**1**) (83% yield). In this reaction, the proton formed by coordination of  $\text{BF}_3 \cdot \text{OEt}_2$  to one of the OH-groups in **10** possibly triggers the cationic rearrangement. When the cyclization is carried out under kinetic conditions (at temperatures below  $-10^\circ\text{C}$ ), a *cis*-decaline framework is formed exclusively. On the other hand, under thermodynamic control, only the *trans*-decaline is obtained. This total synthesis was achieved in eight steps (30% overall yield) from the starting material **26**.

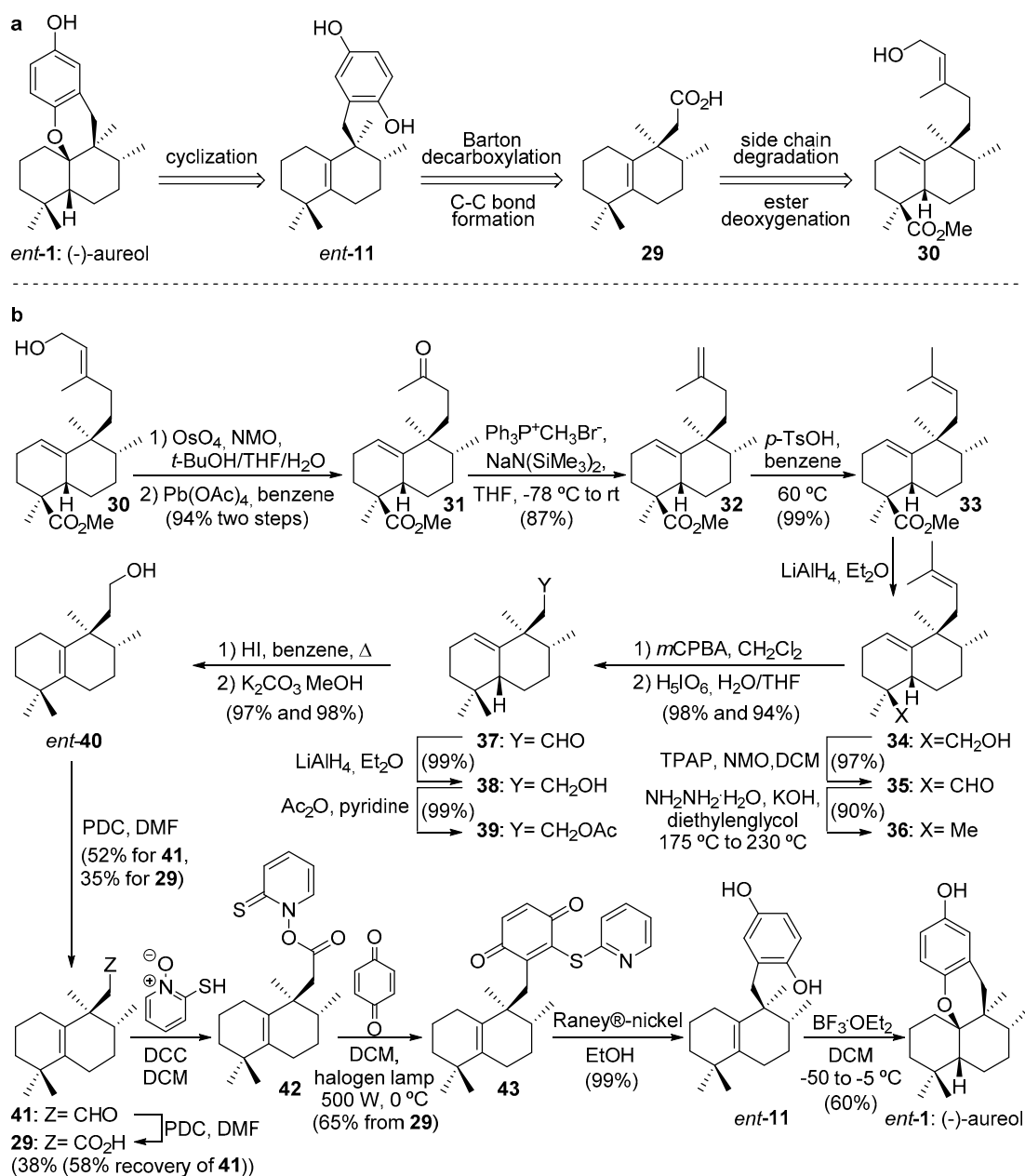
### 2.3. Synthesis of Aureol from Key Intermediate **11**

#### 2.3.1. Marcos's Synthesis of (–)-Aureol

Marcos and colleagues [28] reported the total synthesis of the (–) enantiomer of aureol (*ent*-**1**) from the methyl ester of natural *ent*-halimic acid (Scheme 7a). Their approach was based on: (a) the acid-induced cyclization of sesquiterpene hydroquinone *ent*-**11**, (b) the Barton decarboxylation reaction/*p*-benzoquinone addition sequence and the subsequent reduction with Raney<sup>®</sup> nickel (*ent*-**11** from **29**), and (c) the side-chain degradation of *ent*-halimic acid methyl ester **30** and the subsequent reduction of C-18 methyl ester.

As shown in Scheme 7b the synthesis of (–)-aureol (*ent*-**1**) used *ent*-halimic acid methyl ester **30** as the starting material. The degradation of the side chain of **30** was achieved [29,30] by oxidation with  $\text{OsO}_4$  followed by  $\text{Pb}(\text{OAc})_4$ , which gave ketone **31** (94% yield, two steps). The synthesis of the *endo*-olefin **33** required the Wittig methylenation of **31** (87% yield) and subsequent acid isomerization of **32** (99% yield). In order to remove the C-18 methyl ester, a three steps sequence from **33** to **36** was used, a process which gave a very good global yield. The synthesis of product **39** was achieved in four steps: a) the chemoselective epoxidation of the side-chain double bond in **36** (98% yield), b) the oxidative cleavage with  $\text{H}_5\text{IO}_6$  in  $\text{H}_2\text{O}/\text{THF}$  to afford **37** (94% yield); c) reduction with  $\text{LiAlH}_4$  (99% yield) to give **38** (99% yield), and d) the acetylation of the hydroxy group in **38** to afford **39** (99% yield). The isomerization of the olefin double bond present in acetate **39** with HI (97% yield) followed by the saponification of the acetoxy group (98% yield) gave the rearranged product *ent*-**40**. Finally, the oxidation of *ent*-**40** to acid **29** via aldehyde **41** was achieved with pyridinium dichromate (PDC) in a moderate yield. Once intermediate **29** was available, the key precursor *ent*-**11** of (–)-aureol (*ent*-**1**) could be readily prepared by Barton decarboxylation reaction in the presence of *p*-benzoquinone, a methodology reported by Theodorakis and colleagues [31,32] for the synthesis of ilimaquinone. In this way, when **29** was treated with 2-mercaptopyridine *N*-oxide in the presence of *N,N'*-dicyclohexylcarbodiimide (DCC) a photo labile thio-hydroxamic ester (**42**) was obtained. Then, **43** was prepared by light-induced decarboxylation (halogen lamp 500W) of **42** in the presence of benzoquinone in a 65% yield from **29**. The subsequent reduction of **43** with Raney<sup>®</sup> nickel gave *ent*-**11** in a 99% yield. With the key precursor *ent*-**11** in their hands, the treatment of this compound with  $\text{BF}_3 \cdot \text{Et}_2\text{O}$  at low temperature exclusively afforded (–)-aureol (*ent*-**1**) with complete stereoselectivity (60% yield). This total synthesis was

achieved in 19 steps (10.3% overall yield) from *ent*-halimic acid methyl ester **30** as the chiral pool starting material.

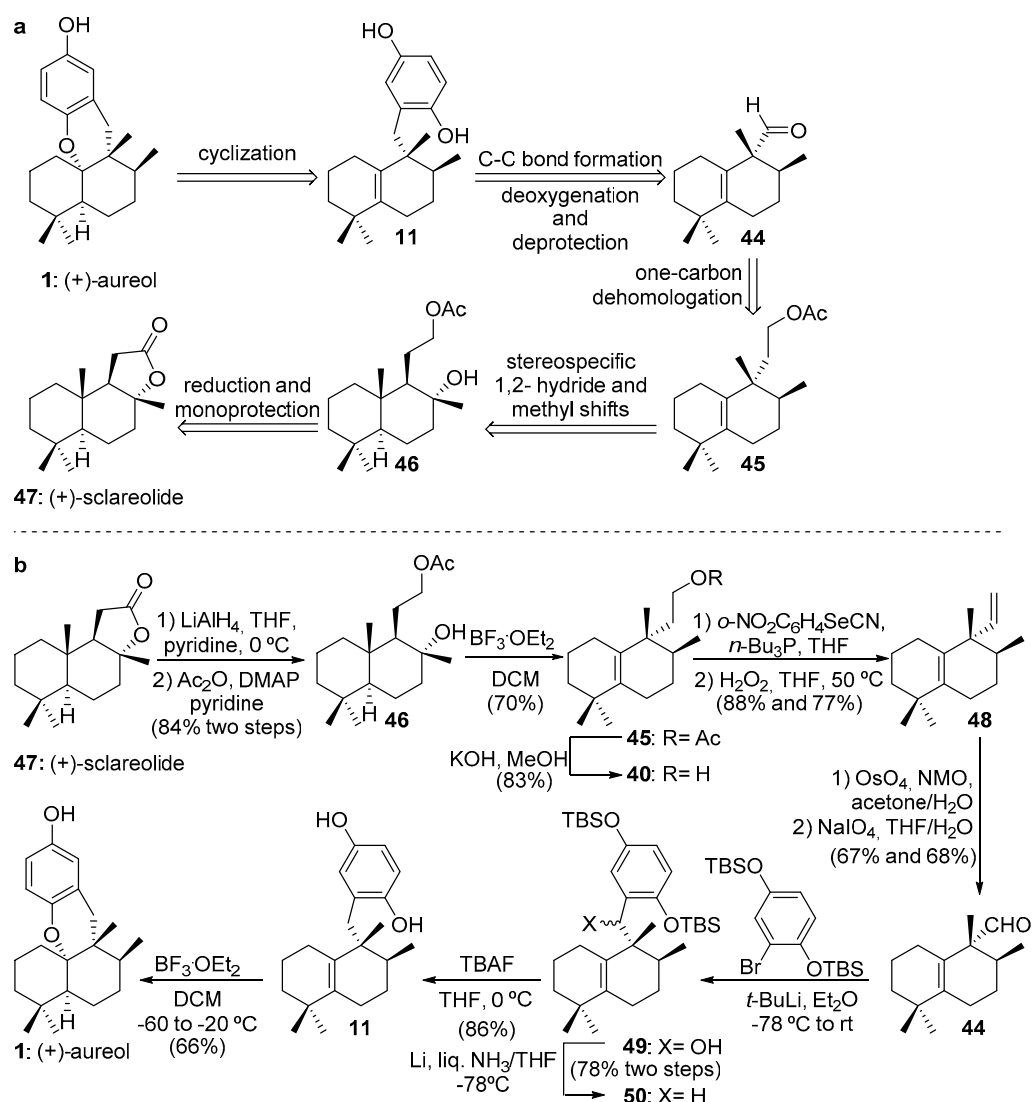


**Scheme 7.** Strategy for the synthesis of (–)-aureol (*ent*-1) according to Marcos and colleagues [26]. (a): Retrosynthetic plan. (b): Synthesis of (–)-aureol (*ent*-1). NMO = *N*-methylmorpholine-*N*-oxide; TPAP = tetra-*n*-propylammonium perruthenate; *m*CPBA = *m*-chloroperoxybenzoic acid; PDC = pyridinium dichromate; DCC = *N,N'*-dicyclohexylcarbodiimide.

### 2.3.2. George's Synthesis of (+)-Aureol

George's group [33] published in 2012 the second total synthesis of (+)-aureol (**1**). Their biosynthetically inspired retrosynthesis of (+)-aureol (**1**) (Scheme 8a) rests upon the biomimetic acid-mediated cyclization of the key tetrasubstituted olefin intermediate **11**, which could be prepared through a process involving the addition of an aryllithium derivative to aldehyde **44**. This aldehyde could be formed using a one-carbon dehomologation sequence from **45**. Another key step in the process is the biomimetic sequence of 1,2-hydride and 1,2-methyl shifts, which converts alcohol **46** into **45**. Finally, the reduc-

tion and selective protection of the commercially available enantiopure starting material (+)-sclareolide (**47**) would form the intermediate **46**.



**Scheme 8.** Strategy for the synthesis of (+)-aureol (**1**) according to George and colleagues [33]. (a) Retrosynthetic plan. (b) Synthesis of (+)-aureol (**1**). DMAP = 4-(dimethylamino)pyridine; NMO = *N*-methylmorpholine-*N*-oxide; TBAF = tetrabutylammonium fluoride.

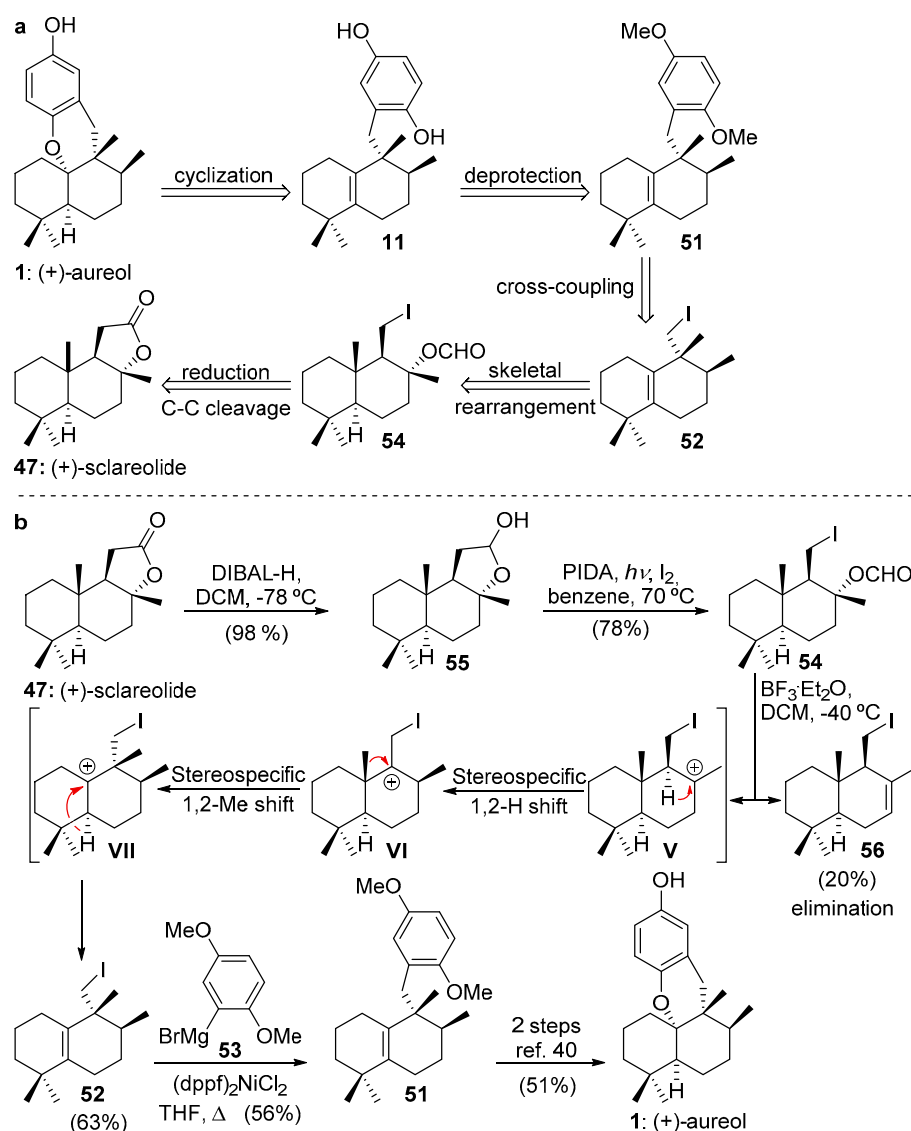
As shown in Scheme 8b, George's synthesis of (+)-aureol (**1**) used **11** as the key intermediate, which was prepared from natural (+)-sclareolide (**47**). Its reduction with LiAlH<sub>4</sub> gave a diol, which was selectively protected at the primary hydroxy group with Ac<sub>2</sub>O in pyridine to afford the acetate **46** in an 84% yield (two steps). Monoacetate **46** was stereoselectively converted to the single stereoisomer olefin **45** (70% yield) in a rearrangement induced by BF<sub>3</sub>·Et<sub>2</sub>O, which occurred via stereospecific sequential 1,2-hydride and 1,2-methyl shifts. Saponification of the acetate in **45** gave alcohol **40** (83% yield), which was readily converted into aldehyde **44** through a one-carbon dehomologation sequence using the Grieco–Sharples elimination protocol [34,35] (67% yield in two steps) followed by oxidative cleavage of the resulting terminal alkene **48** (45% yield in two steps). With aldehyde **44** in their hands, the coupling between **44** and an aryllithium species gave the mixture of diastereomeric benzylic alcohols **49**. In order to remove the OH group, this mixture of alcohols (**49**) was treated with lithium in liquid ammonia followed by NH<sub>4</sub>Cl aqueous solution to afford deoxygenated compound **50** in a 78% yield (two steps). Removal of the TBS protecting groups in **50** with tetrabutylammonium fluoride provided



the key intermediate **11** in an 86% yield. To complete the synthesis of (+)-aureol (**1**), the intermediate **11** was treated with  $\text{BF}_3 \cdot \text{Et}_2\text{O}$  to afford (+)-aureol (**1**) in a 66% yield. This total synthesis was achieved in 12 steps (6% overall yield) from (+)-sclareolide (**47**).

### 2.3.3. Wu's Synthesis of (+)-Aureol

In 2018, Wu and colleagues [36] published the formal synthesis of (+)-aureol (**1**). Their retrosynthesis of (+)-aureol is outlined in Scheme 9a. This retrosynthetic analysis is based on: (a) the biomimetic acid-mediated cyclization of the hydroquinone **11** to generate (+)-aureol (**1**), (b) the removal of the two O-Me protecting groups of **51** to afford the key intermediate **11**, (c) the cross-coupling reaction between alkyl iodide **52** and Grignard reagent **53** to give the intermediate **51**, (d) the rearrangement reaction of **54** to afford **52**, and (e) the reduction of (+)-sclareolide (**47**) and subsequent C-C bond cleavage to give **54**.



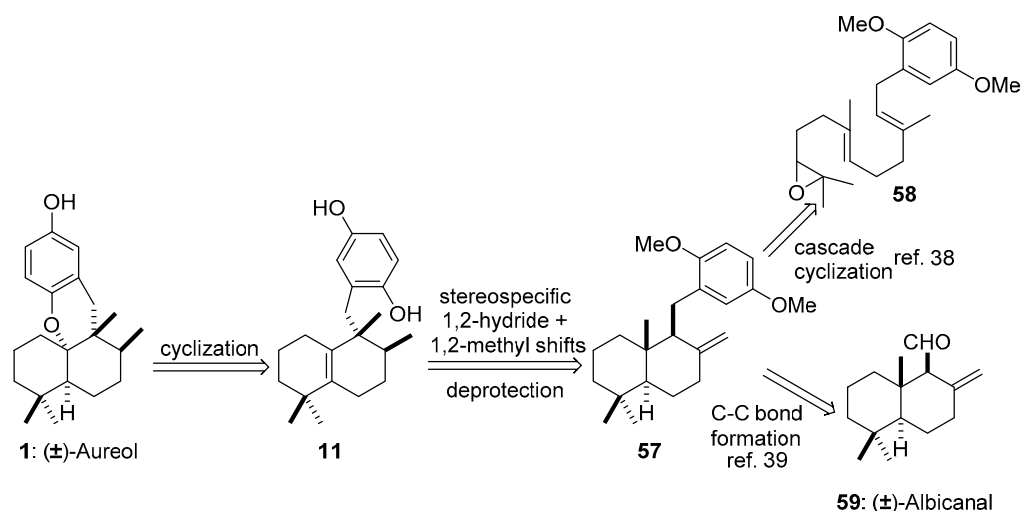
**Scheme 9.** Strategy for the synthesis of (+)-aureol (**1**) according to Wu and colleagues [36]. (a): Retrosynthetic plan. (b): Synthesis of (+)-aureol (**1**). DIBAL-H = diisobutylaluminium hydride; PIDA = (diacetoxyiodo)benzene.

As shown in Scheme 9b, the synthesis of intermediate **11** was carried out starting from commercially available (+)-sclareolide (**47**). Reduction of **47** using diisobutylaluminium hydride (DIBAL-H) generated sclareal (**55**) in a 98% yield. The treatment of **55** under the C-C bond cleavage conditions described by Suárez and colleagues [37] gave drimanal

iodoformate (**54**) in a 78% yield. The crucial step was the  $\text{BF}_3 \cdot \text{Et}_2\text{O}$ -mediated rearrangement of **54**, which occurred via stereospecific sequential 1,2-hydride and 1,2-methyl shifts to generate the desired alkyl iodide **52** (63%), together with a minor amount of by-product **56** (20%). In this reaction, the intermediate carbocations **V-VII** could be involved. With alkyl iodide **52** in their hands, the cross-coupling reaction between Grignard reagent **53** and alkyl iodide **52** generated the key intermediate **51** in a 56% yield. As olefin **51** was an advanced intermediate in the Rosales's synthesis [38,39] of ( $\pm$ )-aureol (**1**), their strategy constituted a formal synthesis of (+)-aureol (**1**). This formal synthesis was completed in four steps (27% overall yield) from starting material (+)-sclareolide (**47**).

#### 2.3.4. Rosales Martínez's Synthesis of ( $\pm$ )-Aureol

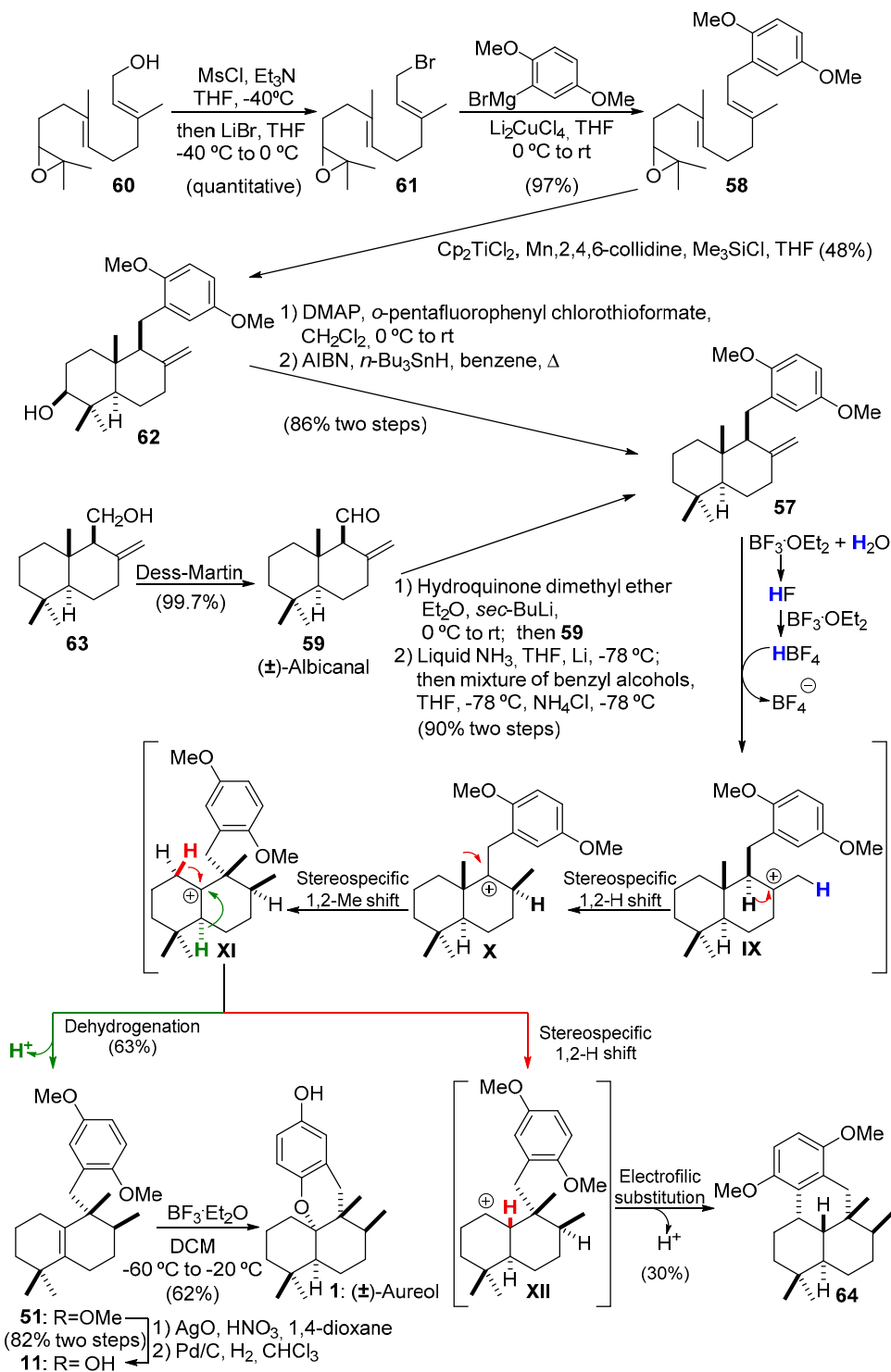
As a part of our efforts directed towards the synthesis of marine terpenoids [40], we embarked on a project aimed at the divergent synthesis of tetracyclic meroterpenoids. Our endeavors started with the racemic preparation of ( $\pm$ )-aureol (**1**) in 2015 [38], a process we later improved in 2020 [39]. This effort continues with the divergent synthesis of other tetracyclic meroterpenoids using aureol (**1**) as a common synthetic intermediate. The retrosynthetic plan for each synthesis is shown in Scheme 10. Our strategy is based on the preparation of ( $\pm$ )-aureol (**1**) through the biomimetic acid cyclization of hydroquinone **11**, an intermediate that could be generated from **57** through a sequence of 1,2-hydride and 1,2-methyl shifts and the subsequent deprotection of both O-Me groups. **57** is an intermediate common to both synthetic approaches. In one of them, **57** is prepared through  $\text{Cp}_2\text{TiCl}$ -catalyzed reductive epoxide cyclization cascade of epoxyfarnesol derivative **58** and the subsequent deoxygenation of the OH-group. In the other, a cross-coupling reaction between albicanal (**59**) and 2-lithiohydroquinone is used.



**Scheme 10.** Retrosynthetic plan of ( $\pm$ )-aureol (**1**) according to Rosales Martínez et al. [38,39].

Initially [38], we pursued the synthesis of the key intermediate **57** using epoxyfarnesol **60** as the starting material (Scheme 11). The one-pot mesylation of product **60** with  $\text{MsCl}$ , and the subsequent addition of  $\text{LiBr}$  quantitatively gave a yield of bromide **61**. The cross-coupling reaction between **61** and 2,5-dimethoxyphenylmagnesium bromide afforded the epoxyfarnesol derivative **58** (97% yield). A very elegant  $\text{Cp}_2\text{TiCl}$ -catalyzed [40] radical cascade cyclization of **58** gave **62** in a moderate 48% yield. The subsequent deoxygenation of alcohol **62** was carried out using the Barton–McCombie procedure, which afforded **57** in an 86% overall yield (two steps). Later [39], the key intermediate **57** was also prepared through a C-C bond-forming reaction between 2-lithiohydroquinone dimethyl ether and ( $\pm$ )-albicanal (**59**) as starting material, which was previously obtained by oxidation of ( $\pm$ )-albicanol (**63**) with the Dess–Martin reagent (99.7% yield). In this way, the coupling of **59** with 2-lithiohydroquinone dimethyl ether gave a mixture of diastereomeric benzylic

alcohols which, without separation, was treated with lithium in liquid  $\text{NH}_3/\text{THF}$  followed by aqueous  $\text{NH}_4\text{Cl}$  to give the deoxygenated product **57** in a 90% yield (two steps). With **57** in our hands, tetrasubstituted olefin **51** was synthesized by biomimetic-type rearrangement of **57** mediated by  $\text{BF}_3 \cdot \text{Et}_2\text{O}$ .



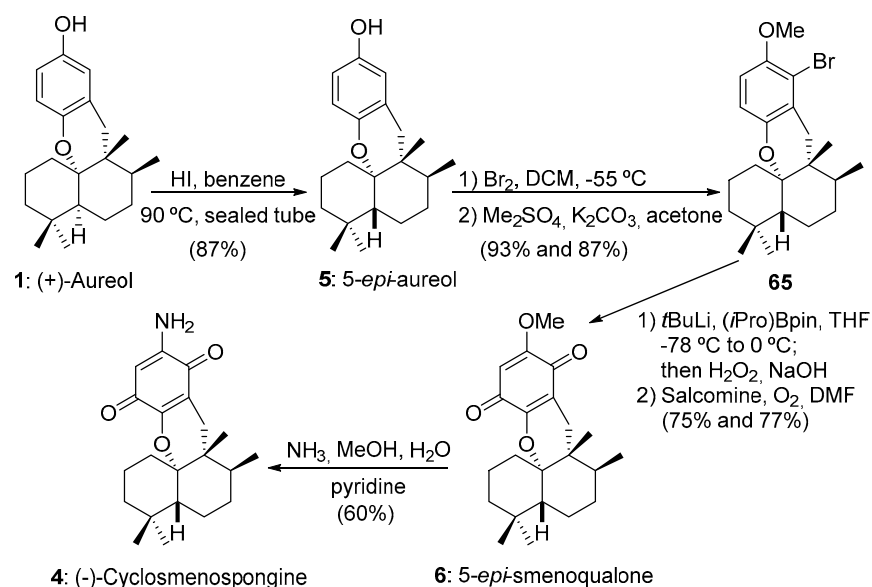
**Scheme 11.** Synthesis of (±)-aureol (**1**) according to Rosales Martínez et al. [38,39]. DMAP = 4-(dimethylamino)pyridine; AIBN = 2,2'-azobis(2-methylpropionitrile).

Under these conditions, **51** was obtained in a 63% yield, together with the by-product **64** in a 30% yield. In this reaction, the intermediate carbocations **IX–XI** could be in-

involved [39]. The cationic rearrangement might be initiated by a proton from HF, which could be formed through hydrolysis of  $\text{BF}_3$ , since it is known that  $\text{BF}_3 \cdot \text{Et}_2\text{O}$  is very moisture sensitive. The demethylation of **51** gave **11** in an 82% yield over the two steps. Finally, the treatment of the hydroquinone **11** with  $\text{BF}_3 \cdot \text{Et}_2\text{O}$  afforded aureol (**1**) (62%). This cyclization was originally explored by Marcos et al. [28] This synthesis of racemic ( $\pm$ )-aureol (**1**) was completed in eight steps (14% overall yield) from the starting material epoxyfarnesol (**60**) or in seven steps (28% yield overall yield) from the starting material ( $\pm$ )-albicanal (**59**).

### 3. Aureol as Pluripotent Late-Stage Intermediate for the Synthesis of Tetracyclic Meroterpenoids

The possibility of using aureol (**1**) as a late-intermediate for the divergent synthesis of other tetracyclic terpenoids stems from the fact that these compounds have differences mostly on the aromatic moiety. Furthermore, the easy epimerization of aureol (**1**) into 5-*epi*-aureol (**5**) previously described by Magauer and colleagues [8] opens the door to the preparation of *trans*-decaline. From both *cis*- or *trans*-decaline frameworks, it should be quite straightforward the access to a library of natural or non-natural tetracyclic meroterpenoid analogues, just by simple variation of the arene moiety. The examples represented in Scheme 12 illustrate how other compounds can be obtained from aureol (**1**). The non-natural 5-*epi*-aureol (**5**) was synthesized by thermal isomerization of (+)-aureol (**1**) using hydroiodic acid in benzene at 90 °C (87% yield) [8]. From 5-*epi*-aureol (**5**), the compounds (–)-cyclomenospongine (**4**) and 5-*epi*-smenoqualone (**6**) were prepared by sequential functionalization of their aromatic core. In this way, selective bromination of **5** with  $\text{Br}_2$ , and the subsequent methylation gave the compound **65** in an excellent yield. The non-natural 5-*epi*-smenoqualone (**6**) was prepared from **65** via a boronation-oxidation sequence in a 58% yield (two steps). Eventually, non-natural **6** was converted to (–)-cyclomenospongine (**4**) via aminolysis (60% yield). In addition, the application of this sequential functionalization of the aromatic core to (+)-aureol (**1**) could be used to prepare natural (+)-smenoqualone (**4**).



**Scheme 12.** Synthesis of (–)-cyclomenospongine (**4**) and 5-*epi*-smenoqualone (**6**) from (+)-aureol (**1**). DMF = *N,N'*-dimethylformamide.

### 4. Conclusions

The divergent synthesis is a valuable tool in the design of efficient routes for the synthesis of natural products using a common intermediate. Although several unified strategies have been reported for some families of natural products, it is desirable to extrapolate this methodology to the synthesis of tetracyclic meroterpenoids. In this context,

this article reviews the synthesis of the marine natural product aureol (1), with special emphasis on their strategies and methodologies. In addition, this natural tetracyclic meroterpenoid can be used as pluripotent late-stage intermediate for the synthesis of other natural and non-natural tetracyclic meroterpenoids. In this article, we proposed a methodology based on a diversification strategy that we believe will be useful in future research for the preparation of other tetracyclic meroterpenoids as substances that could be used as new drugs or in structure–activity relationship studies.

**Author Contributions:** A.R.M.: design and coordination of the project, writing—original draft, writing—review and editing. I.R.-G.: writing—review and editing. J.L.L.-M.: writing—review. All authors have read and agreed to the published version of the manuscript.

**Funding:** This work was supported by the Vicerrectorado de Investigación (Project 2020/00001014) of University of Sevilla (Spain) and by the Vicerrectorado de Investigación e Innovación of University of Almería (Project PPUENTE2020/010).

**Institutional Review Board Statement:** Not applicable.

**Informed Consent Statement:** Not applicable.

**Data Availability Statement:** Not applicable.

**Acknowledgments:** A. Rosales Martínez acknowledges University of the Sevilla for his position as professor and for financial support (Project 2020/00001014).

**Conflicts of Interest:** The authors declare no conflict of interest.

## References

1. Boger, D.L.; Brotherton, C.E. Total synthesis of azafluoranthene alkaloids: Rufescine and imeluteine. *J. Org. Chem.* **1984**, *49*, 4050. [[CrossRef](#)]
2. Li, L.; Chen, Z.; Zhang, X.; Jia, Y. Divergent Strategy in Natural Product Total Synthesis. *Chem. Rev.* **2018**, *118*, 3752–3832. [[CrossRef](#)] [[PubMed](#)]
3. Shimokawa, J. Divergent strategy in natural product total synthesis. *Tetrahedron Lett.* **2014**, *55*, 6156–6162. [[CrossRef](#)]
4. Njardarson, J.T.; Gaul, C.; Shan, D.; Huang, X.-Y.; Danishefsky, S.J. Discovery of Potent Cell Migration Inhibitors through Total Synthesis: Lessons from Structure-Activity Studies of (+)-Migrastatin. *J. Am. Chem. Soc.* **2004**, *126*, 1038–1040. [[CrossRef](#)]
5. Jones, S.B.; Simmons, B.; Mastracchio, A.; MacMillan, D.W.C. Collective synthesis of natural products by means of organocascade catalysis. *Nature* **2011**, *475*, 183–188. [[CrossRef](#)]
6. Katoh, T. Total synthesis of decahydrobenzo[d]xanthene sesquiterpenoids aureol, strongylin A, and stachyflin. Development of a new strategy for the construction of a common tetracyclic core structure. *Heterocycles* **2013**, *87*, 2199–2224. [[CrossRef](#)]
7. Zong, Y.; Wang, W.; Xu, T. Total synthesis of bioactive marine meroterpenoids: The cases of liphagal and frondosin B. *Mar. Drugs* **2018**, *16*, 115. [[CrossRef](#)]
8. Wildermuth, R.; Speck, K.; Haut, F.-L.; Mayer, P.; Karge, B.; Broenstrup, M.; Magauer, T. A modular synthesis of tetracyclic meroterpenoid antibiotics. *Nat. Commun.* **2017**, *8*, 1–9. [[CrossRef](#)] [[PubMed](#)]
9. Djura, P.; Stierle, D.B.; Sullivan, B.; Faulkner, D.J.; Arnold, E.V.; Clardy, J. Some metabolites of the marine sponges *Smenospongia aurea* and *Smenospongia* (s. ident. *Polyfibrospongia*) *echina*. *J. Org. Chem.* **1980**, *45*, 1435. [[CrossRef](#)]
10. Ciminiello, P.; Dell'Aversano, C.; Fattorusso, E.; Magno, S.; Pansini, M. Chemistry of Verongida sponges. 10. Secondary metabolite composition of the Caribbean sponge *Verongula gigantea*. *J. Nat. Prod.* **2000**, *63*, 263–266. [[CrossRef](#)]
11. Wright, A.E.; Rueth, S.A.; Cross, S.S. An antiviral sesquiterpene hydroquinone from the marine sponge *Strongylophora hartmani*. *J. Nat. Prod.* **1991**, *54*, 1108. [[CrossRef](#)]
12. Coval, S.J.; Conover, M.A.; Mierzwa, R.; King, A.; Puar, M.S.; Phife, D.W.; Pai, J.-K.; Burrier, R.E.; Ahn, H.-S.; Boykow, G.C.; et al. Wiedendiol-A and -B, cholesteryl ester transfer protein inhibitors from the marine sponge *Xestospongia wiedenmayeri*. *Bioorg. Med. Chem. Lett.* **1995**, *5*, 605–610. [[CrossRef](#)]
13. Bourguet-Kondracki, M.L.; Martin, M.T.; Guyot, M. Smenoqualone, a novel sesquiterpenoid from the marine sponge *Smenospongia* sp. *Tetrahedron Lett.* **1992**, *33*, 8079. [[CrossRef](#)]
14. Utkina, N.K.; Denisenko, V.A.; Scholokova, O.V.; Makarchenko, A.E. Determination of the Absolute Stereochemistry of Cyclosmenospongine. *J. Nat. Prod.* **2003**, *66*, 1263–1265. [[CrossRef](#)] [[PubMed](#)]
15. Urban, S.; Capon, R.J. Marine sesquiterpene quinones and hydroquinones: Acid-catalyzed rearrangements and stereochemical investigations. *Aust. J. Chem.* **1994**, *47*, 1023–1029. [[CrossRef](#)]
16. Speck, K.; Wildermuth, R.; Magauer, T. Convergent Assembly of the Tetracyclic Meroterpenoid (-)-Cyclosmenospongine by a Non-Biomimetic Polyene Cyclization. *Angew. Chem. Int. Ed.* **2016**, *55*, 14131–14135. [[CrossRef](#)] [[PubMed](#)]

17. Speck, K.; Magauer, T. Evolution of a Polyene Cyclization Cascade for the Total Synthesis of (-)-Cyclospenopongine. *Chem. Eur. J.* **2017**, *23*, 1157–1165. [[CrossRef](#)]
18. Prokof'eva, N.G.; Utkina, N.K.; Chaikina, E.L.; Makarchenko, A.E. Biological activities of marine sesquiterpenoid quinones: Structure-activity relationships in cytotoxic and hemolytic assays. *Comp. Biochem. Physiol. Part B Biochem. Mol. Biol.* **2004**, *139B*, 169–173. [[CrossRef](#)] [[PubMed](#)]
19. Wright, A.E.; Cross, S.S.; Burres, N.S.; Koehn, F. Antiviral and Antitumor Terpene Hydroquinones from Marine Sponge and Methods of Use. U.S. Patent WO9,112,250, 22 August 1991.
20. Longley, R.E.; McConnell, O.J.; Essich, E.; Harmody, D. Evaluation of marine sponge metabolites for cytotoxicity and signal transduction activity. *J. Nat. Prod.* **1993**, *56*, 915. [[CrossRef](#)]
21. Lakshmi, V.; Gunasekera, S.P.; Schmitz, F.J.; Ji, X.; Van der Helm, D. Acid-catalyzed rearrangement of arenarol. *J. Org. Chem.* **1990**, *55*, 4709. [[CrossRef](#)]
22. Nakamura, M.; Suzuki, A.; Nakatani, M.; Fuchikami, T.; Inoue, M.; Katoh, T. An efficient synthesis of (+)-aureol via boron trifluoride etherate-promoted rearrangement of (+)-arenarol. *Tetrahedron Lett.* **2002**, *43*, 6929–6932. [[CrossRef](#)]
23. Suzuki, A.; Nakatani, M.; Nakamura, M.; Kawaguchi, K.; Inoue, M.; Katoh, T. Highly improved synthesis of (+)-aureol via (-)-neoavarone and (-)-neoavarol, by employing salcomine oxidation and acid-induced rearrangement/cyclization strategy. *Synlett* **2003**, 329–332. [[CrossRef](#)]
24. Sakurai, J.; Oguchi, T.; Watanabe, K.; Abe, H.; Kanno, S.-I.; Ishikawa, M.; Katoh, T. Highly efficient total synthesis of the marine natural products (+)-avarone, (+)-avarol, (-)-neoavarone, (-)-neoavarol and (+)-aureol. *Chem. Eur. J.* **2008**, *14*, 829–837. [[CrossRef](#)] [[PubMed](#)]
25. Fukuyama, T.; Lin, S.C.; Li, L. Facile reduction of ethyl thiol esters to aldehydes: Application to a total synthesis of (+)-neothramycin A methyl ether. *J. Am. Chem. Soc.* **1990**, *112*, 7050. [[CrossRef](#)]
26. Yoon, T.; Danishefsky, S.J.; de Gala, S. A Concise Total Synthesis of ( $\pm$ )-Mamanuthaquinone by Using an exo-Diels–Alder Reaction. *Angew. Chem. Int. Ed. Engl.* **1994**, *33*, 853–855. [[CrossRef](#)]
27. Buter, J.; Heijnen, D.; Wan, I.C.; Bickelhaupt, F.M.; Young, D.C.; Otten, E.; Moody, D.B.; Minnaard, A.J. Stereoselective Synthesis of 1-Tuberculosinyl Adenosine; a Virulence Factor of *Mycobacterium tuberculosis*. *J. Org. Chem.* **2016**, *81*, 6686–6696. [[CrossRef](#)]
28. Marcos, I.S.; Conde, A.; Moro, R.F.; Basabe, P.; Díez, D.; Urones, J.G. Synthesis of quinone/hydroquinone sesquiterpenes. *Tetrahedron* **2010**, *66*, 8280–8290. [[CrossRef](#)]
29. Marcos, I.S.; Hernández, F.A.; Sexmero, M.J.; Díez, D.; Basabe, P.; Pedrero, A.B.; García, N.; Sanz, F.; Urones, J.G. Synthesis and absolute configuration of (-)-chettaphanin II. *Tetrahedron Lett.* **2002**, *43*, 1243–1245. [[CrossRef](#)]
30. Marcos, I.S.; Hernández, F.A.; Sexmero, M.J.; Díez, D.; Basabe, P.; Pedrero, A.B.; García, N.; Urones, J.G. Synthesis and absolute configuration of (-)-chettaphanin I and (-)-chettaphanin II. *Tetrahedron* **2003**, *59*, 685–694. [[CrossRef](#)]
31. Ling, T.; Poupon, E.; Rueden, E.J.; Kim, S.H.; Theodorakis, E.A. Unified Synthesis of Quinone Sesquiterpenes Based on a Radical Decarboxylation and Quinone Addition Reaction. *J. Am. Chem. Soc.* **2002**, *124*, 12261–12267. [[CrossRef](#)]
32. Ling, T.; Xiang, A.X.; Theodorakis, E.A. Enantioselective total synthesis of avarol and avarone. *Angew. Chem. Int. Ed.* **1999**, *38*, 3089–3091. [[CrossRef](#)]
33. Kuan, K.K.W.; Pepper, H.P.; Bloch, W.M.; George, J.H. Total Synthesis of (+)-Aureol. *Org. Lett.* **2012**, *14*, 4710–4713. [[CrossRef](#)] [[PubMed](#)]
34. Sharpless, K.B.; Young, M.W. Olefin synthesis. Rate enhancement of the elimination of alkyl aryl selenoxides by electron-withdrawing substituents. *J. Org. Chem.* **1975**, *40*, 947. [[CrossRef](#)]
35. Majetich, G.; Grieco, P.A.; Nishizawa, M. Total synthesis of  $\beta$ -elemenone. *J. Org. Chem.* **1977**, *42*, 2327. [[CrossRef](#)]
36. Wang, J.-L.; Li, H.-J.; Wang, M.; Wang, J.-H.; Wu, Y.-C. A six-step synthetic approach to marine natural product (+)-aureol. *Tetrahedron Lett.* **2018**, *59*, 945–948. [[CrossRef](#)]
37. Concepción, J.I.; Francisco, C.G.; Freire, R.; Hernández, R.; Salazar, J.A.; Suárez, E. Iodosobenzene diacetate, an efficient reagent for the oxidative decarboxylation of carboxylic acids. *J. Org. Chem.* **1986**, *51*, 402. [[CrossRef](#)]
38. Rosales, A.; Muñoz-Bascón, J.; Roldán-Molina, E.; Rivas-Bascón, N.; Padial, N.M.; Rodríguez-Maecker, R.; Rodríguez-García, I.; Oltra, J.E. Synthesis of ( $\pm$ )-Aureol by Bioinspired Rearrangements. *J. Org. Chem.* **2015**, *80*, 1866–1870. [[CrossRef](#)]
39. Rosales Martínez, A.; Enríquez, L.; Jaraíz, M.; Pozo Morales, L.; Rodríguez-García, I.; Díaz Ojeda, E. A Concise Route for the Synthesis of Tetracyclic Meroterpenoids: ( $\pm$ )-Aureol Preparation and Mechanistic Interpretation. *Mar. Drugs* **2020**, *18*, 441. [[CrossRef](#)]
40. Rosales Martínez, A.; Pozo Morales, L.; Díaz Ojeda, E.; Castro Rodríguez, M.; Rodríguez-García, I. The Proven Versatility of  $\text{Cp}_2\text{TiCl}$ . *J. Org. Chem.* **2021**, *86*, 1311–1329. [[CrossRef](#)]



## Article

# Compounds Identified from Marine Mangrove Plant (*Avicennia alba*) as Potential Antiviral Drug Candidates against WDSV, an In-Silico Approach

Mohammed Othman Aljahdali \*, Mohammad Habibur Rahman Molla and Foyсал Ahammad 

Department of Biological Sciences, Faculty of Science, King Abdulaziz University, P.O. Box 80203, Jeddah 21598, Saudi Arabia; mrahmanmolla@stu.kau.edu.sa (M.H.R.M.); fahammad@stu.kau.edu.sa (F.A.)

\* Correspondence: moaljahdali@kau.edu.sa

**Abstract:** Walleye dermal sarcoma virus (WDSV) is a type of retrovirus, which affects most of the adult walleye fishes during the spawning time. The virus causes multiple epithelial tumors on the fish's skin and fins that are liable for more than 50% of the mortality rate of fish around the world. Till now, no effective antiviral drug or vaccine candidates have been developed that can block the progression of the disease caused by the pathogen. It was found that the 582-amino-acid (aa) residues long internal structural gag polyprotein of the virus plays an important role in virus budding and virion maturation outside of the cell. Inhibition of the protein can block the budding and virion maturation process and can be developed as an antiviral drug candidate against the virus. Therefore, the study aimed to identify potential natural antiviral drug candidates from the tropical mangrove marine plant *Avicennia alba*, which will be able to block the budding and virion maturation process by inhibiting the activity of the gag protein of the virus. Initially, a homology modeling approach was applied to identify the 3D structure, followed by refinement and validation of the protein. The refined protein structures were then utilized for molecular docking simulation. Eleven phytochemical compounds have been isolated from the marine plant and docked against the virus gag polyprotein. Three compounds, namely Friedlein (CID244297), Phytosterols (CID12303662), and 1-Triacontanol (CID68972) have been selected based on their docking score  $-8.5$  kcal/mol,  $-8.0$  kcal/mol and  $-7.9$  kcal/mol, respectively, and were evaluated through ADME (Absorption, Distribution, Metabolism and Excretion), and toxicity properties. Finally, molecular dynamics (MD) simulation was applied to confirm the binding stability of the protein-ligands complex structure. The ADME and toxicity analysis reveal the efficacy and non-toxic properties of the compounds, where MD simulation confirmed the binding stability of the selected three compounds with the targeted protein. This computational study revealed the virtuous value of the selected three compounds against the targeted gag polyprotein and will be effective and promising antiviral candidates against the pathogen in a significant and worthwhile manner. Although in vitro and in vivo study is required for further evaluation of the compounds against the targeted protein.



**Citation:** Aljahdali, M.O.; Molla, M.H.R.; Ahammad, F. Compounds Identified from Marine Mangrove Plant (*Avicennia alba*) as Potential Antiviral Drug Candidates against WDSV, an In-Silico Approach. *Mar. Drugs* **2021**, *19*, 253. <https://doi.org/10.3390/md19050253>

Academic Editor: Emiliano Manzo

Received: 9 April 2021

Accepted: 26 April 2021

Published: 28 April 2021

**Publisher's Note:** MDPI stays neutral with regard to jurisdictional claims in published maps and institutional affiliations.

**Keywords:** In-silico drug design; virtual screening; *Avicennia alba*; gag polyprotein; homology modeling; ADMET; molecular dynamics simulation



**Copyright:** © 2021 by the authors. Licensee MDPI, Basel, Switzerland. This article is an open access article distributed under the terms and conditions of the Creative Commons Attribution (CC BY) license (<https://creativecommons.org/licenses/by/4.0/>).

## 1. Introduction

Due to the growing global demand of fish protein, a number of aquaculture industries have been developed to fulfil the demand where capture fisheries are continuously shrinking around the world [1]. Nonetheless, emerging threats originating from different viruses have great influences on fish farms and capture fisheries growth and actual production [2]. Emerging viruses are affecting both farmed and wild fishes, which have tremendous impact on economical aspect around the world [3]. Walleye dermal sarcoma virus (WDSV) is one of them, and crucially impact fishes during their spawning time. It was first isolated from walleye fish (*Stizostedion vitreum*) in the USA [4]. This retrovirus



usually occurs at 4 °C in the winter and infection of the epidermis of fish leads to different types of neoplastic disease. This neoplastic disease is transformed to an invasive tumor within 12–16 weeks and causes the highest mortality of fishes in many countries. [4]. There is no obvious treatment option to control the spread of the virus due to lack of effective therapeutics drug.

The structural proteins of a virus play an important role in viral encapsulation, genome assemble, protection from genome degradation, maturation and releasing the mature virus to make re-infection with the host cellular protein through different mechanism [5,6]. The envelope structure of WDSV and their structural protein carry essential components, which helps viral maturation resulting in releasing of the mature virus and infectivity to the host. The structural and enzymatic proteins of the virus are expressed as gag and gag-pro-pol (and in some cases gag-pro) polyprotein, respectively. The gag polyprotein assembles to form an immature viral particle, which is later matured through different proteolytic cleavages that induces significant structural changes of the protein products. Initially, the viral enzyme protease (PR) domain cleaves the gag-pro-pol into different precursors during or after assembly and budding. The PR then bind with the trans on gag and gag-pro-pol that help to produce mature proteins of the virus. The gag gene is encoded with the viral enzyme protease (PR) which synthesized as a unique large precursor polypeptide and fuse to gag [7]. The gag gene of the WDSV virus also encodes different mature proteins of unknown function that regulate the transcription and RNA processing of the virus. The process is responsible for induction of WDSV and inhibition of the gag polyprotein of the virus can block the transcription process and generate effective antiviral against the virus.

Compounds originated from marine plants have been found to show antiviral and drug like properties for many diseases. The marine plants and their constituents play a vital role in the drug design study as well as animal and human life savior [8]. Different plant herbal extracts have led to identifying single molecule as drug candidates and are being used in different biochemical and biomedical sectors [9]. *Avicennia alba* is a member of true mangrove flowering plants of the genus *Avicennia* and family *Acanthaceae*. This genus contains 11 species and several subspecies with many active biological constituents in this plant. The family members of the *Acanthaceae* have been utilized as traditional and alternative medicine for many years. Previously, leaf extract of *Avicennia marina*, a member of *Avicennia*, has shown activity against replication of herpes simplex virus type-1 (HSV-1) and vaccine strain of polio virus [10]. On the other hand, several phytochemicals such as quercetin, lutolin, baicalein and kaempferol originated from plant extract have been also used as antiviral candidates agents against HIV and Dengue virus for many years [11,12]. Therefore, the extract and subsequent compounds originated from *Avicennia alba* can be utilized as replication inhibitors for different virus as well as WDSV.

Finding viable phytochemicals is a critical objective for the drug discovery [13]. The identification of targeted therapeutics to the fish industries require selection of small bioactive molecules by investigating the action of a molecules with the targeted protein [14]. In-silico drug design techniques are an easy and low time consuming process that can predict the liable compound against a specific drug targets [15]. The ideal compounds against a specific target can be selected based on molecular docking based scoring function and interaction can be documented through the analysis of the different docking poses [16]. The ADMET properties that indicate the efficacy and toxicity of compounds can be easily predicted through computer aided methods, where MD simulation confirm the stability of a drug candidate to the targeted protein. However, it has been difficult to address new drugs, therefore there is a need to progress strong investigation for inventing bioactive compounds by targeting novel protein classes. Therefore, we have planned to utilize an in-silico approach to investigate the new drug candidates against the WSDV virus targeting the gag polyprotein.

## 2. Results

### 2.1. Protein 3D Structure, Refinement, and Validation

The best 3D protein structure was downloaded from the I-TASSER server. The server generated top five models of the gag protein and based on C-score further evaluation has been performed. The lowest C-score was  $-4.73$ . After refinement, the protein model-5 was chosen, where the 3D refine score was 37759.1, GDT-HA score was 0.9747, RMSD value was 0.347, MolProbity 3.473. The RAMPAGE and ProSA-web servers were also used to validate the refined gag protein. Before refinement, the Ramachandran plot analysis of the gag protein found 81.1%, 11.89% and 6.7% residues in the favorable allowed and disallowed regions accordingly, where refined gag protein model showed 91.65, 4.97, and 3.38%, residues in the favorable, allowed and disallowed regions, respectively (Figure 1A). Likewise, the crude model of the gag protein has a Z-score value of  $-4.14$  and after refinement the value has improved to  $-4.75$  (Figure 1B).

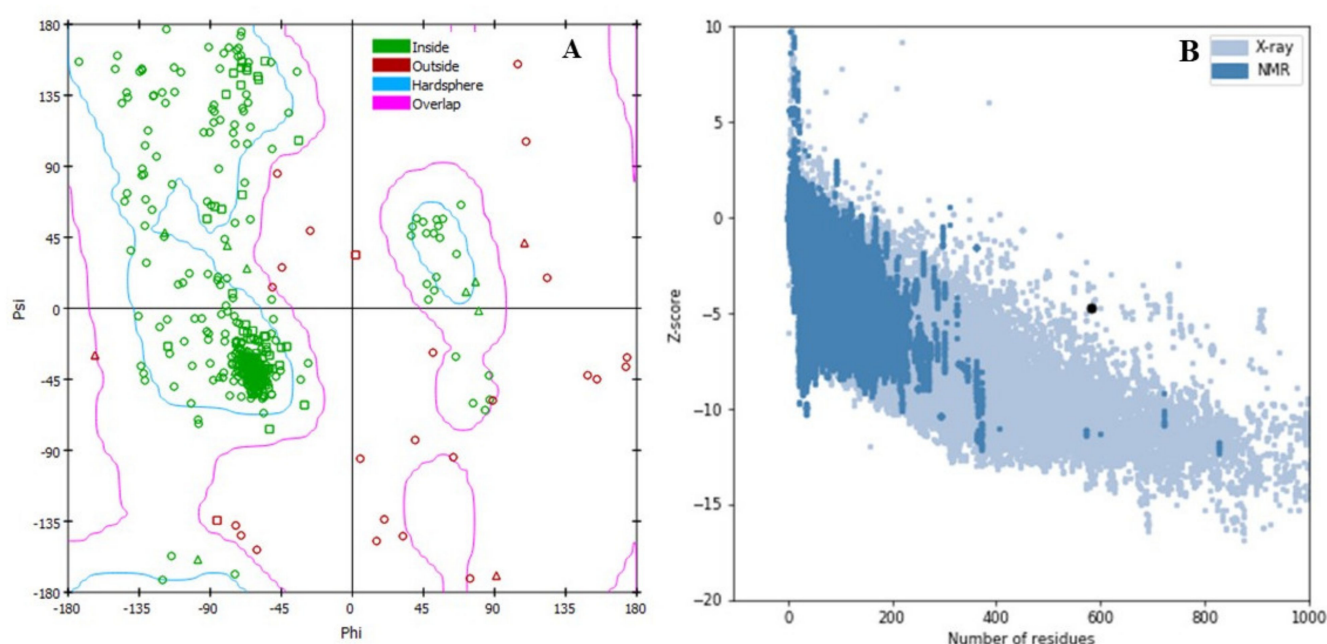


**Figure 1.** Validation of the 3D structure of the gag protein. (A) The Ramachandran plot statistics represent the most favorable, accepted, a disallowed region with a percentage of 91.65, 4.97, and 3.38%, respectively, and (B) the Z-score of refined gag protein  $-4.75$ .

### 2.2. Phytochemical and Protein Preparation

The compounds of marine plant *Avicennia alba* have been retrieved from the popular database IMPPAT. Eleven phytochemical compounds of *Avicennia alba* plant have been retrieved and saved in a 2D (SDF) file format. The compounds have been prepared and optimized during the ligand preparation steps and converted into pdbqt file format for further evaluation. The protein was optimized and prepared for molecular docking process by using AutoDock tool and saved in pdbqt file format for docking.

### 2.3. Active Site Identification and Receptor Grid Generation

Active site (AS) of an enzyme is formed by combining different AA residues in a specific region that are able to make a temporary bond with the substrate known as the binding site. AS of a protein allows to bind with a chemical substrate resulting in a catalyzed reaction. It also helps to stabilize the intermediates of the reaction, where the binding site is a position of a protein or nucleic acid that can recognize a ligand and can make a strong binding interaction with the protein. The study first identified AS of the gag poly peptide from CASTpi server then the combined binding position of the active site was retrieved.

(Figure 2). Analysis of the active pocket of the protein helped to retrieve the binding site residue of the protein (Figure 2). Active site pocket analysis revealed binding site position at MET1, PRO8, LEU13, LYS14, ASP49, GLU59, LEU63, ILE108, THR232, THR233, PRO235, ILE240, GLN250, TYR256, ARG280, GLN313, ARG324, MET402, MET416, THR426 residual positions that have been represented in ball shape with different colors red, green and orange as shown in Figure 2. The binding sites identified by the server have been utilized to generate a receptor grid during molecular docking simulation process and a grid box dimension X = 91.39, Y = 48.45 and Z = 53.14 in angstrom (Å)

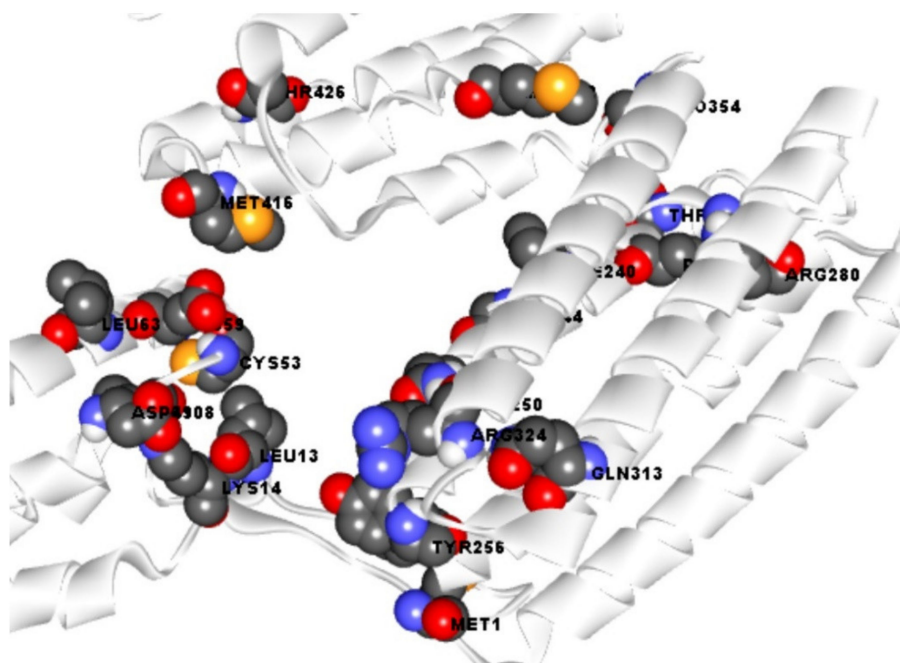


**Figure 2.** Showing the active site and correspondence binding site of gag polyprotein. Ball shapes with red, black, orange, and blue colors, respectively, with their binding site position of the gag polyprotein.

#### 2.4. Molecular Docking Simulation

A possible and accurate drug-like small molecular candidate was not only determined through the molecular docking, but also selected by macromolecule interaction and can also be identified from the method. The docking process can identify both protein and ligands forming best intermolecular frameworks for adjusting with host. Phytochemical compounds and desired proteins were selected, and the best intermolecular interaction determined through the molecular docking study. Eleven phytochemical compounds were utilized for molecular docking process by using PyRx tools AutoDock Vina wizard. The binding affinity showed a distributed range from  $-3.2$  and  $-8.5$  after molecular docking of phytochemicals compound. The top fifty percentage phytochemical compounds have been chosen from the 11 compounds based on the capacity of top binding affinity. The best three compounds, namely Friedlein (CID 244297), Phytosterols (CID12303662), and 1-Triacontanol (CID68972) have been selected based on their docking score  $-8.5$  kcal/mol,  $-8.0$  kcal/mol and  $-7.9$  kcal/mol and further evaluated through different screening methods. The best three compounds selected based on molecular docking score are listed in Table 1 and docking scores for all compounds are listed in Table S1. Additionally, the docking score for the selected three compounds was validated through the re-docking process. The single binding poses of the selected three compounds have been retrieved and re-docked again at the same binding site of the compounds. In this, case the upper and lower RMSD, having the low value, were chosen and the binding affinities found for the compounds were approximately same as previous score. The compounds CID244297,

CID12303662, and CID68972 showed a docking score  $-8.4$  kcal/mol,  $-8.1$  kcal/mol and  $-8.1$  kcal/mol, respectively, and has RMSD value of zero.

**Table 1.** List of selected three compounds identified based on molecular docking score (kcal/mol) and their chemical name, formula, and correspondence PubChem CID.

PubChem CID	Chemical Name	Formula	Binding Affinity (kcal/mol)
CID244297	Friedlein	$C_{30}H_{50}O$	$-8.5$
CID12303662	Phytosterols	$C_{29}H_{50}O$	$-8.0$
CID68972	1-Triacontanol	$C_{30}H_{62}O$	$-7.9$

### 2.5. Protein-Ligand Interaction Analysis

Gag polyprotein with the highest binding score producing compounds has been selected and retrieved to observe the interaction between them. The interaction formed between the selected three ligands with the desired protein was observed by using the BIOVIA Discovery Studio Visualizer tool. For the compound CID244297 it was found to form several hydrogen and hydrophobic bonds with the desired gag polyprotein. The hydrogen bonds found to formed at ALA364 position, where the hydrophobic bonds from at the position ILE240, ILE342, PRO369, and PHE365 position is shown in Figure 3 and the bond types are listed in Table 2.

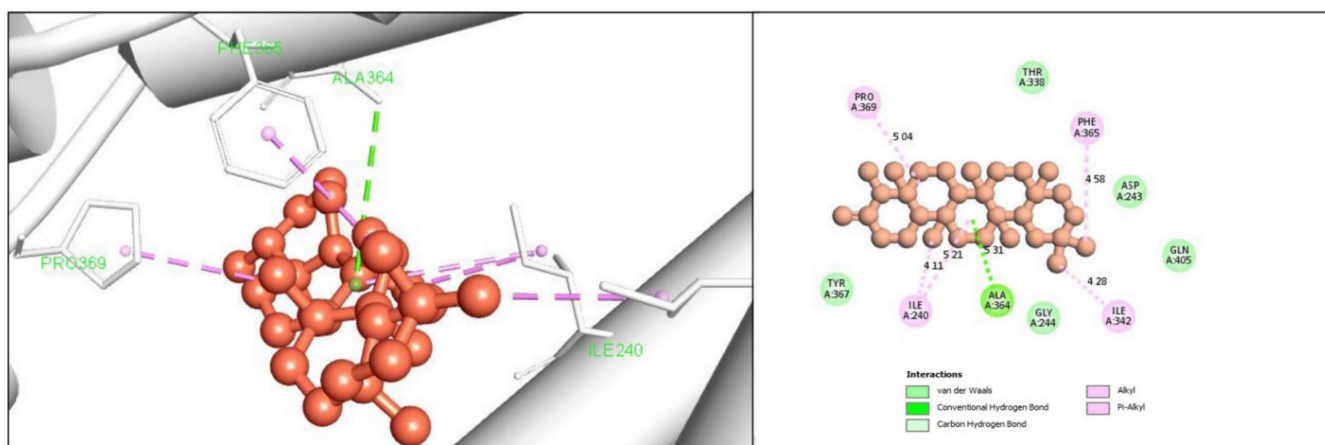


**Figure 3.** Shown the interaction between the compound CID244297 and gag polyprotein. Left side indicate 3D interaction and the right portion indicates 2D interaction of the protein -ligands complex.

**Table 2.** List of bonding interactions between selected four phytochemical with gag protein.

PubChem CID	Residue	Distance	Category	Type
CID244297	ALA364	5.30689	Hydrogen Bond	Conv-H-Bond
	ILE240	5.20546	Hydrophobic	Alkyl
	PRO369	5.03758	Hydrophobic	Alkyl
	ILE240	4.10592	Hydrophobic	Alkyl
	ILE342	4.27502	Hydrophobic	Alkyl
	PHE365	4.58263	Hydrophobic	Pi-Alkyl
CID6897	GLY418	2.86383	Hydrogen Bond	Conv-H-Bond
	PRO420	3.47712	Hydrogen Bond	C-H Bond
	LYS56	4.6933	Hydrophobic	Alkyl
	LYS56	4.99136	Hydrophobic	Alkyl
	LYS368	5.21921	Hydrophobic	Alkyl
	LYS368	5.05134	Hydrophobic	Alkyl

Table 2. Cont.

PubChem CID	Residue	Distance	Category	Type
CID6897	LEU415	5.22063	Hydrophobic	Alkyl
	MET416	5.23747	Hydrophobic	Alkyl
	PRO420	4.55835	Hydrophobic	Alkyl
	PRO420	5.075	Hydrophobic	Alkyl
	LEU415	5.47725	Hydrophobic	Alkyl
	LEU415	4.82065	Hydrophobic	Alkyl
	ILE427	4.51538	Hydrophobic	Alkyl
	LEU415	5.46433	Hydrophobic	Alkyl
	MET416	5.07033	Hydrophobic	Alkyl
CID12303662	LEU63	4.86074	Hydrophobic	Alkyl
	VAL346	4.68285	Hydrogen Bond	Conv-H-Bond
	PHE365	4.64493	Hydrogen Bond	Conv-H-Bond
	PRO369	4.52399	Hydrophobic	Alkyl
	PRO369	5.17641	Hydrophobic	Alkyl
	ILE240	4.62631	Hydrophobic	Alkyl
	PRO369	4.03084	Hydrophobic	Alkyl
	ILE240	4.36608	Hydrophobic	Alkyl
	ILE342	4.65569	Hydrophobic	Alkyl
	ILE342	3.93691	Hydrophobic	Alkyl
ILE240	4.59804	Hydrophobic	Alkyl	
ILE342	4.80551	Hydrophobic	Alkyl	

In the case of compound CID12303662 it has been observed to form several hydrophobic bonds in the ILE240, ILE342, ALA364, ALA364, and PRO369 residual position. Another two conventional hydrogen bonds were found to form at the position of VAL346 and PHE365 AA position as shown in Figure 4 and are listed in the Table 2.

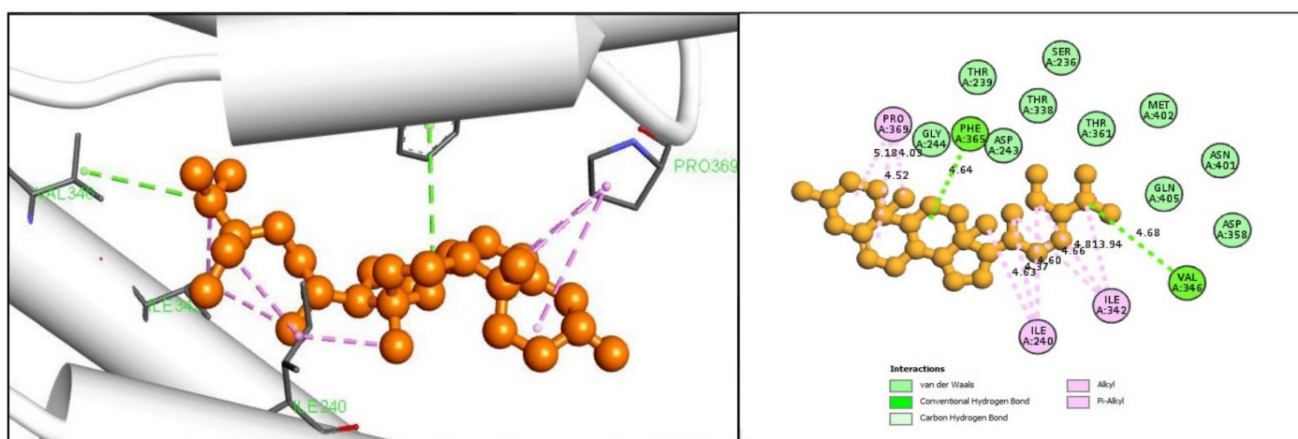


**Figure 4.** Shown the interaction between the compound CID12303662 and gag polyprotein. Left side indicate 3D interaction and the right portion indicates 2D interaction of the protein-ligands complex.

For the compound CID68972 it was found to form the highest binding interaction with the desire protein. The compound has formed three hydrogen bonding interactions at GLY418 and PRO420 positions. A total of fourteen hydrophobic bonds were also found to form with the desired compounds, including alkyl bonds in the LYS56, LYS368, LEU415, MET416, PRO420, ILE427, MET416, LEU63 residual positions as depicted in Figure 5 and listed in Table 2.

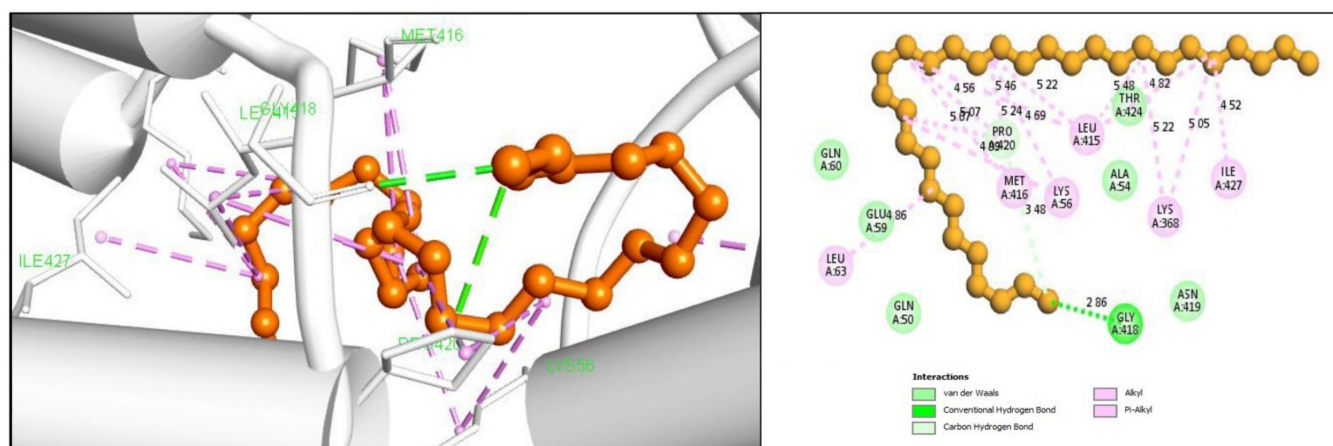


**Figure 5.** Shown the interaction between the compound CID68972 and gag polypeptide. Left side indicate 3D interaction and the right portion indicates 2D interaction of the protein -ligands complex.

### 2.6. ADME Analysis

The analysis of pharmacokinetics (PK) properties analysis, was an indispensable part during drug design and development process. However, it is mainly analyzed at the ADME properties and includes physicochemical properties such as lipophilicity, water solubility, pharmacokinetics, medication likeness and medicinal chemistry and provided the possible hypothesis for selecting the best drug candidates. Before undergoing drugs into the preclinical studies, the analysis of pharmacophore properties can determine the xenobiotic regulation features of a compound. The SwissADME server have been used to determine the pharmacophore properties from the selected three drug-like compounds. The drug-like compounds have a lipophilicity feature which dissolve in fats, oils, and nonpolar solvent. Finally, pharmacophore properties have shown the suitable result with compound thus can be used as an effective and druggable in the study. The pharmacokinetics properties found for the selected three compounds have been listed in the Table 3.

**Table 3.** List of pharmacokinetics includes ADME properties of the selected three compounds. The lists also present different physicochemical properties of the three compounds.

Properties		CID244297	CID12230662	CID68972
Physico-chemical attribute	MW (g/mol)	426.73 g/mol	414.72 g/mol	438.8 g/mol
	Heavy atoms	31	30	31
	Aromatic heavy atoms	0	1	0
	Rotatable bonds	0	6	28
	H-bond acceptors	1	1	1
	H-bond donors	0	1	4
Lipophilicity	Log Po/w	8.46	8.02	7.67
Water solubility	Log S (ESOL)	Soluble	Soluble	Soluble
Pharmacokinetics	GI absorption	Low	Low	Low
Drug-likeness	Lipinski	Yes	Yes	Yes
Medi. Chemistry	Synth. accessibility	Easy	Easy	Easy

Medi. Chemistry = Medicinal chemistry; Synth. Accessibility = Synthetic accessibility.

### 2.7. Toxicity Prediction

To know the adverse effect of a specific compound on animal, plant and human or the outside of the environment, it is important to measure the toxicity of compounds. Therefore, toxicity prediction has become a first and crucial step for selecting any compound as a drug. The toxicity analysis requires different animal models, which is time consuming and expensive process. On the other hand, the computer-based toxicity test is currently

requiring no animal model and is not time consuming and expensive and can be used instead of the conventional method. In-silico toxicity test, we have chosen the selected three compounds through the popular web server admetSAR 2.0 and ProToxII. The server has predicted hepatotoxicity, carcinogenicity, immunotoxicity, mutagenicity, and cytotoxicity by using rat as a target model which given in Table 4.

**Table 4.** List of the drug-induced toxicity profile includes hepatotoxicity, carcinogenicity, immunotoxicity, mutagenicity, cytotoxicity of selected three compounds.

PubChem ID	Hepatotoxicity	Carcinogenicity	Immunotoxicity	Mutagenicity	Cytotoxicity
CID244297	Inactive	No	Inactive	Inactive	Inactive
CID12230662	Inactive	No	Light active	Inactive	Inactive
CID68972	Inactive	No	Inactive	Inactive	Inactive

### 2.8. MD Simulation Analysis

Molecular dynamic simulation has been run for exploring the binding stability of protein-ligand docking complexes. The molecular dynamic simulation also documented evidence based on intermolecular interaction through the orientation time. However, intermolecular interaction confirmation we got from the molecular dynamic simulation that has observed by the 100 ns simulation run between the protein and ligand complex structure. The analysis of RMSD, RMSF and protein ligand interaction mapping has been examined through the simulation trajectories.

### 2.9. RMSD Analysis

The RMSD can measure the average atomic distance of protein and help to characterize the protein [17]. The RMSD value can calculate the difference between observed value and estimated value and a value change between 1–3 Å or 0.1–0.3 nm is reasonably acceptable [18,19]. In our study, the RMSD value for the protein structure (C $\alpha$ ) residues and ligand fit protein were documented from the 100 ns simulation trajectory. The acceptable variation of ligand with protein was calculated from 100 ns interval during RMSD analysis and depicted in Figure 6. However, the RMSD calculated from C $\alpha$  atoms of gag polyprotein and ligand fit protein showed the considerable fluctuation for all the three compounds. The three compound CID244297, CID12230662, CID68972 have found the optimum fluctuation >3.0 Å. The fluctuation for all the three ligands was high before 40 ns simulation time and after 40 ns the fluctuation for all compounds was reduced and showed a state of equilibration resulting in stability of the compound to the binding site of protein.

### 2.10. RMSF Analysis

RMSF provided the information about the local change of protein along with protein chain. The local changes of protein as well as protein chain determined from the RMSF value can help to characterize the protein. Therefore, the RMSF of the protein in complex with the selected phytochemical compounds were calculated for the PubChem CID244297(gray), CID12230662 (Yellow) and CID68972 (red) shown in Figure 7. The highest peak point of the fluctuation has observed between 150 and 155 residual point. The all complex structure has also been fluctuated from 500 to 550 residues due to the location of N-terminal domain. Overall, the fluctuation for all the compounds found optimal compared to the RMSF of the gag protein. Therefore, the compounds will be able to maintains a stable interaction without changing the structure of the protein.

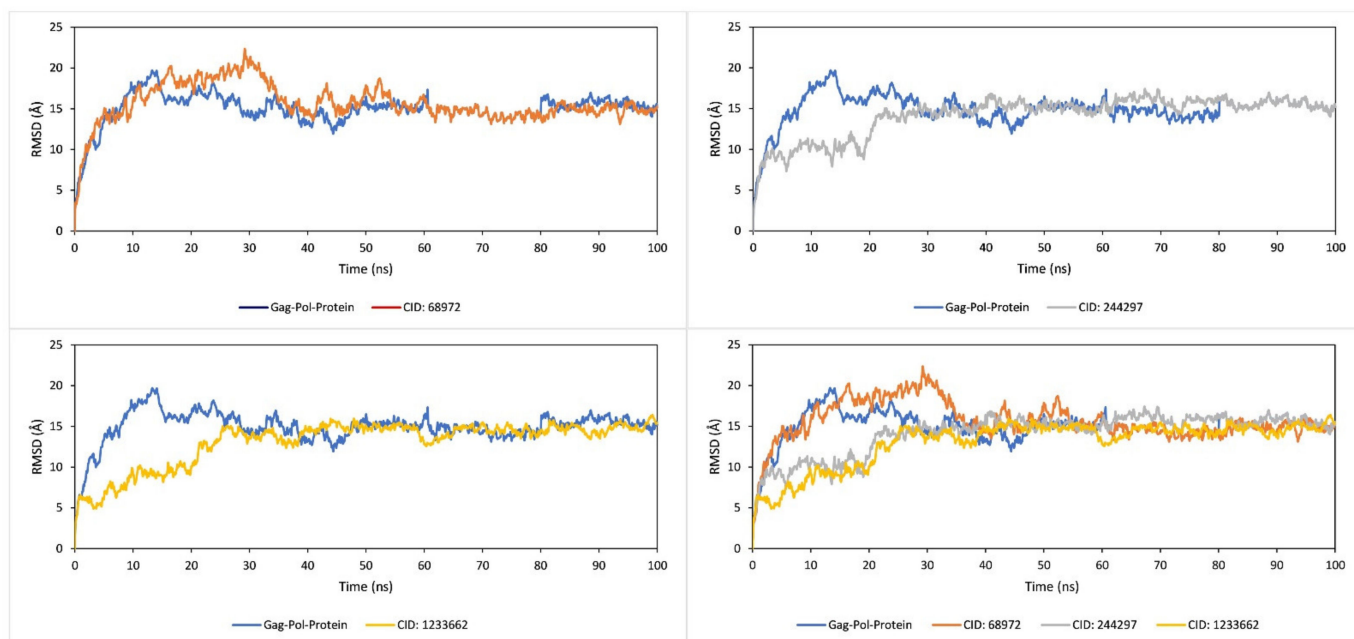


**Figure 6.** RMSD values extracted from the C $\alpha$  atoms (blue curves) of gag polyprotein and natural compounds, where the compounds has shown in CID244297(orange), CID68972 (brown) and CID12230662 (yellow) with regards of 100 ns simulation time.

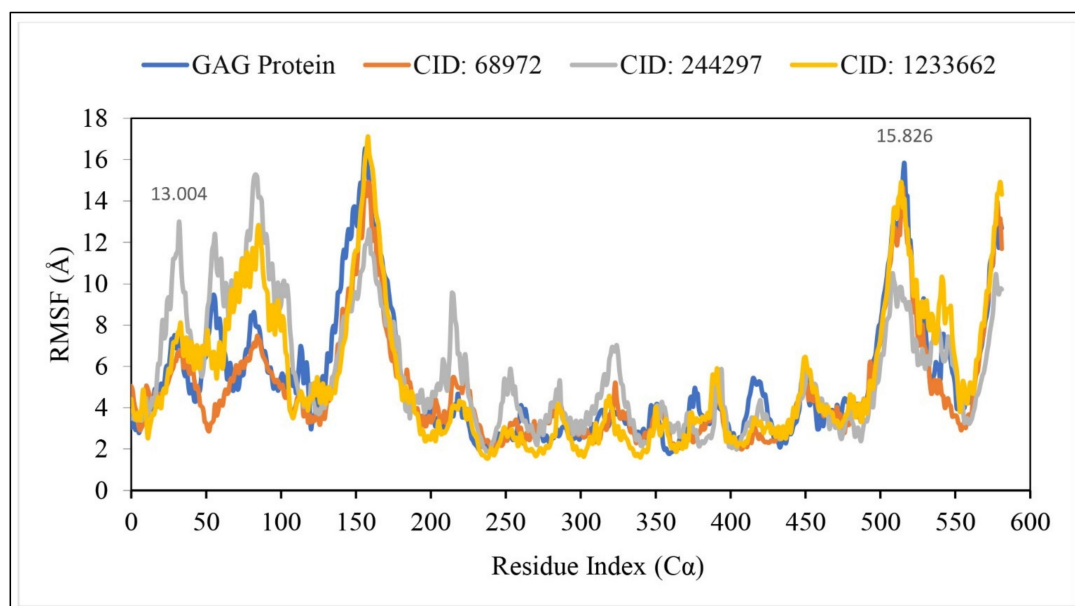


**Figure 7.** Showing the RMSF values extracted from the protein residue index C $\alpha$  atoms of the complex structure viz. CID 244297(gray), CID12230662 (Yellow), CID68972 (red) and gag protein (blue) with respect to 100 ns simulation time.

### 2.11. Protein-Ligand Contact Mapping

The gag protein interactions with the phytochemicals were monitored throughout the analysis of 100 ns MD simulation trajectory. These interactions of the compound's CID244297, CID12230662 and CID68972 have been categorized in different types, like hydrogen bonds, hydrophobic, ionic and water bridge bonds and summarized in the stacked bar charts as shown in the Figure 7. The substantial interaction with catalytic residues shows the significant interaction for all the selected three compounds. The screened compounds have shown the considerable intermolecular contact to the molecular



dynamic simulation interval. It was found that the active residues not only keep contact with intermolecular but also with selected ligands as well as calculated their density for all of three compounds. The depicted figure shows that the dark area orange color indicates ligand in the specific frame with residues of protein (Figure 8). The active pocket of gag protein was derived through the screening of natural compounds, which was established by the analysis of molecular dynamic trajectories. Hence, the screened natural compounds CID244297, CID12230662, and CID68972 will be stable with the gag protein in real life experiments.

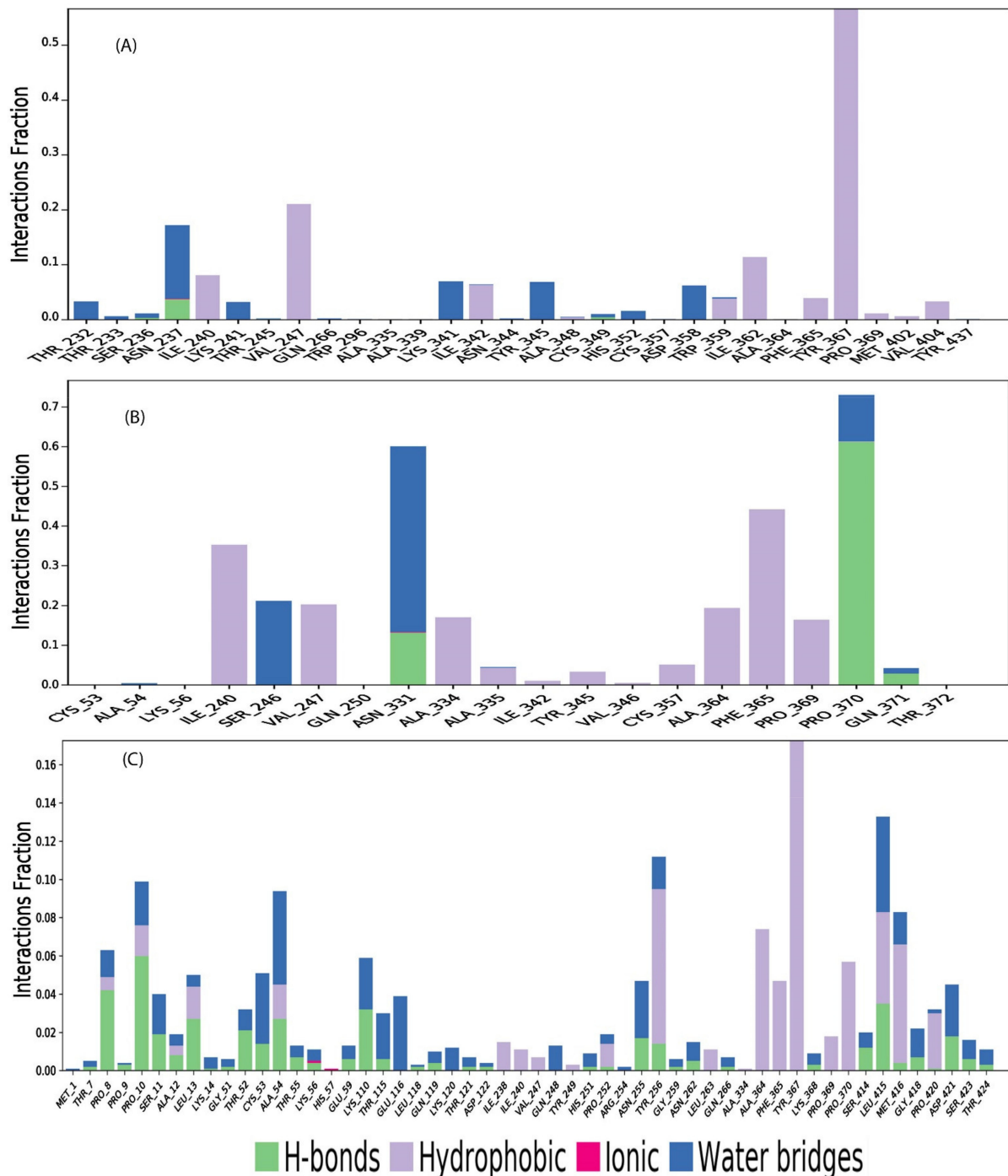


**Figure 8.** The stacked bar charts representing the contact mapping of gag protein with potential natural compounds, i.e., (A) CID244297, (B) CID12230662, and (C) CID68972 extracted from 100 ns simulations trajectory.

### 3. Discussion

In the modern drug design, computer aided drug design (CADD) brings a new medicinal era by providing cost effective processes, reducing time and minimize labor recruitment that make it reasonable in the process of drug discovery. It is an indispensable part as well as a tool for drug design [20]. Therefore, scientists and researchers have been affording the context of biological and synthetic research by the accelerating of CADD. As a result, selecting drug candidate shows that the highest biological efficacy identifying through the molecular docking, ADMET, and molecular dynamic simulation process [21]. A disease can be minimized by understanding the mechanism of the disease, identifying the disease associated protein and ligand binding approach to the protein. Understanding the process can reveal compounds that can interact and inhibit a specific protein resulting blocking the mechanism of disease. CADD help to identify exact target molecule based on their behavior and binding mode of the ligand. On the other hand, molecular docking clarifies the predominate binding modes within a ligand and protein and the MD simulation disclose the complex mechanism of protein ligand interaction. Thus, small molecule candidates can be identified as drug candidates against a specific disease.

The study utilized a compressive drug design approach that helped to screen eleven natural phytochemicals compounds by targeting the gag polyprotein to fight against the WDSV. The best three compounds have been chosen from the eleven compounds which have the highest binding affinity found from the molecular docking score. The higher binding has been documented to the compound CID244297, CID12230662, CID689702 with binding score  $-8.5$ ,  $8.0$  and  $-7.9$  kcal/mol, respectively. The ADME approaches have been utilized to emphasize the metabolite kinetics of small molecular candidates in the body. This was also the time-consuming evaluation process and conventional drug design processes required part of the body of animals or others. The ADME is mainly acting on the drug related to the pharmacokinetic properties. The PK parameters should be optimized before drug design process because it needed to pass standard clinical trial for a promising drug candidate [22]. This property is not only affecting the small molecules permeability across the biological system but also includes molecular weight and polar surface topological area with it. (TPSA). The high molecular weight may cause permeability in the drug candidate and TPSA helps to increase the permeability of lower ones [22]. Lipophilicity is the ability of chemical compound dissolve in polar and non-polar solvents and is expressed by LogP. It not only referred to the inorganic logarithm but also coefficient of the target molecules through the aqueous phase partition. Therefore, it influences various drug molecule's absorption within the body and suggested that lower absorption rate spontaneously correlated to higher logP. However, LogS shows the negative attitude and affect the solubility of the candidate molecules that are considered the lowest value. Hydrogen bonds affect the capacity of drug molecules crossing the bilayer of the membrane, which depends on the number of donors and acceptors of hydrogen bonds. The rotatable bond is overwhelming with oral bioavailability because of their high rational barrier. The PK properties have been implemented to all of compounds and required evaluation has performed that found good value for all of the three compounds.

Moreover, toxicity test has been designed to generated data concerning the adverse effect that can harm or damage an organism. It was documented that about 20% of drug development failed due to the positive range of toxicity. The test of toxicity is indispensable part before drug experiment that is much expensive, and time consume of apply to animal trial [23]. Thus, in-silico alternative methods have been chosen before drug development because of no need to require animal trials and is even time-consuming and reasonable. In this study, three phytochemical compounds identified have shown low toxic effect and have optimize PK properties.

MD simulation helped to determine the physical movements of a compounds within a desired macromolecular environment, which has become an important tool in the CADD process [24]. The MD simulation helps to analyze the stability of the desired drug candidate with a targeted macromolecule. Therefore, MD simulation has been done in this study to

observe the RMSD, RMSF, and ligand-protein interaction of the complex system, which found the optimum RMSD and RMSF value with good protein-ligand contact for all the three compounds. Therefore, the selected three compounds can be design further class of antiviral drug against the WDSV.

## 4. Materials and Methods

### 4.1. Homology Modeling

The WDSV structural gag polyprotein sequence (UniProtKB: O92815) has been retrieved through the UniProtKB (<https://www.uniprot.org/uniprot/O92815>) database accessed on 31 January 2021. To ensure or predict the three-dimensional (3D) structure of the desire protein the retrieved sequence was submitted into the popular online web portal on 31 January 2021 (<https://zhanglab.dcmf.med.umich.edu/I-TASSER/>), namely Iterative Threading Assembly Refinement (I-TASSER) [25]. The I-TASSER server created top five models of the protein structure and provided C-score, TM-score value and root-mean-square deviation (RMSD) of the protein structure. Top protein 3D structure was selected and downloaded as a PDB format considered on the C-score value. The higher value of C-score indicates that the protein model was high confidence from positive to negative numbers.

### 4.2. Model Refinement and Validation

Protein structure refinement has been done after submitting 3D structure into online web-based server on GalaxyRefine (<http://galaxy.seoklab.org/cgi-bin/submit.cgi?type=REFINE>) accessed on 7 February 2021. The RMSD value, energy score and quality of the final structure were identified from the GalaxyRefine server [26]. The maximum and minimum RMSD were determined and the average distance between atoms as well as energy score was used as the parameters to select the refined structure. PyMol v2.3.4 software is used to visualize the refined structure [17]. Ramachandran plot scoring function was used to validate the refine model. Furthermore, Ramachandran plot score (drug design) and z score value is lead to evaluate 3D structure that determine the standard deviation through the main value [27]. However, Z-score plot has documented through the popular server at ProSA-web (<https://prosa.services.came.sbg.ac.at/prosa.php>) accessed on 8 February 2021. The allow and disallow regions of amino acid are considering by Ramachandran plot that was studied through the Rampage server ([https://warwick.ac.uk/fac/sci/moac/people/students/peter\\_cock/python/ramachandran/other/](https://warwick.ac.uk/fac/sci/moac/people/students/peter_cock/python/ramachandran/other/)) accessed on 8 February 2021 [28].

### 4.3. Protein and Ligand Preparation

Prior to docking, refined and validated protein structures need to be prepared. Therefore, chosen 3D structure of gag protein was prepared through AutoDockTools (ADT). The gasteiger charge not only calculated from the protein but also merged and added non-polar and non-polar hydrogen. It also acts as a discarded metal ion and cofactors from its protein. Indian Medicinal Plants, Phytochemistry And Therapeutics (IMPPAT) database available at (<https://cb.imsc.res.in/imppat/home>) has been used for searching the desire plant compound and a total 11 compounds of marine plant *Avicennia alba* were downloaded from the database on 8 February 2021. Selected compounds retrieved from the database that has been set and minimized energy through the Universal Force Field (UFF) designed for individual ligand.

### 4.4. Protein Active Site Identification and Receptor Grid Generation

The refined protein structure of gag protein has been submitted in CASTp 3.0 web server available at <http://sts.bioe.uic.edu/> accessed on 8 February 2021. The server identified different active pockets of the protein and based on the pocket surface area (SA); the first active pocket of the protein has been selected. From the active pocket the binding site residues of the protein has been identified and visualized through BIOVA Discovery

Studio Visualizer Tool 16.1.0. The binding sites identified from the server were utilized for receptor grid generation during molecular docking simulation in PyRx tools.

#### 4.5. Molecular Docking Simulation

Virtual screening of selected compounds was performed through molecular docking process that was carried out by PyRx software. Many potential drugs have been identified against several diseases through the virtual screening software [29]. It is provided Lamarckian genetic algorithm (LGA) as a scoring function included both AutoDock and AutoDock Vina for docking. Molecular docking interaction were proceeding by PyRx tools AutoDock Vina in this study [30]. The BIOVA Discovery Studio Visualizer Tools 16.1.0.41 used for analyzing the complex binding poses [31].

#### 4.6. ADME Analysis

The key criteria of compounds to develop a successful drug candidate is the ADME properties of a compound and should be evaluated. In-silico based molecules ADME predicted at the early stage of drug development can reduce the failure rate in clinical trial, because many drugs were not fit in the clinical trial and its demand before [32]. Therefore, the observation of ADME test is indispensable part of early-stage drug design process. The evacuation of any drug inside of the fish through the urine and feces, are at the final stage that directly affected by the ADME profile [33]. The internal impacts on the fish are on physiochemical properties, hydrophobicity, lipophilicity, gastrointestinal environment, blood brain barrier before excretion. The ADME properties such as bioavailability and solubility profile, and GIT absorption were evaluating through the free accessible server at Swiss-ADME (<http://www.swissadme.ch/>) for the 11 selected compounds accessed on 10 February 2021 [22].

#### 4.7. Toxicity Analysis

To measure the toxicity, in-silico computational techniques have been used for evaluating the safety profile of selected compounds. Therefore, it ensured that compounds have toxic effect which may be critically harmful for the human and animal. The qualitative and qualitative ways were used to evaluate and determine the toxicity profile, where the mutagenicity, carcinogenicity, LD50 value, immunotoxicity were evaluated [34]. The ProTox-II (<https://tox-new.charite.de/for>) web server has been utilized to document the toxicity of selected compound during this study period on 10 February 2021.

#### 4.8. Molecular Dynamic Simulation (MD)

Thermodynamic constancy of the receptor-ligand system was analyzed through the Desmond v3.6 Program [35]. This program supported automated simulation and free energy perturbation (FEP) calculation included with multiple temperatures as prediction of equation of state (EOS). Again, TIP3P water model and OPLS2005 force field was used to run MD simulation [36]. The simulation of the larger complex structure was determined by orthorhombic periodic boundary condition while the system charge and place randomly for stabilizing sodium ions and their system neutralize electrically. The buffer box calculation method was used with the box shape and size 10 Å. NPT ensemble along with periodic boundary condition were used for performing molecular dynamic simulation [37]. The simulation trajectory has been retrieved and analysis through simulation interaction diagram (SID) available at Schrödinger Release 2020-2.

## 5. Conclusions

The WDSV is responsible for the induction of a multifocal benign cutaneous tumor known as WDS that is found with very high frequency in some localities. The effective therapeutics against the virus have not been developed yet to minimize the frequency of the virus infection. Therefore, this study has been developed to search natural and effective antiviral candidates against the virus to hinder cutaneous tumor development. The

study has utilized CADD approaches to develop molecules through homology modeling, molecular docking, ADMET and MD simulation methods, which identified three potential antiviral candidates namely Friedlein, Phytosterols, and 1-Triacontanol against the virus that will be able to reduce the economic losses in fisheries sector. Although further study is suggested (in vitro and in vivo) to evaluate the effectiveness of the compounds against the virus.

**Supplementary Materials:** The following are available online at <https://www.mdpi.com/article/10.3390/md19050253/s1>, Table S1: List of eleven known compound of *Avicennia alba* and their binding affinity towards to the protein generated through molecular docking method.

**Author Contributions:** M.O.A., M.H.R.M. and F.A.; Conceptualization, M.H.R.M. and F.A.; methodology, formal analysis, and writing—original draft preparation, M.O.A.; supervision, writing—review and editing and funding acquisition. All authors have read and agreed to the published version of the manuscript.

**Funding:** This project was funded by National Plan for Science, Technology, and Innovation (MAAR-IFAH), King Abdulaziz City for Science and Technology, the Kingdom of Saudi Arabia award number (14-ENV263-03).

**Institutional Review Board Statement:** Not applicable.

**Informed Consent Statement:** Not applicable.

**Data Availability Statement:** Not applicable.

**Acknowledgments:** The authors acknowledge with thanks to the Science and Technology Unit, King Abdulaziz University for technical support.

**Conflicts of Interest:** The authors declare no conflict of interest.

## References

- Chan, C.Y.; Tran, N.; Pethiyagoda, S.; Crissman, C.C.; Sulser, T.B.; Phillips, M.J. Prospects and challenges of fish for food security in Africa. *Glob. Food Secur.* **2019**, *20*, 17–25. [[CrossRef](#)]
- Walker, P.J.; Winton, J.R. Emerging viral diseases of fish and shrimp. *Vet. Res.* **2010**, *41*, 51. [[CrossRef](#)] [[PubMed](#)]
- Chávez, C.; Dresdner, J.; Figueroa, Y.; Quiroga, M. Main issues and challenges for sustainable development of salmon farming in Chile: A socio-economic perspective. *Rev. Aquac.* **2019**, *11*, 403–421. [[CrossRef](#)]
- Rovnak, J.; Quackenbush, S.L. Walleye dermal sarcoma virus: Molecular biology and oncogenesis. *Viruses* **2010**, *2*, 1984–1999. [[CrossRef](#)]
- Galluzzi, L.; Brenner, C.; Morselli, E.; Touat, Z.; Kroemer, G. Viral Control of Mitochondrial Apoptosis. *PLoS Pathog.* **2008**, *4*, e1000018. [[CrossRef](#)]
- Ahammad, F.; Abd Rashid, T.R.T.; Mohamed, M.; Tanbin, S.; Fuad, F.A.A. Contemporary strategies and current trends in designing antiviral drugs against dengue fever via targeting host-based approaches. *Microorganisms* **2019**, *7*, 296. [[CrossRef](#)]
- Huang, L.; Chen, C. Understanding HIV-1 protease autoprocessing for novel therapeutic development. *Future Med. Chem.* **2013**, *5*, 1215–1229. [[CrossRef](#)] [[PubMed](#)]
- Guo, Z. The modification of natural products for medical use. *Acta Pharm. Sin. B* **2017**, *7*, 119–136. [[CrossRef](#)] [[PubMed](#)]
- Atanasov, A.G.; Waltenberger, B.; Pferschy-Wenzig, E.M.; Linder, T.; Wawrosch, C.; Uhrin, P.; Temml, V.; Wang, L.; Schwaiger, S.; Heiss, E.H.; et al. Discovery and resupply of pharmacologically active plant-derived natural products: A review. *Biotechnol. Adv.* **2015**, *33*, 1582–1614. [[CrossRef](#)] [[PubMed](#)]
- Zandi, K.; Taherzadeh, M.; Yaghoubi, R.; Tajbakhsh, S.; Rastian, Z.; Fouladvand, M.; Sartavi, K. Antiviral activity of *Avicennia marina* against herpes simplex virus type 1 and vaccine strain of poliovirus (An in vitro study). *J. Med. Plants Res.* **2009**, *3*, 771–775.
- Ghildiyal, R.; Prakash, V.; Chaudhary, V.K.; Gupta, V.; Gabrani, R. Phytochemicals as antiviral agents: Recent updates. In *Plant-Derived Bioactives: Production, Properties and Therapeutic Applications*; Springer: Singapore, 2020; pp. 279–295, ISBN 9789811517617.
- Rahman, S.M.M.; Atikullah, M.; Islam, M.N.; Mohaimenul, M.; Ahammad, F.; Islam, M.S.; Saha, B.; Rahman, M.H. Anti-inflammatory, antinociceptive and antiarrhoeal activities of methanol and ethyl acetate extract of *Hemigraphis alternata* leaves in mice. *Clin. Phytosci.* **2019**, *5*, 16. [[CrossRef](#)]
- Choudhari, A.S.; Mandave, P.C.; Deshpande, M.; Ranjekar, P.; Prakash, O. Phytochemicals in cancer treatment: From preclinical studies to clinical practice. *Front. Pharmacol.* **2020**, *10*, 1614. [[CrossRef](#)] [[PubMed](#)]
- Ziegler, S.; Pries, V.; Hedberg, C.; Waldmann, H. Target identification for small bioactive molecules: Finding the needle in the haystack. *Angew. Chem. Int. Ed.* **2013**, *52*, 2744–2792. [[CrossRef](#)]

15. Yin, L.; Zheng, L.; Xu, L.; Dong, D.; Han, X.; Qi, Y.; Zhao, Y.; Xu, Y.; Peng, J. In-silico prediction of drug targets, biological activities, signal pathways and regulating networks of dioscin based on bioinformatics. *BMC Complement. Altern. Med.* **2015**, *15*, 41. [[CrossRef](#)] [[PubMed](#)]
16. Guedes, I.A.; de Magalhães, C.S.; Dardenne, L.E. Receptor-ligand molecular docking. *Biophys. Rev.* **2014**, *6*, 75–87. [[CrossRef](#)]
17. Samad, A.; Ahammad, F.; Nain, Z.; Alam, R.; Imon, R.R.; Hasan, M.; Rahman, M.S. Designing a multi-epitope vaccine against SARS-CoV-2: An immunoinformatics approach. *J. Biomol. Struct. Dyn.* **2020**, 1–17. [[CrossRef](#)]
18. Opo, F.A.D.M.; Rahman, M.M.; Ahammad, F.; Ahmed, I.; Bhuiyan, M.A.; Asiri, A.M. Structure based pharmacophore modeling, virtual screening, molecular docking and ADMET approaches for identification of natural anti-cancer agents targeting XIAP protein. *Sci. Rep.* **2021**, *11*, 4049. [[CrossRef](#)]
19. Ahammad, F.; Alam, R.; Mahmud, R.; Akhter, S.; Talukder, E.K.; Tonmoy, A.M.; Fahim, S.; Al-Ghamdi, K.; Samad, A.; Qadri, I. Pharmacoinformatics and molecular dynamics simulation-based phytochemical screening of neem plant (*Azadirachta indica*) against human cancer by targeting MCM7 protein. *Brief. Bioinform.* **2021**. [[CrossRef](#)]
20. Madhavi Sastry, G.; Adzhigirey, M.; Day, T.; Annabhimoju, R.; Sherman, W. Protein and ligand preparation: Parameters, protocols, and influence on virtual screening enrichments. *J. Comput. Aided Mol. Des.* **2013**, *27*, 221–234. [[CrossRef](#)]
21. Mahmud, S.; Uddin, M.A.R.; Paul, G.K.; Shimu, M.S.S.; Islam, S.; Rahman, E.; Islam, A.; Islam, M.S.; Promi, M.M.; Emran, T.B.; et al. Virtual screening and molecular dynamics simulation study of plant-derived compounds to identify potential inhibitors of main protease from SARS-CoV-2. *Brief. Bioinform.* **2021**, *22*, 1402–1414. [[CrossRef](#)]
22. Daina, A.; Michielin, O.; Zoete, V. SwissADME: A free web tool to evaluate pharmacokinetics, drug-likeness and medicinal chemistry friendliness of small molecules. *Sci. Rep.* **2017**, *7*, 1–13. [[CrossRef](#)] [[PubMed](#)]
23. Bhuiyan, M.A.; Quayum, S.T.; Ahammad, F.; Alam, R.; Samad, A.; Nain, Z. Discovery of potential immune epitopes and peptide vaccine design—A prophylactic strategy against Rift Valley fever virus. *F1000Research* **2020**, *9*, 999. [[CrossRef](#)]
24. Zhou, W.; Wang, Y.; Lu, A.; Zhang, G. Systems pharmacology in small molecular drug discovery. *Int. J. Mol. Sci.* **2016**, *17*, 246. [[CrossRef](#)]
25. Roy, A.; Kucukural, A.; Zhang, Y. I-TASSER: A unified platform for automated protein structure and function prediction. *Nat. Protoc.* **2010**, *5*, 725–738. [[CrossRef](#)]
26. Heo, L.; Park, H.; Seok, C. GalaxyRefine: Protein structure refinement driven by side-chain repacking. *Nucleic Acids Res.* **2013**, *41*, W384–W388. [[CrossRef](#)]
27. Ho, B.K.; Thomas, A.; Brasseur, R. Revisiting the Ramachandran plot: Hard-sphere repulsion, electrostatics, and H-bonding in the  $\alpha$ -helix. *Protein Sci.* **2009**, *12*, 2508–2522. [[CrossRef](#)]
28. Wiederstein, M.; Sippl, M.J. ProSA-web: Interactive web service for the recognition of errors in three-dimensional structures of proteins. *Nucleic Acids Res.* **2007**, *35*, 407–410. [[CrossRef](#)] [[PubMed](#)]
29. Shaker, M.S.; Oppenheimer, J.; Grayson, M.; Stukus, D.; Hartog, N.; Hsieh, E.W.Y.; Rider, N.; Dutmer, C.M.; Vander Leek, T.K.; Kim, H.; et al. COVID-19: Pandemic Contingency Planning for the Allergy and Immunology Clinic. *J. Allergy Clin. Immunol. Pract.* **2020**, *8*, 1477–1488.e5. [[CrossRef](#)] [[PubMed](#)]
30. Ahammad, F.; Fuad, F.A.A. The in silico identification of potent natural bioactive anti-dengue agents by targeting the human hexokinase 2 enzyme. In Proceedings of the 5th International Electronic Conference on Medicinal Chemistry, Basel, Switzerland, 1–30 November 2019; p. 6342. [[CrossRef](#)]
31. Vyas, A.; Saraf, S.; Saraf, S. Cyclodextrin based novel drug delivery systems. *J. Incl. Phenom. Macrocycl. Chem.* **2008**, *62*, 23–42. [[CrossRef](#)]
32. Hadni, H.; Elhallaoui, M. 2D and 3D-QSAR, molecular docking and ADMET properties: In silico studies of azaaurones as antimalarial agents. *New J. Chem.* **2020**, *44*, 6553–6565. [[CrossRef](#)]
33. Yamashita, S.; Inoue, Y.; Maruyama, S.; Murakami, Y.; Yaguchi, H.; Jablonski, M.; Set, S.Y. Saturable absorbers incorporating carbon nanotubes directly synthesized onto substrates and fibers and their application to mode-locked fiber lasers. *Opt. Lett.* **2004**, *29*, 1581. [[CrossRef](#)]
34. Raies, A.B.; Bajic, V.B. In silico toxicology: Computational methods for the prediction of chemical toxicity. *Wiley Interdiscip. Rev. Comput. Mol. Sci.* **2016**, *6*, 147–172. [[CrossRef](#)] [[PubMed](#)]
35. Rinn, W.E. Emotional facial expression in Parkinson's disease: A response to Bowers (2006). *J. Int. Neuropsychol. Soc.* **2007**, *13*, 721–722. [[CrossRef](#)] [[PubMed](#)]
36. Shivakumar, D.; Williams, J.; Wu, Y.; Damm, W.; Shelley, J.; Sherman, W. Prediction of absolute solvation free energies using molecular dynamics free energy perturbation and the opl's force field. *J. Chem. Theory Comput.* **2010**, *6*, 1509–1519. [[CrossRef](#)]
37. Shinoda, W.; Mikami, M. Rigid-body dynamics in the isothermal-isobaric ensemble: A test on the accuracy and computational efficiency. *J. Comput. Chem.* **2003**, *24*, 920–930. [[CrossRef](#)] [[PubMed](#)]



MDPI  
St. Alban-Anlage 66  
4052 Basel  
Switzerland  
Tel. +41 61 683 77 34  
Fax +41 61 302 89 18  
[www.mdpi.com](http://www.mdpi.com)

*Marine Drugs* Editorial Office  
E-mail: [marinedrugs@mdpi.com](mailto:marinedrugs@mdpi.com)  
[www.mdpi.com/journal/marinedrugs](http://www.mdpi.com/journal/marinedrugs)







MDPI  
St. Alban-Anlage 66  
4052 Basel  
Switzerland

Tel: +41 61 683 77 34  
Fax: +41 61 302 89 18

[www.mdpi.com](http://www.mdpi.com)



ISBN 978-3-0365-1940-1